



**HAL**  
open science

# Introduction of ionic liquid via microencapsulation to design enhanced and self-healable epoxy-amine composites

Ting Shi

► **To cite this version:**

Ting Shi. Introduction of ionic liquid via microencapsulation to design enhanced and self-healable epoxy-amine composites. Materials. Université de Lyon, 2022. English. NNT : 2022LYSEI026 . tel-03709308

**HAL Id: tel-03709308**

**<https://theses.hal.science/tel-03709308>**

Submitted on 29 Jun 2022

**HAL** is a multi-disciplinary open access archive for the deposit and dissemination of scientific research documents, whether they are published or not. The documents may come from teaching and research institutions in France or abroad, or from public or private research centers.

L'archive ouverte pluridisciplinaire **HAL**, est destinée au dépôt et à la diffusion de documents scientifiques de niveau recherche, publiés ou non, émanant des établissements d'enseignement et de recherche français ou étrangers, des laboratoires publics ou privés.



N°d'ordre NNT : 2022LYSEI026

**THESE de DOCTORAT DE L'UNIVERSITE DE LYON**  
opérée au sein de  
**L'Institut National des Sciences Appliquées de Lyon**

**Ecole Doctorale N° 34**  
**Ecole Doctorale de Matériaux de Lyon**

**Spécialité de doctorat** : Matériaux Polymères et Composites  
**Discipline** : Matériaux

Soutenue publiquement le 29/03/2022, par :  
**Ting SHI**

---

**Introduction of Ionic Liquid via  
Microencapsulation to Design Enhanced and  
Self-healable Epoxy-Amine Composites**

---

Devant le jury composé de :

BONGIOVANNI Roberta	Professeur (Politecnico di Torino)	Examinatrice
KENNY José Maria	Professeur (Università degli Studi di Perugia)	Rapporteur
DEFOORT Brigitte	Docteur, HDR (ArianeGroup)	Rapporteur
GERARD Jean-François	Professeur (INSA Lyon)	Directeur de thèse
DUCHET-RUMEAU Jannick	Professeur (INSA Lyon)	Co-directrice de thèse
LIVI Sébastien	Maître de Conférences, HDR (INSA Lyon)	Co-directeur de thèse

## Département FEDORA – INSA Lyon - Ecoles Doctorales

SIGLE	ECOLE DOCTORALE	NOM ET COORDONNEES DU RESPONSABLE
<b>CHIMIE</b>	<b>CHIMIE DE LYON</b> <a href="https://www.edchimie-lyon.fr">https://www.edchimie-lyon.fr</a> Sec. : Renée EL MELHEM Bât. Blaise PASCAL, 3e étage secretariat@edchimie-lyon.fr	<b>M. Stéphane DANIELE</b> C2P2-CPE LYON-UMR 5265 Bâtiment F308, BP 2077 43 Boulevard du 11 novembre 1918 69616 Villeurbanne <a href="mailto:directeur@edchimie-lyon.fr">directeur@edchimie-lyon.fr</a>
<b>E.E.A.</b>	<b>ÉLECTRONIQUE, ÉLECTROTECHNIQUE, AUTOMATIQUE</b> <a href="https://edeea.universite-lyon.fr">https://edeea.universite-lyon.fr</a> Sec. : Stéphanie CAUVIN Bâtiment Direction INSA Lyon Tél : 04.72.43.71.70 secretariat.edeea@insa-lyon.fr	<b>M. Philippe DELACHARTRE</b> INSA LYON Laboratoire CREATIS Bâtiment Blaise Pascal, 7 avenue Jean Capelle 69621 Villeurbanne CEDEX Tél : 04.72.43.88.63 <a href="mailto:philippe.delachartre@insa-lyon.fr">philippe.delachartre@insa-lyon.fr</a>
<b>E2M2</b>	<b>ÉVOLUTION, ÉCOSYSTÈME, MICROBIOLOGIE, MODÉLISATION</b> <a href="http://e2m2.universite-lyon.fr">http://e2m2.universite-lyon.fr</a> Sec. : Sylvie ROBERJOT Bât. Atrium, UCB Lyon 1 Tél : 04.72.44.83.62 secretariat.e2m2@univ-lyon1.fr	<b>M. Philippe NORMAND</b> Université Claude Bernard Lyon 1 UMR 5557 Lab. d'Ecologie Microbienne Bâtiment Mendel 43, boulevard du 11 Novembre 1918 69 622 Villeurbanne CEDEX <a href="mailto:philippe.normand@univ-lyon1.fr">philippe.normand@univ-lyon1.fr</a>
<b>EDISS</b>	<b>INTERDISCIPLINAIRE SCIENCES-SANTÉ</b> <a href="http://ediss.universite-lyon.fr">http://ediss.universite-lyon.fr</a> Sec. : Sylvie ROBERJOT Bât. Atrium, UCB Lyon 1 Tél : 04.72.44.83.62 secretariat.ediss@univ-lyon1.fr	<b>Mme Sylvie RICARD-BLUM</b> Institut de Chimie et Biochimie Moléculaires et Supramoléculaires (ICBMS) - UMR 5246 CNRS - Université Lyon 1 Bâtiment Raulin - 2ème étage Nord 43 Boulevard du 11 novembre 1918 69622 Villeurbanne Cedex Tél : +33(0)4 72 44 82 32 <a href="mailto:sylvie.ricard-blum@univ-lyon1.fr">sylvie.ricard-blum@univ-lyon1.fr</a>
<b>INFOMATHS</b>	<b>INFORMATIQUE ET MATHÉMATIQUES</b> <a href="http://edinfomaths.universite-lyon.fr">http://edinfomaths.universite-lyon.fr</a> Sec. : Renée EL MELHEM Bât. Blaise PASCAL, 3e étage Tél : 04.72.43.80.46 infomaths@univ-lyon1.fr	<b>M. Hamamache KHEDDOUCI</b> Université Claude Bernard Lyon 1 Bât. Nautibus 43, Boulevard du 11 novembre 1918 69 622 Villeurbanne Cedex France Tél : 04.72.44.83.69 <a href="mailto:hamamache.kheddouci@univ-lyon1.fr">hamamache.kheddouci@univ-lyon1.fr</a>
<b>Matériaux</b>	<b>MATÉRIAUX DE LYON</b> <a href="http://ed34.universite-lyon.fr">http://ed34.universite-lyon.fr</a> Sec. : Yann DE ORDENANA Tél : 04.72.18.62.44 yann.de-ordenana@ec-lyon.fr	<b>M. Stéphane BENAYOUN</b> Ecole Centrale de Lyon Laboratoire LTDS 36 avenue Guy de Collongue 69134 Ecully CEDEX Tél : 04.72.18.64.37 <a href="mailto:stephane.benayoun@ec-lyon.fr">stephane.benayoun@ec-lyon.fr</a>
<b>MEGA</b>	<b>MÉCANIQUE, ÉNERGÉTIQUE, GÉNIE CIVIL, ACOUSTIQUE</b> <a href="http://edmega.universite-lyon.fr">http://edmega.universite-lyon.fr</a> Sec. : Stéphanie CAUVIN Tél : 04.72.43.71.70 Bâtiment Direction INSA Lyon mega@insa-lyon.fr	<b>M. Jocelyn BONJOUR</b> INSA Lyon Laboratoire CETHIL Bâtiment Sadi-Carnot 9, rue de la Physique 69621 Villeurbanne CEDEX <a href="mailto:jocelyn.bonjour@insa-lyon.fr">jocelyn.bonjour@insa-lyon.fr</a>
<b>ScSo</b>	<b>ScSo*</b> <a href="https://edsciencessociales.universite-lyon.fr">https://edsciencessociales.universite-lyon.fr</a> Sec. : Mélina FAVETON INSA : J.Y. TOUSSAINT Tél : 04.78.69.77.79 melina.faveton@univ-lyon2.fr	<b>M. Christian MONTES</b> Université Lumière Lyon 2 86 Rue Pasteur 69365 Lyon CEDEX 07 <a href="mailto:christian.montes@univ-lyon2.fr">christian.montes@univ-lyon2.fr</a>

\*ScSo : Histoire, Géographie, Aménagement, Urbanisme, Archéologie, Science politique, Sociologie, Anthropologie

# Acknowledgements

First of all, I would like to express my sincerest gratitude to my supervisors, who accepted as their PhD student and accompanied me all the work along the beautiful journey in France. Thank Prof. Jean-François GERARD for his kind guidance and for sharing his knowledge. I benefited a lot from his rigorous academic attitude and open-minded attitude towards research and life. Thank Prof. Jannick DUCHET-RUMEAU for her guidance and kind help on my research, and her smile always makes me feel extremely warm. I also express my great thanks to Dr. Sébastien LIVI for all the discussion on science and showing me the food and culture of Lyon. His passion for both science and life encourage me deeply. Again, thank you all my supervisors for accepting me as your student, all the discussion, corrections of this manuscript, and following my growth during my PhD.

Besides my supervisors, I would like to thank the members of my defense committee who have accepted to review and examine this work. I would like to thank Prof. José Maria KENNY and Dr. Brigitte DEFOORT for reviewing the manuscript, and Prof. Roberta BONGIOVANNI for examining this work. Thanks for their time, interest, insightful remarks, and helpful comments. It is a great honor to have you as my defense committee.

This work was supported by China Scholarship Council (CSC) and done in the laboratory Ingénierie des Matériaux Polymères in INSA Lyon (IMP@INSA). Thanks for the financial support from CSC and all the members in IMP@INSA. Thank Pierre ALCOUFFE for the TEM and SEM analysis, Guilhem QUINTARD and Xavier MORELLE for the mechanical properties, Ahmed BELHADJ for the thermal properties, and Carlos FERNANDEZ DE ALBA for the help of NMR analysis. Thank Isabelle POLO, Mallaouia BENGOUA, and Sylvain BAUDU for their kindly help in the lab. Thank Gabriel PERLI for the help of synthesis. Thank Laurent REMY, Carolina Helena FRANZON, and Younes EL OMARI for the invitation of hanging out. Thank Victor HADDAD, Adrien TOPALIAN for sharing the time in the lab. Thank especially Luxiao CHAI for helping me adapt to the lab quickly. Thank all the professors, technicians, PhD students, and postdoc researchers for your welcome, kindness, and sharing of knowledge during the past three years.

Thank all my best office members. It is really lucky for sharing the same office with you. Thank Dr. Houssém CHABANE for all the help from the very first day when I arrived in France, I will never forget your kindness, your advice, and discussions. Thank Dr. Alexei RADCHENKO for being the only one who accompanied me from the first day to the last day, and thank you for speaking with me in French even if I made hundreds of mistakes, and especially thank you for all the help and all the praises every day. Thank Benoit CAPRIN for showing good local restaurants and your help. Thank Dr. Aude-Héloïse BONARDI for the help of my manuscript. Thank all the Chinese students in the lab. Liutong HOU, Yufei WANG and Hu Qiao for your help and kindness, thank Yiping CHEN for sharing all the exciting moments and experiences together.

I would like to express all my appreciation to my Chinese friends, Xiaokang ZHANG, Xiaoyang YUE, Chenchen CHU, and Hequn LIU for sharing happiness, sadness, anxiety, and hope together. It is all of you that make my life in France happier, more enriched and fulfilled. I do believe it is a kind of special fate that allows us to meet in France and become close friends and we will always cherish this precious friendship in the future. Especially, thank my friends in China, Xiaoyu LIU, Yuxin QING, Mengyue Tian and Boxin HE. Although we are thousands of miles apart, your care and support make me feel extremely warm here in France.

The deepest thanks and love to my beloved parents and my family. It is your support that keeps me bravely pursuing my dream and becoming the person that I want to be.

Finally, thank myself for never giving up even when facing all the difficulties during my PhD, just like all the medical workers in the pandemic COVID-19. Thank myself for always working hard to be a strong, independent, free and better person. There is a long journey to go, I will always keep going forward, just like the old Chinese saying:

路漫漫其修远兮，吾将上下而求索。

Thank you all and love you all.

Ting SHI

Lyon

Mars 2022



*Il faut être l'homme de la pluie et l'enfant du beau temps.*

*You have to be the man of the rain and the child of the good weather.*

风雨中要像个大人，晴空里要做个孩子。

# Abstract

Epoxy networks are the most widely used thermoset materials. Nevertheless, these highly crosslinked networks display a high brittleness, *i.e.* a low toughness, which limits their applications in some specific occasions. Therefore, improving the toughness to prevent crack propagation and healing damages which could occur in the epoxy matrices for low strains is a key issue to extend life span of epoxy-based materials such as fiber-based thermoset composites materials. Ionic liquids (IL) have been considered to design high performance epoxies because of the excellent intrinsic properties and a very large number of combinations of cations and anions. Therefore, this work focuses on improvement of toughness and self-healing property in conventional epoxy-amine networks via a microencapsulation-based strategy. In the first section, phosphonium type ionic liquid was firstly encapsulated in silica shell-based microcapsules which could contribute to the improvement of the toughness of epoxy-amine network. In the second section, an epoxy monomer was encapsulated in poly(urea-formaldehyde) shell-based microcapsule as an extrinsic healing agent and an ionic liquid was incorporated in epoxy-amine-IL network. Self-healing was expected to be achieved at high temperature by the releasing of the epoxy from the breakage of microcapsules and its polymerization induced by the IL. In the last section, a ionic liquid functionalized epoxy monomer was synthesized. This one was first encapsulated in poly(melamine-formaldehyde) shell microcapsules and that were added into different epoxy-amine matrices to design single microcapsule-based self-healing systems. Therefore, this work focused on different strategies via different combinations of ionic liquids and microcapsules designed for epoxy networks. Numerous research routes and technological applications will be offered based on our results.

**Key words** : epoxy-amine network ; ionic liquids ; microencapsulation ; toughness ; self-healing.





# Résumé

La résine époxy est l'un des polymères thermodurcissables les plus largement utilisés pour les applications de haute valeur ajoutée. Leur utilisation est toutefois confrontée au problème de fragilité élevée et de faible ténacité de ce type de polymère hautement réticulé, ce qui limite leurs applications à certains domaines. Par conséquent, améliorer leur ténacité pour freiner la propagation des fissures et guérir les microfissures qui pourraient se créer dans des matrices époxy pourrait conduire à une prolongation de la durée de vie de matériaux polyépoxydes comme les matériaux composites et/ou les adhésifs structuraux. Un liquide ionique (LI) a été adopté pour concevoir un matériau époxy à hautes performances en prenant en compte les excellentes propriétés intrinsèques des liquides ioniques notamment les combinaisons multiples de cations et d'anions. Ces travaux se concentrent sur l'amélioration de la ténacité et de la capacité d'auto-guérison des matrices époxy-amine via une méthodologie déjà largement maîtrisée, celle faisant appel à la microencapsulation.

Dans une première partie, un liquide ionique de type phosphonium a été encapsulé dans une coque de silice pour former des microcapsules capables d'améliorer la ténacité du réseau époxy-amine via les mécanismes de plasticité mis en jeu. Dans la deuxième partie, le monomère époxy a été encapsulé dans une coque de poly(urée-formaldéhyde) et des microcapsules résultantes ont été considérées comme agent cicatrisant extrinsèque combiné à un liquide ionique incorporé dans le réseau époxy-amine. Dans la dernière partie, un monomère époxy liquide ionique, c'est-à-dire un liquide ionique porteur de fonctions époxyde réactives, a été synthétisé. Celui-ci a d'abord été encapsulé dans des microcapsules à coque poly(mélatamine-formaldéhyde) qui ont été ajoutées dans différentes matrices époxy-amine pour concevoir un système d'auto-cicatrisation. En conclusion, ce travail s'est concentré sur différentes stratégies combinant liquides ioniques et composés designer des microcapsules pertinentes pour

des systèmes époxy. Bien entendu, les travaux exposés ouvrent vers de nombreuses applications où l'encapsulation de liquides ioniques fait sens (tribologie, corrosion, etc).

**Mots clés** : réseau époxy-amine ; liquides ioniques ; microencapsulation ; dureté ; auto-guérison.

# Table of Contents

<b>Acknowledgements</b> .....	<b>i</b>
<b>Abstract</b> .....	<b>v</b>
<b>Résumé</b> .....	<b>vii</b>
<b>Table of Contents</b> .....	<b>ix</b>
<b>List of Figures</b> .....	<b>xv</b>
<b>List of Schemes</b> .....	<b>xxiii</b>
<b>List of tables</b> .....	<b>xxv</b>
<b>List of abbreviations and symbols</b> .....	<b>xxvii</b>
<b>General Introduction</b> .....	<b>1</b>
<b>Résumé Étendu</b> .....	<b>5</b>
<b>Chapter 1: Literature Review</b> .....	<b>27</b>
<b>Table of contents</b> .....	<b>28</b>
<b>1.1 Self-healing materials</b> .....	<b>31</b>
1.1.1 Introduction .....	30
1.1.2 Intrinsic self-healing .....	31
1.1.2.1 Self-healing from reversible covalent interactions.....	31
1.1.2.2 Self-healing from reversible non-covalent interactions .....	33
1.1.3 Extrinsic self-healing.....	36
1.1.3.1 Microvascular systems for self-healing.....	37
1.1.3.2 Microcapsules for self-healing .....	39
1.1.4 Conclusion.....	44
<b>1.2 Ionic liquids and epoxy networks</b> .....	<b>44</b>

---

1.2.1 Ionic liquids .....	44
1.2.1.1 Introduction .....	44
1.2.1.2 Applications of ionic liquids.....	45
1.2.2 Epoxy networks .....	49
1.2.2.1 Introduction .....	49
1.2.2.2 Building epoxy networks.....	50
1.2.3 Ionic liquids combined with epoxy networks.....	53
1.2.3.1 As hardener or initiator for curing epoxies.....	53
1.2.3.2 As dispersing aids of nanomaterials/nano-objects within polymers .....	56
1.2.3.3 As flame retardant agents .....	57
1.2.4 Conclusions .....	58
<b>1.3 Microencapsulation .....</b>	<b>58</b>
1.3.1 Introduction .....	58
1.3.2 Synthesis strategies for microencapsulation.....	60
1.3.2.1 Solvent evaporation .....	60
1.3.2.2 Spray drying .....	61
1.3.2.3 <i>In-situ</i> polymerization .....	62
1.3.2.4 Interfacial polymerization .....	63
1.3.3 Applications of microcapsules.....	66
1.3.3.1 Biomedical uses.....	66
1.3.3.2 Food industry.....	67
1.3.3.3 Electronic devices.....	68
1.3.3.4 Polymer composites .....	69
1.3.4 Conclusion.....	71
<b>1.4 Conclusion of Chapter 1 .....</b>	<b>71</b>
<b>References in Chapter 1 .....</b>	<b>73</b>
<b>Chapter 2: Ionic liquid-containing silica microcapsules as functional additives</b>	

---

<b>for epoxy-amine networks .....</b>	<b>87</b>
<b>Table of Contents .....</b>	<b>88</b>
<b>2.1 Introduction .....</b>	<b>89</b>
<b>2.2 Experimental.....</b>	<b>92</b>
2.2.1 Materials .....	92
2.2.2 Experimental .....	93
2.2.3 Characterization methods .....	97
<b>2.3 Characterization of the IL@SiO<sub>2</sub> microcapsules .....</b>	<b>99</b>
2.3.1 Morphology and size distribution of the IL@SiO <sub>2</sub> microcapsules .....	99
2.3.2 Chemical characterization of the IL@SiO <sub>2</sub> microcapsules .....	102
2.3.3 Determination of IL content of the IL@SiO <sub>2</sub> microcapsules .....	103
<b>2.3 Characterization of IL@SiO<sub>2</sub> microcapsule-filled epoxy-amine microcomposites .....</b>	<b>106</b>
2.3.1 Morphology and size distributions of IL@SiO <sub>2</sub> microcapsule-filled epoxy-amine microcomposites.....	106
2.3.2 Thermal and dynamic mechanical properties of IL@SiO <sub>2</sub> microcapsule- filled epoxy-amine microcomposites .....	107
2.3.3 Swelling.....	112
2.3.4 Thermal behavior of neat epoxy networks and IL@SiO <sub>2</sub> microcapsule- filled epoxy microcomposites .....	115
2.3.5 Mechanical performances of IL@SiO <sub>2</sub> microcapsule-filled epoxy-amine microcomposites.....	116
2.3.6 Fracture mechanism of IL@SiO <sub>2</sub> microcapsule-filled epoxy-amine microcomposites.....	118
<b>2.4 Conclusion of Chapter 2 .....</b>	<b>123</b>
<b>References of Chapter 2.....</b>	<b>125</b>

---

<b>Supporting Information of Chapter 2 .....</b>	<b>131</b>
<b>Chapter 3: Synthesis of poly(urea-formaldehyde) microcapsules containing epoxy monomer to design self-healable epoxy-amine-IL materials .....</b>	<b>139</b>
<b>Table of Contents .....</b>	<b>140</b>
<b>3.1 Introduction .....</b>	<b>142</b>
<b>3.2 Experimental.....</b>	<b>144</b>
3.2.1 Materials .....	144
3.2.2 Characterization methods .....	146
<b>3.3 Synthesis and characterization of EP@PUF microcapsules.....</b>	<b>148</b>
3.3.1 Synthesis procedure of EP@PUF microcapsules.....	148
3.3.2 Characterization of EP@PUF microcapsules.....	149
3.3.2.1 Morphology of EP@PUF microcapsules .....	149
3.3.2.2 Determination of chemical nature of EP@PUF microcapsules ...	153
3.3.2.3 Thermal properties of EP@PUF microcapsules.....	154
<b>3.4 Preparation and characterization of epoxy-amine-IL networks.....</b>	<b>159</b>
3.4.1 Sample preparation.....	159
3.4.2 Characterization of epoxy-amine-IL networks.....	160
3.4.2.1 Curing behavior of epoxy-amine-IL networks .....	160
3.4.2.2 Morphology of epoxy-amine-IL networks .....	163
3.4.2.3 Thermal properties of epoxy-amine-IL networks.....	165
3.4.2.4 Mechanical properties of epoxy networks.....	167
<b>3.5 Preparation and characterization of self-healing epoxy-amine-ionic liquids composites filled with EP@PUF microcapsules .....</b>	<b>168</b>
3.5.1 Material processing .....	168
3.5.2 Characterization of EP@PUF microcapsule-filled epoxy-amine-IL materials .....	169

---

3.5.2.1 Morphology of EP@PUF microcapsule-filled epoxy-amine-IL materials .....	169
3.5.2.2 Thermal behavior of EP@PUF microcapsule-filled epoxy-amine-IL materials.....	170
3.5.2.3 Thermal stability of EP@PUF microcapsule-filled epoxy-amine-IL materials.....	172
3.5.2.4 Dynamic mechanical analysis of EP@PUF microcapsule-filled epoxy-amine-IL materials .....	173
3.5.2.5 Self-healing property of EP@PUF microcapsule-filled epoxy-amine-IL materials.....	176
3.5.2.6 Mechanical properties of EP@PUF microcapsule-filled epoxy-amine-IL materials.....	179
<b>3.6 Conclusion of Chapter 3 .....</b>	<b>181</b>
<b>References of Chapter 3 .....</b>	<b>183</b>
<b>Supporting Information of Chapter 3 .....</b>	<b>188</b>
<b>Chapter 4: Encapsulation of ionic liquid epoxy monomer and their self-healing application in epoxy-amine networks.....</b>	<b>191</b>
<b>Table of contents .....</b>	<b>192</b>
<b>4.1 Introduction .....</b>	<b>194</b>
<b>4.2 Experimental.....</b>	<b>195</b>
4.2.1 Materials.....	195
4.2.2 Characterization methods .....	197
<b>4.3 Synthesis and characterization of ILEM@PMF microcapsules .....</b>	<b>200</b>
4.3.1 Synthesis of ILEM.....	200
4.3.2 Synthesis of ILEM@PMF microcapsules .....	201
4.3.3 Characterization of ILEM@PMF microcapsules.....	202



---

4.3.3.1 Selection of the best surfactant to obtain ILEM/H <sub>2</sub> O emulsion...	202
4.3.3.2 Monitoring ILEM@PMF microcapsules synthesis.....	203
4.3.3.3 Influence of synthesis parameters on the morphology and size distribution of ILEM@PMF microcapsules .....	205
4.3.3.4 Chemical structure of ILEM@PMF microcapsules .....	210
4.3.3.5 Thermal behavior and stability of ILEM@PMF microcapsules ..	211
<b>4.4 Preparation and characterization of ILEM@PMF microcapsule-filled epoxy-amine materials .....</b>	<b>214</b>
4.4.1 Material processing .....	215
4.4.2 Characterization of ILEM@PMF microcapsules filled epoxy-amine materials .....	215
4.4.2.1 Local temperature of different epoxy-amine networks .....	215
4.4.2.2 Morphology of ILEM@PMF microcapsule-filled epoxy-amine materials .....	216
4.4.2.3 Thermal properties of ILEM@PMF microcapsule-filled epoxy- amine materials.....	218
4.4.2.4 Dynamic mechanical properties of ILEM@PMF microcapsule- filled epoxy-amine materials .....	219
4.4.2.5 Self-healing property of ILEM@PMF microcapsule-filled epoxy- amine materials.....	220
4.4.2.6 Mechanical properties of ILEM@PMF microcapsule-filled epoxy- amine materials.....	222
<b>4.5 Conclusion.....</b>	<b>223</b>
<b>References of Chapter 4 .....</b>	<b>224</b>
<b>Supporting Information of Chapter 4 .....</b>	<b>229</b>
<b>Chapter 5 Conclusions and perspectives.....</b>	<b>237</b>

# List of Figures

**Figure 1-1** Damage modes in polymer composites

**Figure 1-2** (a) Chemical structure of DGEBA and diamine with DA adducts. (b) thermal induced self-healing mechanism

**Figure 1-3** Construction of covalent cross-linked polymer gel based on reversible covalent acylhydrazone bond

**Figure 1-4** Stages of self-healing mechanism for polymeric segments of random walk character

**Figure 1-5** Self-healing mechanism for a supramolecular material

**Figure 1-6** Proposal of design for the multiphase self-healing brush polymer system

**Figure 1-7** (a) Chemical structures of polyimides **1** and polyamides **2** in Burattini's work and (b) intercalation of pyrenyl end-groups (red) into designed polyimide chain-folds (blue)

**Figure 1-8** Concept of microvascular self-healing system in PMC

**Figure 1-9** Schematic illustration of different hollow fiber self-healing systems

**Figure 1-10** Structure of a microvascular network-embedded self-healing membrane and schematic illustration of the healing mechanism

**Figure 1-11** Solidified resin (circled) providing from releasing curing agents from ruptured PAN fibers

**Figure 1-12** Basic healing concept using microcapsules in PMC left: single microcapsules healing system; right: dual microcapsule healing system

**Figure 1-13** Microscope photos of self-healing coating films

**Figure 1-14** Self-healing evidence from SEM images of fracture surfaces of an epoxy network containing 4 wt% amine-containing and 6 wt% epoxy-containing microcapsules: (a) fracture surface after healing; (b) non-healed fracture surface rinsed with ethanol

**Figure 1-15** (a) SEM micrograph of core-shell bead-on-string morphology prepared by coaxial electrospinning; (b) Release of healing agent in coating after mechanical damage

**Figure 1-16** Some commonly used cations and anions of RTILs

**Figure 1-17** Ethylmethylimidazolium-based ILs

**Figure 1-18** Properties of ionic liquids and application in lithium metal batteries on electrolytes, cathodes and lithium metal anode

**Figure 1-19** Chemical structure of IL P<sub>222-201</sub>-TFSI

**Figure 1-20** Boundary film formation process during sliding ware from IL-filled microcapsules breakage

**Figure 1-21** Chemical structures of the common epoxy resins: (1) DGEBA: diglycidylether of bisphenol A, (2) DGEBF: diglycidylether of bisphenol F, (3) DGEBiphenyl: diglycidylether of biphenyl, (4) Phenol novolac type epoxy, (5) Phenoxy resin

**Figure 1-22** Epoxy network scheme. The network results from the homopolymerization in presence of IL: (blue) IL anion, (red) IL cation, (black) pre-polymer; (green) crosslinks

**Figure 1-23** TEM micrographs of epoxy amine networks modified with: (a) POSS<sup>IB</sup>-triol and (b): IL-g-POSS<sup>IB</sup> at different magnification (b<sub>1</sub>; b<sub>2</sub>), (c) POSS<sup>Ph</sup>-triol and (d): IL-g-POSS<sup>Ph</sup> at different magnifications (d<sub>1</sub>; d<sub>2</sub>)

**Figure 1-24** Solvent evaporation method for fabricating microcapsules

**Figure 1-25** Graphic illustration of typical spray drying system

**Figure 1-26** Conventional synthesis of microcapsules considering *in-situ* polymerization in the O/W emulsion state

**Figure 1-27** Idealized mechanism of particle/capsule formation by interfacial polymerization

**Figure 1-28** (A) Emulsions are prepared by dispersing a polar phase containing anhydrous polyethylenimine (PEI) into a nonpolar phase. (B) A cross-linked polyurea shell forms upon addition of f 2,4-tolylene diisocyanate (TDI) to the continuous phase

**Figure 1-29** Schematic diagram of synthetic process of double layered microcapsules: (a) O/W emulsion; (b) formation of the inner PU layer; (c) condensation of the UF resin; (d) consolidation of the outer layer

**Figure 1-30** Synthesis procedure of IBU microcapsules and the controllable drug release model

**Figure 1-31** Scheme of the capsule geometry and fluorescence microscopy images of single capsules under acidic (pH 6.0, green) and alkaline (pH 9.0, red) pH

**Figure 1-32** Schematic structure of the supercapacitors containing microcapsules

**Figure 1-33** Schematic diagram of microcapsules based self-lubricating mechanism

**Figure 2-1** Schematic synthesis procedure of IL@SiO<sub>2</sub> microcapsules

**Figure 2-2** Preparation of IL@SiO<sub>2</sub> microcapsule-filled epoxy-amine microcomposites

**Figure 2-3** Compact Tensile (CT) test specimen geometry

**Figure 2-4** (a,b) TEM and SEM (c,d) micrographs of IL@SiO<sub>2</sub> microcapsules at different magnifications

**Figure 2-5** EDX spectra of (a) IL@SiO<sub>2</sub> microcapsules and (b) cooper grid

**Figure 2-6** Size distribution of IL@SiO<sub>2</sub> microcapsules

**Figure 2-7** FT-IR spectrum of (a) SDS, (b) CTAB, (c) IL 104, and (d) IL@SiO<sub>2</sub>

**Figure 2-8** TGA traces of (a) IL@SiO<sub>2</sub> microcapsules, (b) IL 104, (c) SDS, (d) CTAB, and (e) nSiO<sub>2</sub> (*i.e.* without IL) (N<sub>2</sub> atmosphere, heating rate 20 K·min<sup>-1</sup>)

**Figure 2-9** TEM micrographs of IL@SiO<sub>2</sub> microcapsule-filled epoxy-amine microcomposites (a)1.0-1; (b)1.0-2; (c)1.0-5; (d) 1.2-1; (e) 1.2-2; (f) 1.2-5; (g) 1.4-1; (h) 1.4-2; (i) 1.4-5

**Figure 2-10** Loss factor ( $\tan \delta$ ) as a function temperature of different epoxy networks (a)  $r=1.0$ ; (b)  $r=1.2$ ; (c)  $r=1.4$  (at 1Hz, heating rate 3 K·min<sup>-1</sup>)

**Figure 2-11** Swelling ratio of different epoxy-amine networks and their corresponding IL@SiO<sub>2</sub> microcapsule-filled microcomposites in THF (at room temperature)

**Figure 2-12** Graphical illustration of swelling model of neat epoxy-amine network: (a) before and (b) after swelling; and IL@SiO<sub>2</sub> microcapsule-filled epoxy-amine microcomposites : (c) before and (d) after swelling

**Figure 2-13** Young's modulus epoxy-amine microcomposite filled with different weight fractions of IL@SiO<sub>2</sub> microcapsules

**Figure 2-14** (a)  $K_{Ic}$  and (b)  $G_{Ic}$  of epoxy-amine microcomposites filled with different weight fractions of IL@SiO<sub>2</sub> microcapsules

**Figure 2-15** SEM micrographs of fracture surface of epoxy-amine composites filled with different weight fractions of IL@SiO<sub>2</sub> microcapsules (a)1.0-0; (b) 1.0-1; (c) 1.0-2; (d) 1.0-5; (e) 1.2-0; (f)1.2-1; (g)1.2-2; (h)1.2-5;(i)1.4-0; (j)1.4-1; (k)1.4-2; (l)1.4-5

**Figure 2-16** Schematic diagram of the crack tip and crack opening displacement (COD)

**Figure S2-1** TEM micrograph of hollow silica nanoparticles (nSiO<sub>2</sub>)

**Figure S2-2** DSC traces of epoxy-amine networks and their corresponding IL@SiO<sub>2</sub> microcapsule-filled microcomposites (N<sub>2</sub> atmosphere, heating rate: 10 K·min<sup>-1</sup>) (a)  $r=1.0$ ; (b)  $r=1.2$ ; (c)  $r=1.4$

**Figure S2-3** Storage modulus and loss modulus as a function of temperature of different IL@SiO<sub>2</sub> microcapsule-filled epoxy microcomposites, Storage modulus ( $E'$ ) : (a)  $r=1.0$ ; (c)  $r=1.2$ ; (e)  $r=1.4$  Loss modulus ( $E''$ ) : (b)  $r=1.0$ ; (d)  $r=1.2$ ; (f)  $r=1.4$

**Figure S2-4** Contact angle with H<sub>2</sub>O on surfaces of IL@SiO<sub>2</sub> microcapsule-filled epoxy microcomposites

**Figure S2-5** TGA traces of different IL@SiO<sub>2</sub> microcapsule-filled epoxy microcomposites (N<sub>2</sub> atmosphere, heating rate: 20 K·min<sup>-1</sup>)

**Figure 3-1** Schematic diagram of the (a) self-healing of scratch (b) and its characterization

**Figure 3-2** Synthesis steps of EP@PUF microcapsules via *in-situ* polymerization

**Figure 3-3** OM images of synthetic procedure of EP@PUF microcapsules (a) O/W emulsion; (b) formation of PUF nanoparticles; (c) formation and solidification of EP@PUF microcapsules;

(d) OM image of EP@PUF microcapsules at reflection mode;

**Figure 3-4** Flow pattern (a) radial flow; (b) axial flow; (c) tangential flow

**Figure 3-5** Diameter distribution of EP@PUF microcapsules

**Figure 3-6** SEM micrographs of (a), (b) EP@PUF microcapsules; (c) surface morphology of EP@PUF microcapsule; (d) broken EP@PUF microcapsule

**Figure 3-7** FTIR spectra of (a) EP@PUF microcapsules and its (b) shell material: pure PUF and (c) core materials: DGEBA+BGE

**Figure 3-8** Characteristic peaks of core (DGEBA+BGE) and shell (PUF) materials in EP@PUF microcapsules

**Figure 3-9** DSC traces of core and shell materials in EP@PUF microcapsules (■) EP@PUF; (●) neat PUF; (▲) DGEBA+BGE (N<sub>2</sub> atmosphere, heating rate: 10 K·min<sup>-1</sup>)

**Figure 3-10** (a) TGA and (b) DTG traces of (▲) EP@PUF microcapsules and their shell material (●, neat PUF) and core material (■, DGEBA+BGE) (N<sub>2</sub> atmosphere, heating rate 20 K·min<sup>-1</sup>)

**Figure 3-11** FTIR spectra of emergent gas while degradation of EP@PUF microcapsules in N<sub>2</sub> atmosphere (heating rate: 10 K·min<sup>-1</sup>)

**Figure 3-12** DSC traces of curing process of epoxy-amine at stoichiometric ratio with different amount of ionic liquid (■) EP + 30 phr PACM; (●) EP + 30 phr PACM + 5 phr IL169; (▲) EP + 30 phr PACM + 10 phr IL169; (▼) EP + 30 phr PACM + 20 phr IL169 (N<sub>2</sub> atmosphere, heating rate: 10 K·min<sup>-1</sup>)

**Figure 3-13** The possible polymerization and structure of epoxy-amine-IL network

**Figure 3-14** DSC traces of curing process of different epoxy-amine-ionic liquid systems (■) EP + 30 phr PACM; (●) EP + 10 phr IL169; (▲) EP + 30 phr PACM + 10 phr IL169; (▼) EP + 20 phr PACM + 10 phr IL169 (N<sub>2</sub> atmosphere, heating rate: 10 K·min<sup>-1</sup>)

**Figure 3-15** TEM micrographs of cured epoxy-amine-IL networks, *i.e.* DGEBA combined with 30 phr PACM with addition of (a,d) 5 phr IL 169; (b, e) 10 phr IL 169; (c, f) 20 phr IL 169

**Figure 3-16** DSC traces of epoxy-amine-IL networks: (■) EP + 30 phr PACM + 5 phr IL169; (●) EP + 30 phr PACM + 10 phr IL169; (▲) EP + 30 phr PACM + 20 phr IL169 (N<sub>2</sub> atmosphere, heating rate: 10 K·min<sup>-1</sup>)

**Figure 3-17** (a) TGA and (b) DTG traces of epoxy-amine-IL networks (■) EP + 30 phr PACM + 5 phr IL169; (●) EP + 30 phr PACM + 10 phr IL169; (▲) EP + 30 phr PACM + 20 phr IL169; (▼) neat IL169 ; (◆) EP + 10 phr IL169 (N<sub>2</sub> atmosphere, heating rate: 20 K·min<sup>-1</sup>)

**Figure 3-18** Design of EP@PUF microcapsule-filled epoxy-amine-IL composites

**Figure 3-19** SEM micrographs of fractured surface of epoxy-amine-IL composites filled with (a) 5 wt%; (b) 10 wt%; (c) 15 wt%; (d) 20 wt% of EP@PUF microcapsules (b)-(f) intact/broken EP@PUF microcapsules and the interfaces

**Figure 3-20** DSC traces of EP@PUF microcapsule-filled epoxy-amine-IL composites (N<sub>2</sub> atmosphere, heating rate: 10 K·min<sup>-1</sup>)

**Figure 3-21** (a) TGA and (b) DTG traces of EP@PUF microcapsule-filled epoxy composites (■) EP + 30PACM + 10IL + 5EP@PUF; (●) EP + 30PACM + 10IL + 10EP@PUF; (▲) EP + 30PACM + 10IL + 15EP@PUF; (▼) EP + 30PACM + 10IL + 5EP@PUF (N<sub>2</sub> atmosphere, heating rate: 20 K·min<sup>-1</sup>)

**Figure 3-22** tan  $\delta$ ,  $G'$ , and  $G''$  vs. temperature curves of EP@PUF microcapsule-filled epoxies (at 1Hz, heating rate 3 K·min<sup>-1</sup>)

**Figure 3-23** Graphical representation of possible structure after healing process

**Figure 3-24** SEM micrographs of scratches on the EP@PUF microcapsule-filled epoxy-amine-IL materials before (left) and after (after) healing: (a)(b) 5 wt%; (c)(d) 10 wt%; and (e)(f) 15 wt% and (g)(h) 20 wt% of EP@PUF microcapsules addition

**Figure 3-25** SEM micrographs of healing surface after fractured toughness test of EP@PUF microcapsule-filled epoxy-amine-IL materials (arrow indicated the release and polymerized healing agent at the fracture surface)

**Figure S3-1** FTIR spectra of emitted gas during degradation of EP@PUF microcapsules under N<sub>2</sub> atmosphere

**Figure S3-2** FTIR spectra of emitted gas at different temperatures EP@PUF microcapsules under N<sub>2</sub> atmosphere

**Figure S3-3** FTIR spectra of emitted gas during degradation of DGEBA+BGE under N<sub>2</sub> atmosphere

**Figure S3-4** FTIR spectra of emitted gas at different temperatures DGEBA+BGE under N<sub>2</sub> atmosphere

**Figure S3-5** FTIR spectra of emitted gas during degradation of neat PUF under N<sub>2</sub> atmosphere

**Figure S3-6** FTIR spectra of emitted gas at different temperatures neat PUF under N<sub>2</sub> atmosphere

**Figure 4-1** Local temperature recording of the sample during curing

**Figure 4-2** Compact Tensile (CT) test specimen geometry

**Figure 4-3** Synthesis route of ILEM@PMF microcapsules via *in-situ* polymerization

**Figure 4-4** ILEM (left) and ILEM@PMF microcapsules (right)

**Figure 4-5** Optical microscope images of ILEM/H<sub>2</sub>O emulsion stabilized by (a) Tween 80; (b) Reax 88A; (c) TX-100; (d) SDBS; (e) PVA; (f) SDBS:PVA=9:1 (surfactant concentration: 1wt%)

**Figure 4-6** Optical microscope images of the formation of ILEM@PMF microcapsules at different times after mixing with prepolymer (TM= transmission mode, RM=reflection mode) (a) 0 min, TM; (b) 120 min TM; (c) 180 min, TM; (d) 180 min, RM

**Figure 4-7** SEM micrographs ((A)-(G)) and size distributions ((a)-(g)) of ILEM@PMF microcapsules prepared with different parameters

**Figure 4-8** ILEM@PMF microcapsules **4** (a) (b) and **5** (d) (e) and morphologies of epoxy-amine networks containing microcapsules **4** (c) and **5** (f)

**Figure 4-9** FTIR spectra of ILEM@PMF microcapsules, core, and shell materials (a) ILEM@PMF microcapsules; (b) shell: neat PMF; (c) core: ILEM

**Figure 4-10** Characteristic peaks in FTIR spectra of core and shell materials of ILEM@PMF microcapsules

**Figure 4-11** DSC traces of (▲) ILEM (■) neat PMF, and (●) ILEM@PMF microcapsules (N<sub>2</sub> atmosphere, heating rate 10 K·min<sup>-1</sup>)

**Figure 4-12** (a) TGA and (b) DTG traces of (▲) core material ILEM and (■) shell material neat PMF and (●) ILEM@PMF microcapsules (N<sub>2</sub> atmosphere, heating rate 20 K·min<sup>-1</sup>)

**Figure 4-13** FTIR spectra of emitted gas during thermal degradation of ILEM@PMF microcapsules under N<sub>2</sub> atmosphere

**Figure 4-14** Preparation of ILEM@PMF microcapsule-filled epoxy-amine materials

**Figure 4-15** Settled and recorded temperature (in the bulk) vs. time during curing of (a) epoxy-PACM; (b) epoxy-TETA; (c) epoxy-Epikure 3223 systems

**Figure 4-16** SEM micrographs of ILEM@PMF microcapsules filled (a)-(c) epoxy-PACM; (d)-(f) epoxy-TETA; (g)-(i) epoxy-Epikure 3223 materials

**Figure 4-17** DSC traces of (a) epoxy-PACM; (b) epoxy-TETA; (c) epoxy-Epikure 3223 based materials (N<sub>2</sub> atmosphere, heating rate 10 K·min<sup>-1</sup>)

**Figure 4-18** tan  $\delta$ ,  $G'/G''$  vs. temperature spectra of ILEM@PMF microcapsules filled (a), (b) epoxy-PACM; (c), (d) epoxy-TETA; (e), (f) epoxy-Epikure 3223 materials (at 1Hz, heating rate 3 K·min<sup>-1</sup>)

**Figure 4-19** SEM micrographs of scratches before (up) and after (down) self-healing for ILEM@PMF microcapsule-filled (a), (b) epoxy-PACM; (c), (d) epoxy-TETA; (e), (f) epoxy-

Epikure 3223-based materials

**Figure S4-1**  $^1\text{H}$  spectrum of ILEM (Chloroform-d)

**Figure S4-2**  $^{19}\text{F}$  NMR spectrum of ILEM (Acetonitrile-d<sub>3</sub>)

**Figure S4-3**  $^1\text{H}$  spectrum of compound **2** (Chloroform-d)

**Figure S4-4**  $^1\text{H}$  spectrum of compound **4** (Chloroform-d)

**Figure S4-5**  $^{19}\text{F}$  spectrum of compound **4** (Chloroform-d)

**Figure S4-6** DSC trace of ILEM ( $\text{N}_2$  atmosphere, heating rate  $10 \text{ K}\cdot\text{min}^{-1}$ )

**Figure S4-7** TGA (■) and DTG (□) traces of ILEM ( $\text{N}_2$  atmosphere, heating rate  $20 \text{ K}\cdot\text{min}^{-1}$ )

**Figure S4-8** FTIR spectra of emitted gas during degradation of ILEM@PMF microcapsules under  $\text{N}_2$  atmosphere

**Figure S4-9** FTIR spectra of emitted gas at different temperatures of ILEM@PMF microcapsules under  $\text{N}_2$  atmosphere

**Figure S4-10** FTIR spectra of emitted gas during degradation of ILEM under  $\text{N}_2$  atmosphere

**Figure S4-11** FTIR spectra of emitted gas at different temperatures of ILEM microcapsules under  $\text{N}_2$  atmosphere

**Figure S4-12** FTIR spectra of emitted gas during degradation of neat PMF under  $\text{N}_2$  atmosphere

**Figure S4-13** FTIR spectra of emitted gas at different temperatures of neat PMF under  $\text{N}_2$  atmosphere

**Figure S4-14** (a) TGA and (b) DTG traces of (■) neat epoxy-PACM networks and (●) ILEM@PMF microcapsule-filled epoxy-PACM materials ( $\text{N}_2$  atmosphere, heating rate  $20 \text{ K}\cdot\text{min}^{-1}$ )

**Figure S4-15** (a) TGA and (b) DTG traces of (■) neat epoxy-TETA networks and (●) ILEM@PMF microcapsule-filled epoxy-TETA materials ( $\text{N}_2$  atmosphere, heating rate  $20 \text{ K}\cdot\text{min}^{-1}$ )

**Figure S4-16** (a) TGA and (b) DTG traces of (■) neat epoxy-Epikure 3223 networks and (●) ILEM@PMF microcapsules filled epoxy-Epikure 3223 materials ( $\text{N}_2$  atmosphere, heating rate  $20 \text{ K}\cdot\text{min}^{-1}$ )





# List of Schemes

**Scheme 1-1** Diels-Alder (DA) reaction

**Scheme 1-2** Synthetic of epoxy monomer with bifunctional Diels-Alder adduct

**Scheme 1-3** the reversible reaction of the sterically hindered amine with an isocyanate-functionalized polymer

**Scheme 1-4** Ring opening polymerization of DCPD catalyzed by a Grubbs' catalyst

**Scheme 1-5** Mechanisms of Friedel-Crafts reactions

**Scheme 1-6** Cure mechanism between epoxy and amine

**Scheme 1-7** Mechanism of epoxy polymerization induced by tertiary amines

**Scheme 1-8** Mechanism of cationic polymerization of epoxy prepolymer

**Scheme 1-9** Proposed mechanism for curing initiated by imidazolium IL of epoxy monomer

**Scheme 1-10** Proposed mechanism for the polymerization of epoxy resin (DGEBA) in the presence of IL 104

**Scheme 1-11** Synthesis of imidazolium ILs-modified POSS

**Scheme 2-1** Hydrolysis and condensation reactions occurring during the sol-gel process

**Scheme 3-1** Reaction mechanism of poly(urea-formaldehyde)

**Scheme 3-2** Hydrogen bond between amine and imidazolium IL

**Scheme 3-3** General mechanism for epoxy-amine curing

**Scheme 4-1** Synthesis of the imidazolium ionic liquid epoxy monomer (ILEM)

**Scheme 4-2** Reaction mechanism of poly(melamine-formaldehyde) (PMF)



# List of tables

**Table 1-1** Description of imidazolium-based ILs considered in Maka's researches

**Table 1-2** Natural and synthetic wall materials in microencapsulation and their main characteristics

**Table 1-3** Functional properties of different microcapsules

**Table 1-4** Different contact materials for microcapsules for food industry

**Table 2-1** Chemical structures of the products used

**Table 2-2** Weight and molar ratios of D.E.R. 332 and PACM for preparing epoxy-amine Networks

**Table 2-3** Microcomposites prepared with different  $r$  values and weight fractions of IL@SiO<sub>2</sub> microcapsules

**Table 2-4** Glass transition temperature ( $T_g$ ) of epoxy-amine networks and their corresponding IL@SiO<sub>2</sub> microcapsule-filled microcomposites with different epoxy-to-amino hydrogen ratios

**Table 2-5** Dynamic mechanical behavior of neat epoxy-amine networks and microcomposites based on different contents IL@SiO<sub>2</sub> microcapsules

**Table 2-6** Degradation temperatures of epoxy-based materials obtained using TGA analysis

**Table 2-7** Yield stress and theoretical crack opening displacement values of neat epoxy-amine networks and microcomposites based on different weight fractions of IL@SiO<sub>2</sub> microcapsules

**Table S2-1** Contact angle and surface energy of IL@SiO<sub>2</sub> microcapsule-filled epoxy-amine microcomposites measured by sessile drop method

**Table S2-2** Fracture toughness and Young's modulus of epoxy-amine microcomposites filled with different weight fractions of IL@SiO<sub>2</sub> microcapsules

**Table 3-1** Summarized chemical structures of the materials used

**Table 3-2** Weight loss temperature of EP@PUF microcapsules and neat components

**Table 3-3** Emitted gas and their characterization from FTIR absorption peaks of EP@PUF microcapsules, shell (PUF), and core (DGEBA+BGE) materials during TGA analysis

**Table 3-4** Formulations considered to design epoxy-amine-ionic liquids networks

**Table 3-5** Weight loss temperatures of epoxy-amine-IL networks and neat IL 169

**Table 3-6** Mechanical properties of different epoxy-amine-IL networks

**Table 3-7** Weight fractions of each component of EP@PUF microcapsule-filled epoxy-amine-IL composites

**Table 3-8**  $T_g$  of different EP@PUF microcapsule-filled epoxy-amine-IL materials

**Table 3-9** Weight loss temperature of EP@PUF microcapsule-filled epoxy-amine-IL materials

**Table 3-10**  $\alpha$  transition temperatures of different EP@PUF microcapsule-filled epoxy-amine-IL materials

**Table 3-11** Mechanical properties of different EP@PUF microcapsule-filled epoxy-amine-IL materials

**Table 4-1** Chemical structures of the products used

**Table 4-2** Thermal properties of ILEM

**Table 4-3** Different synthesis parameters considered for the preparation of ILEM@PMF microcapsules and its serial number of corresponding SEM micrographs

**Table 4-4** Emitted gas characterization from FTIR for ILEM@PMF microcapsules and their corresponding shell (PMF) and core (ILEM) materials by TGA-IR analyses

**Table 4-5** Degradation temperatures of ILEM@PMF microcapsule-filled epoxy-amine composites ( $N_2$  atmosphere, heating rate  $20\text{ K}\cdot\text{min}^{-1}$ )

**Table 4-6** Mechanical properties of ILEM@PMF microcapsule-filled epoxy-amine material at room temperature

# List of Abbreviations and Symbols

## Nomenclature

AA	Ascorbic acid
Al <sub>2</sub> Cl <sub>7</sub> <sup>-</sup>	Dialuminum-heptachloride
AlCl <sub>3</sub>	Aluminium chloride
AlCl <sub>4</sub> <sup>-</sup>	Tetrachloroaluminate
BF <sub>4</sub> <sup>-</sup>	Tetrafluoroborate
BMI	1-n-butyl-3-methylimidazoilum
BMIM	1-Butyl-3-methylimidazolium
BPA	Bisphenol A
BMITF	L-butyl-3-methylimidazolium tetrafluoroborate
CF <sub>3</sub> CO <sub>2</sub> <sup>-</sup>	Trifluoroacetate
CH <sub>2</sub>	Methylene
CH <sub>3</sub> CO <sub>2</sub> <sup>-</sup>	Acetate acetate
CHI	Chitosan
CNF	Carbon nanotube film
COD, $\delta_{tc}$	Crack opening displacement
CTAB	Cetyltrimethylammonium bromide
DA	Diels-alder
DE	Decanoate
DGEBA	Diglycidylether of bisphenol A
DGEBF	Diglycidylether of bisphenol F
DGEBiphenyl	Diglycidylether of biphenyl
DMIM	1,3-Dimethyl-1H-imidazol-3-ium
[DiOImid][I]	N,N'-dioctadecylimidazolium iodide
e/a (r)	Epoxy to amino hydrogen ratio
Epikure 3223	Diethylenetriamine (DETA)
EMI	Electromagnetic interference
EPON-828	Diglycidyl ether of bisphenol A
EtNH <sub>3</sub>	Ethylammonium
Fe <sub>3</sub> O <sub>4</sub>	Iron(II,III) oxide
GP	Graphene oxide/polyaniline
MF	Melamine formaldehyde
MHHPA	Methylhexahydrophthalic anhydride

Mg(OH) <sub>2</sub>	Magnesium hydroxide
MPCMs	Microencapsulated phase change materials
MPF	Furan groups
N(CN) <sub>2</sub> <sup>-</sup>	Cyanide
NH <sub>3</sub> ·H <sub>2</sub> O	Ammonium hydroxide solution
NTf <sub>2</sub> <sup>-</sup>	Bis(trifluoromethylsulfonyl)azanide
NO <sub>2</sub> <sup>-</sup>	Nitrite ion
NO <sub>3</sub>	Nitrate
NP	Nanoparticle
H <sub>2</sub> SO <sub>4</sub>	Sulfuric acid
HBP-Mim	Hyperbranched ionic liquid by trimellitic anhydride, diethylene glycol and 1-methylimidazole
HLB	Hydrophilic–lipophilic balance
IBU	Ibuprofen
IL	Ionic liquid
IL104	Trihexyl(tetradecyl) phosphonium bis(2,4,4-trimethylpentyl) phosphinate
IL 169	Tributyl(ethyl)phosphonium Diethyl Phosphate
IL/H <sub>2</sub> O	Ionic liquid in water
MELI	Ionic liquid epoxy monomer
MELI/H <sub>2</sub> O	MELI in water emulsion
IL@SiO <sub>2</sub>	Ionic liquid containing silica microcapsules
OMIM	1-octyl-3-methylimidazolium
O/O	Oil-in-oil
OTf <sup>-</sup>	Trifluoromethanesulfonate
O/W	Oil-in-water
P <sub>222-201</sub> -TFSI	Triethyl(2-methoxyethyl)phosphonium bis(trifluoromethylsulfonyl) imide
PA6	Polyamide 6
PA-amide	Polyacrylate amide
PACM	4,4-methylene biscyclohexanamine
PAN	Polyacrylonitrile
PANI	Polyaniline
PEI	Polyethylenimine
PF <sub>6</sub> <sup>-</sup>	Hexafluorophosphate
phr	Per hundred
PLA	Poly(lactic acid)
PMC	Polymer matrix composites

PMMA	Poly methyl methacrylate
PMF	Poly melamine formaldehyde
POSS	Polyhedral oligomeric silsesquioxane
PP	Polypropylene
PU	Polyurethane
PVA	Polyvinyl alcohol
PUF	Poly urea formaldehyde
REAX 88A	Sodium salt of a chemically modified low molecular weight kraft lignin
RTIL	Room temperature ionic liquid
SDS	Sodium dodecyl sulfate
SDBS	Sodium dodecylbenzenesulfonate
SiO <sub>2</sub>	Silica
SLN	Solid lipid nanoparticles
S/O/W	Solid-in-oil-in-water
TEA	Triethanolamine
TEOS	Tetraethyl orthosilicate
THAB	Tetrahexylammonium benzoate
THF	Tetrahydrofuran
THTDP	Tetradecyl phosphonium
TiO <sub>2</sub>	Titanium dioxide
TDI	2,4-tolylene diisocyanate
Tween 80	Polyethylene glycol sorbitan monooleate
TX-100	Triton X-100, 2-[4-(2,4,4-trimethylpentan-2-yl)phenoxy]ethanol
UF	Urea-formaldehyde
UV	ultraviolet
W/O	Water-in-oil
W/O/W	Water-in-oil-in-water
wt%	Weight percent
ZnO	Zinc oxide



**Characterization**

$\sigma$	Stress
$\varepsilon$	Strain
$\nu$	Poisson's ratio
$\nu_e$	Crosslink density
$\delta$	Solvent absorbency
$\delta_{tc}$	Crack opening displacement
$\varphi$	Swelling ratio
$\rho$	Density
$\chi_{12}$	Flory solvent-polymer interaction parameter
DLS	Dynamic light scattering
DMA	Dynamic mechanical analysis
DSC	Differential scanning calorimetry
DTG	Derivative thermogravimetric analysis
$E'$	Storage modulus
$E'_R$	Storage modulus at rubbery state
$E$	Young's modulus
EDX	Energy-dispersive X-ray spectroscopy
FTIR	Fourier transform infrared spectroscopy
$F_Q$	Load at the first crack
$G_{IC}$	Critical energy release rate
ICP-AES	Inductively coupled plasma-atomic emission spectrometry
$K_{IC}$	Critical stress intensity factor (Mode I)
$M_n$	Molar mass
$M_c$	Average molecular weight
NMR	Nuclear magnetic resonance
OM	Optical microscopy
POM	Polarizing optical microscopy
$R$	Ideal gas constant
SEM	Scanning electron microscopy
$T_\alpha$	$\alpha$ Relaxation temperature
$T_R$	Temperature at rubbery state
$\tan \delta$	Loss factor
$T_{d \text{ onset}}$	Onset decomposition temperature
$T_{d \text{ max}}$	Maximum decomposition temperature
TEM	Transmission electron microscopy

$T_g$	Glass transition temperature
TGA	Thermogravimetric analysis
$V_p$	Volume fraction of polymer in the swollen polymer



# General Introduction

Polymer matrix composite as well as structural material is a type of lightweight material which displays high mechanical properties can be widely used in different fields. Epoxy materials because of their good chemical stability, thermal properties and mechanical properties can be used as structural adhesives or composite materials used in aerospace and daily life applications. However, the main drawback that limits long term application of epoxy matrix is the high brittleness, which means microcracks can be generated easily in the epoxy matrix when the material is exposed to impact, mechanical or thermal solicitations. Therefore, to prevent the generation and propagation of microcracks is of great importance for prolonging the life span of epoxy-based structures. With the emphasis on such issues, toughened and self-healing materials are of interest to be integrated in real applications. Thus, this work focuses on designing multifunctional epoxy matrices considering ionic liquids via microencapsulation concept as one of the promising strategies. Therefore, to improve the toughness and to offer self-healing ability to epoxy-based materials, microcapsules addition seems to be a promising route. However, how to design the structure of microcapsules, how to choose the nature of shell and core materials, and how to use relevant process were considered in this study.

Based on the literatures and our research objects, this PhD work is divided into following five chapters.

The first chapter is dedicated to report the state of art concerning self-healing materials, combination of ionic liquid and epoxy compounds as well as microencapsulation methods. The first section reviewed the self-healing routes involving intrinsic and/or extrinsic self-healing mechanisms and more precisely extrinsic self-healing mechanisms which are easily tuned for thermoset systems. The second section focused on the combination of ionic liquid and epoxy resin. Ionic liquids were recently founded to be efficient initiators for epoxy polymerization to design epoxy networks with high performances. Because of their nonflammability and liquid nature, ionic liquid can act as flame retardants and self-lubricants. Our study brings new insights for ionic liquids use. The third section describes the microencapsulation, including the physico-chemical basic considerations, main strategies and applications, with a special focus on self-

healing in polymers.

The second chapter is dedicated to the synthesis of the ionic liquid core and the silica shell of the microcapsules. These ones are supposed to be considered as reinforcement in epoxy-amine networks. In a first step, hydrophobic ionic liquid, *i.e.* tetradecyl(trihexyl)phosphonium bis-(2,4,4-trimethylpentyl)phosphinate, denoted as IL104, was encapsulated in silica-shell microcapsules (IL@SiO<sub>2</sub>) by performing a sol-gel reaction in ionic liquid-in-water emulsion. The obtained IL@SiO<sub>2</sub> microcapsules have spherical shape as well as rough surface with a diameter from 0.5 to 2 μm. These microcapsules were added in the epoxy-4,4-methylenebis(cyclohexylamine) (epoxy-PACM) networks as fillers. The addition of that IL@SiO<sub>2</sub> microcapsules to epoxy-amine networks improve the mechanical properties and fracture toughness without damaging the thermal properties.

The third chapter focused on achieving self-healing of epoxy-amine networks. Microcapsules with healing agent inside with large diameter are required to achieve self-healing. The initially proposed latent initiator, *i.e.* Grubbs' catalyst, suffers from a too low decomposition temperature and impacts on the choice of amine hardener. Thus, ionic liquid could be a good alternative and could be applied in high temperature cured polymer thermosets. Therefore, epoxy containing microcapsules with poly(urea-formaldehyde) shell, denoted as EP@PUF, were successfully synthesized and added in epoxy-PACM-IL ternary reactive system as self-healing additive. Before investigating the self-healing performances, the optimal IL content as well as their influence on epoxy matrix were studied. Finally, it was found that 10 wt% of IL in the matrix is the optimal value and self-healing can be achieved by adding more than 10 wt% of EP@PUF microcapsules.

Third chapter related to self-healing in epoxy materials showed that the introduction of a initiator was required for epoxy healing agent. The fourth chapter proposed to achieve self-healing from a strategy considering single microcapsules system without initiator. For such a purpose, a ionic liquid epoxy monomer (ILEM) was synthesized. Therefore, ILEM was encapsulated in poly(melamine-formaldehyde) shell-based microcapsules (ILEM@PMF). The influence of the morphology of the microcapsules and their self-healing performances in different epoxy-amine networks were investigated. It was found that the ILEM cores can polymerize under thermal stimulus. Nevertheless, this ILEM core material could polymerize

when curing temperature is higher than 180 °C. Therefore, these new microcapsules are appropriate for achieving self-healing purpose in low temperature or room temperature cured epoxy-amine materials such as structural adhesives.

To summarize the work done in this study, different types of microcapsules were synthesized for designing functional epoxy materials. The combination of these microcapsules with an ionic liquid was proposed using different routes. Toughening and self-healing purposes have been achieved. The first result of this work can be considered as the proof of concept and more works could be proposed. For example, coaxial electrospinning could be applied to design microvascular networks to achieve self-healing purposes. Epoxy monomer with reversible groups can also be designed for obtaining intrinsic self-healing thermoset materials. Such an approach can be achieved by using the molecular architecture of the ionic liquid epoxy monomer.



# Résumé Étendu

## Chapitre 1 : Étude bibliographique

- **Matériaux autoréparants**

Au cours des dernières années, les composites à matrice polymère (PMC) ont été largement utilisés dans l'industrie automobile et aérospatiale. Ces matériaux présentent de nombreux avantages par rapport aux matériaux métalliques traditionnels, tels que de bonnes propriétés électriques, une stabilité thermique et thermomécanique, de bonnes propriétés mécaniques, une stabilité dimensionnelle, etc. [1-4]

Cependant, lors d'un impact, d'un cyclage mécanique ou de chargements thermiques, des microfissures peuvent être générées dans la matrice généralement fragile comme les matrices époxy et polyesters [5]. Par conséquent, les chercheurs s'efforcent de concevoir des matériaux autoréparants, visant à cicatrifier ces microfissures avant leur propagation afin de prolonger la durée de vie des matériaux PMC.

Selon les mécanismes d'autoréparation rapportés dans la littérature, les matériaux autoréparants peuvent être divisés en deux catégories : matériaux autoréparants intrinsèques et matériaux autoréparants extrinsèques [6]. Dans le mécanisme intrinsèque d'autoréparation, la guérison se fait principalement par les matériaux eux-mêmes par des interactions chimiques, physiques ou supramoléculaires. La guérison extrinsèque fait appel à des additifs. Le recours à des microcapsules ou microcanaux sont les stratégies les plus largement proposées pour obtenir l'autoréparation de matériaux PMC.

Les matériaux autoréparants doivent aussi pallier les inconvénients des polymères fragiles et en raison de leur aptitude à allonger la durée de vie, présentent les performances requises pour différents domaines applicatifs, tels que les expéditions aérospatiales, les revêtements anticorrosion, les dispositifs conducteurs ou certaines applications biologiques.



- **Les liquides ioniques et époxy**

Les liquides ioniques (LIs), également connus sous le nom de liquides ioniques à température ambiante, sont des sels organiques liquides au voisinage de la température ambiante. Le premier d'entre eux, le nitrate d'éthylammonium LI [EtNH<sub>3</sub>][NO<sub>3</sub>], a été découvert par Paul Walden en 1914<sup>[7]</sup>. Depuis cette date, les liquides ioniques sont largement utilisés comme solvants propres, électrolytes ou additifs dans les matériaux polymères en raison de leurs excellentes caractéristiques, notamment une pression de vapeur nulle, une large plage de fonctionnement, une stabilité thermique élevée, une bonne conductivité ionique et une inflammabilité<sup>[8]</sup>.

Le prépolymère époxy est un composé organique avec une fonctionnalité époxy égale ou supérieure à deux. Les groupes époxy peuvent être ouverts par une variété d'espèces chimiques permettant de former des réseaux<sup>[9]</sup>. Par conséquent, divers mécanismes de polymérisation, y compris par étapes ou par croissance de chaîne, peuvent être activés.

Après les recherches de Kowalczyk<sup>[10]</sup> selon lesquelles le tétrafluoroborate de 1-butyl-3-méthylimidazolium (BMITF) peut être utilisé comme agent de réticulation de résines époxy, de nombreux chercheurs proposent d'autres applications pour les liquides ioniques dans les composites époxy. En raison de leurs propriétés uniques, les LIs sont désormais largement utilisés comme durcisseurs, additifs pour aide à la dispersion, à la lubrification ou pour apporter de nouvelles fonctionnalités dans les composites à matrice époxy.

- **Microencapsulation**

La microencapsulation est une méthode efficace pour confiner des matériaux liquides ou solides par des matériaux de paroi (organiques ou inorganiques) afin de préserver les propriétés biologiques, fonctionnelles et physico-chimiques des matériaux du cœur des microcapsules<sup>[11,12]</sup>. Il est nécessaire alors que le matériau de la coque ne réagisse pas avec le matériau du cœur. Dépendant de l'application visée des microcapsules, leur résistance mécanique, la solubilité des matériaux d'écorce, leur biocompatibilité, leur caractère hydroscopique, leurs propriétés diélectriques, leur dégradabilité ou d'autres propriétés spécifiques sont également requises. Par conséquent, sur la base de ces diverses exigences, les matériaux de la coque peuvent être d'origine naturelle ou obtenus par synthèse.

De nombreuses stratégies différentes ont été proposées pour la fabrication de microcapsules. Généralement, les procédés adoptés pour leur préparation peuvent être divisés en trois : (1) Procédés physiques : évaporation de solvant, séchage par pulvérisation, dépôt électrostatique, etc. et (2) Procédés chimiques : polymérisation *in-situ*, polymérisation interfaciale, etc. (3) Procédés physico-chimiques : coacervation (séparation de phases), etc. Ces méthodes sont désormais largement appliquées en microencapsulation pour obtenir des microcapsules adaptées aux différentes applications<sup>[13,14]</sup>.

### • Références

- [1] Senthilkumar, K.; Saba, N.; Rajini, N.; Chandrasekar, M.; Jawaid, M.; Siengchin, S.; Alotman, O. Y., Mechanical properties evaluation of sisal fibre reinforced polymer composites: A review. *Construction and Building Materials*. **2018**, 174, 713-729.
- [2] Saba, N.; Jawaid, M.; Alotman, O. Y.; Paridah, M. T., A review on dynamic mechanical properties of natural fibre reinforced polymer composites. *Construction and Building Materials*. **2016**, 106, 149-159.
- [3] Forintos, N.; Czigany, T., Multifunctional application of carbon fiber reinforced polymer composites: electrical properties of the reinforcing carbon fibers—a short review. *Composites Part B: Engineering*. **2019**, 162, 331-343.
- [4] Chen, H.; Ginzburg, V. V.; Yang, J.; Yang, Y.; Liu, W.; Huang, Y.; Du, L.; Chen, B., Thermal conductivity of polymer-based composites: fundamentals and applications. *Prog. Polym. Sci.* **2016**, 59, 41-85.
- [5] Blaiszik, B. J.; Kramer, S. L. B.; Olugebefola, S. C.; Moore, J. S.; Sottos, N. R.; White, S. R., Self-healing polymers and composites. *Annu. Rev. Mater. Res.* **2010**, 40, 179-211.
- [6] Song, M. M.; Wang, Y. M.; Liang, X. Y.; Zhang, X. Q.; Zhang, S.; Li, B. J., Functional materials with self-healing properties: a review. *Soft Matter*. **2019**, 15, 6615-6625
- [7] Walden, P., Molecular weights and electrical conductivity of several fused salts. *Bull. Acad. Imper. Sci. (St. Petersburg)*. **1914**, 1800, 405-422.
- [8] H, O.-B.; Magna, L., Ionic liquids perspectives for organic and catalytic reactions. *J. Mol. Catal. A: Chem.* **2002**, 182-183, 419-437.
- [9] Vakil, U. M.; Martin, G. C., Crosslinked epoxies network structure characterization and physical-mechanical properties. *J. Appl. Polym. Sci.* **1992**, 46, 2089-2099.
- [10] Kowalczyk, K.; Spychaj, T., Ionic liquids as convenient latent hardeners of epoxy resins. *Polimery*. **2003**, 48, 833-835
- [11] Bansode, S. S.; Banarjee, S. K.; Gaikwad, D. D.; Jadhav, S. L.; Thorat, R. M., Microencapsulation: a review. *International Journal of Pharmaceutical Sciences Review and Research*. **2010**, 1, 38-43.

- [12] Bakry, A. M.; Abbas, S.; Ali, B.; Majeed, H.; Abouelwafa, M. Y.; Mousa, A.; Liang, L., Microencapsulation of oils: a comprehensive review of benefits, techniques, and applications. *Comprehensive Reviews in Food Science and Food Safety*. **2016**, 15, 143-182.
- [13] I Ré, M., Microencapsulation by spray drying. *Drying Technol.* **1998**, 16, 1195-1236.
- [14] Thies, C., In: Mark HF, editor. Microencapsulation. *Encyclopedia of Polymer Science and Technology*. Hoboken: John Wiley & Sons, Inc., **2002**.

## Chapitre 2 : Microcapsules à coquille de silice et noyau liquide ionique pour matériaux polyépoxydes

### • Introduction

Les résines époxy, en raison de leur propriétés physiques et chimiques exceptionnelles, ont été largement appliquées dans le domaine de l'automobile, de l'aérospatiale, etc, mais leur grande fragilité reste leur principal inconvénient. <sup>[1]</sup>. Par conséquent, leur modification par des additifs externes tels que des caoutchoucs liquides, les thermoplastiques ou des nanoparticules a été étudiée dans de nombreuses recherches. Néanmoins, l'ajout de caoutchoucs ou de thermoplastiques de basse température de transition vitreuse ( $T_g$ ), faisant appel à la génération d'une phase ductile, un mécanisme de séparation de phase induit par la polymérisation a une influence négative sur leurs propriétés thermomécaniques. Les modifications par des nanoparticules rencontrent la difficulté de dispersion <sup>[2]</sup>.

Jusqu'à présent, il existe peu de travaux sur l'encapsulation de liquides ioniques (LI) de type phosphonium, en particulier pour leurs applications dans des matériaux polymères thermodurcissables. Dans ce chapitre, des microcapsules de silice ( $LI@SiO_2$ ) contenant le LI de type phosphonium ont été synthétisés avec succès pour la première fois et ont été ajoutés dans les réseaux époxy-amine comme additif multifonctionnel. Ce chapitre est donc divisé en deux parties : *i*) Synthèse et caractérisation des microcapsules  $LI@SiO_2$  ; *ii*) Préparation et caractérisation des matériaux  $LI@SiO_2$ /époxy-amine. La préparation et la nature des microcapsules  $LI@SiO_2$  sont alors analysées.

### • Synthèse et caractérisation de microcapsules $IL@SiO_2$

Le concept de base est celui de considérer un procédé sol-gel au sein d'une émulsion IL dans eau (O/W) stabilisée à l'aide de tensioactifs. Le tetraethyl orthosilicate (TEOS) est alors utilisé comme précurseur de silice qui constituera l'écorce <sup>[3,4]</sup>. Le tétradécyl(trihexyl)phosphonium bis-(2,4,4triméthypentyl)phosphinate, noté LI 104, a été sélectionné comme liquide ionique et le SDS et le CTAB ont été choisis comme co-tensioactifs <sup>[5]</sup> pour stabiliser le LI 104 dans la solution aqueuse. Lorsque l'émulsion a été bien stabilisée,

TEOS a été ajouté dans des conditions basiques pour former l'enveloppe de silice à la surface des gouttelettes de liquide ionique. La procédure de synthèse est schématiquement donnée dans la Figure 1.

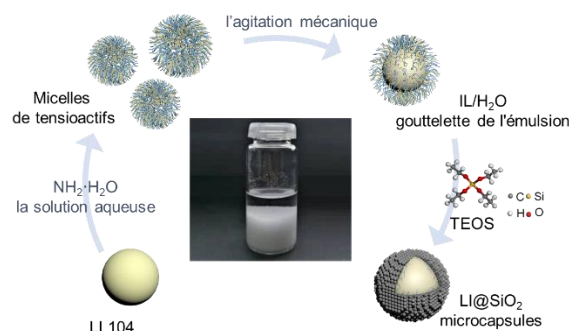


**Figure 1** Procédure de synthèse des microcapsules LI@SiO<sub>2</sub>

Les microcapsules obtenues ont une forme sphérique, une structure cœur-coquille désirée et une surface rugueuse comme le montrent les micrographies MET et MEB de la Figure 2 (a)(b). La distribution des diamètres des microcapsules LI@SiO<sub>2</sub> a également été caractérisée par diffusion dynamique de la lumière (DLS). Les microcapsules ont une distribution de taille centrée à 10-15 µm comme le montre la Figure (c).

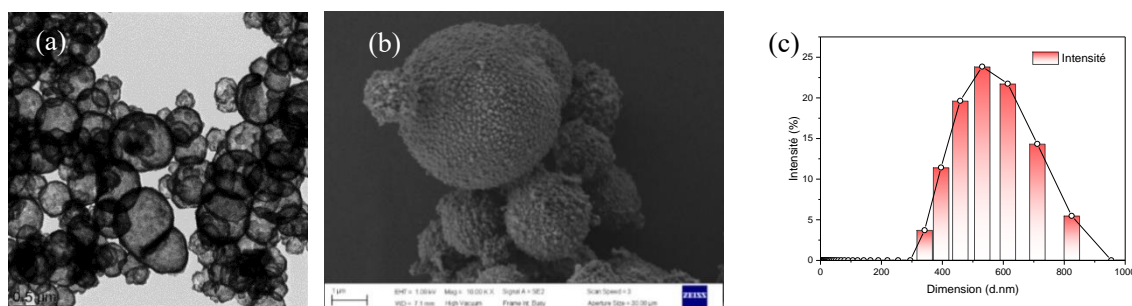


**Figure 2** Micrographies (a) MET et (b) MEB et (c) distributions des diamètres des microcapsules LI@SiO<sub>2</sub>

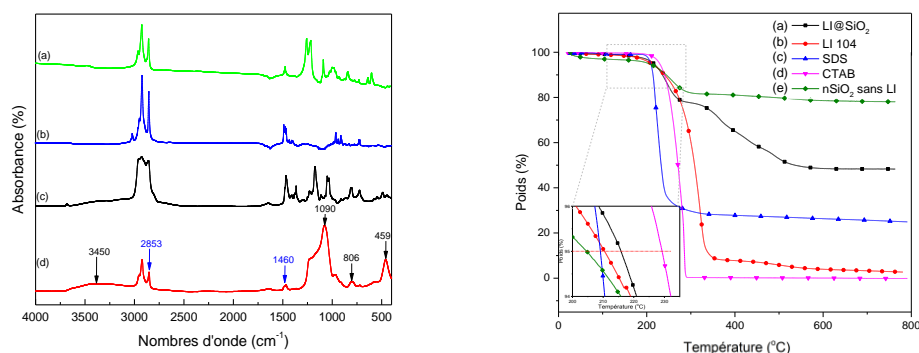


**Figure 3** Spectres FTIR et ATG des microcapsules LI@SiO<sub>2</sub>

Ces caractérisations montrent que les microcapsules à enveloppe de silice et noyau liquide ionique ont été synthétisées avec succès ce qui leur permet dans une étape suivante d'être ajoutées dans les systèmes époxy-amine afin d'étudier leurs performances en tant que microcapsules de renforcement et d'autoréparation des réseaux époxy finaux.

- **Préparation et caractérisation de microcapsules LI@SiO<sub>2</sub> dans des réseaux époxy-amine**

Des microcapsules IL@SiO<sub>2</sub> ont été ajoutées dans une matrice polymère issue de la copolymérisation d'un monomère époxy (DGEBA, D.E.R. 332) et de 4,4-méthylènebis(cyclohexylamine) (PACM). Différents rapports stoechiométriques époxy/amine et différentes fractions massiques de microcapsules LI@SiO<sub>2</sub> ont été considérés pour étudier les propriétés des matériaux époxy obtenus. Les propriétés thermiques et les propriétés mécaniques des différents matériaux époxy ont été analysées et les résultats ont été présentés dans le Tableau 1.

**Tableau 1** Propriétés thermiques ( $T_g$ ,  $T_{d\ onset}$ , et  $T_{d\ max}$ ) et mécaniques ( $E$ ,  $K_{IC}$ , et  $G_{IC}$ ) de différents matériaux époxy

Matériel	$T_g$ <sup>(a)</sup> (°C)	$T_{d\ onset}$ <sup>(b)</sup> (°C)	$T_{d\ max}$ <sup>(b)</sup> (°C)	$E$ <sup>(c)</sup> (GPa)	$K_{IC}$ <sup>(c)</sup> (MPa·m <sup>1/2</sup> )	$G_{IC}$ <sup>(c,d)</sup> (kJ·m <sup>-2</sup> )
1.0-0	156	359	378	1.10 ± 0.04	0.55 ± 0.05	0.25
1.0-1	165	361	379	1.20 ± 0.05	0.69 ± 0.07	0.35
1.0-2	170	352	378	1.26 ± 0.06	0.76 ± 0.04	0.41
1.0-5	171	353	377	1.30 ± 0.04	0.80 ± 0.06	0.44
1.2-0	104	352	380	1.24 ± 0.03	0.56 ± 0.06	0.23
1.2-1	116	359	381	1.30 ± 0.06	0.65 ± 0.08	0.29
1.2-2	127	363	380	1.40 ± 0.03	0.76 ± 0.07	0.36
1.2-5	142	359	380	1.50 ± 0.06	0.81 ± 0.06	0.38
1.4-0	83	329	380	1.42 ± 0.05	0.60 ± 0.05	0.22
1.4-1	109	363	382	1.64 ± 0.06	0.68 ± 0.05	0.25
1.4-2	125	352	383	1.70 ± 0.04	0.77 ± 0.06	0.31
1.4-5	135	356	384	1.68 ± 0.05	0.82 ± 0.05	0.35

<sup>(a)</sup> analyses DSC (vitesse de chauffage : 10 K·min<sup>-1</sup>, atmosphère : N<sub>2</sub>)

<sup>(b)</sup> analyses ATG (vitesse de chauffage : 20 K·min<sup>-1</sup>, atmosphère : N<sub>2</sub>)

<sup>(c)</sup> à température ambiante

<sup>(d)</sup> calculé à partir de la valeur moyenne de  $E$  and  $K_{IC}$

- **Principaux résultats**

Des microcapsules à écorce de silice (LI@SiO<sub>2</sub>) obtenues par procédé sol-gel en émulsion LI/H<sub>2</sub>O à l'aide de tensioactifs et contenant un liquide ionique de type phosphonium ont été synthétisées avec succès. La forme sphérique et la structure noyau-enveloppe avec une large gamme de tailles de microcapsules LI@SiO<sub>2</sub> ont été caractérisées par MET, MEB et DLS. La polydispersité des diamètres a été associée à l'équilibre dynamique du LI dans l'émulsion aqueuse. La spectroscopie IRTF, l'analyse élémentaire et l'EDX ont prouvé que les liquides ioniques ont été encapsulés avec succès par la coque de silice. La stabilité thermique élevée a été révélée par analyses ATG, montrant ainsi que les microcapsules LI@SiO<sub>2</sub> peuvent être des additifs idéaux dans les réseaux époxy-amine polymérisés à haute température. Ainsi, les liquides ioniques encapsulés offrent un véritable potentiel et une polyvalence pour les matrices thermodurcissables en tant qu'additifs fonctionnels.

Dans la deuxième partie du Chapitre 2, les microcapsules LI@SiO<sub>2</sub> obtenues ont été dispersées dans des réseaux époxy-amine. La morphologie, les propriétés thermiques et mécaniques des matériaux époxy ont été caractérisées par différentes méthodes. Par microscopie MET il a été confirmé que les microcapsules LI@SiO<sub>2</sub> restent intactes dans la matrice réseau époxy-amine finale et que celles-ci sont bien dispersées. Les caractérisations DSC et mécaniques ont montré que de petites quantités de microcapsules LI@SiO<sub>2</sub> peuvent favoriser les propriétés thermiques et mécaniques des matériaux car celles-ci jouent le rôle de charges renforçantes. Pour être plus précis, en considérant un rapport  $r$  donné, avec une fraction massique croissante de microcapsules LI@SiO<sub>2</sub>, la température de transition vitreuse et le module de Young des réseaux LI@SiO<sub>2</sub>-époxy-amine augmentent. De même, en considérant un même rapport stœchiométrique  $r$ , lorsque la fraction massique de microcapsules augmente, la ténacité  $K_{Ic}$  et l'énergie de fracture des LI@SiO<sub>2</sub>-époxy amine sont plus encore augmentées. Avec une fraction massique fixe de microcapsules LI@SiO<sub>2</sub>, les mêmes effets sont encore plus significatifs pour un rapport  $r$  élevé. Des tests de sorption et des analyses mécaniques dynamiques (AMD) ont montré également que les microcapsules LI@SiO<sub>2</sub> peuvent améliorer la résistance aux solvants des matériaux époxy grâce aux interactions créées aux interfaces

microcapsule-époxy [6]. Enfin, le mécanisme de cicatrisation via le remplissage des fissures a été étudié et prouvé par microscopie MEB [7,8], répondant ainsi à l'objectif d'autoréparation.

En conclusion, des microcapsules LI@SiO<sub>2</sub> ont été synthétisées avec succès et se sont avérées être des charges micrométriques renforçantes dans le réseau époxy-amine puisque elles permettent d'augmenter la ténacité, puis généralement les propriétés mécaniques sans avoir d'effet négatif sur les propriétés thermomécaniques de la matrice époxy.

#### • Références

- [1] Shin, H.; Kim, B.; Han, J.-G.; Lee, M. Y.; Park, J. K.; Cho, M., Fracture toughness enhancement of thermoplastic/epoxy blends by the plastic yield of toughening agents: a multiscale analysis. *Composites Science and Technology*. **2017**, 145, 173-180.
- [2] Sasidharan S, Anand A. Epoxy-based hybrid structural composites with nanofillers: a review. *Industrial & Engineering Chemistry Research*, 2020, 59(28): 12617-12631.
- [3] Weiss, E.; Dutta, B.; Kirschning, A.; Abu-Reziq, R., BMIm-PF<sub>6</sub>@SiO<sub>2</sub> microcapsules: particulated ionic liquid as a new material for the heterogenization of catalysts. *Chemistry of Materials*. **2014**, 26, 4781-4787.
- [4] Yang, M.; Zhu, X.; Ren, G.; Men, X.; Guo, F.; Li, P.; Zhang, Z., Tribological behaviors of polyurethane composite coatings filled with ionic liquid core silica gel shell microcapsules. *Tribology Letters*. **2015**, 57, 9.
- [5] Zhou, D.; Liu, R.; He, Y.-B.; Li, F.; Liu, M.; Li, B.; Yang, Q.-H.; Cai, Q.; Kang, F., SiO<sub>2</sub> hollow nanosphere-based composite solid electrolyte for lithium metal batteries to suppress lithium dendrite growth and enhance cycle life. *Advanced Energy Materials*. **2016**, 6, 1-10.
- [6] Kenyon, A. S.; Nielsen, L. E., Characterization of Network Structure of Epoxy Resins by Dynamic Mechanical and Liquid Swelling Tests. *Journal of Macromolecular Science: Part A - Chemistry*. **1969**, 3, 275-295.
- [7] AJ, K.; YOUNG, R., Fracture behavior of polymers. *App. Sci. Publishers, London*. **1983**.
- [8] Liebowitz, H., Fracture: an advanced treatise. Volume VII. Fracture of nonmetals and composites. *Elsevier*, **1972**.



## Chapitre 3 : Synthèse des microcapsules contenant un composé époxy et conception de nouveaux matériaux liquides ioniques époxy-amine autoréparants

### • Introduction

Le mécanisme d'auto-réparation extrinsèque est un mécanisme intéressant et générique pour réaliser une auto-guérison dans des matériaux polymères thermodurcissables en général. Mais il peut toutefois être limité par la température de réticulation de la matrice polymère ou le coût élevé du système à double microcapsules <sup>[1,2]</sup>. Par conséquent, ce chapitre propose une solution basée sur un système de microcapsules de nature unique à cœur époxy avec un liquide ionique ajouté dans le réseau époxy-amine et qui interviendra comme amorceur. Ce système pourra alors être appliqué pour les matériaux époxy polymères à haute température. Ce chapitre est divisé en trois parties : *i*) Synthèse et caractérisation de microcapsules de poly(urée-formaldéhyde) à cœur prépolymère époxy ; *ii*) Caractérisation des réseaux époxy-amine-LI et formulation optimale, c'est-à-dire, optimisation de la fraction de LI; *iii*) Préparation et caractérisation des composites époxy-amine-LI chargés microcapsules EP@PUF.

### • Synthèse et caractérisation des microcapsules EP@PUF

La synthèse de microcapsules de poly(urée-formaldéhyde) contenant de l'époxy (EP@PUF) par polymérisation *in-situ* <sup>[3]</sup> implique principalement trois étapes, comme le montre la Figure 4.

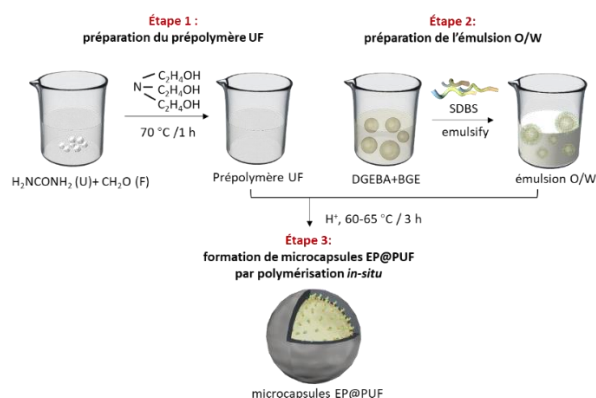


**Figure 4** Étapes de synthèse de microcapsules EP@PUF par polymérisation *in-situ*

## • Préparation et caractérisation des réseaux époxy-amine-LI

Afin d'étudier la réactivité du LI tributyl(éthyl)phosphonium diéthyl phosphate (LI 169) dans la matrice époxy et la fraction massique optimale de LI 169, la cinétique de polymérisation de ces systèmes réactifs et les propriétés finales des réseaux époxy-amine-LI ont été étudiées. La Figure 6 montre les thermogrammes DSC permettant une sélection des différents réseaux époxy-amine-LI et le Tableau 2 résume les propriétés finales des réseaux époxy-amine intégrant 5, 10 et 20 phr de liquide ionique LI 169.

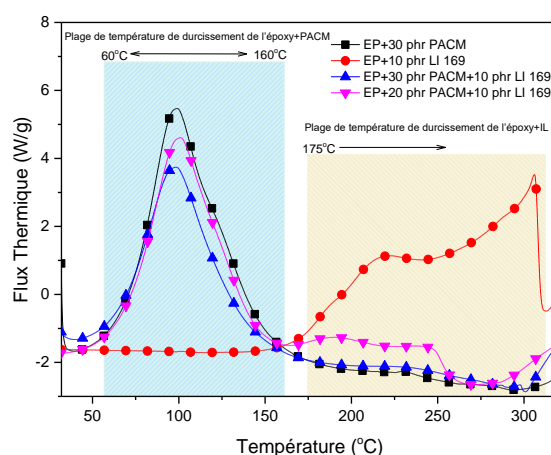


**Figure 5** Thermogrammes DSC de systèmes réactifs époxy-amine et/ou LI 169

(vitesse de chauffage :  $10 \text{ K}\cdot\text{min}^{-1}$ , atmosphère :  $\text{N}_2$ )

Comme le montre la Figure 5, LI 169 n'a pas influence dramatique sur la réticulation du prépolymère époxy avec le comonomère diamine. Celui-ci est capable d'amorcer la polymérisation de l'excès de monomère époxy dans le réseau après le durcissement de la matrice [4]. Par conséquent, le LI 169 pourrait être appliqué en tant qu'amorceur de polymérisation d'un agent cicatrisant de matériaux époxy cicatrisants cuits à haute température.

Les propriétés thermiques et mécaniques des réseaux époxy-amine-LI ont été caractérisées pour déterminer la fraction massique optimale de LI 169. Les résultats dans le Tableau 2 ont montré que le LI 169 joue le rôle de plastifiant dans le réseau époxy-amine et est dispersé sous forme de nanophases. Sa présence aura une influence négative sur les propriétés thermiques mais avec un effet positif sur les propriétés mécaniques. En prenant en compte ces effets, 10 phr

sera retenu comme fraction massique optimale de LI 169 au sein du système réactif prépolymère époxy-amine.

**Tableau 2** Propriété thermique et propriété mécanique des composites époxy-amine-LI

Matériaux	$T_g/^\circ\text{C}$ <sup>(a)</sup>	$T_{d\text{ onset}}/^\circ\text{C}$ <sup>(b)</sup>	$T_{d\text{ max}}/^\circ\text{C}$ <sup>(b)</sup>	$E/\text{GPa}$ <sup>(c)</sup>	$K_{IC}/\text{MPa}\cdot\text{m}^{1/2}$ <sup>(c)</sup>
EP + 30 PACM+5 LI 169	151	333	370	1.3±0.02	0.60±0.05
EP+30 PACM+10 LI 169	135	328	365	1.6±0.03	0.63±0.04
EP+30 PACM+20 LI 169	118	313	364	1.6±0.02	0.68±0.04

<sup>(a)</sup> analyses DSC (vitesse de chauffage :10 K·min<sup>-1</sup>, atmosphère : N<sub>2</sub>)

<sup>(b)</sup> analyses ATG (vitesse de chauffage :20 K·min<sup>-1</sup>, atmosphère : N<sub>2</sub>)

<sup>(c)</sup> à température ambiante

- **Préparation et caractérisation de matériaux époxy-amine-LI autoréparant avec microcapsules EP@PUF**

Des microcapsules EP@PUF ont été ajoutées à différentes fractions massiques dans une matrice époxy-amine-LI (10 phr de LI 169 selon l'étude précédente). Les propriétés thermiques et mécaniques ont été étudiées et les résultats sont résumés dans le Tableau 3. La capacité d'autoréparation des matériaux a été caractérisée par microscopie MEB en observant la rayure effectuée sur le film avant et après le processus de guérison comme le montre la Figure 6.

**Tableau 3** Propriétés thermiques et mécaniques des matériaux époxy-amine-LI/microcapsules EP@PUF

Matériaux	$T_g/^\circ\text{C}$ <sup>(a)</sup>	$T_{d\text{ onset}}/^\circ\text{C}$ <sup>(b)</sup>	$T_{d\text{ max}}/^\circ\text{C}$ <sup>(b)</sup>		$E/\text{GPa}$ <sup>(c)</sup>	$K_{IC}/\text{MPa}\cdot\text{m}^{1/2}$ <sup>(c)</sup>
			$T_{d\text{ max1}}$	$T_{d\text{ max2}}$		
EP+30PACM+10LI+5EP@PUF	130	324	--	374	1.6±0.01	0.66±0.02
EP+30PACM+10LI+10EP@PUF	124	308	264	373	1.5±0.05	0.71±0.03
EP+30PACM+10LI+15EP@PUF	123	287	257	375	1.5±0.02	0.77±0.02
EP+30PACM+10LI+20EP@PUF	113	282	258	377	1.4±0.02	0.81±0.05

<sup>(a)</sup> analyses DSC (vitesse de chauffage :10 K·min<sup>-1</sup>, atmosphère : N<sub>2</sub>)

<sup>(b)</sup> analyses ATG (vitesse de chauffage :20 K·min<sup>-1</sup>, atmosphère : N<sub>2</sub>)

<sup>(c)</sup> à température ambiante

- **Principaux résultats**

Le prépolymère époxy a été encapsulé dans une coque de poly(urée-formaldéhyde) (PUF) sous forme de microcapsules EP@PUF, qui ont été ajoutées dans les systèmes époxy pour permettre une auto-guérison des réseaux. Le phosphate de diéthyle de tributyl(éthyl)phosphonium comme liquide ionique (LI 169) a été considéré comme amorceur pour le prépolymère époxy confiné pour avoir une plage de température de polymérisation différente de celle de la copolymérisation du réseau à base de 4,4'-méthylènebis(cyclohexylamine) (PACM) et DGEBA. Ainsi, le LI 169 permet une réaction de l'agent cicatrisant époxy libéré par la rupture des microcapsules EP@PUF. Après avoir considéré les effets positifs et négatifs liés à la présence de LI 169 dans les réseaux époxy-amine, une fraction optimale de Li 169 dans le système réactif époxy-amine a été déterminée à 10 phr.

Par la suite, différentes fractions massiques de microcapsules EP@PUF ont été ajoutées dans un réseau époxy-amine-LI en tant qu'additif d'auto-cicatrisation et les propriétés thermiques, d'auto-cicatrisation et les propriétés mécaniques de ces derniers ont été étudiées. Les résultats des analyses thermiques DSC et TGA ont montré que l'ajout de microcapsules EP@PUF affecte faiblement  $T_g$  et la température de dégradation des matériaux finaux en raison des faibles interactions entre microcapsules et matrice et de la faible température de décomposition des microcapsules EP@PUF par rapport à celle de la matrice polymère. La microscopie MEB a été utilisée pour caractériser la capacité d'auto-guérison des matériaux en observant une rayure sur le matériau avant et après la cicatrisation. Il a été montré qu'un nombre suffisant de microcapsules EP@PUF (> 10 % en poids) dans la matrice polymère peut garantir la libération de l'agent de cicatrisation et la capacité d'auto-guérison des matériaux.

Ainsi, si l'ajout de microcapsules EP@PUF dans une matrice époxy peut abaisser le module de Young mais améliorer la résistance à la rupture de matériaux composites époxy-amine-LI/ microcapsules EP@PUF, celui-ci peut offrir une solution d'autoréparation aux matrices époxy <sup>[5,6]</sup>.

---

- **Références**

- [1] Szabó, T.; Molnár-Nagy, L.; Bognár, J.; Nyikos, L.; Telegdi, J., Self-healing microcapsules and slow release microspheres in paints. *Prog. Org. Coat.* **2011**, *72*, 52-57.
- [2] Yin, T.; Rong, M.; Zhang, M.; Yang, G., Self-healing epoxy composites – Preparation and effect of the healant consisting of microencapsulated epoxy and latent curing agent. *Composites Science and Technology.* 2007, *67*, 201-212.
- [3] Yuan, L.; Liang, G.-Z.; Xie, J.-Q.; Guo, J.; Li, L., Thermal stability of microencapsulated epoxy resins with poly(urea–formaldehyde). *Polymer Degradation and Stability.* **2006**, *91*, 2300-2306.
- [4] Leclère, M.; Livi, S.; Maréchal, M.; Picard, L.; Duchet-Rumeau, J., The properties of new epoxy networks swollen with ionic liquids. *RSC Advances.* **2016**, *6*, 56193-56204.
- [5] Lee, J.; Zhang, M.; Bhattacharyya, D.; Yuan, Y. C.; Jayaraman, K.; Mai, Y. W., Micromechanical behavior of self-healing epoxy and hardener-loaded microcapsules by nanoindentation. *Materials Letters.* **2012**, *76*, 62-65.
- [6] Brown, E. N.; White, S. E.; Sottos, N. R., Microcapsule induced toughening in a self-healing polymer composite. *Journal of Materials Science.* **2004**, *39*, 1703-1710.

## Chapitre 4 : Encapsulation de monomère époxy liquide ionique et application à l'auto-cicatrisation de réseaux époxy-amine

### • Introduction

Dans le domaine des polymères thermodurcissables, les monomères liquides ioniques (MLI) représentent une réelle opportunité pour la conception de nouveaux matériaux polymères intelligents et (multi)fonctionnels avec des propriétés améliorées telles que la stabilité thermique, les performances mécaniques, les propriétés barrières aux gaz ou à l'eau, le caractère antibactérien, et les propriétés d'auto-guérison <sup>[1,2]</sup>. Un monomère époxy liquide ionique (MELI), tel que celui synthétisé dans cette étude, peut être polymérisé pour construire des matériaux à hautes performances <sup>[3]</sup> et peut être appliqué comme agent de comblement en l'intégrant dans un système de cicatrisation fait de microcapsules uniques. Il existe toutefois peu de travaux sur l'encapsulation de tel type de LI réactif dans des microcapsules. Par conséquent, ce chapitre se concentre sur: *i*) Synthèse d'un nouveau monomère époxy liquide ionique avec deux groupes époxy et leur encapsulation dans une coque PMF pour obtenir des microcapsules (MELI@PMF); *ii*) Application à l'auto-cicatrisation de différents matériaux époxy-amine.

### • Synthèse et caractérisation de monomère époxy liquide ionique (MELI) cœur des microcapsules (MELI@PMF)

Le schéma de la synthèse du monomère liquide ionique imidazolium (MELI) difonctionnel est donné dans le Schéma 1 <sup>[4]</sup> et la synthèse des microcapsules de poly(mélaamine-formaldéhyde) (MELI@PMF) par polymérisation *in-situ* est décrite à la Figure 7. Différents paramètres de synthèse ont été étudiés pour sélectionner la morphologie optimale des microcapsules MELI@PMF. Il a été montré qu'un rapport noyau-enveloppe à 1.31 et une agitation sous 300 tr/min permettent d'obtenir des microcapsules MELI@PMF avec la morphologie souhaitée. Des micrographies de microscopie MEB et la distribution de leurs diamètres sont données (Figure 8).

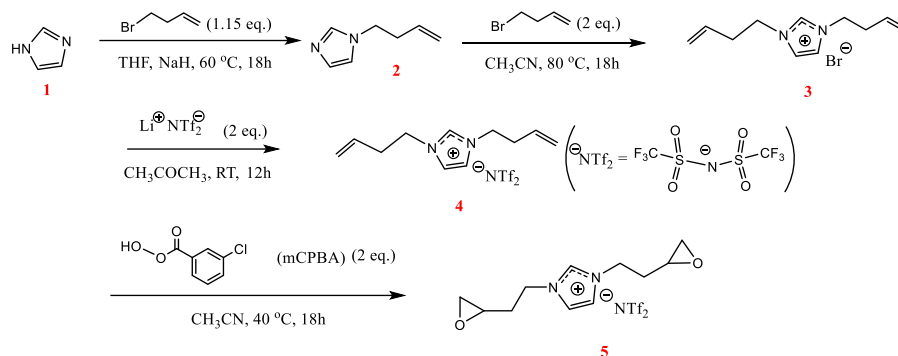


Schéma 1 Synthèse du monomère liquide ionique difonctionnel (MELI)

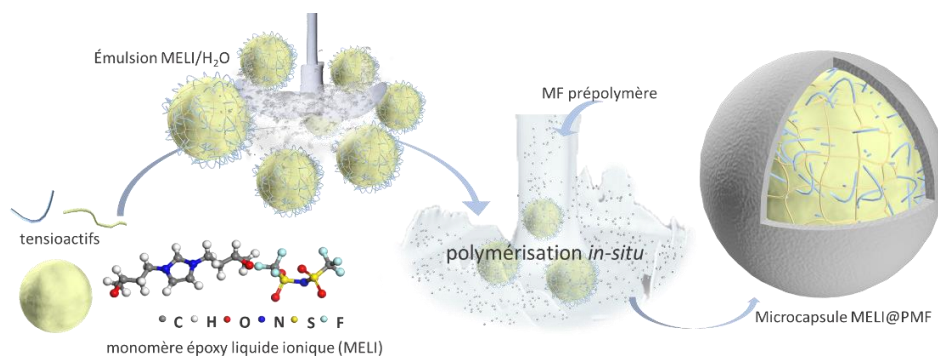


Figure 7 Préparation de microcapsules contenant le monomère époxy liquide ionique (MELI) contenant des microcapsules

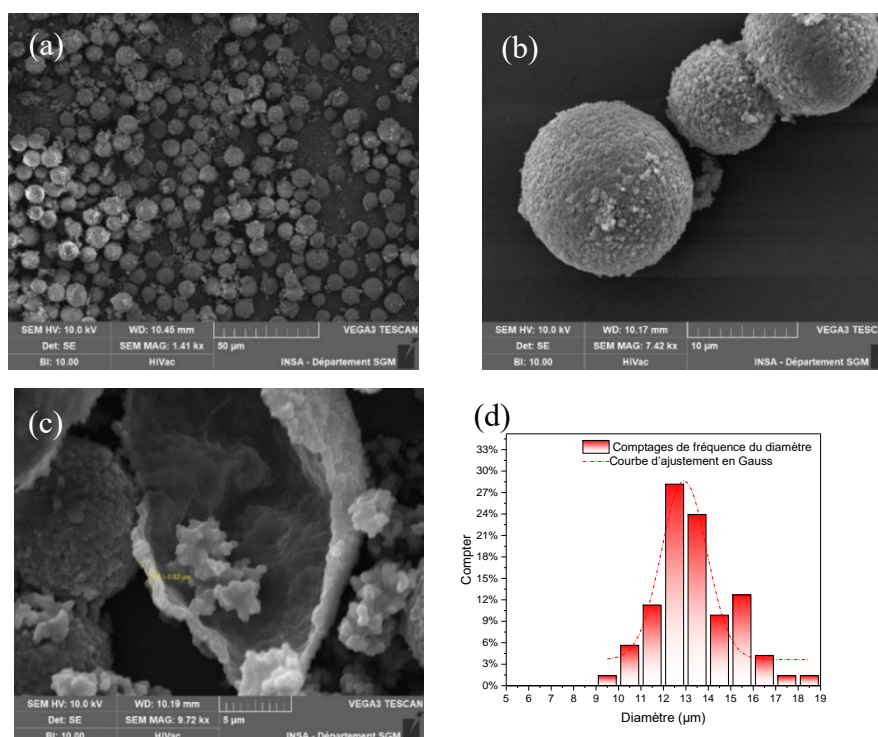
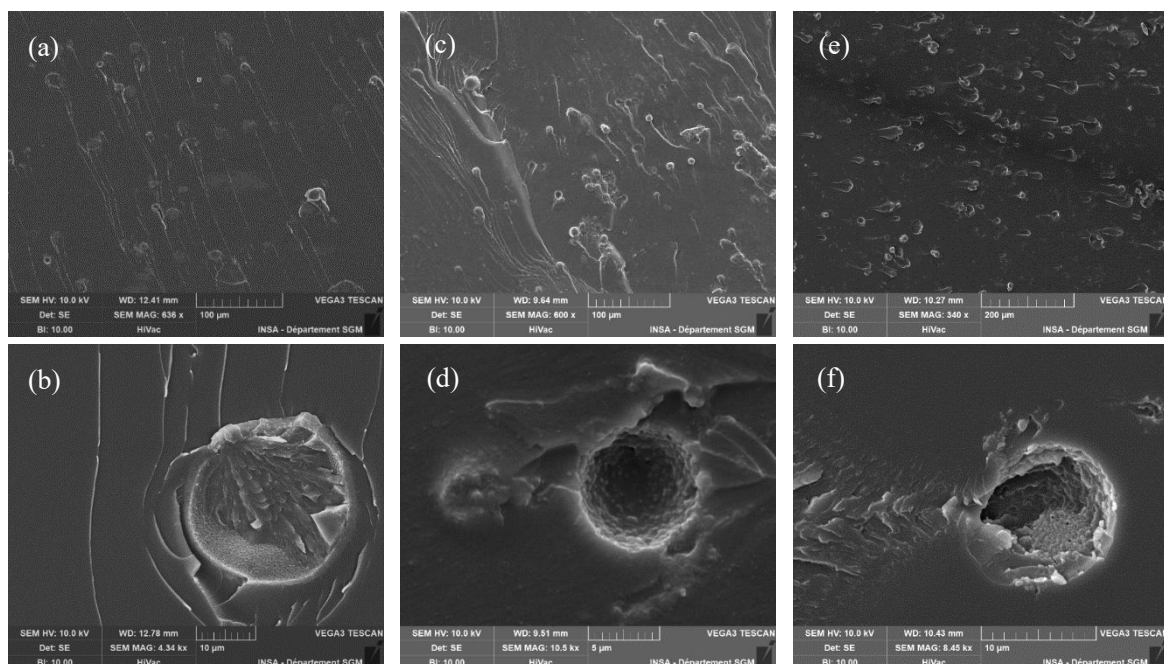


Figure 8 Micrographies MEB (a-c) et distribution de diamètres (d) des microcapsules MELI@PMF

- **Préparation et caractérisation des matériaux époxy avec microcapsules MELI@PMF**

Des microcapsules MELI @PMF ont été ajoutées dans différentes matrices époxy résultant de la polymérisation d'un prépolymère époxy avec différentes amines nécessitant différentes températures de cuisson, à savoir la 4,4'-méthylènebis(cyclohexylamine) (PACM), la triéthylènetétramine (TETA) et l'Epikure 3223 (diéthylènetriamine, DETA). Les micrographies MEB des matrices obtenues sont données Figure 9. Le monomère MELI comme agent de cicatrisation peut être polymérisé avant qu'il ne procède à la cicatrisation (comme montré Figure 9 (d)) en raison de la température nécessaire pour la cuisson du réseau et de la température atteinte avec l'exothermie de la réaction [5,6]. Par conséquent, pour atteindre un objectif d'auto-guérison, la température en volume de la matrice époxy pendant le processus de cuisson doit rester inférieure à la température de polymérisation du MELI. Par conséquent, les comonomères TETA et Epikure 3223 peuvent être considérés les plus appropriés pour le design de système époxy auto-réparables avec des microcapsules synthétisées dans ce travail.

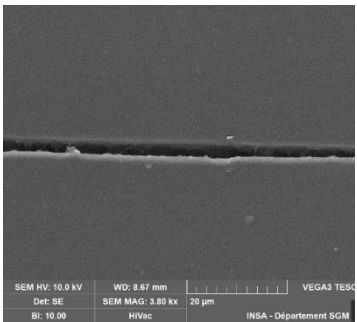
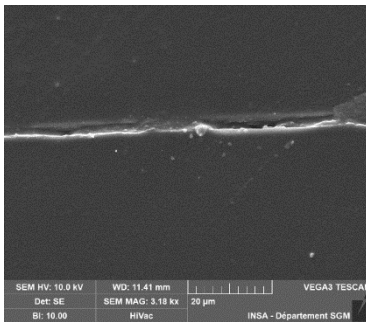
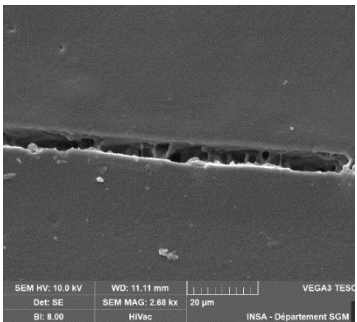
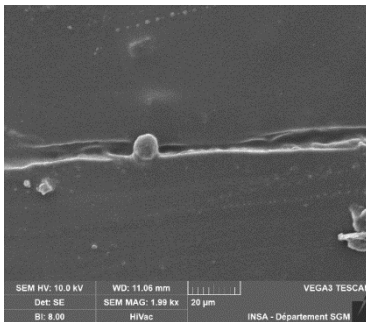


**Figure 9** Micrographies MEB de matériaux époxy avec microcapsules MELI@PMF à base de matrices époxy de différentes nature (a) (b) époxy-PACM; (c) (d) époxy-TETA; (e) (f) époxy-Epikure 3223;



Les propriétés thermiques et mécaniques ainsi que la capacité d'auto-guérison des matériaux époxy-TETA et époxy-Epikure 3223 avec des microcapsules MELI@PMF ont été caractérisées et les résultats sont donnés Tableau 4.

**Tableau 4** Propriétés thermiques, mécaniques et d'auto-guérison de matériaux époxy-TETA et époxy-Epikure 3223 incluant des microcapsules MELI@PMF

Matériaux	Auto-guérison		Caractéristiques	
	avant	après		
époxy-TETA- MELI@PMF			$T_g/^\circ\text{C}$	150
			$T_{d\text{ onset}}/^\circ\text{C}$	330
			$T_{d\text{ max}}/^\circ\text{C}$	368
			$E/\text{GPa}$	$1.5 \pm 0.04$
			$K_{IC}/\text{MPa} \cdot \text{m}^{1/2}$	$0.72 \pm 0.06$
époxy- Epikure3223- MELI@PMF			$T_g/^\circ\text{C}$	135
			$T_{d\text{ onset}}/^\circ\text{C}$	330
			$T_{d\text{ max}}/^\circ\text{C}$	364
			$E/\text{GPa}$	$1.4 \pm 0.02$
			$K_{IC}/\text{MPa} \cdot \text{m}^{1/2}$	$0.73 \pm 0.06$

### • Principaux résultats

Un monomère époxyde difonctionnel de type liquide ionique, noté MELI, a été synthétisé avec succès. Différentes méthodes de caractérisation ont montré que ces MELI ont une bonne stabilité thermique et peuvent homopolymériser à une température donnée. Ce nouveau monomère époxy de type liquide ionique a alors été encapsulé dans une coque de polyméline-formaldéhyde (PMF) par une méthode de polymérisation *in-situ*.

Les performances des microcapsules MELI@PMF dans différents réseaux époxy-amine nécessitant différentes plages de température de cuisson compte-tenu de la nature des comonomères amines utilisées ont été étudiées. Les amines PACM (80 °C - 160 °C), TETA

(60 °C - 125 °C), Epikure 3223 (DETA, 20 °C - 120 °C) ont ainsi été choisies comme durcisseurs. Parmi les trois systèmes époxy-amine, les microcapsules MELI@PMF ont montré une meilleure capacité d'auto-guérison dans le système époxy-Epikure 3223 à l'opposé du système époxy-PACM. Cet effet peut être aisément relié à la température 'vue' par le liquide ionique fonctionnel lors de la réaction exothermique des époxydes et des amines qui conduit alors à la polymérisation. Dans ce dernier cas, le MELI n'est alors plus disponible pour parvenir à une auto-cicatrisation. Par conséquent, une réticulation à température ambiante et/ou une limitation de l'exothermie semblent être les plus adaptées pour éviter ces problèmes et empêcher d'initier la polymérisation de MELI dans les microcapsules MELI@PMF.

## Références

- [1] Muldoon, M. J.; Gordon, C. M., Synthesis of gel-type polymer beads from ionic liquid monomers. *J. Polym. Sci., Part A: Polym. Chem.* **2004**, 42, 3865-3869
- [2] Chardin, C.; Durand, A.; Jarsalé, K.; Rouden, J.; Livi, S.; Baudoux, J., Sulfonimides versus ketosulfonamides as epoxidized imidazolium counterions: towards a new generation of ionic liquid monomers. *New J. Chem.* **2021**, 45, 2953-2957.
- [3] Livi, S.; Chardin, C.; Lins, L. C.; Halawani, N.; Pruvost, S.; Duchet-Rumeau, J.; Gérard, J.-F.; Baudoux, J., From ionic liquid epoxy monomer to tunable epoxy-amine network: reaction mechanism and final properties. *ACS Sustainable Chemistry & Engineering.* **2019**, 7, 3602-3613.
- [4] McDanel W M, Cowan M G, Carlisle T K, et al. Cross-linked ionic resins and gels from epoxide-functionalized imidazolium ionic liquid monomers[J]. *Polymer*, **2014**, 55(16): 3305-3313.
- [5] Bonin, H. W.; Bui, V. T.; Pak, H.; Poirier, E.; Harris, H., Radiation effects on aluminum-epoxy adhesive joints. *J. Appl. Polym. Sci.* **1998**, 67, 37-47.
- [6] Amin, K. G.; Patel, M. P.; Patel, R. G., Studies on the curing kinetics and thermal stability of the novel tetrafunctional epoxy resin. *Die Angewandte Makromolekulare Chemie.* **1999**, 266, 46-49.

## Chapitre 5 : Conclusion et perspectives

### • Conclusion

En résumé, ce travail a proposé différentes stratégies pour synthétiser différents types de microcapsules comme additif fonctionnel dans les réseaux époxy-amine. Les principales conclusions sont les suivantes :

- La synthèse de microcapsules de silice chargées d'un liquide ionique type phosphonium (microcapsules LI@SiO<sub>2</sub>) a été réussie. Les microcapsules ont été ajoutées dans des réseaux époxy-amine de rapports stoechiométriques différents et il a été montré que celles-ci pourraient jouer le rôle de renforcement ;
- La capacité d'auto-guérison des matrices époxy-amine a été prouvée en introduisant des microcapsules chargées en monomère époxy (EP@PUF) dans la matrice ternaire des époxy-amine-LI. La fraction massique de microcapsule EP@PUF est proportionnelle à l'effet d'auto-guérison, mais une fraction trop élevée pourra affecter les performances thermiques et/ou mécaniques des matériaux époxy finaux ;
- L'encapsulation d'un nouveau monomère époxy liquide ionique dans des microcapsules PMF (MELI@PMF) est également décrite. Différents paramètres de synthèse ont été discutés et la morphologie des microcapsules préparées sous différents paramètres a également été étudiée. Les performances de ces microcapsules MELI@PMF comme additif d'auto-cicatrisation dans différents composites époxy-amine ont été étudiées. Il est montré que la température de cuisson de la matrice époxy doit être inférieure à la température de polymérisation du MELI afin que celui-ci puisse jouer son rôle d'agent cicatrisant.

### • Perspective

Ce travail propose un concept lié à l'introduction de différentes microcapsules dans différents types de matrices époxy pour apporter une fonctionnalité, celle de l'autoréparation. Pour mener plus loin ces premiers travaux, plusieurs autres études pourraient être envisagées :

- L'électrofilage ou électrofilage coaxial serait un procédé adapté pour confiner des

liquides ioniques dans le cœur des fibres à l'image de canaux microvasculaires pour designer des membranes fonctionnelles ;

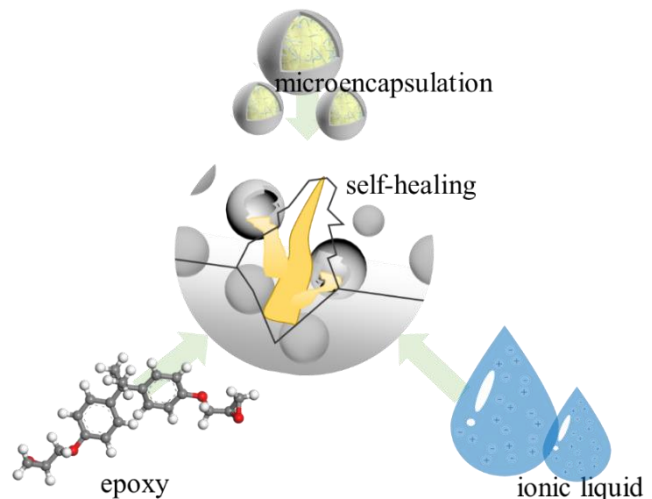
- La conception d'une bibliothèque de liquides ioniques époxy avec des anions ou des cations de différentes natures pour les introduire dans les microcapsules ou au cœur des fibres.



# Chapter 1 :

## Literature Review

This literature review will start from a general introduction on the self-healing following by the structure property relationships between ionic liquid and epoxy networks. Finally, the microencapsulation and their applications including self-healing for polymer matrix composites will be discussed. It is a general overview of related research background and a specific introduction will be included in each chapter. The first part will introduce two main categories of self-healing mechanisms that were widely used in material science, *i.e.* giving basic concepts of self-healing. Examples considering different healing mechanisms, including the epoxy composites, will be also reviewed to have a better understanding. The second part will briefly introduce epoxy resins, ionic liquids and especially their combination, including multifunctional roles of ionic liquids in epoxy networks. The third part will review the methodology of microencapsulation, including basic concepts, classifications and applications. Therefore, this literature review will give a macro concept from purpose, material to method of this PhD work, which can help to have an overview of the background and theoretical support.



---

# Table of contents

<b>1.1 Self-healing materials</b> .....	<b>30</b>
1.1.1 Introduction.....	30
1.1.2 Intrinsic self-healing.....	31
1.1.2.1 Self-healing from reversible covalent interactions.....	31
1.1.2.2 Self-healing from reversible non-covalent interactions .....	33
1.1.3 Extrinsic self-healing .....	36
1.1.3.1 Microvascular systems for self-healing .....	37
1.1.3.2 Microcapsules for self-healing.....	39
1.1.4 Conclusion .....	44
<b>1.2 Ionic liquids and epoxy networks .....</b>	<b>44</b>
1.2.1 Ionic liquids.....	44
1.2.1.1 Introduction.....	44
1.2.1.2 Applications of ionic liquids .....	45
1.2.2 Epoxy networks.....	49
1.2.2.1 Introduction.....	49
1.2.2.2 Building epoxy networks .....	50
1.2.3 Ionic liquids combined with epoxy networks.....	53
1.2.3.1 As hardener or initiator for the curing of epoxy prepolymer .....	53
1.2.3.2 As dispersing aids of nanomaterials/nano-objects within polymers .....	56
1.2.3.3 As flame retardant agents.....	57
1.2.4 Conclusions.....	58
<b>1.3 Microencapsulation .....</b>	<b>58</b>
1.3.1 Introduction.....	58

---

1.3.2 Synthesis strategies for microencapsulation.....	60
1.3.2.1 Solvent evaporation.....	60
1.3.2.2 Spray drying.....	61
1.3.2.3 <i>In-situ</i> polymerization.....	62
1.3.2.4 Interfacial polymerization.....	63
1.3.3 Applications of microcapsules.....	66
1.3.3.1 For biomedical uses.....	66
1.3.3.2 In food industry.....	67
1.3.3.3 In electronic devices.....	68
1.3.3.4 In polymer composites.....	69
1.3.4 Conclusion.....	71
<b>1.4 Conclusion of Chapter 1.....</b>	<b>71</b>
<b>References in Chapter 1.....</b>	<b>73</b>



## 1.1 Self-healing materials

### 1.1.1 Introduction

Nowadays, polymer matrix composites (PMC) have been widely used in industry, such as automotive, aerospace, wind turbine, etc. These materials have many advantages compared to traditional metal materials, according to their light weight, good electrical properties, thermal stability, good mechanical properties, dimensional stability, etc [1-4]. However, under continuous impact or cyclic mechanical force or thermal loads, microcracks or other defects are prone to be generated in brittle polymer matrices such as epoxy and polyesters as shown in Figure 1-1 [5]. Therefore, inspired by self-healing ability of living creatures in the nature, researchers are making efforts to design self-healable polymer materials, aiming at healing the microcracks before the cracks propagation to extend the lifetime of PMC materials. Self-healing materials have overcome the drawbacks of brittle polymers and due to their flexibility, intelligence, and long lifetime, it is an ideal and innovating choice for different fields, such as aerospace, coatings for anticorrosion, conductive devices or some biological applications.

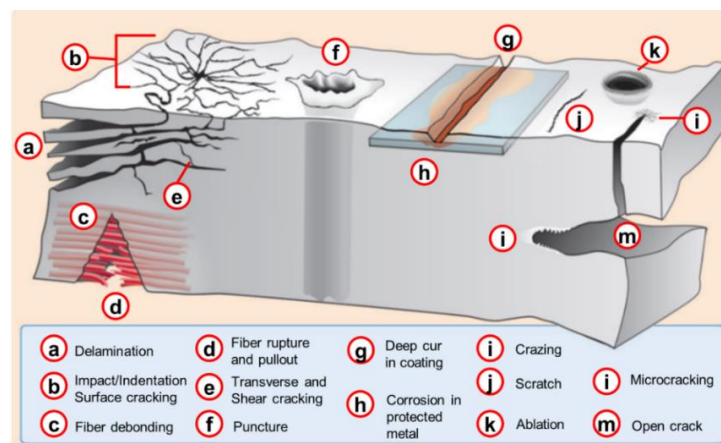


**Figure 1-1** Damage modes in polymer composites [5]

According to the need of external stimulus and/or extra healing agent, self-healing materials can be divided into two main categories: intrinsic self-healing materials and extrinsic self-healing materials [6]. In the intrinsic self-healing mechanism, the healing behavior occurs from the materials themselves via chemical, physical, or supramolecular interactions [7, 8]. By contrast, extrinsic healing behavior takes place by using additional healing additives or healing agents. Microcapsule and microvascular solutions are the most widely used strategies to achieve

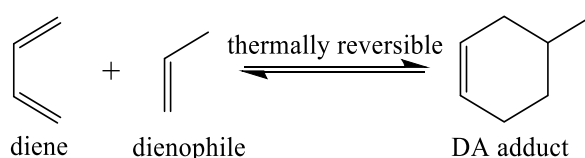
extrinsic self-healing purpose. In the following part, specific examples will be given for a better explanation of intrinsic and extrinsic self-healing mechanisms in different types of materials.

## 1.1.2 Intrinsic self-healing

### 1.1.2.1 Self-healing from reversible covalent interactions

Cracks lead to structural breakages of molecular chains or structural changes of molecules. Intrinsic self-healing mechanisms, are usually based on reversible reactions/bonds, physical or supramolecular interactions between the molecular chains of polymer materials.

Intrinsic self-healing achieved from dynamic reactions/bonds allows breaking and rebuilding chemical bonds in a chemical reaction repeatedly under certain conditions. For example, Diels-Alder (DA) reactions which happen between a conjugated diene and a substituted alkene to form a substituted cyclohexene derivative, was first proposed by Otto Diels and Kurt Alder in 1928 [9]. Scheme 1-1 presents the most common DA reaction between a diene and a dienophile. It should be noticed that DA reaction is thermally reversible, the DA adduct is so thermally instable under high temperature that the substituted cyclohexene derivative will decompose to regenerate the original diene and dienophile [10]. Such reaction could be a good choice to achieve intrinsic self-healing involving breakages of molecular chains by using DA adducts.



**Scheme 1-1** Diels-Alder (DA) reaction

In the real practice, Bai *et al* [11] have designed a crosslinked system from the copolymerization of new diamine crosslinker having two Diels–Alder (DA) adducts and conventional diglycidyl ether of bisphenol A (DGEBA) epoxy prepolymer. (Figure 1-2 (a)). This new crosslinked epoxy network with local DA adducts on the diamine can be thermally cleaved and reformed, thereby allowing the crosslinked polymer to fill or heal cracks and scratches. The thermally induced self-healing mechanism is described in Figure 1-2 (b). The authors have pointed out that the cleavable/healable moiety is within the amine crosslinker, rather than the epoxy monomer.

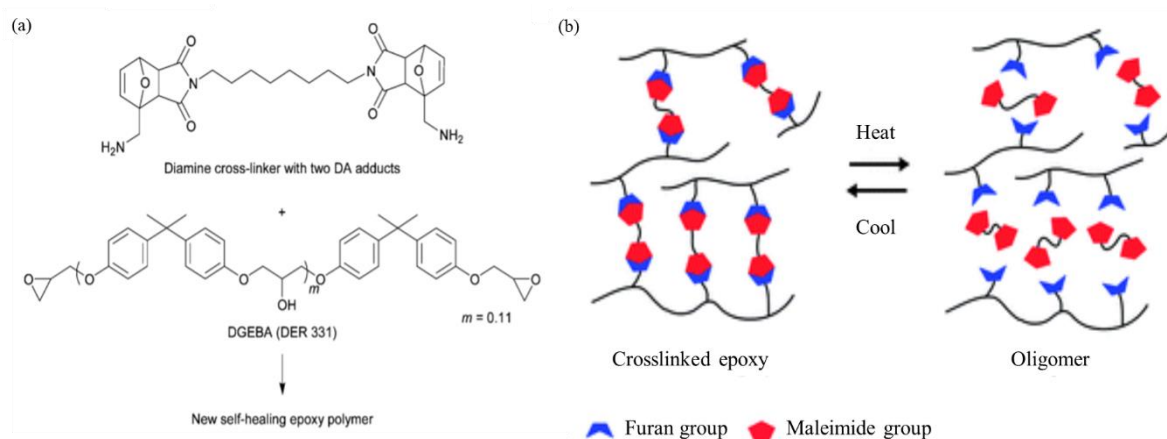
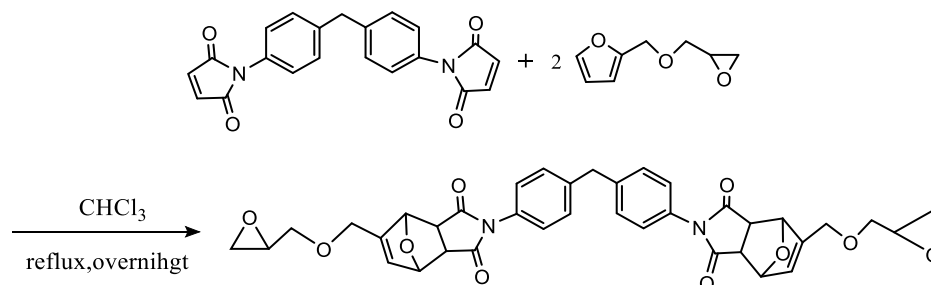


**Figure 1-2** (a) Chemical structure of DGEBA and diamine with DA adducts; (b) thermal induced self-healing mechanism <sup>[11]</sup>

To design self-healable epoxy network which is not limited by hardener, it is required to introduce such reversible groups on the epoxy chains. For example, Amendola *et al* <sup>[12]</sup> have synthesized epoxy monomer with bifunctional Diels-Alder adduct as shown in Scheme 1-2. This DA adduct containing epoxy monomer possesses an intrinsic self-healing ability when it is cured with ordinary hardener.



**Scheme 1-2** Synthetic of epoxy monomer with bifunctional Diels-Alder adduct <sup>[12]</sup>

Reversible covalent bonds were also employed to design self-healable polymer materials. For example, Deng *et al* <sup>[13]</sup> reported a novel type of self-healing “dynamic” covalent system by using acylhydrazones reversible bonds. The authors succeeded in condensation of acylhydrazones at the end of a poly(ethylene oxide) (PEO) (A2) with aldehyde groups in tris[(4-formylphenoxy)methyl]ethane (B3), which can form a crosslinked network. The obtained polymer gel was able to undergo cleavage under mild acidic conditions and reshape the polymer gel back to its original state by increasing the pH value, as shown in Figure 1-3.

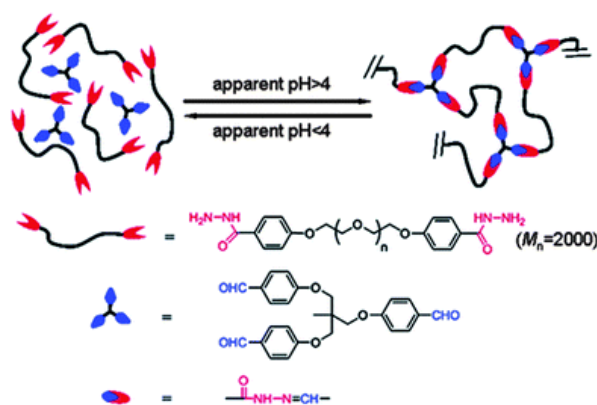
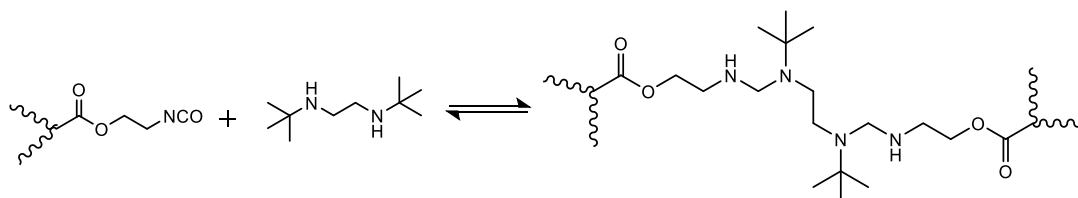


**Figure 1-3** Construction of covalent cross-linked polymer gel based on reversible covalent acylhydrazone bond <sup>[13]</sup>

A reversible reaction between a sterically hindered amine with an isocyanate-functionalized polymer was also considered to prepare intrinsically self-healing polymers. Zechel *et al* <sup>[14]</sup> synthesized crosslinked methacrylates with dynamic urea bonds as reversible crosslinking moieties with a sterically hindered amine, as shown in Scheme 1-3. Because of the reversibility of the formed urea bonds in sterically hindered urea, the obtained polymer can be converted into the starting compounds (isocyanate and amine) by a simple thermal treatment.



**Scheme 1-3** the reversible reaction of the sterically hindered amine with an isocyanate-functionalized polymer <sup>[14]</sup>

### 1.1.2.2 Self-healing from reversible non-covalent interactions

Unlike chemical reactions for self-healing mentioned above, non-covalent interactions for achieving self-healing are mainly related to the mobility of polymer chains and reversible non-covalent interactions in the bulk materials, including chain interdiffusion and supramolecular interactions.

#### Chain interdiffusion

A certain class of ionomers <sup>[15]</sup> and epoxy-amine networks <sup>[16]</sup> are reported to have the ability to self-heal instantaneously without external intervention after the damage, depending

on mainly chain interdiffusion. This self-healing phenomenon can be explained by the physical model put forward by Wool and O'Connor in 1981 [17]. This simple and universal mechanism based on chain interdiffusion as shown in Figure 1-4, involves the following aspects: (1) surface rearrangement; (2) surface approach; (3) wetting; (4) diffusion; and (5) randomization [18]. However, this process is strongly related to molecular interdiffusion that takes place at (or above) the glass transition temperature ( $T_g$ ) at which polymer segments are mobile enough for efficient self-repairing [19].

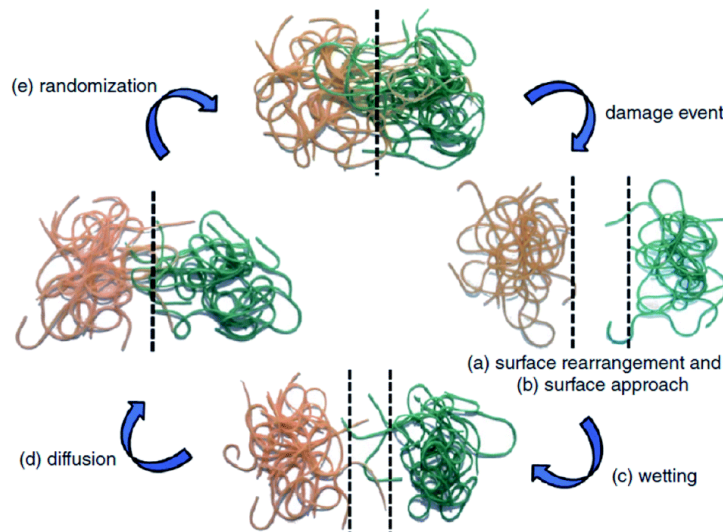


**Figure 1-4** Stages of self-healing mechanism for polymeric segments of random walk character [17, 18]

### Supramolecular interactions

Supramolecular chemistry includes aspects of physics and biology and deals with interactions between molecules, which concern non-covalent interactions between molecules such as hydrogen bonding, metal coordination, hydrophobic forces, Van Der Waals forces,  $\pi$ - $\pi$  interactions or electrostatic effects [20]. These non-covalent interactions are involved for healing damages within networks through reversibility and dynamics of networks. Self-healing mechanisms for a supramolecular material are described in Figure 1-5 [21]. When the material is damaged, the weak supramolecular bonds or clusters are broken preferentially. Even though the supramolecular bonding stay unassociated on the fractured surface for a while, the supramolecular bonds or clusters are reformed again when the broken parts are brought into contact to heal the crack.

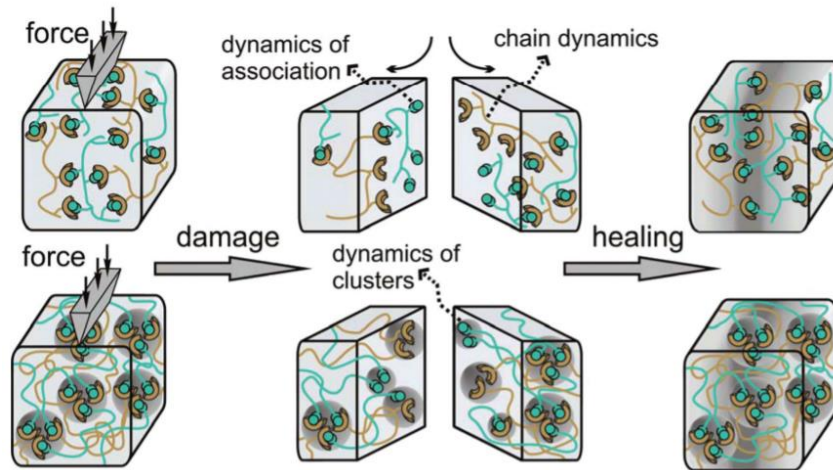


**Figure 1-5** Self-healing mechanism for a supramolecular material [21]

For example, a hydrogen-bonding brush polymer with high Young's modulus and extensibility that self-assembles into a hard/soft two-phase system with the self-healing ability was reported by Chen [22]. As shown in Figure 1-6, they designed a polymer with a polystyrene backbone as the hard phase with high  $T_g$  and polyacrylate amide (PA-amide) brushes as the soft phase with low  $T_g$ , and the polyvalent hydrogen-bonding sites ensure the self-assemble capacity to form a hydrogel with two-phase nanostructure. It can spontaneously self-heal as a single-component solid material without any external stimuli, healing agents, plasticizer or solvent.

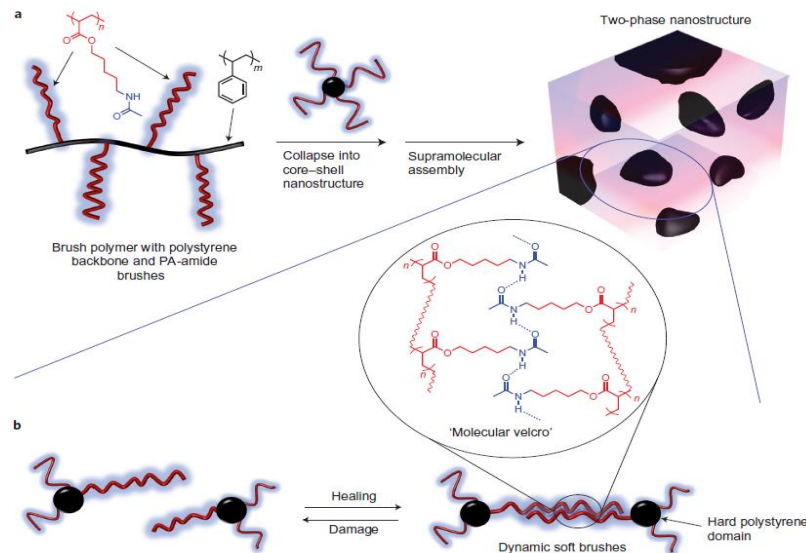


**Figure 1-6** Proposal of design for the multiphase self-healing brush polymer system [22]

Non-covalent interactions such as  $\pi$ - $\pi$  stacking are also used to design self-healable supramolecular polymer system. For example, Burattini *et al* [23] designed a complexation of chain-folding polyimide with the pyrenyl end-capped polyamide via electronically-

complementary  $\pi$ - $\pi$  interaction (Figure 1-7). The finally polymer showed enhanced mechanical properties and a thermally reversible self-healing ability.

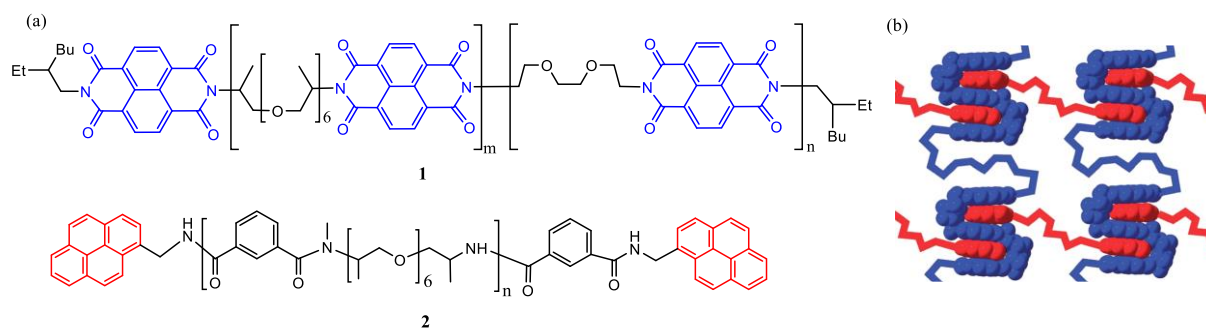


**Figure 1-7** (a) Chemical structures of polyimides **1** and polyamides **2** in Burattini's work and (b) intercalation of pyrenyl end-groups (red) into designed polyimide chain-folds (blue)

In summary, intrinsic self-healing mechanisms involving either reversible reactions, dynamic bonds, physical rearrangements of polymer chains or supramolecular interactions are based on the intrinsic properties of materials. Because of the reversible feature of such interactions, multi healing times may be achieved for different materials [6]. However, limitations of intrinsic self-healing mechanisms were also noticed for different situations. The material itself has to be designed with self-healable unit at molecular level and in some cases, self-healing processes need specific stimulus or condition, such as temperature, pH or UV irradiation, which may limit a wide range of applications. Differently, extrinsic self-healing mechanism relies on external healing agent, which can be used in various types of materials that don't possess the above reversible interactions.

### 1.1.3 Extrinsic self-healing

As mentioned before, some polymer materials without any molecular modification do not display the ability to healing itself because the intrinsic mechanism always requires specific structure or reactive groups in the molecule chains. In order to achieve self-healing property, external healing agents need to be introduced in materials. Such agents are usually introduced as microcapsules or macrovascular system and contribute to heal the crack when needed. In some cases, researchers combined various methods to achieve a better self-healing efficiency. In the following sections, some examples will be given for both microcapsule and macrovascular-based systems.

### 1.1.3.1 Microvascular systems for self-healing

Like blood vessels in the human body, similar structures of micro-channels containing healing agent are embedded in the polymer matrix. Such a route is known as microvascular self-healing. Healing agent for polymer network is sequestered in capillaries or hollow channels, which may be interconnected when the material is damaged [5]. In this concept, removeable or non-removeable hollow tubes, wires or mandrels have been embedded in to polymer matrix to form microvascular networks [24]. Figure 1-8 shows the basic concept of microvascular in polymer composites given by Kathleen *et al* [25]. When microcracks are generated in PMC matrix, microvascular channels are broken and release the healing agent. Usually, there are two components to heal the cracks as the healing agent reacts in the presence of catalyst already dispersed in the PMC matrix. Hollow fibers are the most common choice of microvascular in PMC materials, *i.e.* hollow glass fiber [26-28] or core-shell fibers processed by coaxial electrospinning [29].

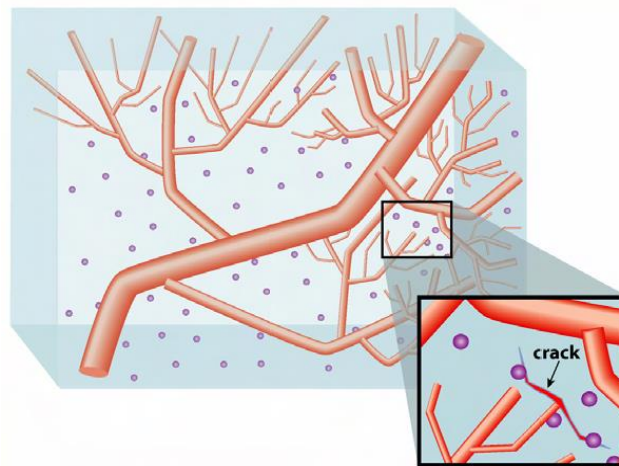


**Figure 1-8** Concept of microvascular self-healing system in PMC [25]

R.S. Trask and I.P. Bond [30] reported the self-healing composites by using glass hollow fiber, which can act both as storage of functional agents for composite self-repair and reinforcement. The typical hollow fibers-based self-healing concerns three approaches: (1) one-part resin system, (2) two-part resin and hardener system, or (3) a resin system with a catalyst or hardener contained within the matrix [31], as shown in Figure 1-9.



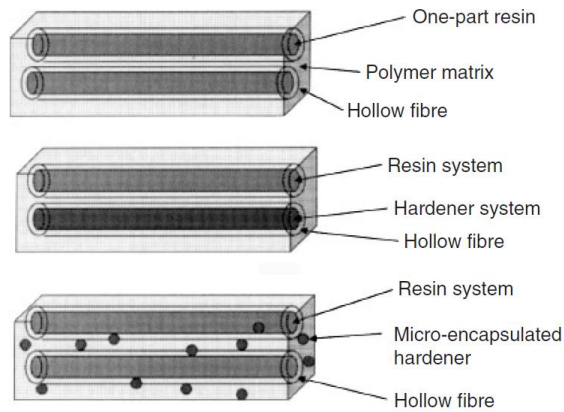


**Figure 1-9** Schematic illustration of different hollow fiber self-healing systems [30]

For example, Kim *et al* [32] have developed a membrane with a methylene diphenyl diisocyanate contained fluorinated ethylene propylene capillary tubes. The healing agent is released from the tubes when damage occurred in the membrane. The released healing agent undergoes a water-induced reaction to form an expanded polyurethane/polyurea matrix to heal the crack. The self-healing mechanism was shown in Figure 1-10.

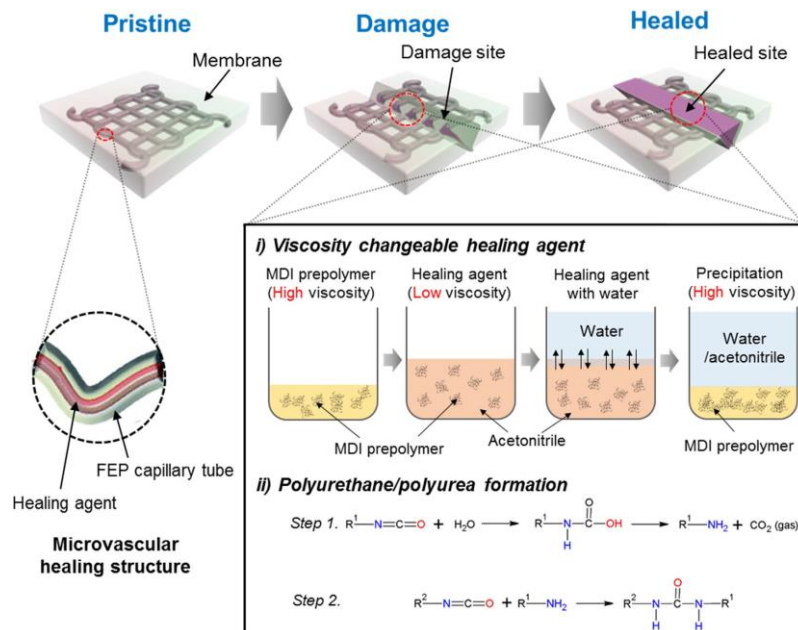


**Figure 1-10** Structure of a microvascular network-embedded self-healing membrane and schematic illustration of the healing mechanism [32]

Neisiany *et al* [33] have prepared microfibers with polyacrylonitrile (PAN) shell and dual components (epoxy or amine) core which are fabricated by coaxial electrospinning technique to construct a two-parts resin healing system. Core-shell nanofibers with smooth and continuous surface without beads were achieved. When these two types of fibers are broken by external damage, the epoxy prepolymer and curing agent are released and react at room temperature. Figure 1-11 shows the SEM image of broken nanofibers releasing epoxy and amine healing agents cured to get a solid-state material. These dual components fiber fabricated by coaxial electrospinning technique is a promising component in polymers and carbon fiber composites to achieve self-healing.

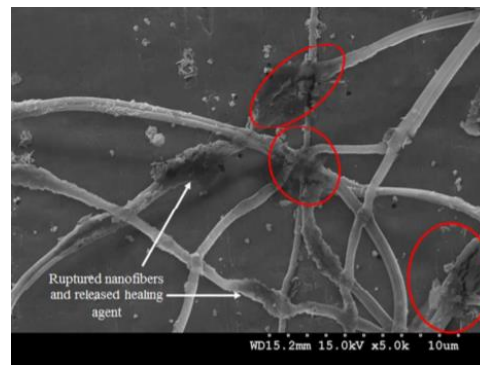


**Figure 1-11** Solidified resin (circled) providing from releasing curing agents from ruptured PAN fibers [33]

### 1.1.3.2 Microcapsules for self-healing

Microencapsulation is a method for packaging different components as microparticles having an organic or inorganic shell. The isolated microcapsules can release core compounds under certain conditions, such as temperature [34, 35] or pH [36-38]. Compared with microvascular network, the separated microcapsules are easy to process and to incorporate in the polymer materials. In PMC materials, different core compounds used as healing agents could be encapsulated in a shell material and the obtained microcapsules could be embedded in polymer matrix. Single microcapsules healing system or dual microcapsule healing system, could be considered (Figure 1-12). Both of them relate to the same principle: the wall of the microcapsules provides protection and a controllable release of core compound which will heal the damages when cracks are generated in the material.

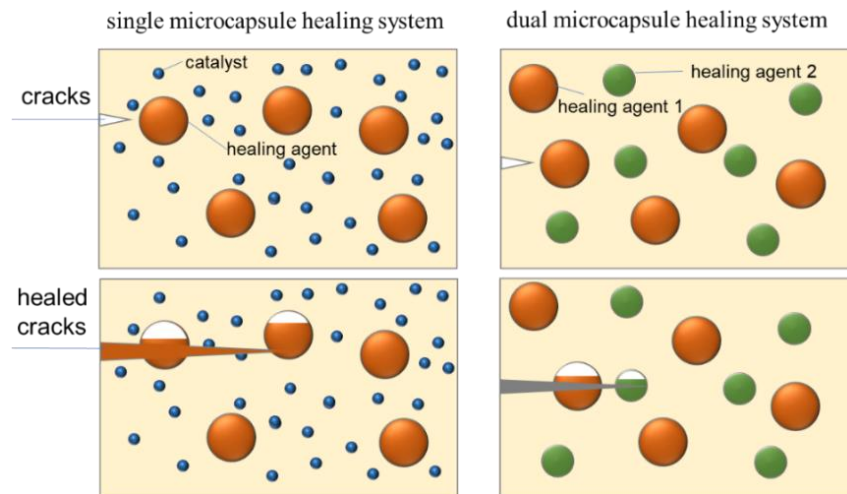


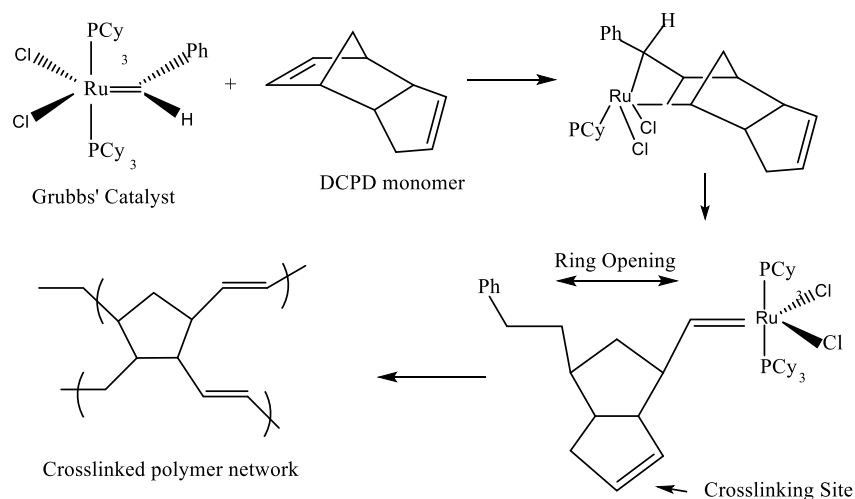
**Figure 1-12** Basic healing concept using microcapsules in PMC

left: single microcapsules healing system; right: dual microcapsule healing system

For the single microcapsules system, only the main healing agent was encapsulated, whereas the catalyst or the latent hardener/initiator, such as Grubbs' catalyst<sup>[39]</sup> was embedded in the polymer matrix. When the healing agent released from the microcapsules rupture, it could react with pre-embedded catalyst or latent hardener/initiator. For the dual microcapsule system, self-healing also occurs from the released healing agent in the presence of catalyst/initiator in the bulk of the material, but in the dual microcapsule system, both healing agent and the corresponding hardener or initiator were encapsulated into two different types of microcapsules. Compared with single microcapsule system, additional synthesis of microcapsules is required and the healing efficiency is relied on the content of the two microcapsules. While the higher stability of hardener in the microcapsules for dual microcapsule system compared to latent ones provides more choices and variety. In the following part, specific examples and research status of the literature on microcapsules for self-healing PMC will be introduced in detail.

For the single microcapsule system, the most common reaction is the Grubbs' catalyzed ring-opening polymerization of released dicyclopentadiene (DCPD), which is illustrated in Scheme 1-4. The role of the crystal morphology and dissolution kinetics of Grubbs' catalyst is very important for self-healing capability and healing efficiency in the PMC materials. In fact, Jones *et al*<sup>[40]</sup> has investigated the influence of two crystal polymorph of Grubbs' catalyst on the healing effect in epoxy composites. They have found that the crystal polymorph influences

the catalyst's thermal stability and the smallest crystals undergo the fastest dissolution kinetics, leading to a high concentration of catalyst in the healing agent before any significant reaction has started. Nevertheless, small size catalyst particles showed a reduced reactivity when exposed to amines for certain periods of time. As a consequence, it may limit their self-healing performances for epoxy-amine matrix-based composites.



**Scheme 1-4** Ring opening polymerization of DCPD catalyzed by a Grubbs' catalyst <sup>[41]</sup>

Another choice of core compound for single microcapsule system is linseed oil which can be considered as a healing agent due to its ability to form films from atmospheric oxidation. For instance, Suryanarayana *et al* <sup>[42]</sup> have prepared linseed oil filled microcapsules for healing the cracks in coatings. Microcapsules were synthesized by *in-situ* polymerization in oil/water (O/W) emulsion, with a poly(urea–formaldehyde) copolymer as shell material. It is proved that obtained microcapsules have rough morphology and good thermal stability. Self-healing performances of colored linseed oil-filled microcapsules were observed by optical microscopy (OM) from the healing of a crack in a coating. Figure 1-13 shows the OM images of optical microscopy of colored films formed by released linseed oil. It is shown that the initial open length of the crack is gradually reduced and is filled after 90 s. The authors demonstrated that linseed oil as healing component undergoes an oxidation from the atmospheric oxygen to form continuous material filling the cracks.

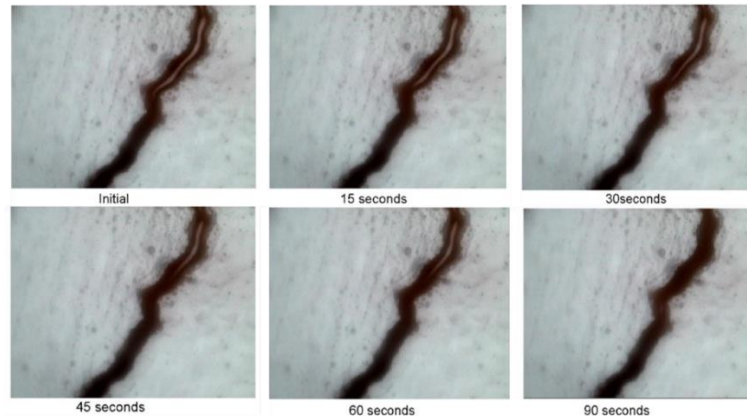


**Figure 1-13** Microscope photos of self-healing coating films [42]

For dual microcapsule system, healing agents and hardener/initiator were encapsulated into two different types of microcapsules which are embedded together in the matrix. The conditions for self-healing require the break of both microcapsules and the release of core compounds at the same time. For example, Jin *et al* [43] have prepared two types of microcapsules containing modified aliphatic polyamine and a diluted epoxy monomer respectively. When these two types of microcapsules were broken during cracks generation and growth, the healing agents will react to fill the cracks under room temperature condition for 48 h. The authors found that the best amine-to-epoxy microcapsules mass ratio is 4:6. When 7 wt% amine-containing and 10.5 wt% epoxy-containing microcapsules were in epoxy network, a promising healing efficiency of 91% was achieved. Figure 1-14 shows the surface morphology of cross section of a microcapsule-filled epoxy before and after the healing process. It is obvious that the crack tails on the cross surface are disappeared after the cracks are healing by epoxy and amine reaction product.

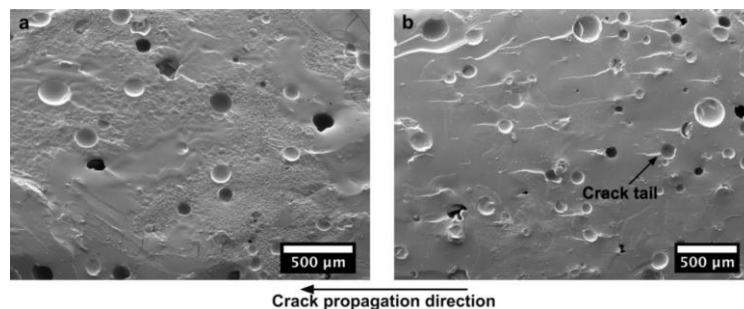


**Figure 1-14** Self-healing evidence from SEM images of fracture surfaces of an epoxy

network containing 4 wt% amine-containing and 6 wt% epoxy-containing microcapsules: (a) fracture surface after healing; (b) non-healed fracture surface rinsed with ethanol [43]

Indeed, microcapsule in self-healing application is not only limited to single separated microcapsules prepared from conventional synthetic methods. Park *et al* [44] reported a novel self-healing coating produced by coaxial electrospinning with capsules as healing agent container. Differing from the traditional uniform fiber morphology, they have obtained a bead-on-string fiber morphology, as shown in Figure 1-15 (a). It can be seen that a large number of special microcapsules containing healing agent were strung among the fibers. When the coating was exposed to mechanical damage, these microcapsules were broken releasing the healing agent as shown in Figure 1-15 (b). One major advantage of this process is that this unique bead-on-string structure was obtained only by physical forces instead of using chemical reaction in emulsion. Such a route avoids complex process or other unfavorable effects.

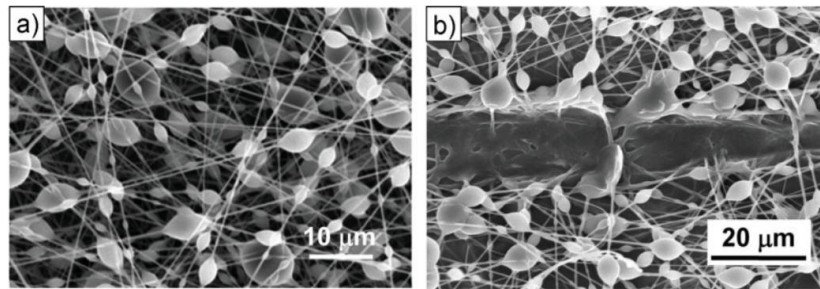


**Figure 1-15** (a) SEM micrograph of core-shell bead-on-string morphology prepared by coaxial electrospinning; (b) Release of healing agent in coating after mechanical damage [44]

In this section, literature focus about self-healing routes, different healing mechanisms and corresponding applications were introduced. It can be summarized that intrinsic healing mechanism proceeds from different types of interactions between molecules or components requiring specific chemical structures of the materials themselves. Such a route gives the higher healing efficiency as no extra healing additives are required and become healing processes could be repeat several times. On the other hand, the extrinsic healing route which involves external healing agent whether as microcapsules or as microvascular network, provides a greater universality in the choices of repair components. Nevertheless, for conventional polymer, *i.e.* already defined in chemical nature, the self-healing mechanism cannot consider the intrinsic healing mechanism.

### 1.1.4 Conclusion

To conclude, inspired by the extensive self-healing behavior in living creatures, development of self-healable materials such as self-healable polymers have been considered as one of the most important requirements for durability, *i.e.* for the development of sustainable materials. There are two main routes of self-healing mechanisms: intrinsic self-healing mechanism vs. extrinsic self-healing mechanism. Intrinsic self-healing route relates to the reversible interactions while extrinsic self-healing route needs additional self-healing agents accompanied with different embedding technology of healing agents. While compared the way of introducing healing agents, intrinsic self-healing mechanism provide a reliable healing effect and avoid problems such as inadequate stability of extra healing agent and complex preparation process [45]. While extrinsic self-healing mechanism can be widely applied in different materials without limitations by the chemical structure of the material itself and higher mobility and compatibility of extrinsic self-healing mechanism allow it to be used in a wider range of materials.

## 1.2 Ionic liquids and epoxy networks

### 1.2.1 Ionic liquids

#### 1.2.1.1 Introduction

Ionic liquids (IL), also known as room temperature ionic liquids (IL or RTIL), are organic salts that are liquid at closed room temperature. The first RTIL, *i.e.* ethylammonium nitrate [EtNH<sub>3</sub>][NO<sub>3</sub>], was discovered by Paul Walden in the year of 1914 [46]. Thirty years later, an ionic liquid based on chloroaluminate was described in US patent as a new route for solubilization of cellulose with ionic liquid [47]. Later, in 1967, C. Gardner *et al* have applied tetrahexylammonium benzoate (THAB), which is a liquid salt at room temperature, as solvent for numerous organic compounds. The intrinsic conductance and electrochemical inertness of ILs promote them as promising solvents for electrochemistry [48]. Edward *et al* [49] have firstly studied the electrochemistry of organometallics and an alkylaromatic in RTIL based on tetraalkylammonium cation and chloroaluminate anion. Afterwards, Robinson *et al* [50] have studied AlCl<sub>3</sub>-*n*-butylpyridinium chloride system. The variability of anions and cations leads to

numerous combinations and tunability of ionic liquid properties. Figure 1-16 shows some commonly used cations and anions among RTIL <sup>[51]</sup>.

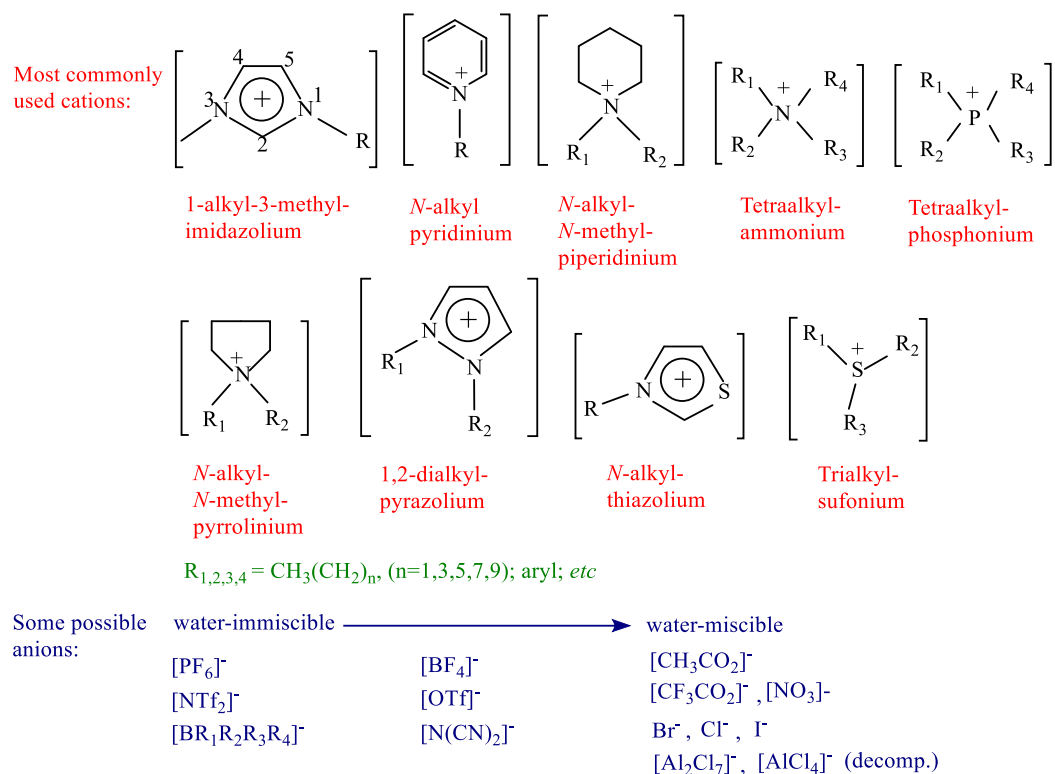


**Figure 1-16** Some commonly used cations and anions of RTILs <sup>[51]</sup>

### 1.2.1.2 Applications of ionic liquids

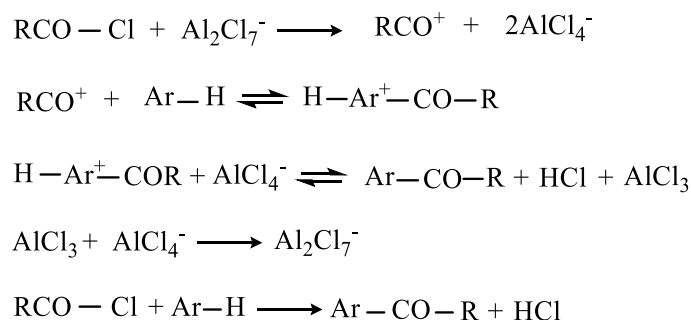
Combinations of various anions and cations can tailor the properties of RTILs. Nevertheless, some common characteristics <sup>[52]</sup> for RTILs could be listed including: negligible vapor pressure, non-flammability, high ionic conductivity <sup>[53]</sup>, non-volatility and high thermal stability <sup>[54]</sup>, etc. As a consequence, RTILs are widely used in different research fields and the main applications of RTILs are described in this section.

#### As clean solvents

One of the most attractive features of ILs is their negligible vapor pressure, *i.e.* no emission of volatile organic compounds. As a consequence, ILs offer an excellent alternative of conventional solvents for the green chemistry <sup>[55]</sup>. The great versatility (cation/anion) of ILs opens new perspectives for numerous applications. Jeffery *et al* <sup>[56]</sup> have firstly considered a the mixture of 1-methyl-3-ethylimidazolium chloride and aluminum chloride as solvent which can also act as catalyst of Friedel-Crafts reactions. The authors reported that Lewis acid species,



such as  $\text{Al}_2\text{Cl}_7^-$ , played the role of functional catalyst for Friedel-Crafts reactions. The reaction mechanism can be described as follows:



**Scheme 1-5** Mechanisms of Friedel-Crafts reactions

Most recently, researchers considered the use of RTIL for transition metal catalysis. Jairton *et al* <sup>[57]</sup> have reported for the first time the use of 1-n-butyl-3-methylimidazolium hexafluorophosphate ( $[\text{BMI}][\text{PF}_6]$ ) as a medium for stabilization of transition-metal in biphasic hydrogenation systems, which leads to very good cyclic performance. The RTILs have replaced conventional organic solvents according to their good solubility of hydrogen and many alkenes, resulting in a multiphase reaction and recovery ability <sup>[58]</sup>.

**As electrolytes**

Because of their high relative ion concentration, the fact that they do not have vapor pressure and display low melting points, ILs are considered as relevant electrolytes in electrochemical devices <sup>[59]</sup>. Solar radiation being one of the clean and renewable energies has a great potential for construction of photovoltaic devices. However, despite of the sensitivity of expensive dyes and the use of iodide/triiodide as redox couple that will limit the performance of the dye-sensitized solar cells <sup>[60, 61]</sup>, volatile organic electrolytes make difficult design packaging of dye-sensitized solar cells. Therefore, the non-volatile, chemically and thermally stable RTILa could be considered as promising alternatives for electrolytes <sup>[62]</sup>. The challenges of imidazolium ionic liquids for solar cells are related to their high viscosity that limit the mass-transport, Dai *et al* <sup>[63]</sup> have investigated the performance of three different ethylmethylimidazolium-based ILs with various types of anions (Figure 1-17): tricyanomethanide (TCM), dicyanamide (DCA), and thiocyanate (SCN) for dye-sensitized solar cells. The authors have found that the TCM IL displayed the lower viscosity, the lower

hygroscopy and a sufficiently high conductivity, compared to DCA IL. The SCN IL is also a very promising anion when a light intensity is less than 30% of sun light intensity.

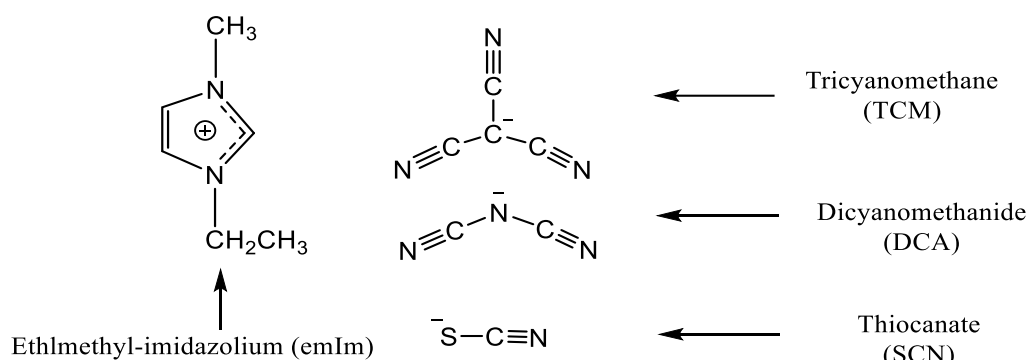


**Figure 1-17** Ethylmethylimidazolium-based ILs [63]

Lithium metal batteries are burgeoning electrochemical devices that are widely used in portable electronic devices, electric vehicles, grid energy storage systems, aerospace, etc [64-66]. ILs, because of their high ion conductivity, non-volatile behavior and unique physicochemical properties, have shown a great potential in lithium metal batteries and played tunable roles [67]. ILs can be applied as electrolyte solvents [68], additives of composite electrolytes [69] or filler in solid electrolytes [70], as well as wetting agents to interfaces between solid electrolytes and electrodes [71]. Figure 1-18 schematically reports the properties of ionic liquids and applications in lithium metal batteries on electrolytes, cathodes and lithium metal anode.

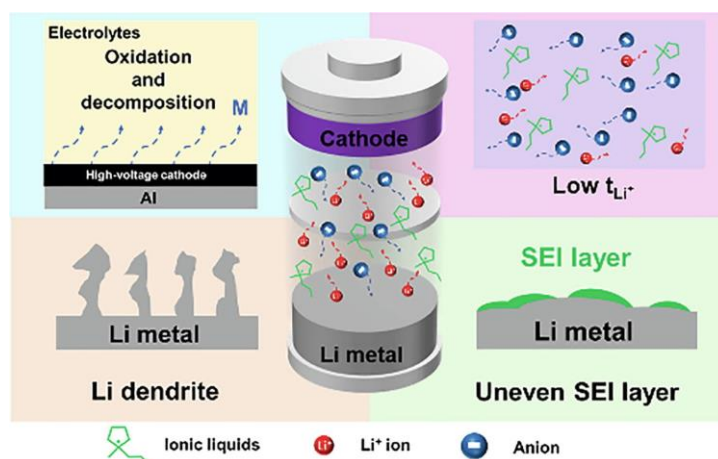


**Figure 1-18** Properties of ionic liquids and applications in lithium metal-based batteries as electrolytes, cathodes, and lithium metal anode [67]

Phosphonium-based room temperature ionic liquids contribute also to a broad and promising range that possess non-conventional properties that can be applied in the field of electrochemical applications <sup>[72]</sup> including high performance lithium metal batteries. For example, Katsuhiko *et al* <sup>[73]</sup> have built a lithium battery electrolyte based on triethyl(2-methoxyethyl)phosphonium bis (trifluoromethylsulfonyl) imide (P<sub>222-201</sub>-TFSI, chemical structure are shown in Figure 1-19), which exhibited high thermal stability with favorable transport property compared to traditional ammonium electrolyte.

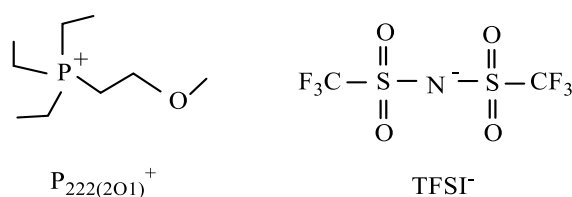


**Figure 1-19** Chemical structure of IL P<sub>222-201</sub>-TFSI

### *As self-lubricants for polymers*

Besides being considered as green solvents and catalysts for chemical syntheses and electrochemistry conduction, ionic liquid can also act as a self-lubricant for polymers according to recently published papers, which can overcome some drawbacks of some traditional lubricants. For example, ionic liquids can be applied at high temperature due to their high thermal stability while some traditional mineral oil cannot be used at high temperature <sup>[74]</sup>. Park <sup>[75]</sup> showed that phosphonium-based ILs with different anions (decanoate, tetrafluoroborate) can act as potential plasticizers and lubricants for polylactic acid (PLA). It was found that these two ILs were well dispersed and partially miscible with PLA at 5 wt% content. While, tetradecyl phosphonium tetrafluoroborate ([THTDP][BF<sub>4</sub>]) is a more relevant multifunctional additive than trihexyl tetradecyl phosphonium decanoate ([THTDP][DE]) for PLA, because [THTDP][BF<sub>4</sub>] offers a better balance between polymer degradation ability versus beneficial contribution as lubricant.

ILs as versatile lubricants represents as a great importance in industry <sup>[76]</sup>, such as metal contact <sup>[77-79]</sup> and polymer composites <sup>[80, 81]</sup>. Sanes *et al* <sup>[82]</sup> have reported IL 1-octyl-3-methylimidazolium tetrafluoroborate ([OMIM]BF<sub>4</sub>) and ZnO nanoparticles could be added to the epoxy system at the same time. According to their work, the residual depth of scratch can

be reduced and the stiffness of epoxy resin can be increased due to the effect of [OMIM]BF<sub>4</sub> on segmental chain mobility. As reported, ILs can reduce the wear coefficient by 50% and the wear rate by two orders of magnitude compared to neat epoxy resin.

In addition to direct addition to a polymer medium, ILs could also be encapsulated in microcapsules as “latent” lubricants when needed. Li *et al* [83] have used a different strategy to introduce ILs within the final epoxy network from the fabrication and use of IL filled polysulfone microcapsules. The authors reported that when 20 wt% of IL containing microcapsules were added in the epoxy material, the friction coefficient and specific wear rate of composites were reduced by 66.7 % and 64.9 %, respectively. The effective boundary film formed by released IL from broken microcapsules is the mechanism of self-lubricating (Figure 1-20).

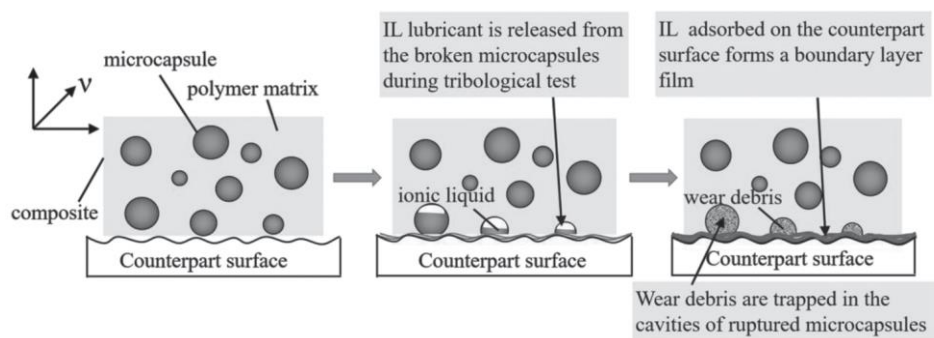


**Figure 1-20** Boundary film formation process during sliding wear from IL-filled microcapsules breakage [83]

Except the applications for green chemistry, electrochemical fields and lubricant applications, ILs can also play various roles combined with thermoset polymer matrices, including epoxy resins. These new combinations have led to additional opportunities for ILs to design PMC materials. For these reasons, combination between epoxy networks and ILs will be introduced in the following section.

## 1.2.2 Epoxy networks

### 1.2.2.1 Introduction

Epoxy resin is an organic polymer compound containing two or more epoxy groups, which can lead to a thermosetting network according to the chemical reactivity of the epoxy groups to

be opened by a variety of compounds containing active hydrogen leading to 3D-networks. Because of their good mechanical properties [84], dimensional stability [85], dielectric properties [86] and chemical stability [87], epoxy networks are considered for aerospace applications [88-90], industrial areas [91] and daily life applications [92]. According to their chemical structure, epoxy resin can be divided into several groups: (1) DGEBA: diglycidylether of bisphenol A, (2) DGEBF: diglycidylether of bisphenol F, (3) DGEbiphenyl: diglycidylether of biphenyl, (4) Phenol novolac type epoxy, (5) Phenoxy resin [93], and their chemical structures are illustrated in Figure 1-21.

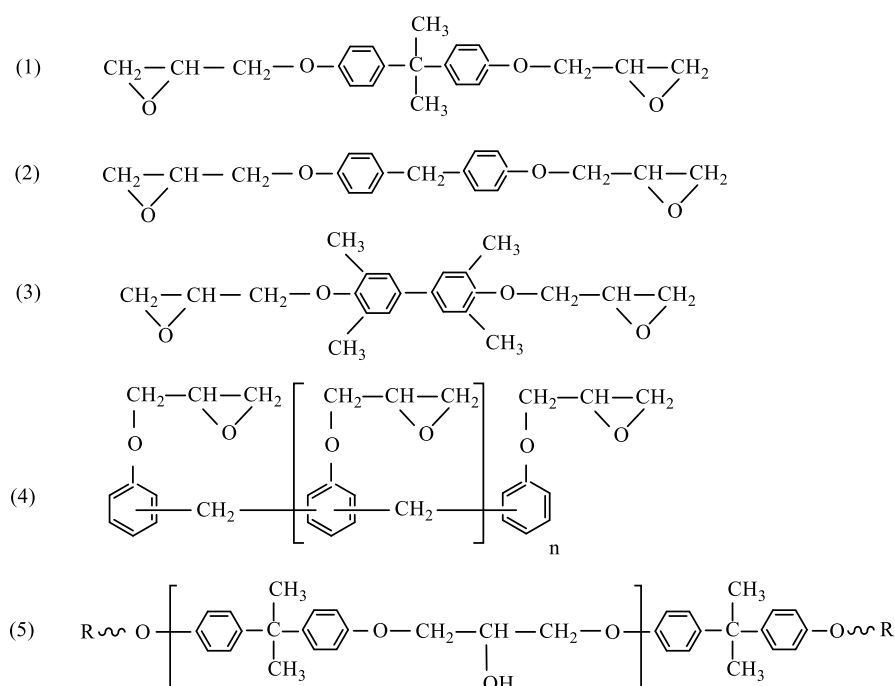


**Figure 1-21** Chemical structures of the common epoxy resins: (1) DGEBA: diglycidylether of bisphenol A, (2) DGEBF: diglycidylether of bisphenol F, (3) DGEbiphenyl: diglycidylether of biphenyl, (4) Phenol novolac type epoxy, (5) Phenoxy resin

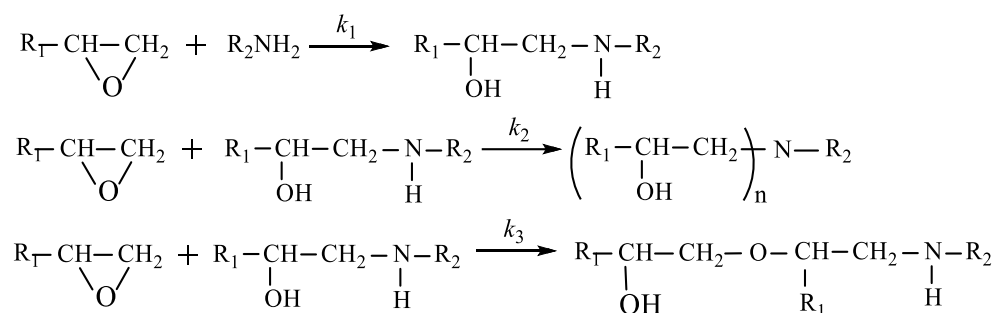
### 1.2.2.2 Building epoxy networks

Epoxy combined with/without comonomers such as diamine or anhydride lead to polymer network with reliable mechanical properties [94].

#### Step-growth polymerization

In step-growth polymerization, a bi-functional or multifunctional monomer will react to form first dimers, trimers, oligomers including long chain polymer chains according to step-by-

step succession reaction. Based on this protocol, amines, phenols, mercaptans, or acids could be considered as curing agents. Let us consider amine as an example, reacting with epoxy groups according to stoichiometric ratio, the reaction between epoxy prepolymer and amine according to step-growth polymerization mechanism can be theoretically described in Scheme 1-6. When there are more epoxy groups or when the secondary amino groups are too inactive to continue the opening of the epoxy rings, the side reaction also named etherification will take place. Generally, using a curing agent with a high curing temperature leads to a cured epoxy material with good heat resistance and thermal properties. For addition polymerization type, curing temperature and heat resistance increase with the hardener nature in the following order: aliphatic polyamine < alicyclic polyamine < aromatic polyamine  $\approx$  phenolic < acid anhydride.



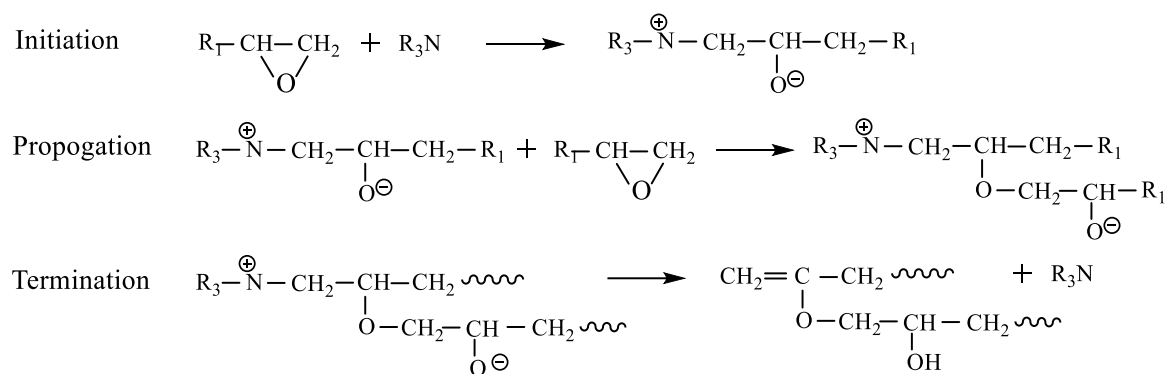
**Scheme 1-6** Cure mechanism between epoxy and amine

### Chain-growth polymerization

A step-growth reaction happened between two molecules with same or different degree of polymerization and monomers will transfer into dimers, trimers and finally long chain polymers which is based on their functional group. Differ from the step growth polymerization, in chain-growth polymerization, the monomer is consumed steadily but the degree of polymerization can increase very quickly after chain initiation. Chain-growth polymerization contains several steps: chain initiation, chain propagation, chain termination and chain transfer, but the latter two steps are not necessary in a chain-growth polymerization. There are different types of chain growth polymerizations, such as radical polymerization, ionic polymerization, coordination polymerization, etc. And for epoxy monomer, polymerization was usually initiated by anions or cations.

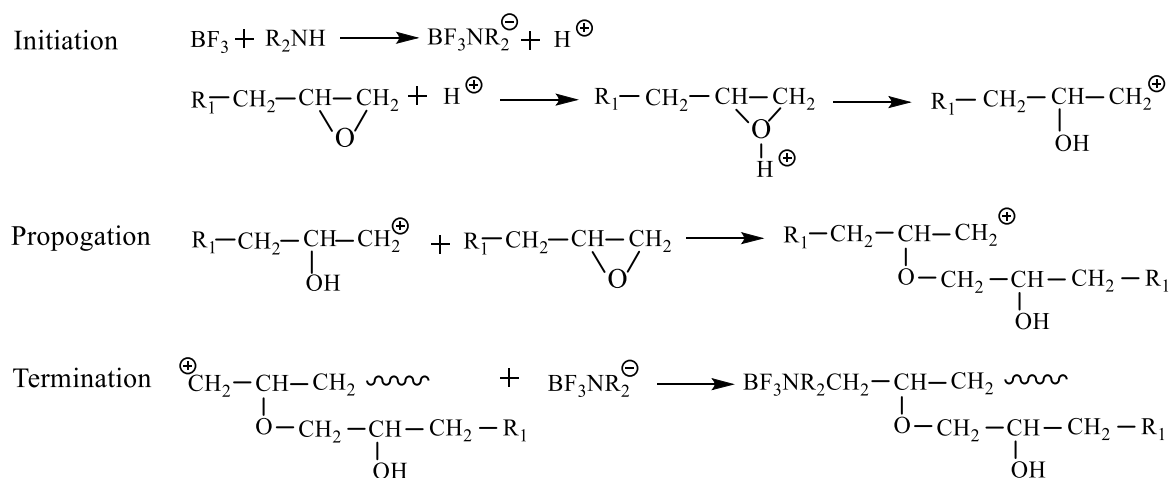
Nucleophilic and electrophilic species can both react with epoxy group, which initiate

chain polymerization of epoxy monomers. In fact, the curing agent based on this chain-growth polymerization mechanism plays a catalytic role in the reaction. This kind of material mainly triggers the epoxy ring open polymerization reaction among epoxy molecules to form the crosslinked polymer, while the curing agent itself does not participate in the cross-linked network. Lewis bases such as tertiary amines, imidazoles, ammonium salts are initiators of anionic chain polymerization. For example, the epoxy polymerization induced by tertiary amines can be roughly described in Scheme 1-7.



**Scheme 1-7** Mechanism of epoxy polymerization induced by tertiary amines

Lewis acids such as diaryl iodonium, triarylsulfonium or arene diazonium can initiate cationic polymerization. Similar to the anionic chain polymerization, there are also three steps in cationic polymerization: initiation, chain propagation and chain termination. By considering boron trifluoride as an example, the cationic polymerization of epoxy prepolymer can be described in Scheme 1-8.



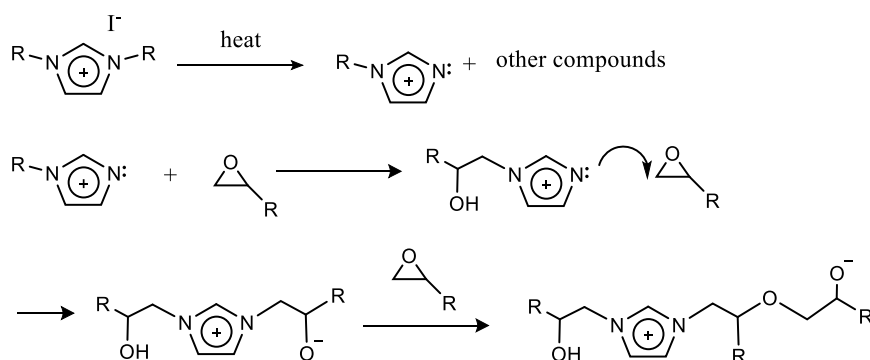
**Scheme 1-8** Mechanism of cationic polymerization of epoxy prepolymer

### 1.2.3 Ionic liquids combined with epoxy networks

After the research done by Kowalczyk <sup>[95]</sup> on 1-butyl-3-methylimidazolium tetrafluoroborate (BMITF) which can be used as hardener of epoxy resin, numerous researchers are trying to find more applications for ionic liquids in epoxy composites. It is because of its unique properties that ionic liquids are widely used as hardener, dispersing agents, lubricant or other functional additives in epoxy matrix composites. Some remarkable combinations of epoxy chemistry and ionic liquids were generally introduced, leading to the reported overview for the applications of ionic liquid in polymer matrix composites, especially in epoxy composites.

#### 1.2.3.1 As hardener or initiator for the curing of epoxy prepolymer

The ionic pair nature of ILs and the ionic polymerization mechanisms with epoxy monomer provide the theoretical evidence that IL could act as hardener for epoxy monomers. As reported by Kowalczyk <sup>[95]</sup>, 1-butyl-3-methylimidazolium tetrafluoroborate (BMITF) can be used as hardener for bisphenol A based epoxy resin (Epidian 6, E6, epoxy equivalent weight 185). As a consequence, researchers have paid more attention on IL hardeners to further investigate the IL-epoxy networks and their resulting properties. Imidazolium IL is a broad family that can be considered for hardeners of epoxy prepolymers. Reaction mechanisms of imidazolium ILs (coupled with inert iodide anion)-initiated epoxy crosslinking reported in several researches <sup>[96-99]</sup> is demonstrated in Scheme 1-9.



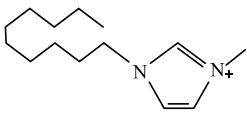
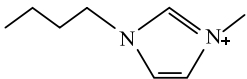
**Scheme 1-9** Proposed mechanism for curing initiated by imidazolium IL of epoxy monomer <sup>[99]</sup>

Maka *et al* <sup>[100]</sup> have chosen imidazolium-type ILs differing by the alkyl chain length of imidazolium cation and different anions to form IL-epoxy networks before investigating the



final properties of resulting IL-epoxy networks. The considered imidazolium-based ILs are presented in Table 1-1. In a first step, basic anions such as  $\text{N}(\text{CN})_2^-$  and  $\text{Cl}^-$  undergo deuterium exchange with imidazolium cation. In a second step, a pyridine-type of nitrogen involved in the imidazole derivative reacts with the epoxy group to form a 1:1 adduct. Subsequently, the anionic polymerization between epoxy prepolymers proceeds to form the final epoxy network. The authors also found that different cation size, anion type and concentration of imidazolium-based ILs have a huge influence on the curing kinetics and resulting properties of IL-epoxy networks. For example, the curing temperature with epoxy of imidazolium-based IL combined with  $\text{N}(\text{CN})_2^-$  anion is lower than that associated with  $\text{BF}_4^-$  anion and imidazolium IL having a decyl substituent group has slightly higher onset curing temperature.

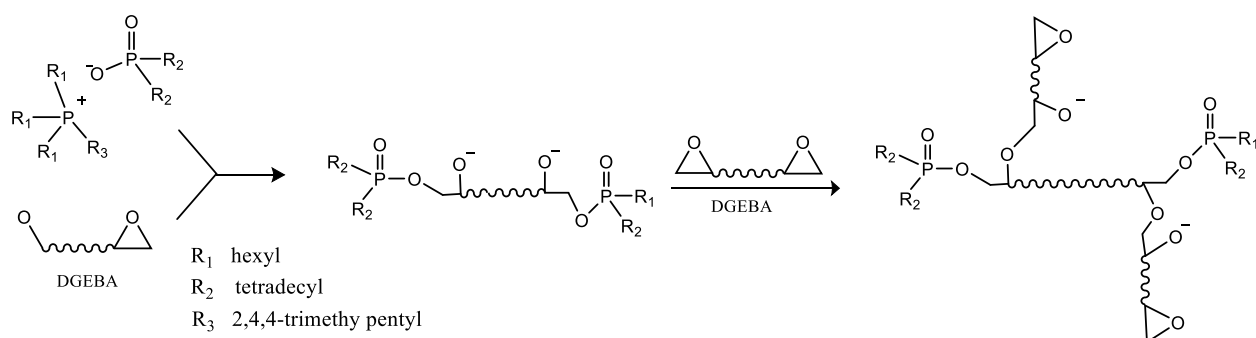
**Table 1-1** Description of imidazolium-based ILs considered in Maka's researches <sup>[100]</sup>

Cations	Anions	Acronym
	$\text{Cl}^-$	[DMIM]Cl
	$\text{BF}_4^-$	[DMIM]BF <sub>4</sub>
	$\text{N}(\text{CN})_2^-$	[DMIM]N(CN) <sub>2</sub>
	$\text{BF}_4^-$	[BMIM]BF <sub>4</sub>
	$\text{N}(\text{CN})_2^-$	[BMIM]N(CN) <sub>2</sub>

Apart from acting directly as initiator for epoxy prepolymers, the role as curing initiator of imidazolium-based ionic liquids with long alkyl chains combined with diamines leading to the epoxy amine networks was also reported. Soares *et al* <sup>[101]</sup> studied the role of imidazolium-based ionic liquid for epoxy-amine curing. For example, N,N'-dioctadecylimidazolium iodide was added to DGEBA and 4,4'-methylenebis(3-chloro-2,6-diethylaniline) (MCDEA) comonomers at various weight fractions. The presence of imidazolium-based ionic liquid led to a decrease of the glass transition temperature of the resulting network. As the onset temperature for curing such reactive system decrease with IL content, it could be concluded that IL has a promoting effect on the epoxy-amine copolymerization. In addition, one can deduce decomposition products of the imidazolium-based IL are responsible for this catalytic

effect. The final homogeneous epoxy networks display very good dynamic mechanical properties compared to conventional networks from a weight addition (1–5 phr) of imidazolium-based ionic liquid.

Phosphonium-based ILs, as one of the main categories of ILs, are also used as curing agents for epoxy compounds [102]. Small amount of phosphonium-based type IL could result in IL-epoxy networks with improved properties, including thermal properties and high hydrophobicity. For example, trihexyl(tetradecyl) phosphonium bis(2,4,4-trimethylpentyl)phosphinate (IL104) was considered as model IL to explain the previously proposed mechanism for bisphenol A-based epoxy prepolymer (DGEBA) polymerization [103], (Scheme 1-10). Nguyen [104] also mentioned that the nature of the anion has a huge influence on the curing behavior of phosphonium-based IL/DGEBA systems because of their different basicity among anions. For example, phosphate anion has a lower basicity than phosphinate anion which possesses longer alkyl group. As a consequence, the phosphonium phosphate-based IL will have a higher curing temperature than that of phosphonium phosphinate-based IL.



**Scheme 1-10** Proposed mechanism for the polymerization of epoxy resin (DGEBA) in the presence of IL 104 [103]

Because of the ion pairs nature for the various ILs, the dielectric properties could be enhanced simultaneously due to the high ion conductivity of IL confined in the epoxy network architecture. Lefort *et al* [105] have used phosphonium-based IL to initiate the polymerization of DGEBA. An increase of the segmental mobility was observed for the resulting networks. In fact, a significant increase of the DC conductivity until 2 decades higher than a conventional epoxy/anhydride system has achieved for such network. As IL could act also as a plasticizer, a decrease of the glass transition temperature was noticed (Figure 1-22).

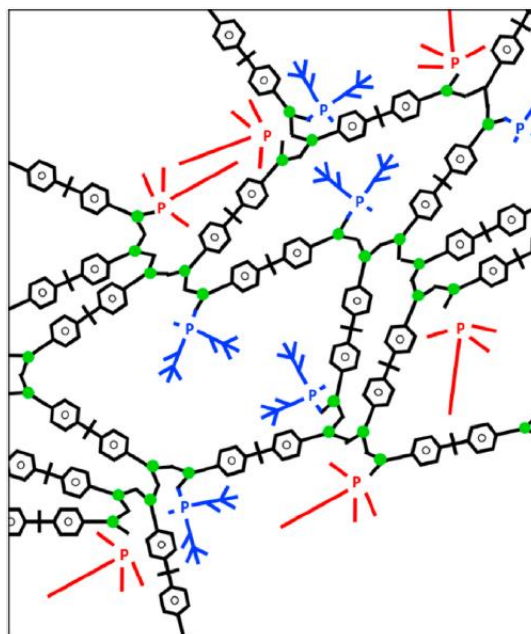
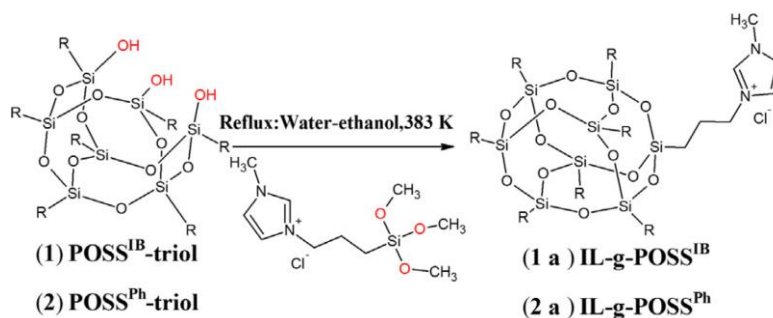


**Figure 1-22** Epoxy network scheme. The network results from the homopolymerization in presence of IL: (blue) IL anion, (red) IL cation, (black) pre-polymer; (green) crosslinks <sup>[105]</sup>

### 1.2.3.2 As dispersing aids of nanomaterials/nano-objects within polymers

Ionic liquids can be considered as reactants, initiators as well as components being able to participate to the curing process of epoxy networks. In addition, ILs can also be used as processing aids of nanomaterials/nano-objects in polymer materials. As known, properties of materials at nanoscale could differ from those of bulk matter <sup>[106]</sup>. As a consequence, emerging nanomaterials have been developed for various application: environment applications <sup>[107]</sup>, biomedicine <sup>[108]</sup>, structure materials <sup>[106]</sup>, etc. Getting a high dispersion level of nano-particles remains a very difficult task which limits a huge development of polymer nanocomposites <sup>[109]</sup>. Conventional dispersion tools of such nano-particles in polymer matrices remain difficult due to agglomeration <sup>[110]</sup>. Therefore, surface modification including tailoring the particles or nano-objects surface using ILs is one of the most popular strategies <sup>[111]</sup>. Chabane *et al* <sup>[112]</sup> successfully grafted imidazolium-based ionic liquid as tethered ligands to polyhedral oligomeric silsesquioxane (POSS) cubes to obtain POSS-supported ILs whose chemical structure is presented in Scheme 1-11.



**Scheme 1-11** Synthesis of imidazolium ILs-modified POSS <sup>[112]</sup>

Two kinds of obtained POSS-supported ILs, denoted IL-g-POSS<sup>IB</sup> and IL-g-POSS<sup>Ph</sup> respectively, were added into epoxy networks. It is shown in Figure 1-23, IL-functionalized POSS (IL-g-POSS<sup>IB</sup> and IL-g-POSS<sup>Ph</sup>) were found to be well dispersed in epoxy networks compared to the unmodified POSS (POSS<sup>IB</sup>-triol, POSS<sup>Ph</sup>-triol, IL-g-POSS<sup>IB</sup>, and IL-g-POSS<sup>Ph</sup>) (Figure 1-23).

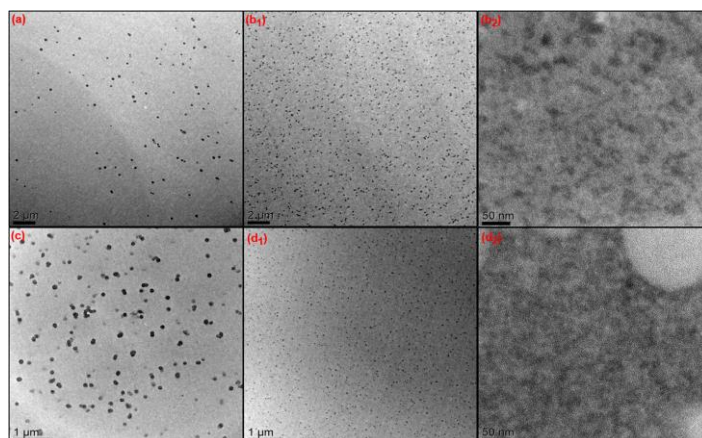


**Figure 1-23** TEM micrographs of epoxy amine networks modified with: (a) POSS<sup>IB</sup>-triol and (b) IL-g-POSS<sup>IB</sup> at different magnification (b<sub>1</sub>; b<sub>2</sub>), (c) POSS<sup>Ph</sup>-triol and (d) IL-g-POSS<sup>Ph</sup> at different magnifications (d<sub>1</sub>; d<sub>2</sub>) <sup>[112]</sup>

### 1.2.3.3 As flame retardant agents

ILs were also used to lead an efficient flame-retardant behavior of epoxy network. For example, Xiao *et al* <sup>[113]</sup> have introduced a phosphonate-based IL named 1-vinyl-3-(diethoxyphosphoryl)-propylimidazolium bromide into an epoxy resin. Because of the presence of phosphonate-based IL which can promote the formation of a compact and stable phosphorus-rich residual char inhibiting the heat transfer and degradation of epoxy resin, an enhanced fire

resistance was observed. Based on similar concept, Chabane *et al* <sup>[114]</sup> synthesized ionic liquid supported on oligomeric silsesquioxane nanoclusters (POSS) as flame retardant additives of epoxy composites. In their study, imidazolium-based IL was combined to chloride ( $\text{Cl}^-$ ) and bistrifluoromethanesulfonimide ( $\text{NTf}_2^-$ ) anions which were grafted onto the POSS nanoclusters as additives of epoxy-amine networks. Such resulting organic-inorganic nanomaterials not only display an improved flame retardancy behavior, but also improve the mechanical behavior.

### 1.2.4 Conclusions

This part has briefly introduced ionic liquid (IL), epoxy and combination of epoxy and IL through different methods. The advantages of ILs related to their zero vapor pressure, thermal stability, numerous combinations and approaches of anions and cations make possible to consider them for green chemistry as solvents or catalysts. Epoxy resins are widely used as thermoset materials due to their good mechanical properties and dielectric properties. The combination of these two components could generate from a synergistic effect an expected behavior. In fact, numerous researches have revealed the potential roles of ILs in epoxy-based materials, including their role as curing initiator, processing aids, compatibilizers, lubricants, or other functional additive contribution.

## 1.3 Microencapsulation

### 1.3.1 Introduction

Microencapsulation is an effective method to confine a liquid or a solid material using a continuous organic or inorganic wall material to preserve the biological, functional, and physico-chemical properties of core materials <sup>[115, 116]</sup>. Materials in different states, *i.e.* liquids <sup>[117]</sup> such as oil <sup>[118-120]</sup>, aqueous solution <sup>[121, 122]</sup>, or solid <sup>[123]</sup>, can be considered as core materials for microencapsulation. Meanwhile, for shell materials, there are several basic rules: (1) shell material should be stable and not react with core material; (2) shell material should have certain mechanical strength to prevent the microcapsule from damaging during processing; (3) shell material should be non-toxic in food industry or biomedical applications; (4) solubility, hygroscopicity, dielectric property, or degradability can also be acquired for specific

applications. Based on these principles, considering natural or synthetic wall materials (Table 1-2), different applications of microcapsules are listed in Table 1-3.

**Table 1-2** Natural and synthetic wall materials in microencapsulation and their main characteristics

Classification	Shell materials	Main features
Natural materials	- Proteins: collagen, albumin and gelatin <sup>[124]</sup>	Non-toxic, good biocompatibility, low cost, poor mechanical properties, poor resistance to high temperature
	- Carbohydrates: starch, agarose, chitosan, and carrageenan <sup>[125]</sup>	
	- Chemically modified carbohydrates: poly dextran, poly starch	
Synthetic materials	- Biodegradable polymers: lactides, glycolides, poly anhydrides and poly(alkyl cyanoacrylates), etc.	Good film formation, good mechanical strength, easy to prepare, high price, poor biocompatibility
	- Non-biodegradable polymers: poly methyl methacrylate (PMMA), glycidyl methacrylate, acrolein, epoxy polymers	
	Inorganic materials	Silica <sup>[126]</sup> , glass <sup>[127]</sup> , ceramics <sup>[128]</sup>

**Table 1-3** Functional properties of different microcapsules

	Core Material	Encapsulant	Functional properties
Drugs	Amphotericin B, doxorubicin, cytarabine, doxorubicin, etc. <sup>[129]</sup>	Phospholipids	Drug delivery
Nutrients	Vitamins B <sub>2</sub> /C, $\alpha$ -tocopherol, essential oils <sup>[130]</sup>	Chitosan or modified chitosan	Protection and controlled release of bioactive food ingredients
Synthetic components	Ionic liquids <sup>[131]</sup> , epoxy <sup>[132]</sup> , DCPD <sup>[133]</sup> , linseed oil <sup>[42]</sup> , etc.	Synthetic materials	Self-lubricant or self-healing function in polymer materials

### 1.3.2 Synthesis strategies for microencapsulation

According to different routes for designing core-shell materials, various strategies have been proposed for the fabrication of microcapsules. Usually, depending on the preparation processes, these methods can be divided into three main routes: (1) Physical processes: such as solvent evaporation, spray drying, electrostatic deposition, etc; (2) Chemical processes: such as *in-situ* polymerization, interfacial polymerization, etc; (3) Physicochemical processes: such as coacervation (phase separation), etc. [134]. Solvent evaporation, spray drying as physical process, *in-situ* polymerization, and interfacial polymerization as chemical process are commonly used methods in industry.

#### 1.3.2.1 Solvent evaporation

Solvent evaporation for fabricating microcapsules is widely used in pharmaceutical industries, which can facilitate a controllable drug release of a drug or other functional core material [135]. Figure 1-24 has demonstrated the common procedure of solvent evaporation method for microencapsulation.

Basically, the core material to be microencapsulated by solvent evaporation method is dissolved in the shell material solution, which is immiscible in the third, *i.e.* the liquid phase (solvent for shell material). Then, the mixture is stirred continuously and sometimes accompanied with heating. The microcapsules are then obtained after completed evaporation of the solvent [136]. While the choice of the solvent and the dispersing liquid phase are dependent on the hydrophilicity and hydrophobicity of the core and shell components [137], different systems may be considered such as oil-in-water (O/W) [138], water-in-oil (W/O) [139], oil-in-oil (O/O) [140], water-in-oil-in-water (W/O/W) [141, 142], or solid-in-oil-in-water (S/O/W) [143] emulsions. In addition, the stirring speed, the solvent concentration, or the evaporation rate will have an important effect on the morphology of the obtained microcapsules.

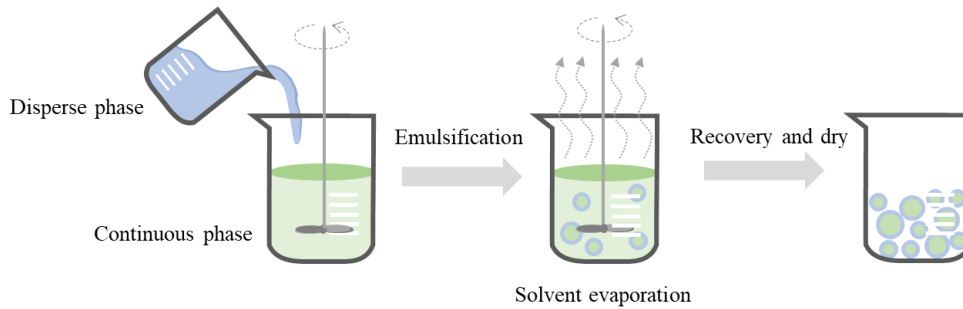


**Figure 1-24** Solvent evaporation method for fabricating microcapsules

### 1.3.2.2 Spray drying

Spray drying is one of the most popular methods for microencapsulation, such as for conversion of liquid flavor compounds into easy-to-handle solid state microcapsules [144]. Spray drying is suitable for heat sensitive compounds as it can produce powder directly from a solution or slurry with good quality, low water activity, and storage ability [145]. In the food industry, spray drying is one of the oldest and most popular technologies for microencapsulation of different ingredients because of its low cost, flexibility, and high quality of products [146] while the most important drawback of spray drying is the limited number of suitable shell materials [147]. The Figure 1-25 illustrates the conventional spray drying process. In the spray drying process, five steps are involved: *i*) liquid feed, *ii*) atomization, *iii*) droplet-air contact, *iv*) droplet drying and *v*) separation [148]. For example, fish oil was microencapsulated in a sugar beet pectin and glucose syrup shell by spray drying [149]. In the latter example, the average oil droplet size was significantly influenced by the composition of the emulsion and the homogenization pressure. However, a high proportion of non-encapsulated components, *i.e.* higher than 50%, was not introduced in the microcapsules.

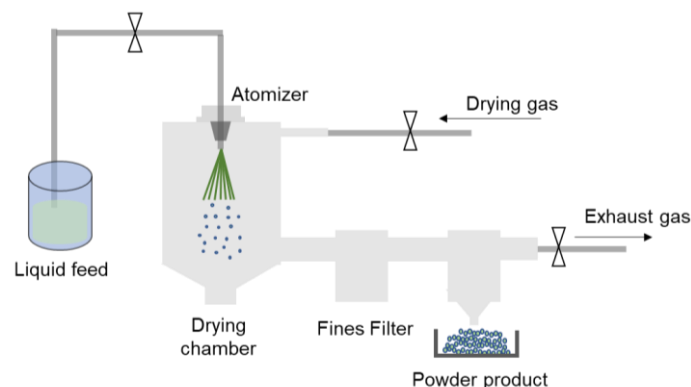


**Figure 1-25** Graphic illustration of typical spray drying system



Shamaei *et al* <sup>[150]</sup> have studied the influence of shell material and spray drying parameters on the physico-chemical properties of walnut oil-filled microcapsules. Three different shell materials including skim milk powder (SMP), SMP + Tween 80, and SMP + maltodextrin were compared for emulsion. The inlet drying air temperature and feed atomization pressure were also investigated. The authors found that increasing the inlet drying pressure and feed atomization temperature led to an increase of the microencapsulation efficiency and contributed to decrease the moisture content while decreasing the atomization pressure will increase the particles size. Among the three shell materials, the highest microencapsulation efficiency was obtained by using a mixture SMP and Tween 80.

### 1.3.2.3 *In-situ* polymerization

*In-situ* polymerization is one of the most widely used chemical process for fabricating microcapsules with synthetic material (polymers in most cases). In fact, *in-situ* polymerization has many advantages for microcapsules with core/shell structure control, such as size and shell thickness tailoring. Thus, microcapsules with tailored mechanical properties and improved thermal stability could be obtained <sup>[151, 152]</sup>. In addition, this method can lead to high yield rate of encapsulation and inexpensive involved costs <sup>[153]</sup>. As the prepolymer will form in the continuous phase <sup>[154]</sup>, typical shell materials are considered such as urea-formaldehyde <sup>[155-157]</sup> and melamine-formaldehyde systems <sup>[153, 158, 159]</sup>. Conventional processing protocol is given in Figure 1-26.

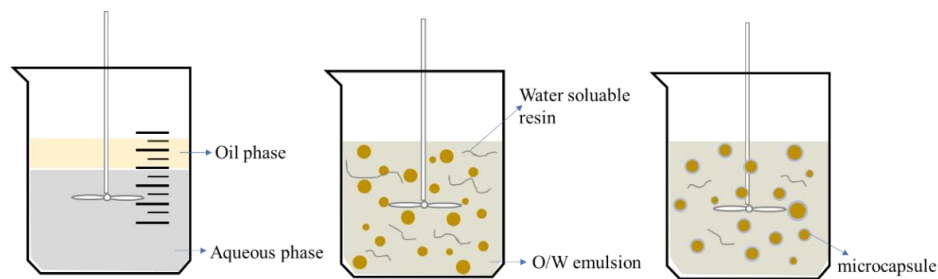


**Figure 1-26** Conventional synthesis of microcapsules considering *in-situ* polymerization in the O/W emulsion state

For example, Hwang <sup>[160]</sup> used such *in-situ* polymerization process to fabricate microcapsules. The authors have prepared melamine-formaldehyde shell microcapsules containing peppermint oil from such *in-situ* polymerization process involving Tween 20 as

emulsifier. The microcapsules with melamine-formaldehyde shell have good durability and reasonable heat-resistance characteristics. These ones are able to release their fragrance via the destruction of the shell instead of a passive diffusion at room temperature. First, the peppermint oil was emulsified by Tween 20 under mechanical stirring to form an oil-in-water (O/W) emulsion. Then, the pre-prepared prepolymer was added in the O/W emulsion for encapsulation reaction. For the *in-situ* polymerization process, the polymerization occurs mainly in the continuous phase and the surface of dispersed oil droplets form the rigid polymer shell. The microcapsules by *in-situ* polymerization could display a perfect sphere shape while sometimes due to shear forces occurring for various dispersion methods could lead to a broad distribution of particles sizes and shapes.

#### 1.3.2.4 Interfacial polymerization

Interfacial polymerization is another common chemical method for polymer shell based microencapsulation, which differs from *in-situ* polymerization in which polymerization takes place in the continuous phase. In the interfacial polymerization process, the monomer will be directly introduced in the disperse phase or the continuous phase of the emulsion. The shell will be polymerized directly at the interface of the disperse phase and continuous phase. There are two possibilities during the particle/capsule formation process as shown in Figure 1-27: (1) the oligomers formed at the early stage are highly soluble in the droplets; (2) the oligomers at the early stage are highly insoluble in the droplets <sup>[161]</sup>.

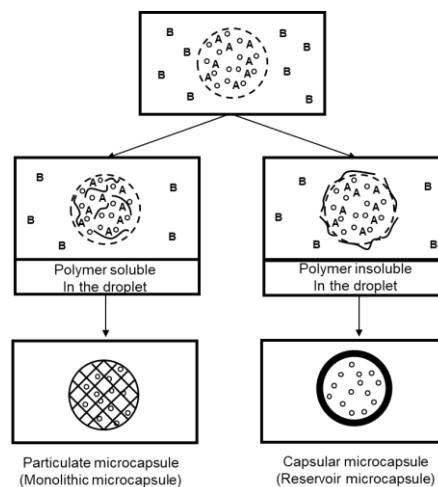


**Figure 1-27** Idealized mechanism of particle/capsule formation by interfacial polymerization <sup>[161]</sup>

Microcapsules obtained via interfacial polymerization are considered for encapsulation of various compounds such as adhesives, agrochemicals, live cells, enzymes, flavors, fragrances, drugs, and dyes, in whether water-in-oil (W/O) or oil-in-water (O/W) emulsions interfaces. In some researches, oil-in-oil (O/O) emulsion is also used for fabricating microcapsules [162-164]. For O/W emulsions, polymerization between polyfunctional isocyanates and diamines for synthesizing polyurea microcapsules is usually considered. For instance, Scarfato *et al* [165] have synthesized polyurea microcapsules containing active essential oils for agricultural applications by interfacial polymerization. The obtained microcapsules are suitable for realizing sustained release systems. Wang *et al* [166] also prepared microcapsules by interfacial polymerization between polyamines and a pyromellitic diester diacid chloride to obtain polyamide microcapsules in which diacid chloride and dye were encapsulated. The obtained microcapsules are stable in a dry or non-polar environment but undergo controlled release at pH 7.4 and accelerated release at pH 5 and pH 10. The release rate of core component is dependent on the by the crosslinking degree of the polymer shell. Phase changed emulsion, W/O emulsion, was considered to encapsulate hydrophilic materials. Hayashi *et al* [167] have encapsulated erythritol as a phase change material into a polyurethane shell. They demonstrated that isocyanate species are required to obtain microcapsules, such as toluene diisocyanate, diphenyl methane diisocyanate, hexamethylenediisocyanate, among which toluene diisocyanate showed the largest heat density and the highest microencapsulation efficiency.

Compared with interfacial polymerization in O/W and W/O emulsions, O/O emulsions are hardly used for microencapsulation because of the difficulty during the stabilization process of the emulsion and the polymerization control. For example, Kobašlija *et al* [168] have prepared microcapsules with polyurea shell by interfacial polymerization in oil-in-oil emulsion, including methanol-in-cyclohexane, formamide-in-cyclohexane, and N,N-dimethylformamide-in-cyclohexane emulsions. Actually, the conventional interfacial polymerization is processed mostly in O/W or W/O emulsion. The authors also suggested that oil-in-oil emulsions could be an alternative to commonly used approaches. As shown in Figure 1-28, the authors used polar protic or aprotic solvent-in-cyclohexane emulsions to template the formation of polyurea microcapsules and set up a model for interfacial polymerization of oil-in-oil emulsions. The changes of the observable characteristics, such as capsule sizes, are monitored as a function of

the input parameters, such as monomer concentration or stirring speed.

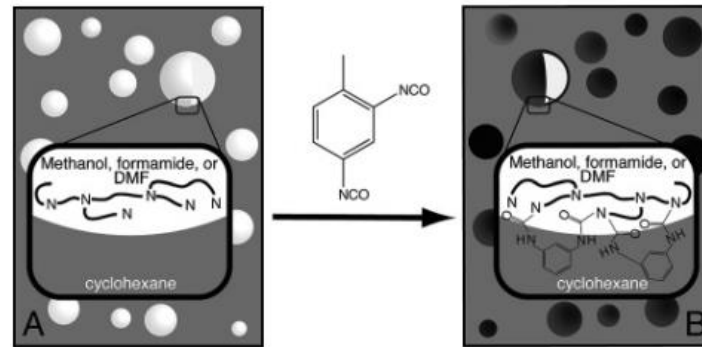


**Figure 1-28** (A) Emulsions are prepared by dispersing a polar phase containing anhydrous polyethylenimine (PEI) into a nonpolar phase; (B) A cross-linked polyurea shell forms upon addition of 2,4-toluene diisocyanate (TDI) to the continuous phase <sup>[168]</sup>

In addition to the use of a separated polymerization process to produce a single shell for microcapsules, these two strategies were combined to fabricate multi-shell microcapsules. For example, Li *et al* <sup>[169]</sup> have used both interfacial polymerization and *in-situ* polymerization to obtain mono dispersed polyurea-urea formaldehyde double layered microcapsules. As shown in Figure 1-29, polyurea microcapsules were synthesized during a first step by interfacial polymerization as the inner layer. In a next step, urea-formaldehyde (UF) resin was deposited to form the outer protective layer by *in-situ* polymerization. This combination of different strategies leads to double layered shell microcapsules. This type of ultra-thick shell displays presented an improved thermal stability compared to traditional microcapsules with a single shell.

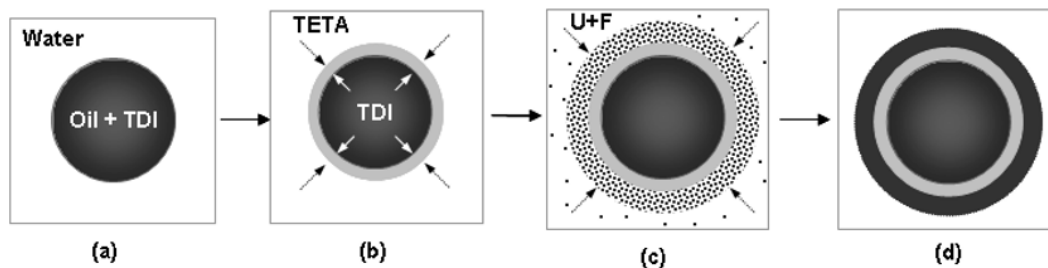


**Figure 1-29** Schematic diagram of synthetic process of double layered microcapsules: (a) O/W emulsion; (b) formation of the inner PU layer; (c) condensation of the UF resin; (d) consolidation of the outer layer <sup>[169]</sup>

Apart from the four methods that have been mentioned above, electrostatically self-assembly <sup>[170]</sup> and coacervation (phase separation) <sup>[171, 172]</sup> are also used to fabricate various kinds of microcapsule. Overall, the choice of synthesis method for preparing microcapsules should be based on the nature of core and shell components, the encapsulation efficiency and cost.

### 1.3.3 Applications of microcapsules

#### 1.3.3.1 For biomedical uses

During the past few decades, increasing researches of microcapsules for biomedical applications such as drug delivery, biosensors, and bioreactors have received a widespread attention <sup>[173]</sup> because of high payloads of active substances <sup>[174]</sup>. In fact, one of the main advantages of microcapsules is protection of sensitive drugs from drastic environment (such as pH exposure) as well as reduction of the number of drug administrations for the patients <sup>[175]</sup>. Kalaycioglu *et al* <sup>[176]</sup> prepared nano-in-micro ibuprofen (IBU)-filled microcapsules using a layer-by-layer method having an increased efficiency, a high surface area, a tunable structure, and a multi-functionality. Figure 1-30 presents the synthesis procedure of IBU microcapsules and the related drug release model. As, shown in Figure 1-30, solid lipid nanoparticles (SLN) were used to create a negatively charged shell and gold nanoparticles (AuNP) and chitosan (CHI) were used as positively charged shell, in order to tune the ascorbic acid (AA) release kinetics.

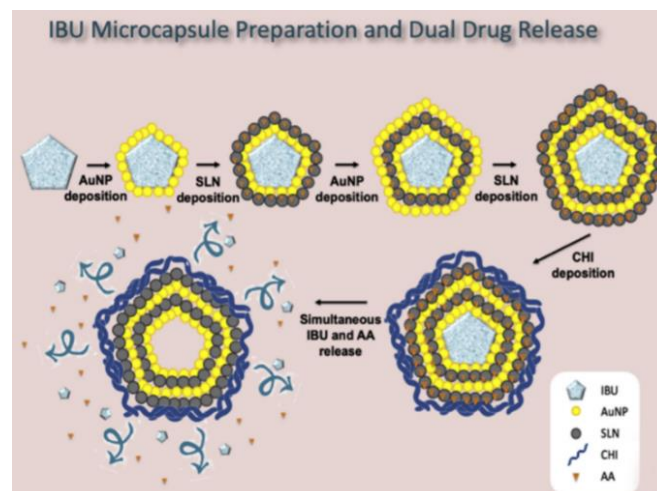


**Figure 1-30** Synthesis procedure of IBU microcapsules and the controllable drug release model <sup>[176]</sup>

Apart from drug delivery, biosensors are also an important part for the use of microcapsules for biomedical applications. Kreft *et al* <sup>[177]</sup> reported a new kind of mobile pH-sensor for monitoring the pH inside the living cells by loading high molecular weight seminaphtho-rhodafluor-1-dye (SNARF-1-dextran conjugate) in polyelectrolyte microcapsules. They demonstrated that SNARF-1 shows a dramatical pH-dependent emission shift from green to red under different pH environment as there is no change after the encapsulation process. Figure 1-31 shows the structure of microcapsules and fluorescence effect of this pH-sensor at acidic and alkaline circumstances. They have successfully followed the pH change of the local environment of SNARF-1-filled microcapsules in human breast cancer cells and fibroblasts when the pH changes.

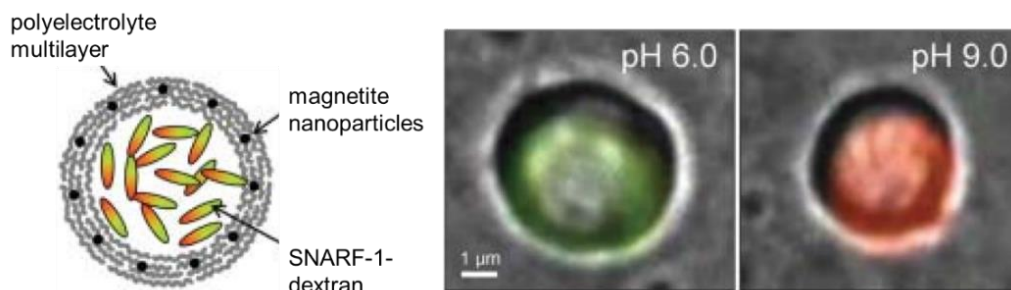


**Figure 1-31** Scheme of the capsule geometry and fluorescence microscopy images of single capsules under acidic (pH 6.0, green) and alkaline (pH 9.0, red) pH <sup>[177]</sup>

### 1.3.3.2 In food industry

In the food industry, food quality could be improved by encapsulating flavors, leavening agents, vitamins, and enzymes could in microcapsules <sup>[178]</sup>. For example, wall materials of microcapsules can prevent the ingredients from oxidation or undesirable interactions and stabilize some sensitive components such as vitamins and minerals. Several microencapsulated strategies can be applied in the food industry, such as spray drying, fluidized bed coating, solvent extraction, coacervation, co-crystallization and liposome formation. Contact materials in food industry have basic requirements, including non-toxicity, compatibility with food content and mechanical performances, etc. There are six main categories for contact materials for microcapsules in food industry, which are summarized in Table 1-4.

**Table 1-4** Different contact materials for microcapsules for food industry

Classifications	Specific types
Gums	Gum arabic, agar, sodium alginate, carrageenan
Carbohydrates	Starch, dextran, sucrose, corn syrup
Celluloses	Carboxymethylcellulose, methylcellulose, ethylcellulose, nitrocellulose, acetylcellulose, cellulose acetate-phthalate, cellulose acetate-butylate-pgthalate
Lipids	Wax, paraffin, tristearin, stearic acid, monoglycerides, diglycerides, beeswax, oils, fats, hardened oils
Inorganic materials	Calcium sulfate, silicates, clays
Proteins	Gluten, casein, gelatin, albumin

### 1.3.3.3 In electronic devices

Xu *et al* <sup>[179]</sup> have fabricated microcapsules are used in constructing flexible supercapacitors by encapsulating the phase change materials into a polymer. Then, this microencapsulated phase change materials (MPCMs) are implanted into 3D porous reduced graphene oxide/polyaniline (GP) frameworks on the surface of carbon nanotube film (CNF) to create a new flexible supercapacitor. The structure of this new supercapacitor is shown in Figure 1-32. N-octadecane was encapsulated by melamine-formaldehyde resin by *in-situ* polymerization, which is for assembling of the flexible supercapacitor. The n-octadecane will undergo a phase change when the temperature changes, in which the endothermic effect will suppress the temperature fluctuation in order to enhance the stability of supercapacitor.

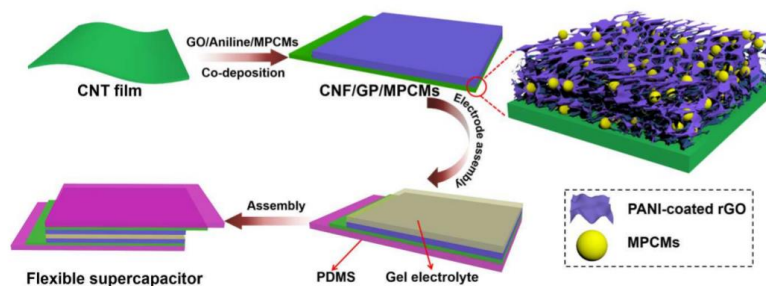


**Figure 1-32** Schematic structure of the supercapacitors containing microcapsules <sup>[179]</sup>

### 1.3.3.4 In polymer composites

Because of the processability, compatibility with polymer and polyfunctionality nature of the core/shell structure, microcapsules were also widely used as functional components in the polymer matrix composites. For instance, some of the polymer materials are facing the problem of poor performance in fire. As a consequence, fire retardants are used to improve the flame retardancy of polymer composites. Microcapsule is one of the efficient routes for introducing these additives in the polymer matrix to suppress the smoke or toxic gases. There are several advantages of microcapsules in flame retardant: (1) reducing the water solubility of flame retardants; (2) increasing the compatibility of flame retardants with the polymer matrix; (3) changing of the appearance and physical state of flame retardancy; (4) protection and increasing of the pyrolysis temperature of flame retardants; (5) prevention of the release of toxic gas and smoke <sup>[180]</sup>. Magnesium hydroxide ( $\text{Mg}(\text{OH})_2$ ) <sup>[181, 182]</sup>, red phosphorus <sup>[183, 184]</sup>, ammonium dihydrogen phosphate <sup>[185-187]</sup> are the conventionally used core materials in refractory materials.

Because of the core-shell structure and the controllable release feature, self-lubricating is another major application of microcapsules in polymer matrix composites. Due to the mobility of microcapsules, encapsulated-lubricant microcapsules can automatically lubricate the material whenever and wherever friction occurs. So, they have drawn great attention of researches for self-lubricate field applications <sup>[188]</sup>. Figure 1-33 demonstrates the expected self-lubricating mechanism induced by microcapsules.

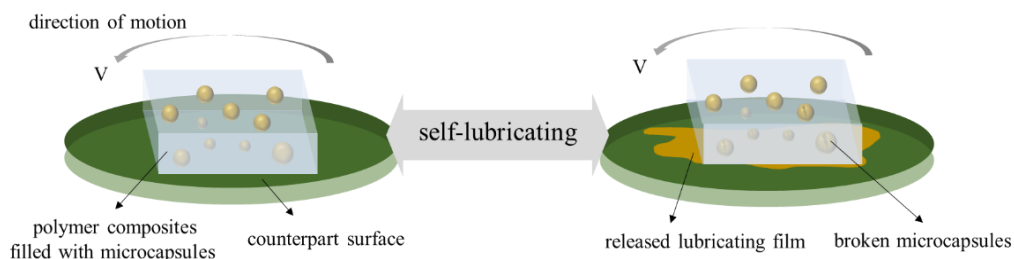


**Figure 1-33** Schematic diagram of microcapsules based self-lubricating mechanism

Li *et al* <sup>[189]</sup> have prepared  $\text{SiO}_2$  wrapped polystyrene microcapsules with a lubricant oil-filled microcapsules. The microcapsules have excellent dispersibility in epoxy coatings which display favorable antifriction effects. Despite of silica shell, polymer shell microcapsules are also studied for self-lubricating application, for example polysulfone shell <sup>[83]</sup>, polyurethane



shell or even double shell such as polysulfone/silica hybrid<sup>[190]</sup> or polyurethane/graphene oxide hybrid<sup>[191]</sup> as shell material. Compared with the shell material, core materials for self-lubricating microcapsules offers more choices. Wax, ionic liquids, tung oil<sup>[192]</sup>, etc can all be considered as lubricant oil for core components.

For the material working under harsh condition such as spacecraft or aircraft and materials which need to avoid electromagnetic interference (EMI) caused by proliferation such as electronic devices<sup>[193]</sup>, shielding property such as ultraviolet (UV) shielding, or electromagnetic shielding properties are required. Microcapsules encapsulated with proper shielding compounds can achieve these aims easily and universally. Specifically, metal-based and magnetic materials are favorable for electromagnetic shielding applications. For example, Jiang *et al*<sup>[194]</sup> encapsulated phase change materials (liquid paraffin containing magnetic nanoparticles, Fe<sub>3</sub>O<sub>4</sub>) into silica shell via interfacial polycondensation in a reverse emulsion. The obtained microcapsules showed a cup-like morphology core-shell structure, which has been proved a promising electromagnetic shielding additive in polyimide film. The authors also succeeded introducing magnetic particles as Fe<sub>3</sub>O<sub>4</sub>/SiO<sub>2</sub> hybrid shell to design new magnetic microcapsules, which can also absorb the electromagnetic radiations of conventional radar wavelength<sup>[195]</sup>. In the UV shielding field, nano-titanium dioxide (TiO<sub>2</sub>) is an ideal candidate for their stability, photocatalytic properties and non-toxicity. Hong *et al*<sup>[196]</sup> added anatase nano-TiO<sub>2</sub> during polymerization process of polyurethane microcapsules to obtain a multifunctional microcapsules. The obtained spherical microcapsules have rough surfaces and attached particles. These ones can be applied for photocatalysis and UV resistance in polymer coatings.

Polymer matrix materials could undergo cyclic thermal or mechanical loads or other damages during long-term use, resulting in micro-cracks in the matrix. As a consequence, self-healing property is required to prolong the life time and prevent final damage. Microcapsules which can encapsulate healing agents and release them as microcracks happen in the matrix. Therefore, they can be considered as one of the convenient and universe methods based on extrinsic self-healing mechanism to achieve self-healing in the polymer composites. Common structure and examples will be given in details in the <1.1.3.2 Microcapsules for self-healing > section.

### 1.3.4 Conclusion

To conclude, this part generally introduced the microencapsulation and summarized different strategies and examples of microcapsules and their applications in different fields. For microencapsulation, physical and chemical procedures consist of spray drying, solvent evaporation, in-situ polymerization, interfacial polymerization, etc. were applied based on the different features of core and shell materials. It is also found that the properties of emulsion or suspension played a very important role on the morphology, size distribution as well as their properties of final microcapsules. Therefore, choosing appropriate core and shell materials and preparation methods will enable the preparation of microcapsules with different functions.

### 1.4 Conclusion of Chapter 1

Self-healing is one of the basic abilities of living organisms in the nature which can help them repair damages and extend their lives. Similarly, the self-healing concept is also introduced into numerous industrial materials to prolong their lifetime through different strategies. Therefore, intrinsic self-healing mechanism based on reversible interaction of molecular chains and extrinsic self-healing mechanism based on external healing agent are developed and applied in the real practice. Compared with intrinsic self-healing, without modifying material in the molecular level, only by introducing packed healing agent can achieve self-healing ability is the reason for which extrinsic self-healing mechanism is widely applied in polymer matrix materials, including epoxy composites.

Ionic liquids are salts in the liquid state with a melting temperature  $< 100$  °C consisting in numerous anions/cations combinations. Their low vapor pressure, inflammability and high ion conductivity make them widely used in organic synthesis, electrochemical devices and materials science. Epoxy resin is widely applied as structural parts, adhesives and coatings in industry, aerospace field and marine areas because of its excellent physical and chemical advantages, but microcracks are generated easily due to the inherent brittleness. According to the latest researches, ionic liquids are used directly as initiators and dispersing aids of nano-objects in epoxy composites to improve the toughness, but introduction of ionic liquids via microencapsulation for epoxy composites as enhancement or self-healing agent are remained vacant.

Reviewing previous studies, dicyclopentadiene with Grubbs' catalyst, linseed oil by oxidation, epoxy and amine microcapsules as dual healing agents are existing strategies for self-healing of epoxy composites but some limitations still exist. For example, high sensibility of Grubbs' catalyst of temperature or exposure to amine hardener, complex synthesis steps and homogeneous dispersion in dual microcapsule system. Therefore, considering the role of initiator of ionic liquids in the epoxy network construction and the multifunction of ionic liquids in epoxy composites, these questions would be put forward: *i)* Is phosphonium-based ionic liquid can be encapsulated by silica microcapsules and introduced in epoxy composites as reinforcement? *ii)* Is ionic liquid can be used as for healing agents in high temperature cured epoxy composites? *iii)* Is there a new single microcapsule system without initiator/hardener can achieve self-healing purpose in different polymer composites with minimum limitations?

Overall, based on the general overview, this PhD work will aim at ionic liquid and epoxy composites via encapsulation strategy to answer the three questions above. Therefore, Chapter 1 gave an overview of the three main subjects in this work: self-healing, ionic liquids and epoxy composites, and microencapsulation. More details will be introduced again in the beginning of each chapter.

## References in Chapter 1

- [1] Senthilkumar, K.; Saba, N.; Rajini, N.; Chandrasekar, M.; Jawaid, M.; Siengchin, S.; Alotman, O. Y., Mechanical properties evaluation of sisal fibre reinforced polymer composites: A review. *Construction and Building Materials*. **2018**, 174, 713-729.
- [2] Saba, N.; Jawaid, M.; Alotman, O. Y.; Paridah, M. T., A review on dynamic mechanical properties of natural fibre reinforced polymer composites. *Construction and Building Materials*. **2016**, 106, 149-159.
- [3] Forintos, N.; Czigany, T., Multifunctional application of carbon fiber reinforced polymer composites: electrical properties of the reinforcing carbon fibers—a short review. *Composites Part B: Engineering*. **2019**, 162, 331-343.
- [4] Chen, H.; Ginzburg, V. V.; Yang, J.; Yang, Y.; Liu, W.; Huang, Y.; Du, L.; Chen, B., Thermal conductivity of polymer-based composites: fundamentals and applications. *Prog. Polym. Sci.* **2016**, 59, 41-85.
- [5] Blaiszik, B. J.; Kramer, S. L. B.; Olugebefola, S. C.; Moore, J. S.; Sottos, N. R.; White, S. R., Self-healing polymers and composites. *Annu. Rev. Mater. Res.* **2010**, 40, 179-211.
- [6] Song, M. M.; Wang, Y. M.; Liang, X. Y.; Zhang, X. Q.; Zhang, S.; Li, B. J., Functional materials with self-healing properties: a review. *Soft Matter*. **2019**, 15, 6615-6625.
- [7] Hia, I. L.; Vahedi, V.; Pasbakhsh, P., Self-healing polymer composites: prospects, challenges, and applications. *Polym. Rev. (Philadelphia, PA, U. S.)*. **2016**, 56, 225-261.
- [8] Scheiner, M.; Dickens, T. J.; Okoli, O., Progress towards self-healing polymers for composite structural applications. *Polymer*. **2016**, 83, 260-282.
- [9] Diels, O.; Alder, K., Synthesen in der hydroaromatischen Reihe. *Justus Liebigs Ann. Chem.* **1928**, 460, 98-122.
- [10] Liu, Y.-L.; Chuo, T.-W., Self-healing polymers based on thermally reversible Diels–Alder chemistry. *Polymer Chemistry*. **2013**, 4, 2194-2205.
- [11] Bai, N.; Simon, G. P.; Saito, K., Investigation of the thermal self-healing mechanism in a cross-linked epoxy system. *RSC Advances*. **2013**, 3, 20699-20707.
- [12] Amendola, E.; Council, N. R., Epoxy thermosets with self-healing ability. *Journal of Materials Science and Chemical Engineering*. **2015**, 3, 162-167.
- [13] Deng, G.; Tang, C.; Li, F.; Jiang, H.; Chen, Y., Covalent cross-linked polymer gels with reversible sol–gel transition and self-healing properties. *Macromolecules*. **2010**, 43, 1191-1194.
- [14] Zechel, S.; Geitner, R.; Abend, M.; Siegmann, M.; Enke, M.; Kuhl, N.; Klein,

- M.; Vitz, J.; Gräfe, S.; Dietzek, B.; Schmitt, M.; Popp, J.; Schubert, U. S.; Hager, M. D., Intrinsic self-healing polymers with a high E-modulus based on dynamic reversible urea bonds. *NPG Asia Materials*. **2017**, 9, 420-427.
- [15] Kalista, S. J.; Ward, T. C.; Oyetunji, Z., Self-Healing of Poly(Ethylene-co-Methacrylic Acid) Copolymers Following Projectile Puncture. *Mechanics of Advanced Materials and Structures*. **2007**, 14, 391-397.
- [16] Rahmathullah, M. A. M.; Palmese, G. R., Crack-healing behavior of epoxy-amine thermosets. *J. Appl. Polym. Sci*. **2009**, 113, 2191-2201.
- [17] Wool, R. P.; O'Connor, K. M., A theory crack healing in polymers. *J. Appl. Phys*. **1981**, 52, 5953-5963.
- [18] Döhler, D.; Michael, P.; Binder, W., *Principles of Self-Healing Polymers*. 2013.
- [19] Willocq, B.; Odent, J.; Dubois, P.; Raquez, J.-M., Advances in intrinsic self-healing polyurethanes and related composites. *RSC Advances*. **2020**, 10, 13766-13782.
- [20] Lehn, J.-M., Supramolecular chemistry. *Science*. **1993**, 260, 1762-1764.
- [21] Herbst, F.; Döhler, D.; Michael, P.; Binder, W. H., Self-healing polymers via supramolecular forces. *Macromol. Rapid Commun*. **2013**, 34, 203-220.
- [22] Chen, Y.; Kushner, A. M.; Williams, G. A.; Guan, Z., Multiphase design of autonomic self-healing thermoplastic elastomers. *Nat. Chem*. **2012**, 4, 467-472.
- [23] Burattini, S.; Colquhoun, H. M.; Fox, J. D.; Friedmann, D.; Greenland, B. W.; Harris, P. J.; Hayes, W.; Mackay, M. E.; Rowan, S. J., A self-repairing, supramolecular polymer system: healability as a consequence of donor-acceptor pi-pi stacking interactions. *Chem Commun (Camb)*. **2009**, 6717-6719.
- [24] Saeed, M.-U.; Chen, Z.; Li, B., Manufacturing strategies for microvascular polymeric composites: A review. *Composites Part A: Applied Science and Manufacturing*. **2015**, 78, 327-340.
- [25] Toohey, K. S.; White, S. R.; Lewis, J. A.; Sottos, N. R., Development of a protocol for microvascular self-healing. In *Proceedings of the 1st International Conference on Self-Healing Materials*, Noordwijk aan Zee, Hollandia, 2007.
- [26] Kling, S.; Czigány, T., Damage detection and self-repair in hollow glass fiber fabric-reinforced epoxy composites via fiber filling. *Composites Science and Technology*. **2014**, 99, 82-88.
- [27] Nademi, M.; Mozaffari, A.; Farrokhbadi, A. In *A new self healing method in composite laminates using the hollow glass fiber*, Key Engineering Materials, Trans Tech Publ: 2011; pp 548-551.
- [28] Sun, L.; Yu, W. Y.; Ge, Q. In *Experimental research on the self-healing performance of micro-cracks in concrete bridge*, Advanced Materials Research, Trans Tech Publ: 2011; pp 28-32.
- [29] Wu, X. F.; Rahman, A.; Zhou, Z.; Pelot, D. D.; Sinha - Ray, S.; Chen, B.; Payne, S.; Yarin, A. L., Electrospinning core - shell nanofibers for interfacial toughening and

- self - healing of carbon - fiber/epoxy composites. *J. Appl. Polym. Sci.* **2013**, 129, 1383-1393.
- [30]Bleay, S.; Loader, C.; Hawyres, V.; Humberstone, L.; Curtis, P., A smart repair system for polymer matrix composites. *Composites Part A: Applied Science and Manufacturing.* **2001**, 32, 1767-1776.
- [31]Trask, R. S.; Bond, I. P., Biomimetic self-healing of advanced composite structures using hollow glass fibres. *Smart Mater. Struct.* **2006**, 15, 704-710.
- [32]Kim, S.-R.; Getachew, B. A.; Kim, J.-H., Toward microvascular network-embedded self-healing membranes. *J. Membr. Sci.* **2017**, 531, 94-102.
- [33]Neisiany, R. E.; Khorasani, S. N.; Kong Yoong Lee, J.; Ramakrishna, S., Encapsulation of epoxy and amine curing agent in PAN nanofibers by coaxial electrospinning for self-healing purposes. *RSC Advances.* **2016**, 6, 70056-70063.
- [34]Gao, C.; Leporatti, S.; Moya, S.; Donath, E.; Möhwald, H., Swelling and shrinking of polyelectrolyte microcapsules in response to changes in temperature and ionic strength. *Chemistry—A European Journal.* **2003**, 9, 915-920.
- [35]Greene, L. C.; Meyers, P. A.; Springer, J. T.; Banks, P. A., Biological evaluation of pesticides released from temperature-responsive microcapsules. *Journal of agricultural and food chemistry.* **1992**, 40, 2274-2278.
- [36]Lv, W.; Feng, J.; Yan, W.; Faul, C. F., Self-assembly and pH response of electroactive liquid core–tetra (aniline) shell microcapsules. *Journal of Materials Chemistry B.* **2014**, 2, 4720-4725.
- [37]Yang, C.; Wu, H.; Yang, X.; Shi, J.; Wang, X.; Zhang, S.; Jiang, Z., Coordination-enabled one-step assembly of ultrathin, hybrid microcapsules with weak pH-response. *ACS Appl. Mater. Interfaces.* **2015**, 7, 9178-9184.
- [38]Déjugnat, C.; Sukhorukov, G. B., pH-responsive properties of hollow polyelectrolyte microcapsules templated on various cores. *Langmuir.* **2004**, 20, 7265-7269.
- [39]Liu, X.; Sheng, X.; Lee, J. K.; Kessler, M. R.; Kim, J. S., Rheokinetic evaluation of self-healing agents polymerized by Grubbs catalyst embedded in various thermosetting systems. *Composites Science and Technology.* **2009**, 69, 2102-2107.
- [40]Jones, A. S.; Rule, J. D.; Moore, J. S.; White, S. R.; Sottos, N. R., Catalyst morphology and dissolution kinetics of self-healing polymers. *Chemistry of Materials.* **2006**, 18, 1312-1317.
- [41]Rusakov, D. A.; Lyapkov, A. A.; Korotkova, E. I.; Thanh, N. V.; Cuong, T. Q.; Zamanova, M. K., Correlation between Temperature Setting and DCS Complex Peak Energy and in ROMP of Dicyclopentadiene. *Procedia Chemistry.* **2014**, 10, 490-493.
- [42]Suryanarayana, C.; Rao, K. C.; Kumar, D., Preparation and characterization of microcapsules containing linseed oil and its use in self-healing coatings. *Prog. Org. Coat.* **2008**, 63, 72-78.
- [43]Jin, H.; Mangun, C. L.; Stradley, D. S.; Moore, J. S.; Sottos, N. R.; White, S. R., Self-healing thermoset using encapsulated epoxy-amine healing chemistry. *Polymer.* **2012**, 53,

581-587.

[44] Park, J. H.; Braun, P. V., Coaxial electrospinning of self-healing coatings. *Adv Mater.* **2010**, *22*, 496-499.

[45] Chen, X.; Zhu, J.; Luo, Y.; Chen, J.; Ma, X.; Bukhvalov, D.; Liu, H.; Zhang, M.; Luo, Z., Molecular dynamics simulation insight into the temperature dependence and healing mechanism of an intrinsic self-healing polyurethane elastomer. *Physical Chemistry Chemical Physics.* **2020**, *22*, 17620-17631.

[46] Walden, P., Molecular weights and electrical conductivity of several fused salts. *Bull. Acad. Imper. Sci. (St. Petersburg).* **1914**, 1800, 405-422.

[47] Charles, G. Cellulose solution. 1934.

[48] Swain, C. G.; Ohno, A.; Roe, D. K.; Brown, R.; Maugh, T., Tetrahexylammonium benzoate, a liquid salt at 25 °, a solvent for kinetics or electrochemistry. *Journal of the American Chemical Society.* **1967**, *89*, 2648–2649.

[49] Chum, H. L.; Koch, V. R.; Miller, L. L.; Osteryoung, R. A., Electrochemical scrutiny of organometallic iron complexes and hexamethylbenzene in a room temperature molten salt. *Journal of the American Chemical Society.* **1975**, *97*, 3264-3265.

[50] Robinson, J.; Osteryoung, R. A., An electrochemical and spectroscopic study of some aromatic hydrocarbons in the room temperature molten salt system aluminum chloride-n-butylpyridinium chloride. *Journal of the American Chemical Society.* **1979**, *101*, 323-237.

[51] Plechkova, N. V.; Seddon, K. R., Applications of ionic liquids in the chemical industry. *Chem. Soc. Rev.* **2008**, *37*, 123-150.

[52] H, O.-B.; Magna, L., Ionic liquids perspectives for organic and catalytic reactions. *J. Mol. Catal. A: Chem.* **2002**, *182-183*, 419-437.

[53] Shim, Y.; Kim, H. J., Dielectric relaxation, ion conductivity, solvent rotation, and solvation dynamics in a room-temperature ionic liquid. *The Journal of Physical Chemistry B.* **2008**, *112*, 11028-11038.

[54] Ngo, H. L.; LeCompte, K.; Hargens, L.; McEwen, A. B., Thermal properties of imidazolium ionic liquids. *Thermochim. Acta.* **2000**, *357-358*, 97-102.

[55] Earle, M. J.; Seddon, K. R., Ionic liquids Green solvents for the future. *Pure and Applied Chemistry.* **2000**, *72*, 1391-1398.

[56] Boon, J. A.; Levisky, J. A.; Pflug, J. L.; Wilkes, J. S., Friedel-crafts reactions in ambient-temperature molten salts. *The Journal of Organic Chemistry.* **1986**, *51*, 480-483.

[57] Dupont, J.; Fonseca, G. S.; Umpieere, A. P.; Fichtner, P. F. P.; Teixeira, S. R.; 124(16), d. j. u., Transition-metal nanoparticles in imidazolium ionic liquids recyclable catalysts for biphasic hydrogenation reactions. *Journal of the American Chemical Society.* **2002**, *124*, 4228-4229.

[58] P, W.; W, K., Ionic liquids—new “solutions” for transition metal catalysis. *Angew. Chem. Int. Ed.* **2000**, *39*, 3772-3789.

[59] Ishikawa, M.; Sugimoto, T.; Kikuta, M.; Ishiko, E.; Kono, M., Pure ionic liquid

electrolytes compatible with a graphitized carbon negative electrode in rechargeable lithium-ion batteries. *Journal of power sources*. **2006**, 162, 658-662.

[60] Gorlov, M.; Kloo, L., Ionic liquid electrolytes for dye-sensitized solar cells. *Dalton Trans.* **2008**, 2655-2666.

[61] O'Regan, B.; Grätzel, M., A low-cost high-efficiency solar cell based on dye-sensitized colloidal TiO<sub>2</sub> films. *Nature*. **1991**, 353, 737-740.

[62] Welton, T., Ionic liquids in catalysis. *Coordination Chemistry Reviews*. **2004**, 248, 2459-2477.

[63] Dai, Q.; Menzies, D. B.; MacFarlane, D. R.; Batten, S. R.; Forsyth, S.; Spiccia, L.; Cheng, Y.-B.; Forsyth, M., Dye-sensitized nanocrystalline solar cells incorporating ethylmethylimidazolium-based ionic liquid electrolytes. *C. R. Chim.* **2006**, 9, 617-621.

[64] Armand, M.; Tarascon, J.-M., Building better batteries. *Nature*. **2008**, 451, 652-657.

[65] Lin, D.; Liu, Y.; Cui, Y., Reviving the lithium metal anode for high-energy batteries. *Nat. Nanotechnol.* **2017**, 12, 194-206.

[66] Scrosati, B., Recent advances in lithium ion battery materials. *Electrochim. Acta*. **2000**, 45, 2461-2466.

[67] Liu, K.; Wang, Z.; Shi, L.; Jungsuttiwong, S.; Yuan, S., Ionic liquids for high performance lithium metal batteries. *Journal of Energy Chemistry*. **2021**, 59, 320-333.

[68] Armand, M.; Endres, F.; MacFarlane, D. R.; Ohno, H.; Scrosati, B., Ionic-liquid materials for the electrochemical challenges of the future. *Nat. Mater.* **2009**, 8, 621-629.

[69] Lombardo, L.; Brutti, S.; Navarra, M. A.; Panero, S.; Reale, P., Mixtures of ionic liquid-Alkylcarbonates as electrolytes for safe lithium-ion batteries. *Journal of Power Sources*. **2013**, 227, 8-14.

[70] Tian, X.; Yang, P.; Yi, Y.; Liu, P.; Wang, T.; Shu, C.; Qu, L.; Tang, W.; Zhang, Y.; Li, M., Self-healing and high stretchable polymer electrolytes based on ionic bonds with high conductivity for lithium batteries. *Journal of Power Sources*. **2020**, 450, 227629-227634.

[71] Wang, Z.; Tan, R.; Wang, H.; Yang, L.; Hu, J.; Chen, H.; Pan, F., A metal - organic - framework - based electrolyte with nanowetted interfaces for high - energy - density solid - state lithium battery. *Adv. Mater. (Weinheim, Ger.)*. **2018**, 30, 1704436-1704442.

[72] J, K.; A, F.; MacFarlane, D. R., Phosphonium-based ionic liquids: an overview. *Australian journal of chemistry*. **2009**, 62, 309-321.

[73] Tsunashima, K.; Yonekawa, F.; Sugiya, M., A lithium battery electrolyte based on a room-temperature phosphonium ionic liquid. *Chem. Lett.* **2008**, 37, 314-315.

[74] Jiménez, A. E.; Bermúdez, M. D.; Iglesias, P., Lubrication of Inconel 600 with ionic liquids at high temperature. *Tribology International*. **2009**, 42, 1744-1751.

[75] Park, K.; Ha, J. U.; Xanthos, M., Ionic liquids as plasticizers/lubricants for polylactic acid. *Polym. Eng. Sci.* **2010**, 50, 1105-1110.

[76] Ye, C.; Liu, W.; Chen, Y.; Yu, L., Room-temperature ionic liquids: a novel versatile



- lubricant. *Chem Commun (Camb)*. **2001**, 2244-2245.
- [77] Wang, H.; Lu, Q.; Ye, C.; Liu, W.; Cui, Z., Friction and wear behaviors of ionic liquid of alkylimidazolium hexafluorophosphates as lubricants for steel/steel contact. *Wear*. **2004**, 256, 44-48.
- [78] Lu, Q.; Wang, H.; Ye, C.; Liu, W.; Xue, Q., Room temperature ionic liquid 1-ethyl-3-hexylimidazolium-bis (trifluoromethylsulfonyl)-imide as lubricant for steel–steel contact. *Tribology International*. **2004**, 37, 547-552.
- [79] Mu, Z.; Zhou, F.; Zhang, S.; Liang, Y.; Liu, W., Effect of the functional groups in ionic liquid molecules on the friction and wear behavior of aluminum alloy in lubricated aluminum-on-steel contact. *Tribology International*. **2005**, 38, 725-731.
- [80] Minami, I., Ionic liquids in tribology. *Molecules*. **2009**, 14, 2286-2305.
- [81] Ma, Y.; Li, Z.; Wang, H.; Li, H., Synthesis and optimization of polyurethane microcapsules containing [BMIm]PF<sub>6</sub> ionic liquid lubricant. *Journal of colloid and interface science*. **2019**, 534, 469-479.
- [82] Sanes, J.; Carrión, F. J.; Bermúdez, M. D., Effect of the addition of room temperature ionic liquid and ZnO nanoparticles on the wear and scratch resistance of epoxy resin. *Wear*. **2010**, 268, 1295-1302.
- [83] Li, H.; Wang, Q.; Wang, H.; Cui, Y.; Zhu, Y.; Wang, B., Fabrication of thermally stable polysulfone microcapsules containing [EMIm][NTf<sub>2</sub>] ionic liquid for enhancement of in situ self - lubrication effect of epoxy. *Macromolecular Materials and Engineering*. **2016**, 301, 1473-1481.
- [84] Yamini, S.; Young, R. J., The mechanical properties of epoxy resins. *Journal of materials science*. **1980**, 15, 1823-1831.
- [85] Aiach, D.; Malone, W. F.; Sandrik, J., Dimensional accuracy of epoxy resins and their compatibility with impression materials. *J. Prosthet. Dent*. **1984**, 52, 500-504.
- [86] Qing, Y.; Zhou, W.; Luo, F.; Zhu, D., Microwave electromagnetic properties of carbonyl iron particles and Si/C/N nano-powder filled epoxy-silicone coating. *Physica B: Condensed Matter*. **2010**, 405, 1181-1184.
- [87] Uddin, M.; Chan, H.; Chow, C., Thermal and chemical stability of a spin-coated epoxy adhesive for the fabrication of a polymer optical waveguide. *Chemistry of materials*. **2004**, 16, 4806-4811.
- [88] Toldy, A.; Szolnoki, B.; Marosi, G., Flame retardancy of fibre-reinforced epoxy resin composites for aerospace applications. *Polymer degradation and stability*. **2011**, 96, 371-376.
- [89] Jakubinek, M. B.; Ashrafi, B.; Zhang, Y.; Martinez-Rubi, Y.; Kingston, C. T.; Johnston, A.; Simard, B., Single-walled carbon nanotube–epoxy composites for structural and conductive aerospace adhesives. *Composites Part B: Engineering*. **2015**, 69, 87-93.
- [90] Prolongo, S.; Gude, M.; Sanchez, J.; Urena, A., Nanoreinforced epoxy adhesives for aerospace industry. *The Journal of Adhesion*. **2009**, 85, 180-199.
- [91] Spee, T.; Van Duivenbooden, C.; Terwoert, J., Epoxy resins in the construction industry.

---

*Annals of the New York Academy of Sciences*. **2006**, 1076, 429-438.

[92] Bascom, W.; Cottington, R.; Jones, R.; Peyser, P., The fracture of epoxy - and elastomer - modified epoxy polymers in bulk and as adhesives. *J. Appl. Polym. Sci.* **1975**, 19, 2545-2562.

[93] Ueki, T.; Nishijima, S.; Izumi, Y., Designing of epoxy resin systems for cryogenic use. *Cryogenics*. **2005**, 45, 141-148.

[94] Vakil, U. M.; Martin, G. C., Crosslinked epoxies network structure characterization and physical-mechanical properties. *J. Appl. Polym. Sci.* **1992**, 46, 2089-2099.

[95] Kowalczyk, K.; Spychaj, T., Ionic liquids as convenient latent hardeners of epoxy resins. *Polimery*. **2003**, 48, 833-835.

[96] Ham, Y. R.; Kim, S. H.; Shin, Y. J.; Lee, D. H.; Yang, M.; Min, J. H.; Shin, J. S., A comparison of some imidazoles in the curing of epoxy resin. *Journal of Industrial and Engineering Chemistry*. **2010**, 16, 556-559.

[97] Jíšová, V., Curing mechanism of epoxides by imidazoles. *J. Appl. Polym. Sci.* **1987**, 34, 2547-2558.

[98] Cho, Y.-S.; Lee, H.-K.; Shim, M.-J.; Kim, S.-W., Effects of additive on electrical tree behavior in epoxy resin. *Journal of Industrial and Engineering Chemistry*. **1997**, 3, 171-176.

[99] Guenther Soares, B.; Livi, S.; Duchet-Rumeau, J.; Gerard, J. F., Preparation of epoxy/MCDEA networks modified with ionic liquids. *Polymer*. **2012**, 53, 60-66.

[100] Maka, H.; Spychaj, T.; Pilawka, R., Epoxy resin/ionic liquid systems: the influence of imidazolium cation size and anion type on reactivity and thermomechanical properties. *Industrial & Engineering Chemistry Research*. **2012**, 51, 5197-5206.

[101] Soares, B. G.; Livi, S.; Duchet-Rumeau, J.; Gerard, J.-F., Synthesis and characterization of epoxy/MCDEA networks modified with imidazolium-based ionic liquids. *Macromolecular Materials and Engineering*. **2011**, 296, 826-834.

[102] Nguyen, T. K. L.; Livi, S.; Soares, B. G.; Pruvost, S.; Duchet-Rumeau, J.; Gérard, J.-F., Ionic liquids: a new route for the design of epoxy networks. *ACS Sustainable Chemistry & Engineering*. **2015**, 4, 481-490.

[103] Silva, A. A.; Livi, S.; Netto, D. B.; Soares, B. G.; Duchet, J.; Gérard, J.-F., New epoxy systems based on ionic liquid. *Polymer*. **2013**, 54, 2123-2129.

[104] Nguyen, T. K. L. New generation of epoxy networks based on ionic liquids: From structuration to final properties. PhD Thesis, Université de Lyon, 2016.

[105] Lefort, T.; Duchet-Rumeau, J.; Livi, S.; Bachellerie, D.; Pruvost, S., Dielectric behaviour of an epoxy network cured with a phosphonium-based ionic liquid. *Polymer*. **2021**, 222, 123645-123654.

[106] Rahman, I. A.; Padavettan, V., Synthesis of silica nanoparticles by sol-gel: size-dependent properties, surface modification, and applications in silica-polymer nanocomposites—a review. *Journal of Nanomaterials*. **2012**, 2012, 1-15.

[107] Klabunde, K. J.; Erickson, L.; Koper, O.; Richards, R., Review of nanoscale

materials in chemistry: environmental applications. In *Nanoscale Materials in Chemistry: Environmental Applications*, 2010; pp 1-13.

[108] Hamidi, M.; Azadi, A.; Rafiei, P., Hydrogel nanoparticles in drug delivery. *Advanced drug delivery reviews*. **2008**, 60, 1638-1649.

[109] Krishnamoorti, R., Strategies for dispersing nanoparticles in polymers. *MRS Bull.* **2007**, 32, 341-347.

[110] Mackay, M. E.; Tuteja, A.; Duxbury, P. M.; Hawker, C. J.; Van Horn, B.; Guan, Z.; Chen, G.; Krishnan, R. S., General strategies for nanoparticle dispersion. *Science*. **2006**, 311, 1740-1743.

[111] Shi, F.; Ma, Y.; Ma, J.; Wang, P.; Sun, W., Preparation and characterization of PVDF/TiO<sub>2</sub> hybrid membranes with ionic liquid modified nano-TiO<sub>2</sub> particles. *J. Membr. Sci.* **2013**, 427, 259-269.

[112] Chabane, H.; Livi, S.; Benes, H.; Ladavière, C.; Ecorchard, P.; Duchet-Rumeau, J.; Gérard, J.-F., Polyhedral oligomeric silsesquioxane-supported ionic liquid for designing nanostructured hybrid organic-inorganic networks. *European Polymer Journal*. **2019**, 114, 332-337.

[113] Xiao, F.; Wu, K.; Luo, F.; Guo, Y.; Zhang, S.; Du, X.; Zhu, Q.; Lu, M., An efficient phosphonate-based ionic liquid on flame retardancy and mechanical property of epoxy resin. *Journal of Materials Science*. **2017**, 52, 13992-14003.

[114] Chabane, H.; Livi, S.; Morelle, X. P.; Sonnier, R.; LoïcDumazert; Duchet-Rumeau, J.; Gérard, J.-F., Synthesis of new ionic liquid-grafted metal-oxo nanoclusters – Design of nanostructured hybrid organic-inorganic polymer networks. *Polymer*. **2021**, 224, 123721-123731.

[115] Bansode, S. S.; Banarjee, S. K.; Gaikwad, D. D.; Jadhav, S. L.; Thorat, R. M., Microencapsulation: a review. *International Journal of Pharmaceutical Sciences Review and Research*. **2010**, 1, 38-43.

[116] Bakry, A. M.; Abbas, S.; Ali, B.; Majeed, H.; Abouelwafa, M. Y.; Mousa, A.; Liang, L., Microencapsulation of oils: a comprehensive review of benefits, techniques, and applications. *Comprehensive Reviews in Food Science and Food Safety*. **2016**, 15, 143-182.

[117] Gun, W. J.; Routh, A. F., Formation and characterization of pH-responsive liquid core microcapsules. *Langmuir*. **2013**, 29, 12541-12548.

[118] Dong, Z.; Ma, Y.; Hayat, K.; Jia, C.; Xia, S.; Zhang, X., Morphology and release profile of microcapsules encapsulating peppermint oil by complex coacervation. *J. Food Eng.* **2011**, 104, 455-460.

[119] Hong, K.; Park, S., Melamine resin microcapsules containing fragrant oil: synthesis and characterization. *Materials Chemistry and Physics*. **1999**, 58, 128-131.

[120] Yu, F.; Li, Z.; Zhang, T.; Wei, Y.; Xue, Y.; Xue, C., Influence of encapsulation techniques on the structure, physical properties, and thermal stability of fish oil microcapsules by spray drying. *Journal of Food Process Engineering*. **2017**, 40, e12576-e12584.

- [121] Atkin, R.; Davies, P.; Hardy, J.; Vincent, B., Preparation of aqueous core/polymer shell microcapsules by internal phase separation. *Macromolecules*. **2004**, *37*, 7979-7985.
- [122] Bean, K.; Black, C. F.; Govan, N.; Reynolds, P.; Sambrook, M. R., Preparation of aqueous core/silica shell microcapsules. *Journal of colloid and interface science*. **2012**, *366*, 16-22.
- [123] Leclercq, S.; Harlander, K. R.; Reineccius, G. A., Formation and characterization of microcapsules by complex coacervation with liquid or solid aroma cores. *Flavour Fragr. J.* **2009**, *24*, 17-24.
- [124] R, P. N.; A, P. D.; D, B. P.; Vikram, P.; Darshan, M., Microsphere as a novel drug delivery. *International Journal of Pharmacy & Life Sciences*. **2011**, *2*, 992-997.
- [125] Solanki, N., Microspheres an innovative approach in drug delivery system. *MOJ Bioequivalence & Bioavailability*. **2018**, *5*, 56-58.
- [126] Fujiwara, M.; Shiokawa, K.; Tanaka, Y.; Nakahara, Y., Preparation and formation mechanism of silica microcapsules (hollow sphere) by water/oil/water interfacial reaction. *Chemistry of materials*. **2004**, *16*, 5420-5426.
- [127] Rottman, C.; Gans, O.; Biagini, F.; Lapidot, N., Advanced sunscreens: UV absorbers entrapped in sol-gel glass microcapsules. *Journal of Sol-Gel Science and Technology*. **2002**, *23*, 268-270.
- [128] Sowman, H. G. Non-vitreous ceramic metal oxide microcapsules and process for making same. 1982.
- [129] Martinez Rivas, C. J.; Tarhini, M.; Badri, W.; Miladi, K.; Greige-Gerges, H.; Nazari, Q. A.; Galindo Rodriguez, S. A.; Roman, R. A.; Fessi, H.; Elaissari, A., Nanoprecipitation process: From encapsulation to drug delivery. *Int. J. Pharm.* **2017**, *532*, 66-81.
- [130] Akbari-Alavijeh, S.; Shaddel, R.; Jafari, S. M., Nanostructures of chitosan for encapsulation of food ingredients. In *Biopolymer Nanostructures for Food Encapsulation Purposes*, 2019; pp 381-418.
- [131] Luo, Q.; Pentzer, E., Encapsulation of Ionic Liquids for Tailored Applications. *ACS Appl Mater Interfaces*. **2020**, *12*, 5169-5176.
- [132] Yuan, L.; Liang, G.-Z.; Xie, J.-Q.; Guo, J.; Li, L., Thermal stability of microencapsulated epoxy resins with poly(urea-formaldehyde). *Polymer Degradation and Stability*. **2006**, *91*, 2300-2306.
- [133] Brown, E. N.; Kessler, M. R.; Sottos, N. R.; White, S. R., In situ poly (urea-formaldehyde) microencapsulation of dicyclopentadiene. *Journal of microencapsulation*. **2003**, *20*, 719-730.
- [134] I Ré, M., Microencapsulation by spray drying. *Drying Technol.* **1998**, *16*, 1195-1236.
- [135] Li, M.; Rouaud, O.; Poncelet, D., Microencapsulation by solvent evaporation: state of the art for process engineering approaches. *Int. J. Pharm.* **2008**, *363*, 26-39.
- [136] Kentepozidou, A.; Kiparissides, C., Production of water-containing polymer

- microcapsules by the complex emulsion solvent evaporation technique. Effect of process variables on the microcapsule size distribution. *Journal of Microencapsulation*. **1995**, 12, 627-638.
- [137] Deshmukh, R.; Wagh, P.; Naik, J., Solvent evaporation and spray drying technique for micro- and nanospheres/particles preparation: A review. *Drying Technol.* **2016**, 34, 1758-1772.
- [138] Yang, C.-Y.; Tsay, S.-Y.; Tsiang, R.-C., An enhanced process for encapsulating aspirin in ethyl cellulose microcapsules by solvent evaporation in an O/W emulsion. *Journal of microencapsulation*. **2000**, 17, 269-277.
- [139] Iwata, M.; McGinity, J., Preparation of multi-phase microspheres of poly (D, L-lactic acid) and poly (D, L-lactic-co-glycolic acid) containing a W/O emulsion by a multiple emulsion solvent evaporation technique. *Journal of microencapsulation*. **1991**, 9, 201-214.
- [140] Uchida, T.; Yagi, A.; Oda, Y.; Goto, S., Microencapsulation of ovalbumin in poly (lactide-co-glycolide) by an oil-in-oil (O/O) solvent evaporation method. *Journal of microencapsulation*. **1996**, 13, 509-518.
- [141] Shin, M. J.; Shin, Y. J.; Hwang, S. W.; Shin, J. S., Microencapsulation of imidazole curing agent by solvent evaporation method using W/O/W emulsion. *J. Appl. Polym. Sci.* **2013**, 129, 1036-1044.
- [142] Meng, F.; Ma, G.; Liu, Y.; Qiu, W.; Su, Z., Microencapsulation of bovine hemoglobin with high bio-activity and high entrapment efficiency using a W/O/W double emulsion technique. *Colloids and surfaces B: Biointerfaces*. **2004**, 33, 177-183.
- [143] Takada, S.; Yamagata, Y.; Misaki, M.; Taira, K.; Kurokawa, T., Sustained release of human growth hormone from microcapsules prepared by a solvent evaporation technique. *Journal of Controlled Release*. **2003**, 88, 229-242.
- [144] Soottitantawat, A.; Yoshii, H.; Furuta, T.; Ohkawara, M.; Linko, P., Microencapsulation by spray drying influence of emulsion size on the retention of volatile compounds. *J. Food Sci.* **2003**, 68, 2256-2262.
- [145] Carneiro, H. C. F.; Tonon, R. V.; Grosso, C. R. F.; Hubinger, M. D., Encapsulation efficiency and oxidative stability of flaxseed oil microencapsulated by spray drying using different combinations of wall materials. *J. Food Eng.* **2013**, 115, 443-451.
- [146] Correa-Filho, L. C.; Lourenco, M. M.; Moldao-Martins, M.; Alves, V. D., Microencapsulation of beta-carotene by spray drying: effect of wall material concentration and drying inlet temperature. *Int J Food Sci.* **2019**, 2019, 8914852.
- [147] Desai, K. G. H.; Jin Park, H., Recent developments in microencapsulation of food ingredients. *Drying Technol.* **2005**, 23, 1361-1394.
- [148] Patel, R. P.; Patel, M. P.; Suthar, A. M., Spray drying technology an overview. *Indian Journal of Science and Technology*. **2009**, 2, 44-47.
- [149] Drusch, S., Sugar beet pectin: a novel emulsifying wall component for microencapsulation of lipophilic food ingredients by spray-drying. *Food Hydrocolloids*. **2007**,

21, 1223-1228.

- [150] Shamaei, S.; Seiedlou, S. S.; Aghbashlo, M.; Tsotsas, E.; Kharaghani, A., Microencapsulation of walnut oil by spray drying: effects of wall material and drying conditions on physicochemical properties of microcapsules. *Innovative Food Science & Emerging Technologies*. **2017**, 39, 101-112.
- [151] Liu, G.; Xie, B.; Fu, D.; Wang, Y.; Fu, Q.; Wang, D., Preparation of nearly monodisperse microcapsules with controlled morphology by in situ polymerization of a shell layer. *Journal of Materials Chemistry*. **2009**, 19, 6605-6609.
- [152] Zhang, G. S., Z, Mechanical properties of melamine-formaldehyde microcapsules. *Journal of microencapsulation*. **2001**, 18, 593-602.
- [153] Lee, H.; Lee, S.; Cheong, I.; Kim, J., Microencapsulation of fragrant oil via in situ polymerization: effects of pH and melamine-formaldehyde molar ratio. *Journal of microencapsulation*. **2002**, 19, 559-569.
- [154] B, J. I.; H, S. J.; J, C. H., Synthesis of microcapsule containing oil phase via in situ polymerization. *Journal of materials science*. **2005**, 40, 1031-1033.
- [155] Mao, J.; Yang, H.; Zhou, X., In situ polymerization of uniform poly (urea–formaldehyde) microcapsules containing paraffins under the high-speed agitation without emulsifier. *Polym. Bull*. **2012**, 69, 649-660.
- [156] Fan, C.; Zhou, X., Effect of emulsifier on poly (urea–formaldehyde) microencapsulation of tetrachloroethylene. *Polym. Bull*. **2011**, 67, 15-27.
- [157] Sarkar, S.; Kim, B., Synthesis of graphene oxide–epoxy resin encapsulated urea–formaldehyde microcapsule by in situ polymerization process. *Polym. Compos*. **2018**, 39, 636-644.
- [158] Konuklu, Y.; Paksoy, H. O.; Unal, M.; Konuklu, S., Microencapsulation of a fatty acid with poly (melamine–urea–formaldehyde). *Energy Convers. Manage*. **2014**, 80, 382-390.
- [159] Yin, D.; Ma, L.; Geng, W.; Zhang, B.; Zhang, Q., Microencapsulation of n - hexadecanol by in situ polymerization of melamine - formaldehyde resin in emulsion stabilized by styrene - maleic anhydride copolymer. *International Journal of Energy Research*. **2015**, 39, 661-667.
- [160] Hwang, J.-S.; Kim, J.-N.; Wee, Y.-J.; Jang, H.-G.; Kim, S.-H.; Ryu, H.-W., Preparation and characterization of melamine-formaldehyde resin microcapsules containing fragrant oil. *Biotechnol. Bioprocess Eng*. **2006**, 11, 332-336.
- [161] Arshady, R., Preparation of microspheres and microcapsules by interfacial polycondensation techniques. *Journal of Microencapsulation*. **1989**, 6, 13-28.
- [162] Kobašlija, M.; McQuade, D. T., Polyurea Microcapsules from Oil-in-Oil Emulsions via Interfacial polymerization. *Macromolecules*. **2006**, 39, 6371-6375.
- [163] Shukla, P.; Sivaram, S., Microencapsulation of the water-soluble pesticide monocrotophos by an oil in oil interfacial polyaddition method. *Journal of microencapsulation*. **1999**, 16, 517-521.

- [164] Bouchemal, K.; Briançon, S.; Chaumont, P.; Fessi, H.; Zydowicz, N., Microencapsulation of dehydroepiandrosterone (DHEA) with poly (ortho ester) polymers by interfacial polycondensation. *Journal of microencapsulation*. **2003**, 20, 637-651.
- [165] Scarfato, P.; Avallone, E.; Iannelli, P.; De Feo, V.; Acierno, D., Synthesis and characterization of polyurea microcapsules containing essential oils with antigerminative activity. *J. Appl. Polym. Sci.* **2007**, 105, 3568-3577.
- [166] Wang, H.-C.; Grolman, J. M.; Rizvi, A.; Hisao, G. S.; Rienstra, C. M.; Zimmerman, S. C., pH-triggered release from polyamide microcapsules prepared by interfacial polymerization of a simple diester monomer. *ACS Macro Letters*. **2017**, 6, 321-325.
- [167] Hayashi, Y.; Fuchigami, K.; Taguchi, Y.; Tanaka, M., Preparation of microcapsules containing erythritol with interfacial polycondensation reaction by using the (W/O) emulsion. *Journal of Encapsulation and Adsorption Sciences*. **2014**, 4, 132-140.
- [168] Kobašlija, M.; McQuade, D. T., Polyurea microcapsules from oil-in-oil emulsions via interfacial polymerization. *Macromolecules*. **2006**, 39, 6371-6375.
- [169] Li, G.; Feng, Y.; Gao, P.; Li, X., Preparation of mono-dispersed polyurea-urea formaldehyde double layered microcapsules. *Polym. Bull.* **2008**, 60, 725-731.
- [170] Parker, R. M.; Zhang, J.; Zheng, Y.; Coulston, R. J.; Smith, C. A.; Salmon, A. R.; Yu, Z.; Scherman, O. A.; Abell, C., Electrostatically directed self - assembly of ultrathin supramolecular polymer microcapsules. *Advanced functional materials*. **2015**, 25, 4091-4100.
- [171] Arshady, R., Microspheres and microcapsules, a survey of manufacturing techniques Part II: Coacervation. *Polym. Eng. Sci.* **1990**, 30, 905-914.
- [172] Burgess, D. J., Complex coacervation: microcapsule formation. In *Macromolecular complexes in chemistry and biology*, Springer: 1994; pp 285-300.
- [173] Tong, W.; Song, X.; Gao, C., Layer-by-layer assembly of microcapsules and their biomedical applications. *Chem. Soc. Rev.* **2012**, 41, 6103-6124.
- [174] Hu, S.-H.; Tsai, C.-H.; Liao, C.-F.; Liu, D.-M.; Chen, S.-Y., Controlled rupture of magnetic polyelectrolyte microcapsules for drug delivery. *Langmuir*. **2008**, 24, 11811-11818.
- [175] S, J. S.; A.Seethadevi; Prabha, K. S.; P.Muthuprasanna; P.Pavitra, Microencapsulation: a review. *International journal of Pharma and Bio Sciences*. **2012**, 3, 509-531.
- [176] Kalaycioglu, G. D.; Aydogan, N., Layer-by-layer coated microcapsules with lipid nanodomains for dual-drug delivery. *Colloids and Surfaces A: Physicochemical and Engineering Aspects*. **2020**, 584, 124037-124047.
- [177] Kreft, O.; Javier, A. M.; Sukhorukov, G. B.; Parak, W. J., Polymer microcapsules as mobile local pH-sensors. *Journal of Materials Chemistry*. **2007**, 17, 4471-4476.
- [178] Arshady, R., Microcapsules for food. *Journal of Microencapsulation*. **1993**, 10, 413-435.
- [179] Xu, X.-y.; Liu, J.-h.; Ouyang, X.; Cui, L.; Hong, J.; Meng, X.; Qin, S.; Liu, C.; Tang, J.; Chen, D.-Z., *In-situ* temperature regulation of flexible supercapacitors by

designing intelligent electrode with microencapsulated phase change materials. *Electrochim. Acta.* **2020**, 334, 135551-135561.

[180] Wang, B.; Sheng, H.; Shi, Y.; Hu, W.; Hong, N.; Zeng, W.; Ge, H.; Yu, X.; Song, L.; Hu, Y., Recent advances for microencapsulation of flame retardant. *Polymer Degradation and Stability.* **2015**, 113, 96-109.

[181] Chang, S.; Xie, T.; Yang, G., Effects of polystyrene-encapsulated magnesium hydroxide on rheological and flame-retarding properties of HIPS composites. *Polymer degradation and stability.* **2006**, 91, 3266-3273.

[182] Chang, S.; Xie, T.; Yang, G., Effects of shell thickness of polystyrene - encapsulated Mg(OH)<sub>2</sub> on flammability and rheological properties of high - impact polystyrene composites. *Polym. Int.* **2007**, 56, 1135-1141.

[183] Wang, H.; Meng, X.; Wen, B.; Gao, X.; Zhang, S.; Yang, M., A simple route for the preparation of red phosphorus microcapsule with fine particle distribution. *Materials Letters.* **2008**, 62, 3745-3747.

[184] Chang, S.; Zeng, C.; Yuan, W.; Ren, J., Preparation and characterization of double - layered microencapsulated red phosphorus and its flame retardance in poly (lactic acid). *J. Appl. Polym. Sci.* **2012**, 125, 3014-3022.

[185] Giraud, S.; Bourbigot, S.; Rochery, M.; Vroman, I.; Tighzert, L.; Delobel, R.; Poutch, F., Flame retarded polyurea with microencapsulated ammonium phosphate for textile coating. *Polymer Degradation and Stability.* **2005**, 88, 106-113.

[186] Vroman, I.; Giraud, S.; Salaün, F.; Bourbigot, S., Polypropylene fabrics padded with microencapsulated ammonium phosphate: Effect of the shell structure on the thermal stability and fire performance. *Polymer degradation and Stability.* **2010**, 95, 1716-1720.

[187] Giraud, S.; Bourbigot, S.; Rochery, M.; Vroman, I.; Tighzert, L.; Delobel, R., Microencapsulation of phosphate: application to flame retarded coated cotton. *Polymer Degradation and Stability.* **2002**, 77, 285-297.

[188] Li, H.; Ma, Y.; Li, Z.; Cui, Y.; Wang, H., Synthesis of novel multilayer composite microcapsules and their application in self-lubricating polymer composites. *Composites Science and Technology.* **2018**, 164, 120-128.

[189] Li, H.; Li, S.; Li, F.; Li, Z.; Wang, H., Fabrication of SiO<sub>2</sub> wrapped polystyrene microcapsules by Pickering polymerization for self-lubricating coatings. *Journal of colloid and interface science.* **2018**, 528, 92-99.

[190] Li, H.; Ma, Y.; Li, Z.; Ji, J.; Zhu, Y.; Wang, H., High temperature resistant polysulfone/silica double-wall microcapsules and their application in self-lubricating polypropylene. *RSC advances.* **2017**, 7, 50328-50335.

[191] Li, H.; Chen, S.; Li, Z.; Feng, Y.; Zhang, M., Preparation of PU/GO hybrid wall microcapsules and their self-lubricating properties for epoxy composites. *Colloids and Surfaces A: Physicochemical and Engineering Aspects.* **2020**, 596, 124729-124735.

[192] Li, H.; Cui, Y.; Wang, H.; Zhu, Y.; Wang, B., Preparation and application of



---

polysulfone microcapsules containing tung oil in self-healing and self-lubricating epoxy coating. *Colloids and Surfaces A: Physicochemical and Engineering Aspects*. **2017**, 518, 181-187.

[193] Yun, J.; Im, J. S.; Lee, Y.-S.; Kim, H.-I., Effect of oxyfluorination on electromagnetic interference shielding behavior of MWCNT/PVA/PAAc composite microcapsules. *European Polymer Journal*. **2010**, 46, 900-909.

[194] Jiang, F.; Wang, X.; Wu, D., Magnetic microencapsulated phase change materials with an organo-silica shell: design, synthesis and application for electromagnetic shielding and thermal regulating polyimide films. *Energy*. **2016**, 98, 225-239.

[195] Jiang, F.; Wang, X.; Wu, D., Design and synthesis of magnetic microcapsules based on n-eicosane core and Fe<sub>3</sub>O<sub>4</sub>/SiO<sub>2</sub> hybrid shell for dual-functional phase change materials. *Appl. Energy*. **2014**, 134, 456-468.

[196] Hong, W.; Wang, R.; Li, N.; Gao, L.; Jiao, T., Facile preparation and excellent ultraviolet shielding application of polyurethane - TiO<sub>2</sub> composite microcapsules. *Particle & Particle Systems Characterization*. **2021**, 38, 1-9.

## Chapter 2:

# Ionic liquid-containing silica microcapsules as functional additives for epoxy-amine networks

Up to now, very few studies are reported on microcapsules containing phosphonium ionic liquids for self-healing applications in thermoset polymer materials. In this chapter, silica microcapsules containing phosphonium ionic liquid (IL@SiO<sub>2</sub>) were successfully designed for the first time and added into the epoxy-amine networks. Then, the thermal and mechanical properties were investigated for the IL@SiO<sub>2</sub> microcapsules filled epoxy-amine microcomposites. Therefore, this chapter is composed of two parts: *i*) synthesis and characterization of IL@SiO<sub>2</sub> microcapsules; *ii*) influence of IL@SiO<sub>2</sub> microcapsules on the physical properties of the epoxy-amine microcomposites.

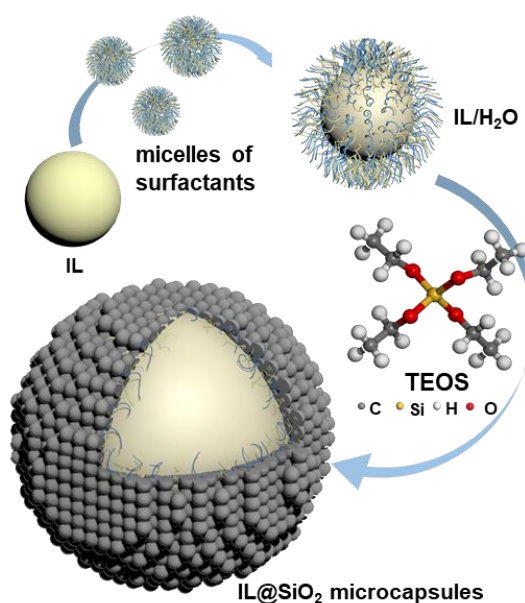


## Table of Contents

<b>2.1 Introduction .....</b>	<b>89</b>
<b>2.2 Experimental.....</b>	<b>92</b>
2.2.1 Materials.....	92
2.2.2 Experimental .....	93
2.2.3 Characterization methods .....	97
<b>2.3 Characterization of the IL@SiO<sub>2</sub> microcapsules .....</b>	<b>99</b>
2.3.1 Morphology and size distribution of the IL@SiO <sub>2</sub> microcapsules .....	99
2.3.2 Chemical characterization of the IL@SiO <sub>2</sub> microcapsules .....	102
2.3.3 Determination of IL content of the IL@SiO <sub>2</sub> microcapsules .....	103
<b>2.3 Characterization of IL@SiO<sub>2</sub> microcapsule-filled epoxy-amine microcomposites ..</b>	<b>106</b>
2.3.1 Morphology and size distributions of IL@SiO <sub>2</sub> microcapsule-filled epoxy-amine microcomposites.....	106
2.3.2 Thermal and dynamic mechanical properties of IL@SiO <sub>2</sub> microcapsule-filled epoxy-amine microcomposites.....	107
2.3.3 Swelling.....	112
2.3.4 Thermal behavior of neat epoxy networks and IL@SiO <sub>2</sub> microcapsule-filled epoxy microcomposites.....	115
2.3.5 Mechanical performances of IL@SiO <sub>2</sub> microcapsule-filled epoxy-amine microcomposites.....	116
2.3.6 Fracture mechanism of IL@SiO <sub>2</sub> microcapsule-filled epoxy-amine microcomposites .....	118
<b>2.4 Conclusion of Chapter 2 .....</b>	<b>123</b>
<b>References of Chapter 2.....</b>	<b>125</b>
<b>Supporting Information of Chapter 2 .....</b>	<b>131</b>

## 2.1 Introduction

According to the literature dedicated to thermoset-based polymer composites (PMC), it is well-known that when such structural materials are damaged, various strategies could be deployed to extend their lifetime. Among these ones, the type of damage must also be taken into consideration in order to propose relevant repair strategies. For example, if the damage is accessible such as matrix cracks, the simplest approach consists into a direct injection of an epoxy reactive system to fill the crack space but if fiber fractures, a recovery of the fiber integrity remains impossible. Epoxy resins are one of the most widely used types of thermosetting systems according to their good mechanical properties and chemical stability of the resulting networks, leading to their intensive integration in automotive, aerospace, or marine applications [1]. Nevertheless, the high crosslinking density of epoxy networks always results in low fracture toughness and high brittleness [2], *i.e.* solutions are required to induce them a better resistance to the microcrack propagation. Numerous strategies have been developed by using reactive rubbers [3-5], thermoplastics [6], block copolymers, or nanoparticles [7] in order to improve the fracture toughness of epoxy networks. Nevertheless, the addition of rubber or low  $T_g$  thermoplastic has a negative influence on the mechanical properties of modified networks. Dispersion of nanofillers is also proposed to enhance properties [8]. Toughening mechanisms strongly depend on different additives [9]. The role of the rubber in toughened epoxies is to relieve stress concentration in the matrix by promoting cavitation mechanism, *i.e.* through the formation of shear yielding [10]. Similar mechanisms involving the role of the plastic zone can be also applied for elastomers and thermoplastics [11]. However, the toughening mechanism involving rigid particles with or without surface modification and functionalization still need to be scrutinized and further discussed for each case [12], *e.g.* the particle size, particle shape or surface modification.

In the last decade, ionic liquid (IL) has emerged as new compound to be considered for polymer-based materials broadening the applications ranges. Due to their unique set of physicochemical properties as well as their numerous chemical structures, ILs offer promising new pathways to design new (multi)functional objects and materials. Indeed, considering ionic liquids in polymer science grow very rapidly in recent years by using them as solvents or as

interfacial agents in multiphase polymer-based materials such as polymer blends or organic-inorganic hybrid materials as well as functional additives. More recently, ILs have generated a growing interest in the field of thermosetting polymers such as epoxies or cyanate esters<sup>[13]</sup> or new IL-epoxy networks<sup>[14]</sup>. Applied to epoxy networks, ILs offer new pathways for designing novel networks by considering ILs as unreactive or reactive additives. Currently, numerous works reported in the literature relate the key role of ionic liquids as functional components within epoxy prepolymers. In fact, they could act as catalysts of epoxy-amine reactions or initiators of anionic polymerizations<sup>[15, 16]</sup>, dispersing aids<sup>[17]</sup>, or compatibilizers in epoxy-thermoplastic blends. In addition to all of those studies dedicated to the addition of ILs into epoxy reactive systems for conventional purposes, Sanes *et al*<sup>[18]</sup> have recently investigated the influence of ILs on the tribological performances of epoxy-amine network surfaces as these ones are known to be of interest as lubricating agents<sup>[19]</sup>. In their study, these authors prepared reactive systems based on an epoxy prepolymer which are cured with a mixture of diamines combined with different amounts (from 7 to 12 wt.%) of imidazolium-IL, *i.e.* 1-octyl-3-methylimidazolium tetrafluoroborate, in order to evaluate the self-healing ability of the resulting epoxy surfaces<sup>[20]</sup>.

Still in the field of tribological applications, encapsulation of ionic liquids in a silica or thermoplastic shell has also caught the attention to prepare ionic liquid core/silica shell microcapsules which can be applied as self-lubricant additives in a polymer matrix. A Chinese team has developed an innovative *in-situ* self-lubrication route based on the preparation of polymer microcapsules containing ionic liquids for epoxy-amine thermoset matrices. In fact, Li *et al*<sup>[21]</sup> have designed polysulfone (PSU) microcapsules containing imidazolium-IL in order to reduce the frictional coefficients between a metal surface and an epoxy matrix. For such a purpose, encapsulated IL/PSU microcapsules of 128  $\mu\text{m}$ -diameter were prepared. The influence of the microcapsule content (from 0 to 30 wt.%) on the tribological performances was investigated. Even if this approach may be difficult to apply due to the IL viscosity, the bipolar nature and the existence of ionic interactions, such a route appears to be promising for the design of self-healable polymer materials. Other authors such as Luo *et al*<sup>[22]</sup> have reported a method to trap imidazole-IL in a polymer shell by microencapsulation in order to propose a new solvent for extraction. Inorganic components can be good candidates for designing the

shell of such IL containers. More specifically, silica was considered for preparing nano/microcapsules for controlled release applications <sup>[23]</sup> thanks to its good mechanical properties <sup>[24]</sup> and biocompatibility <sup>[25, 26]</sup>. Recently, Abu-Reziq *et al* <sup>[27]</sup> have used lignosulfonic acid to stabilize ionic liquid in water in order to prepare a silica shell from an interfacial sol-gel process. The obtained microcapsules showed good performances as heterogeneous catalysts. Yang *et al* <sup>[28]</sup> have used the same ionic liquid as core component and a natural emulsifier, *i.e.* gelatin, to obtain microcapsules which can improve tribological behavior of polyurethane composite materials.

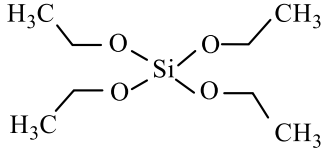
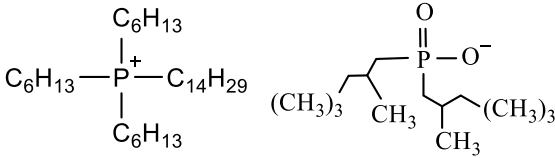
According to the state-of-art on IL encapsulation, to our knowledge, there are no publications reporting the encapsulation of phosphonium ionic liquids in a silica shell and only few studies focused on encapsulation methods of ILs, and very few on the integration of ionic liquids in an encapsulated form in PCM materials. Their applications in a thermosetting polymer matrix such as epoxy-based ones remain vacant. Therefore, this work focuses on the use of phosphonium-based type ionic liquids contained in silica microcapsules (IL@SiO<sub>2</sub>) as fillers to design epoxy/amine-based microcomposites. In order to identify the role of the interactions between the microcapsule surface and the polymer chains and how the microcapsules may have a reinforcing effect on the epoxy-amine network, different stoichiometric epoxy-to-amino hydrogen ratio were considered. Besides, different weight fractions of IL@SiO<sub>2</sub> microcapsules were added in the epoxy/amine network to optimize the performances of epoxy composites. Thus, the thermal, thermomechanical, large strain mechanical, and fracture behaviors were studied. The observed fracture improvement could be explained according to the proposed toughening mechanisms. From these results, new routes could be proposed to design high performance materials from the introduction of ionic liquids contained in microcapsules.

## 2.2 Experimental

### 2.2.1 Materials

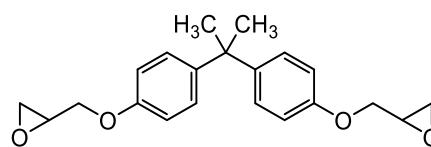
Surfactants, *i.e.* sodium dodecyl sulfate (SDS) and cetyltrimethylammonium bromide (CTAB), tetraethyl orthosilicate (TEOS), and ammonium hydroxide solution ( $\text{NH}_3 \cdot \text{H}_2\text{O}$ ) were purchased from Sigma-Aldrich and used as received. An ionic liquid based on tetradecyl(trihexyl)phosphonium cation and bis-(2,4,4-trimethylpentyl)phosphinate anion, denoted Cyphos IL 104, was provided by Cytec Solvay, Inc. The well-known bisphenol A diglycidyl ether (DGEBA, D.E.R. 332) was combined with the 4,4'-methylenebis(cyclohexylamine) (PACM) as a comonomer to prepare epoxy-amine networks. These compounds were purchased from Sigma-Aldrich and used as received without any further purification. Acetone used as solvent was purchased from Carlo ERBA Reagent. All the chemical structures of the products are summarized in Table 2-1.

**Table 2-1** Chemical structures of the products used

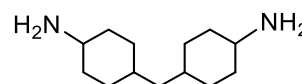
Materials and abbreviations	Chemical formula
Sodium dodecyl sulfate (SDS)	$\text{CH}_3(\text{CH}_2)_{10}\text{CH}_2\text{O}-\overset{\text{O}}{\parallel}{\text{S}}-\text{O}^- \text{Na}^+$
Cetyltrimethylammonium bromide (CTAB)	$\text{H}_3\text{C}(\text{H}_2\text{C})_{15}-\overset{\text{CH}_3}{\underset{\text{CH}_3}{\text{N}^+}}-\text{CH}_3 \text{Br}^-$
tetraethyl orthosilicate (TEOS)	
Ionic liquid (IL 104) tetradecyl(trihexyl)phosphonium bis-(2,4,4-trimethylpentyl)phosphinate	

Epoxy resin

Bisphenol A diglycidyl ether (DEGBA D.E.R. 332,  
epoxide equivalent weight, 171 – 175 g/eq)



4,4-methylene bis(cyclohexylamine)  
(PACM)



---

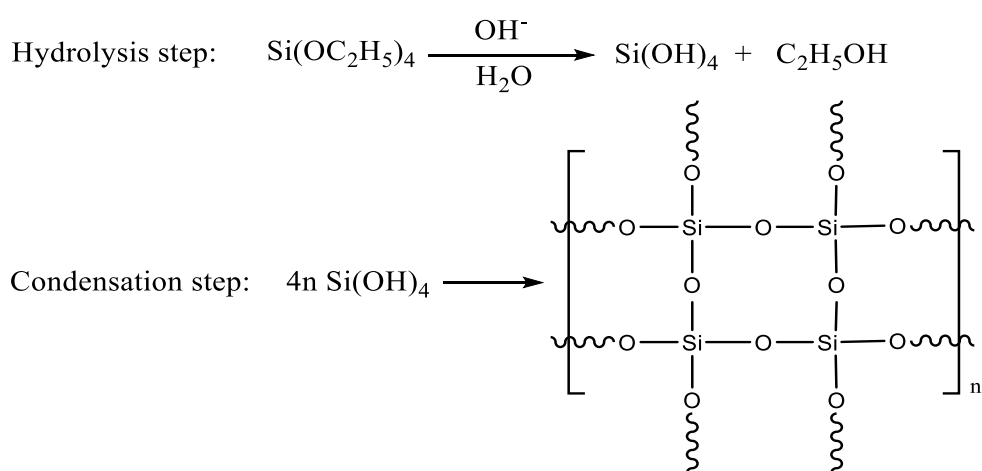
### 2.2.2 Experimental

To obtain silica shell microcapsules, the first step refers to the dispersion of the hydrophobic core compound in water to form an oil in water emulsion (O/W) and then a sol-gel process is processed to form silica shell around the suspended droplets to form microcapsules. In this work, phosphonium-based ionic liquid IL 104 was selected as core material. To our knowledge, the hydrophilic emulsifiers with HLB values of 10-18 are suitable for O/W emulsions [29]. Thus, different kinds of surfactants are reported in the literature to prepare the ionic liquid in water (IL/H<sub>2</sub>O) emulsion. For example, ionic surfactants (such as CTAB, SDS [30], REAX 88A [31,32]), non-ionic surfactants (such as Triton X-100 [33]), and natural surfactants (such as gelatin [28]) were taken into account. However, only by using a combination of SDS and CTAB can we obtain the microcapsules with ideal morphology. To stabilize ionic liquid in water, the surfactant should have good interactions with both aqueous phase and ionic liquid phase. The combination of CTAB and SDS could form stable spherical vesicles in aqueous solution to get a stabilization of the ionic liquid droplets in aqueous solution for given between SDS:CTAB molar ratio [34,35]. The combination of SDS (HLB = 20) and CTAB (HLB = 8.8) [36] at a given molar ratio will provide an ideal HLB value for O/W emulsion [37]. In the second step, the siliceous precursor TEOS is hydrolyzed and condensed at the surface of oil droplets due to the Coulombic forces [38] to form the silica shell.

In the first step, the cationic surfactant, CTAB, and anionic surfactant, SDS, were added at the same time in water until they were fully dissolved. In the aqueous solution, the electrostatic interactions between the positively and negatively charged head groups of CTAB and SDS will drive these molecules to assemble into vesicles in water. When the hydrophobic



ionic liquid, IL 104, was added in the mixture, the long alkyl chains of IL 104 will help them to migrate and turn to vesicles and stabilize to form IL in water emulsion (IL/H<sub>2</sub>O) under stirring. In the next step, in order to obtain microcapsules with a silica shell, tetraethoxysilane (TEOS) was chosen as the siliceous precursor and sol-gel process was catalyzed by ammonium hydroxide. Specifically, TEOS will transfer to the IL - water interface to undergo the hydrolysis and then condensation at the surface of IL/H<sub>2</sub>O emulsion droplets to form the silica shell. The hydrolysis and condensation steps during the sol-gel process are presented in Scheme 2-1. Finally, the white precipitate can be collected by centrifugation and dried.



**Scheme 2-1** Hydrolysis and condensation reactions occurring during the sol-gel process

Typically, 0.20 g of SDS and 0.40 g of CTAB were added in 54 mL deionized water followed by the addition of 1.00 mL of NH<sub>3</sub>·H<sub>2</sub>O. Then, the mixture was stirred under magnetic stirring and kept at 68 °C for 1.5 h in order to obtain a homogeneous solution. Next, 1.00 g of IL 104 was added in the aqueous solution and vigorously stirred at 68 °C for an additional time of 5 h until obtaining ionic liquid in water (IL/H<sub>2</sub>O) emulsion, characterized by a milky appearance. After that, 1.50 g TEOS was dripped slowly into the IL/H<sub>2</sub>O emulsion to perform a sol-gel reaction to form the silica shell. The sol-gel process proceeded at the same temperature for two hours and 80 °C for two extra hours. Finally, white precipitate was formed and collected by centrifugation at 4,000 rpm for 10 min. The final product was washed three times with deionized water and acetone then dried at 60 °C for 24 h. Figure 2-1 illustrates the synthetic procedure of IL@SiO<sub>2</sub> microcapsules synthesis.

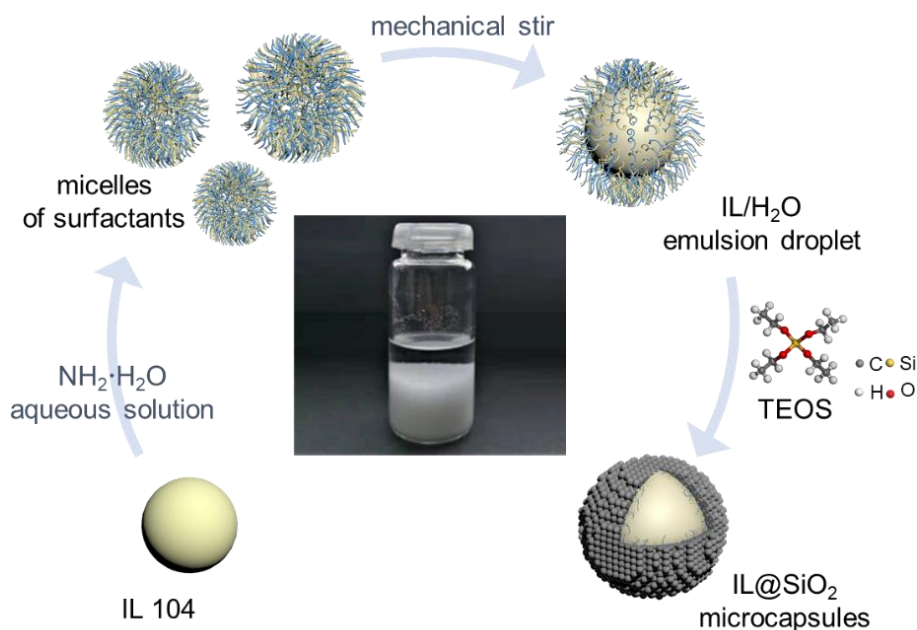


**Figure 2-1** Schematic synthesis procedure of IL@SiO<sub>2</sub> microcapsules

In order to investigate the reinforcement effect of IL@SiO<sub>2</sub> microcapsules in epoxy microcomposites, several reactive systems with different epoxy-to-amino hydrogen ratio ( $r$ ) were selected. The weights and molar ratios of DGEBA and PACM for each  $r$  value are listed in Table 2-2. Moreover, various amounts of IL@SiO<sub>2</sub> microcapsules were introduced in the epoxy-amine system to evaluate the thermal and mechanical properties of obtained IL@SiO<sub>2</sub> microcapsules reinforced epoxy-amine microcomposites. Abbreviations of all different samples with different  $r$  value and mass fraction of IL@SiO<sub>2</sub> microcapsules are listed in Table 2-3.

**Table 2-2** Weight and molar ratios of D.E.R. 332 and PACM for preparing epoxy-amine networks

$r^*$	DGEBA (phr)	PACM (phr)	Weight ratio of DGEBA/PACM
1.0	100	30.4	3.3
1.2	100	26.0	3.8
1.4	100	22.0	4.3

\*  $r$  is the epoxy-to-amino hydrogen ratio

**Table 2-3** Microcomposites prepared with different  $r$  values and weight fractions of IL@SiO<sub>2</sub> microcapsules

Material	$r^*$	IL@SiO <sub>2</sub> wt. fraction (%)	Material	$r^*$	IL@SiO <sub>2</sub> wt. fraction (%)	Material	$r^*$	IL@SiO <sub>2</sub> wt. fraction (%)
1.0-0		0	1.2-0		0	1.4-0		0
1.0-1	1.0	1	1.2-1	1.2	1	1.4-1	1.4	1
1.0-2		2	1.2-2		2	1.4-2		2
1.0-5		5	1.2-5		5	1.4-5		5

\*  $r$  is epoxy-to-amino hydrogen ratio

The preparation procedure of IL@SiO<sub>2</sub> microcapsule-filled epoxy-amine networks is schematically illustrated in Figure 2-2. Usually, IL@SiO<sub>2</sub> microcapsules were added in a given amount of acetone and the mixture was sonicated for 1 h. Then, the given amount of epoxy resin (DGEBA, D.E.R 332) was added and the mixture was kept in ultrasonic bath for an additional hour to get a better dispersion of IL@SiO<sub>2</sub> microcapsules. After, the mixture was put in the vacuum oven at 60 °C overnight to remove the solvent. After that, according to the epoxy-to-amino hydrogen ratio ( $r$ ), the related amount of PACM was added and the mixture was mixed under mechanical stirring at 60 °C. Finally, the mixture was degassed using a vacuum bell jar for 10 min and cured at 80 °C for 2 h and post-cured at 160 °C in an oven for 2 h.

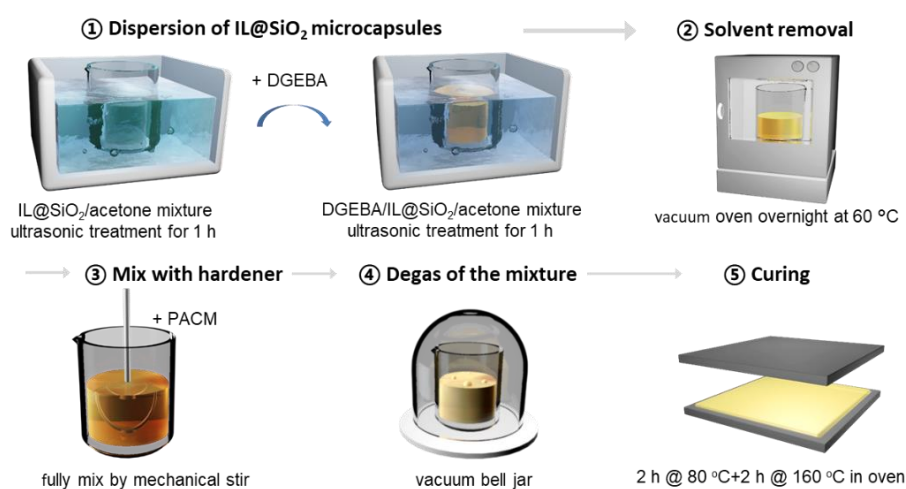


**Figure 2-2** Preparation of IL@SiO<sub>2</sub> microcapsule-filled epoxy-amine microcomposites

### 2.2.3 Characterization methods

The morphology of the IL@SiO<sub>2</sub> microcapsules was characterized by transmission electron microscope (TEM). Phillips CM 120 TEM equipped with electron diffraction spectroscopy (EDS) was operating at an accelerating voltage of 120 kV. IL@SiO<sub>2</sub> microcapsules were dispersed in deionized water and then ultrasonic treatment was carried out for 30 min to ensure a good dispersion. Then a small amount of the suspension was dropped on the carbon-coated copper grid. After 10 min, a tissue paper was slightly approached to the grid to remove the excess water for TEM observation. To characterize polymer microcomposites, the samples were cut using ultramicrotomy and collected on a carbon film-coated cooper grid.

Scanning electron microscope (SEM) at low resolution was carried out using a TESCAN VEGA3 microscope from TESCAN ANALYTICS operating at an accelerate voltage of 10 kV. SEM microscopy at high resolution was carried out using a ZEISS MERLIN COMPACT microscope operating at an accelerate voltage of 1 kV. To prepare the specimen, dried powder of IL@SiO<sub>2</sub> microcapsules and cross sections of epoxy composites were pasted on the sample holder using a carbon tape. The specimens were coated with gold using a sputter coater to prevent charge accumulation on the surface. The sputter coating process was performed at a current of 30 mA for 90 s.

Thermogravimetric analysis (TGA) was carried out using a Q500 thermogravimetric analyzer from TA Instruments. The analysis was performed from 30 to 700 °C at a heating rate of 20 K·min<sup>-1</sup> under nitrogen atmosphere.

Dynamic light scattering (DLS) performed using Nano Series instrument ZEN 3600 (Nano-Zeta Sizer) from Malvern Instruments was used to determine the size distribution of the IL@SiO<sub>2</sub> microcapsule. IL@SiO<sub>2</sub> microcapsules were dispersed in large amount of deionized water and then ultrasonic treatment was carried out for 30 min in order to obtain a good dispersion.

The reagents and IL@SiO<sub>2</sub> microcapsules were characterized using Fourier transform infrared (FTIR) spectroscopic analysis (Thermo Scientific Nicolet iS10 Spectrometer) in transmission mode (64 scans, resolution 4 cm<sup>-1</sup>).

Elemental analysis was carried out by CREALINS Co. using Inductively Coupled Plasma-

Atomic Emission Spectrometry (ICP-AES) (Thermofisher Instrument).

Differential Scanning Calorimetry (DSC) measurements on epoxy microcomposites were carried out by using Q10 (TA Instrument) from 20 to 250 °C at a heating rate of 10 K·min<sup>-1</sup> under nitrogen flow of 50 mL·min<sup>-1</sup>.

Compression tests were carried out using a MTS machine operating with a 5 kN load cell. The samples geometry was based on ISO 604:2002 standard *i.e.* 5\*5\*16 mm<sup>3</sup>. The Young's modulus ( $E$ ) was determined from  $\sigma$  (stress) vs.  $\varepsilon$  (strain) curves in the linear region.

Mode I stress intensity factor ( $K_{IC}$ ) of epoxy-amine networks and related microcomposites were determined on compact tension specimens according to the ISO 13586:2018(E) standards (Figure 2-2). The notch was formed using a milling cutter and the initial crack also known as natural crack was made by tapping a fine razor blade into the notch. The length of initial crack to width ratio ( $\alpha/w$ ) has to keep between 0.2 and 0.8. The fracture toughness test was carried out using a MTS tensile machine equipped with a 1 kN load cell operating at tensile speed at 10 mm·min<sup>-1</sup>.  $K_{IC}$  was calculated according to equation 2-1:

$$K_{IC} = f(\alpha/w) \frac{F_Q}{h\sqrt{w}} \quad (\text{equation 2-1})$$

where  $\alpha$  (m) is the length of initial crack,  $w$  (m) and  $h$  (m) are the width and thickness of specimen, respectively.  $F_Q$  (N) is the final load at the first crack. The  $f(\alpha/w)$  value is a geometrical factor which can be calculated using equation 2-2:

$$f(\alpha/w) = \frac{(2+\alpha)}{(1-\alpha)^{3/2}} \times (0.886 + 4.64\alpha - 13.32\alpha^2 + 14.72\alpha^3 - 5.64\alpha^4) \quad (\text{equation 2-2})$$

The critical energy release ( $G_{IC}$ ) can be calculated from equation 2-3 and the value of  $K_{IC}$ , Young's modulus ( $E$ ), and Poisson's coefficient ( $\nu$ ). 0.35 for  $\nu$  were considered according to the values related in the literature for epoxy networks [39, 40].

$$G_{IC} = \frac{(1-\nu^2) \cdot K_{IC}^2}{E} \quad (\text{equation 2-3})$$

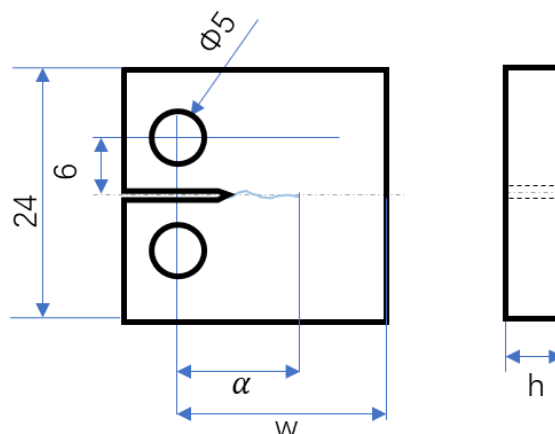


**Figure 2-3** Compact Tensile (CT) test specimen geometry

Dynamic mechanical analyses (DMA) were carried out using a ARES-G2 type rotational rheometer from TA Instruments. The analyses were carried out for 0.01% dynamic strain at a frequency of 1 Hz and a heating rate of 3 K·min<sup>-1</sup> from 35 to 250 °C.

Swelling tests were carried out at room temperature. Tetrahydrofuran (THF) was chosen as good solvent for epoxy resin. Each specimen (1 × 5 × 5 mm<sup>3</sup>) was immersed in THF at room temperature until the equilibrium was reached. THF uptake ( $\delta$ ) was determined by weighing the swollen polymer (dried with paper after taken from the THF) and calculated according to the following 2-4 equation.

$$\delta = \frac{m_t - m_o}{m_o} \text{ (equation 2-4)}$$

where  $m_o$  and  $m_t$  were the weight of the sample before swelling and the weight after swelling, respectively.

## 2.3 Characterization of the IL@SiO<sub>2</sub> microcapsules

### 2.3.1 Morphology and size distribution of the IL@SiO<sub>2</sub> microcapsules

The surface morphology and the size distribution of IL@SiO<sub>2</sub> microcapsules were characterized by transmission electron (TEM) and scanning electron (SEM) microscopies. Figure 2-4 shows TEM and SEM micrographs of IL@SiO<sub>2</sub> microcapsules at different magnifications. These ones reveal the core-shell structure and the roughness of obtained IL@SiO<sub>2</sub> microcapsules. TEM micrographs (Figure 2-4 (a), (b)) confirm the synthesis of

IL@SiO<sub>2</sub> microcapsules having sizes from 0.5 to 2 μm. The resulting distribution of particle sizes of the IL@SiO<sub>2</sub> microcapsules can be explained by the synthesis protocol involving a sol-gel process in O/W emulsion medium. The dispersed oil droplets in the emulsion, *i.e.* IL, are always in constant motion. As a consequence, if the interfacial membrane of the IL droplets in the emulsion breaks during the collision, two droplets could coalesce to form larger size droplets [41]. That's why the presence of an emulsifier is required to keep the emulsion stable. However, the droplets are subjected to different shear forces field leading to a broad droplet size distribution [42, 43]. The shell thickness of microcapsules could be estimated from image analysis and was founded to be 100 nm. On the SEM micrograph in Figure 2-4 (d), it is also worth noting the roughness of the silica microcapsules highlighting the formation of colloidal silica nanoparticles onto their surface.

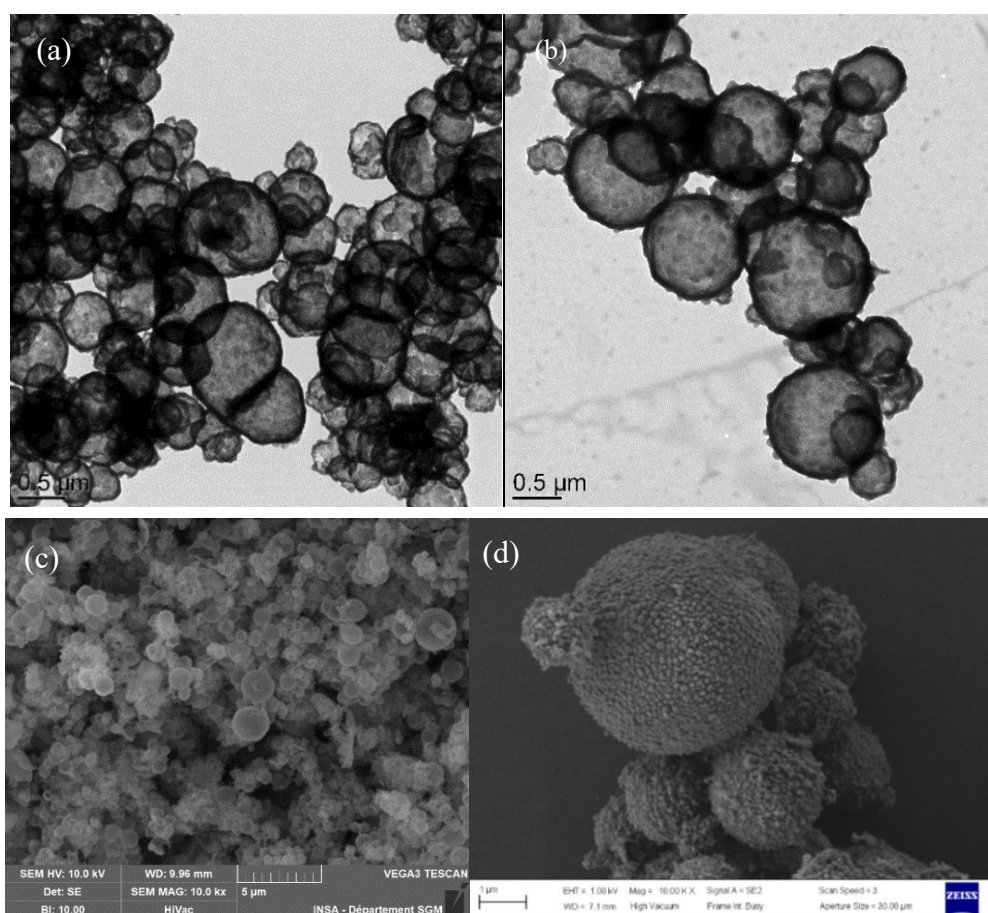


**Figure 2-4** (a,b) TEM and SEM (c,d) micrographs of IL@SiO<sub>2</sub> microcapsules at different magnifications

Moreover, energy-dispersive X-ray spectroscopy (EDX) combined with TEM was used to determine the location of phosphonium ionic liquid in the IL@SiO<sub>2</sub> microcapsules. The EDX spectra were presented in Figure 2-5. Compared to the carbon film supported copper grids (Figure 2-5 (b)) used as reference substrate, silicon and phosphorus-rich compounds can be clearly distinguished in IL@SiO<sub>2</sub> microcapsules (Figure 2-5 (a)) confirming that the phosphonium IL was well encapsulated into a silica shell.

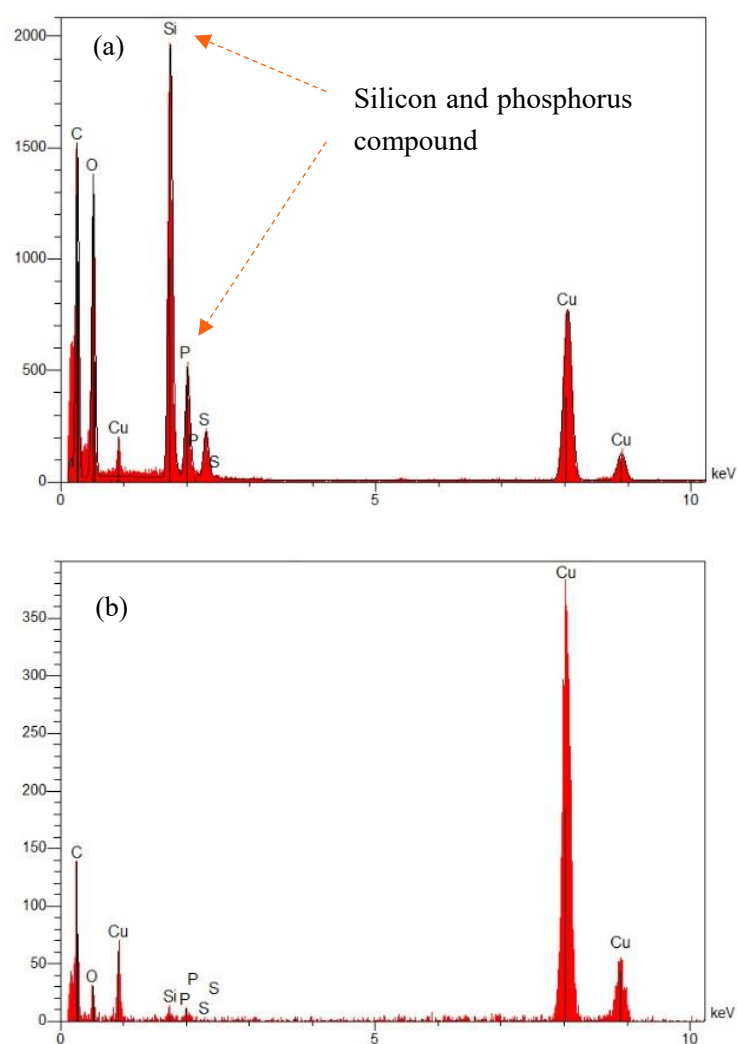


**Figure 2-5** EDX spectra of (a) IL@SiO<sub>2</sub> microcapsules and (b) copper grid

As mentioned, dynamic light scattering (DLS) was considered to quantify the microcapsule size distribution which was already observed by electron microscopies. The DLS spectrum presented in Figure 2-6 evidences a relatively narrow distribution of particle sizes in agreement with the conclusions from TEM and SEM analyses. IL@SiO<sub>2</sub> microcapsules have



size in the range from 0.5  $\mu\text{m}$  to 2  $\mu\text{m}$ . As mentioned previously, the polydispersity of microcapsule size is associated to the dynamic character of IL/H<sub>2</sub>O emulsion droplets [42].

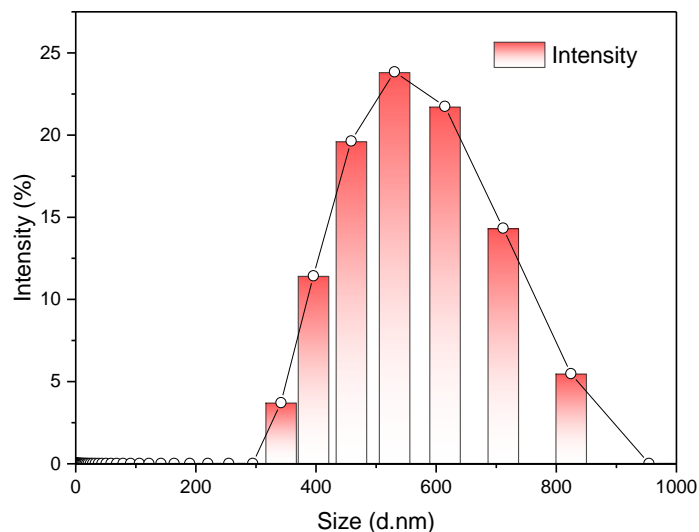


**Figure 2-6** Size distribution of IL@SiO<sub>2</sub> microcapsules

### 2.3.2 Chemical characterization of the IL@SiO<sub>2</sub> microcapsules

Fourier-transform infrared spectroscopy (FTIR) was used to investigate the chemical structure of IL@SiO<sub>2</sub> microcapsules. The spectra of IL@SiO<sub>2</sub> microcapsules, IL 104, and CTAB and SDS surfactants are given in Figure 2-7. The absorption peak at 1,090  $\text{cm}^{-1}$  corresponds to the anti-symmetric stretching vibrations of Si-O-Si bonds as well the absorption peaks at 806  $\text{cm}^{-1}$  and 459  $\text{cm}^{-1}$  which are assigned to symmetric stretching vibration and bending vibration of Si-O bonds. These bonds evidence for the existence of the SiO<sub>2</sub>-rich shell for the IL@SiO<sub>2</sub> microcapsules. Moreover, the stretching vibration of carbon-hydrogen bonds (C-H, 2,853-2,860  $\text{cm}^{-1}$ ) and bending vibration of methylene groups ( $-\text{CH}_2-$ , 1,460  $\text{cm}^{-1}$ ) were assigned to the alkyl chains of IL 104 and the hydrophobic moieties of the surfactants. Compared to the strong absorption peaks of initial chemicals, these relatively weak absorption peaks corresponding to aliphatic chains can be additional evidence to prove that IL 104 is well encapsulated. In addition, the similar features spectra for IL 104 and IL@SiO<sub>2</sub> microcapsules also confirmed the efficient encapsulation of IL 104. In order to know the weight fractions of IL 104 and silica shell, further analytical characterizations should be carried out.

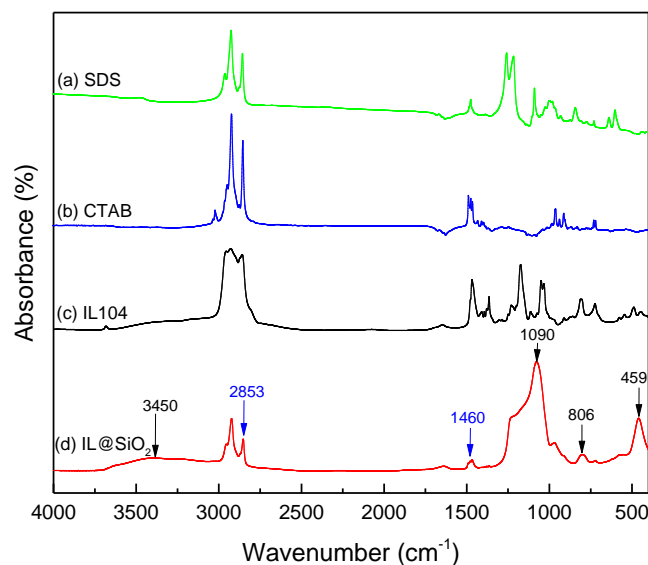


**Figure 2-7** FT-IR spectrum of (a) SDS, (b) CTAB, (c) IL 104, and (d) IL@SiO<sub>2</sub>

### 2.3.3 Determination of IL content of the IL@SiO<sub>2</sub> microcapsules

Thermogravimetric analysis (TGA) was carried out to characterize the thermal stability as well as the IL content in IL@SiO<sub>2</sub> microcapsules. In order to confirm the presence of IL 104 into IL@SiO<sub>2</sub>, silica nanospheres (nSiO<sub>2</sub>), *i.e.* without IL, were also prepared using the same procedure. The synthetic procedure of nSiO<sub>2</sub> and their corresponding TEM micrographs (Figure S2-1) are described in the Supporting Information. TGA traces of IL@SiO<sub>2</sub> microcapsules, IL 104, surfactants, and nSiO<sub>2</sub> (without IL) are presented in Figure 2-8. It can be seen that the first degradation step occurs below 300 °C for IL@SiO<sub>2</sub> microcapsules and nSiO<sub>2</sub> due to the decomposition of surfactants, *i.e.* CTAB and SDS. In addition, the onset decomposition temperature ( $T_{d \text{ onset}}$ ) which is defined for 5 % wt. loss. for IL 104, SDS, and CTAB were found to be 208, 209, and 229 °C, respectively. For IL@SiO<sub>2</sub> microcapsules, the  $T_{d \text{ onset}}$  is 216 °C that is slightly higher than the neat IL 104 one (208 °C). This can be explained by the protection of the ionic liquid by the silica shell and the resistance of internal pressure. Compared with nSiO<sub>2</sub> without IL, it is obvious that there is another degradation stage (320 °C - 570 °C) taking place, which can be assigned to the degradation of IL 104 in the IL@SiO<sub>2</sub> microcapsules. Regarding the complex degradation process, it was found that the total weight

loss of IL@SiO<sub>2</sub> microcapsules was found to be closed to 51 wt%.

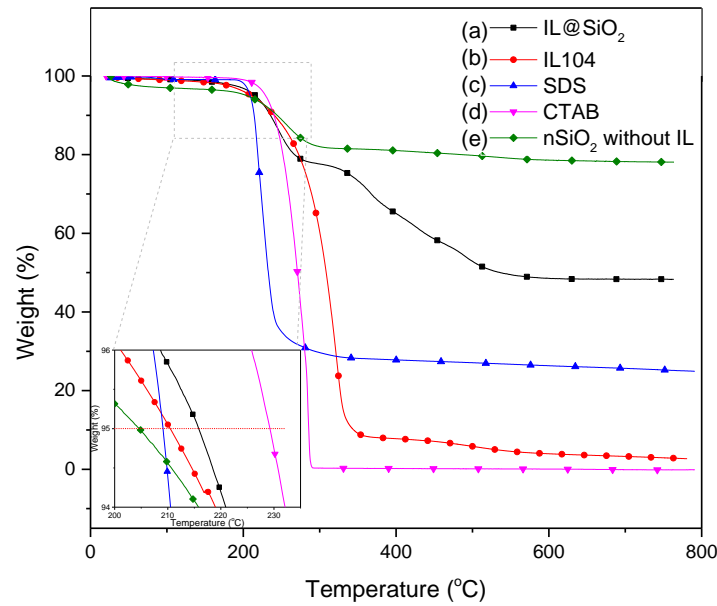


**Figure 2-8** TGA traces of (a) IL@SiO<sub>2</sub> microcapsules, (b) IL 104, (c) SDS, (d) CTAB, and (e) nSiO<sub>2</sub> (*i.e.* without IL) (N<sub>2</sub> atmosphere, heating rate 20 K·min<sup>-1</sup>)

In order to quantify the IL 104 content in the silica microcapsules, elemental analysis was carried on. Silicon (Si) and phosphorous (P) mainly concern the elements from the shell and core material respectively. The elemental mass fractions of Si and P in IL@SiO<sub>2</sub> microcapsules were found to be 19.1 and 1.5 %, respectively. Therefore, according to the mass fraction of these two elements in the starting materials, one can estimate the corresponding SiO<sub>2</sub> and IL 104 contents in the IL@SiO<sub>2</sub> microcapsules according to the following equations 2-5 and 2-6, respectively.

$$\omega_{SiO_2/IL@SiO_2} = \frac{\omega_{Si/IL@SiO_2}}{\omega_{Si/SiO_2}} \quad (\text{equation 2-5})$$

$$\omega_{P/IL@SiO_2} = \frac{\omega_{P/IL@SiO_2}}{\omega_{P/IL}} \quad (\text{equation 2-6})$$

where  $\omega_{Si/SiO_2}$  and  $\omega_{P/IL}$  are the mass fractions of Si or P elements in SiO<sub>2</sub> or in IL 104 respectively,

$\omega_{Si/IL@SiO_2}$  and  $\omega_{P/IL@SiO_2}$  are the mass fractions of Si or P elements in IL@SiO<sub>2</sub> microcapsules from the elemental analyses,

$\omega_{SiO_2/IL@SiO_2}$  and  $\omega_{IL/IL@SiO_2}$  are the calculated mass fractions of SiO<sub>2</sub> and IL 104 in

IL@SiO<sub>2</sub> microcapsules. Therefore, after the calculation based on elemental analysis, it can be estimated that about 41 wt.% of silica and 20 wt.% IL 104 are contained in the IL@SiO<sub>2</sub> microcapsules. The calculated mass fraction of silica is in agreement with the residual weight fraction measured by TGA after a complete degradation. Compared to the previous works about encapsulation of imidazolium ionic liquid ([Bmim][PF<sub>6</sub>]), 66 wt.% IL loading for Weiss<sup>[27]</sup> and 31 wt.% for Zhang<sup>[28]</sup>, we have reached a lower encapsulated mass fraction of IL. This result could be explained as the phosphonium ionic liquid used in this work has a higher viscosity because of its longer alkyl chain. As a consequence, its stabilization in aqueous solution is more difficult. Therefore, higher amounts of surfactants were required lowering the mass fraction of ionic liquid in the resulting IL@SiO<sub>2</sub> microcapsules.

To sum up, IL@SiO<sub>2</sub> microcapsules with a silica shell containing phosphonium IL 104 core were successfully synthesized from one pot sol-gel process within an IL/H<sub>2</sub>O emulsion stabilized with surfactants. Several characterization techniques were employed to characterize the obtained IL@SiO<sub>2</sub> microcapsules. It has been proved that this new type of IL@SiO<sub>2</sub> microcapsules have ideal sphere morphology, core-shell structure, and good thermal stability. Up to now, there were not many researches on ionic liquids encapsulated in silica microcapsules which has been applied as functional additives in thermoset polymer composites.

Therefore, the designed IL@SiO<sub>2</sub> microcapsules were introduced as reinforcing fillers in epoxy-amine networks in order to study their effect on the final properties of resulting microcomposites. It can be speculated that the core-shell structure and other features of IL@SiO<sub>2</sub> microcapsules will influence the mechanical behavior of the epoxy matrix. Therefore, in the following part, IL@SiO<sub>2</sub> microcapsules were incorporated in epoxy-amine networks and different methods such as TEM, SEM, DMA, etc., were employed to characterize the morphologies, dynamic mechanical properties and mechanical properties of the microcomposites. Finally, the mechanisms involved in fracture of such microcomposites are discussed according to the models reported in the literature.

## 2.3 Characterization of IL@SiO<sub>2</sub> microcapsule-filled epoxy-amine microcomposites

### 2.3.1 Morphology and size distributions of IL@SiO<sub>2</sub> microcapsule-filled epoxy-amine microcomposites

Dispersion and morphology of fillers in polymer matrix often have non-negligible influence on the physical properties of polymer composites. So, the dispersion and morphology of IL@SiO<sub>2</sub> microcapsules in the epoxy-amine microcomposites were characterized by transmission electron microscope (TEM). Figure 2-9 shows TEM micrographs of epoxy microcomposites for  $r$  equal to 1.0 and various weight fractions of IL@SiO<sub>2</sub> microcapsules at different magnifications (similar morphologies are observed for the different stoichiometry ratios). As shown in Figure 2-9, spherical geometry, *i.e.* circular cross section on TEM micrographs, of microcapsules can be seen which demonstrates that the microcapsules were not broken during processing of the microcomposites, *i.e.* mixing step.

Silica-based fillers such as fumed silica without any surface modification are likely to aggregate which limits their reinforcement effect or even leads to negative effects on the properties of polymer composites [44]. For example, Constantinescu [45] and Battistella [46] have reported that non-functionalized fumed silica nanoparticles have poor ability to be dispersed in epoxy matrix. As a consequence, no improvement could be reached compared to the neat epoxy due to the poor dispersion state issued from the weak chemical interactions between fumed nanosilica surface and epoxy network chains. For example, for nanosilica/epoxy materials [47], silica remains as large agglomerates and the addition of imidazolium IL as dispersing agent can contribute to a better morphology and interfacial adhesion. Nevertheless, according to our study, IL@SiO<sub>2</sub> microcapsules synthesized by sol-gel in IL/H<sub>2</sub>O emulsion having a core-shell structure and a rough surface [48] have good dispersibility, *i.e.* a good ability to be dispersed in epoxy-amine reactive systems. The role of the roughness of the surface of the IL@SiO<sub>2</sub> microcapsules may enhance the interfacial strength between the silica surface and organic phase.

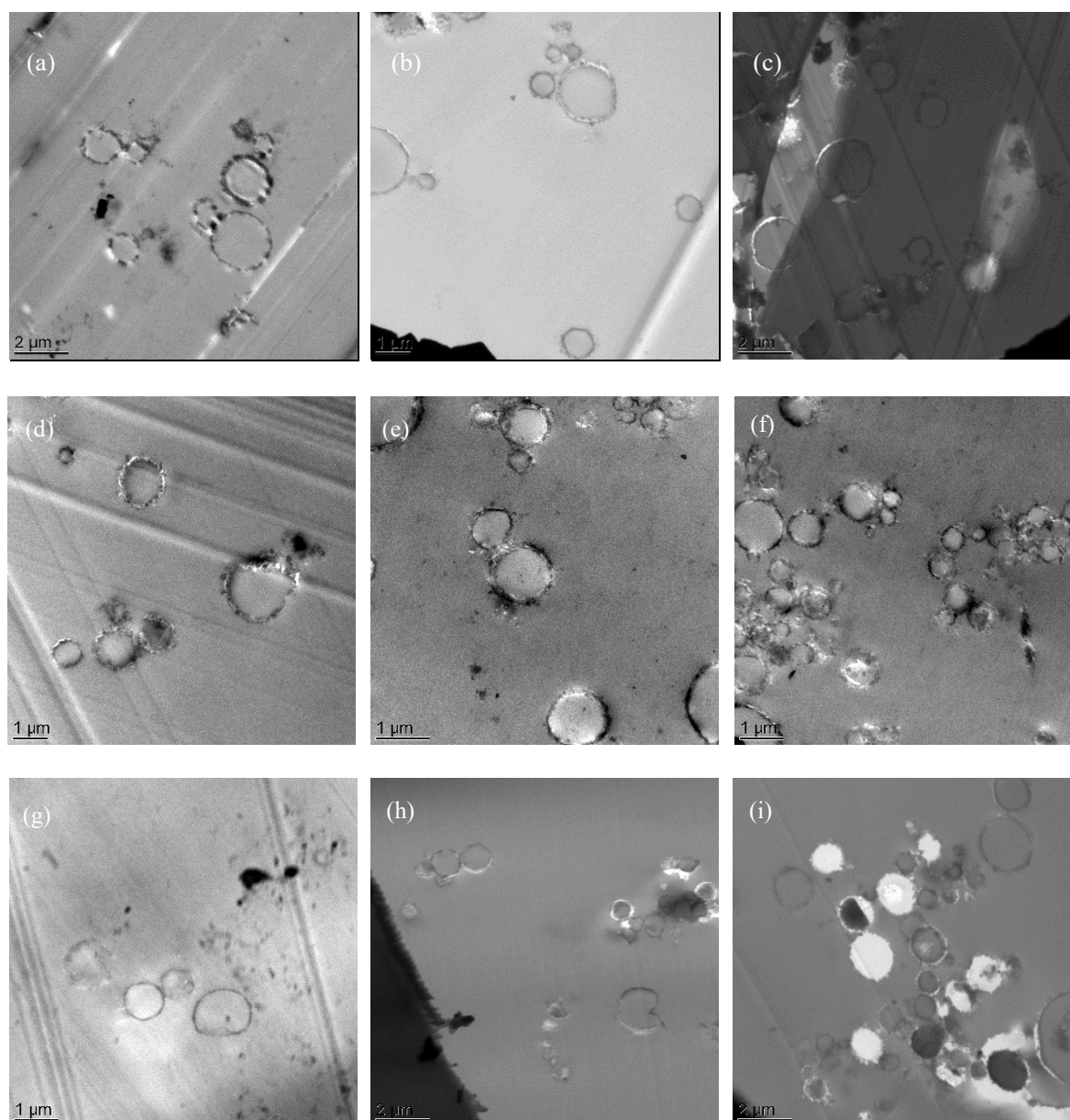


**Figure 2-9** TEM micrographs of IL@SiO<sub>2</sub> microcapsule-filled epoxy-amine microcomposites (a) 1.0-1; (b) 1.0-2; (c) 1.0-5; (d) 1.2-1; (e) 1.2-2; (f) 1.2-5; (g) 1.4-1; (h) 1.4-2; (i) 1.4-5

### 2.3.2 Thermal and dynamic mechanical properties of IL@SiO<sub>2</sub> microcapsule-filled epoxy-amine microcomposites

Thermal properties, including glass transition temperature,  $T_g$ , of IL@SiO<sub>2</sub> microcapsule-filled epoxy microcomposites were characterized by differential scanning calorimetry (DSC). All the  $T_g$  values of different materials are summarized in Table 2-4 while all the DSC curves are given in Figure S2-1 in the Supporting Information of Chapter 2.

**Table 2-4** Glass transition temperature ( $T_g$ ) of epoxy-amine networks, *i.e.* their corresponding IL@SiO<sub>2</sub> microcapsule-filled microcomposites with different epoxy-to-amino hydrogen ratios

Materials	$T_g$ (°C)	Materials	$T_g$ (°C)	Materials	$T_g$ (°C)
1.0-0	156	1.2-0	104	1.4-0	83
1.0-1	165	1.2-1	116	1.4-1	109
1.0-2	170	1.2-2	127	1.4-2	125
1.0-5	171	1.2-5	142	1.4-5	135

As expected, the epoxy-to-aminohydrogen ratio has a significant influence on the  $T_g$  value. For the same weight fraction of IL@SiO<sub>2</sub> microcapsules, the epoxy-amine network prepared at the stoichiometric ratio ( $r=1.0$ ) has the highest  $T_g$ . While for the non-stoichiometric epoxy-amine system ( $r=1.2$  or  $r=1.4$ ), the lack of curing agents, *i.e.* amine comonomer, resulted in a lower crosslink density, inducing more flexibility, as a consequence, a lower  $T_g$  [49].

For the same epoxy-to-amino hydrogen ratio,  $T_g$  increased with the increasing number of IL@SiO<sub>2</sub> microcapsules in the epoxy-amine microcomposites. Compared with epoxy-amine microcomposites cured at stoichiometric ratio ( $r=1$ ), IL@SiO<sub>2</sub> microcapsules led to a more dramatical improvement on  $T_g$  for non-stoichiometric ( $r=1.2$  or  $r=1.4$ ) matrix materials, indicating that unreacted groups could interact at the IL@SiO<sub>2</sub> microcapsules surface hindering segmental motion of polymer chains. For IL@SiO<sub>2</sub> microcapsule-filled epoxy networks, it can be seen that these IL@SiO<sub>2</sub> microcapsules have a positive effect on the thermal properties of epoxy-amine microcomposites. Compared to the results of Rosso *et al* [50], the addition of sol-gel silica nanoparticles with surface modification at 5 vol % improved the stiffness and toughness while promoting a plasticizing effect, *i.e.* a decrease of  $T_g$ . Such an effect of plasticizing induced by the surface treatment of silica surface also happened for other colloidal silica filled epoxy composites [51]. In fact, the surface modification induced the formation of an interface softer than the bulk matrix.

In order to confirm the existence of strong interactions between polymer chains and the surface of IL@SiO<sub>2</sub> microcapsules, dynamic mechanical analysis (DMA) has been carried out.

Figure 2-10 shows curves of loss factor ( $\tan \delta$ ) as a function of temperature of different epoxy networks and their corresponding microcomposites prepared with different  $r$  ratios. Storage modulus ( $E'$ ) and loss modulus ( $E''$ ) curves are also shown in Figure S2-3 in supporting information of Chapter 2. Considering the Young's modulus ( $E$ ) can be related to the second derivative with respect to strain ( $\varepsilon$ ) of the Helmholtz free energy ( $A$ )<sup>[52, 53]</sup>, written as equation 2-7:

$$E = \left( \frac{\partial^2 A}{\partial \varepsilon^2} \right)_T \quad (\text{equation 2-7})$$

and the definition of Helmholtz free energy<sup>[54]</sup> in equation 2-8 involving internal energy ( $U$ ) and entropy ( $S$ ):

$$A = U - TS \quad (\text{equation 2-8})$$

therefore, the Young's modulus can be written as equation 2-9:

$$E = \left( \frac{\partial^2 U}{\partial \varepsilon^2} \right)_T - T \left( \frac{\partial^2 S}{\partial \varepsilon^2} \right)_T \quad (\text{equation 2-9})$$

Assuming homogeneous epoxy networks for which the internal energy will not change with deformation at a given temperature, the change of entropy governs the value of their modulus as one is affected by the structure and the crosslink density. Thus, according to the rubber elasticity theory<sup>[55]</sup>, the elastic modulus is related to the molecular weight between crosslinks ( $M_c$ ) and volume density ( $\rho$ ) (2-10):

$$E = \frac{3RT\rho}{M_c} \quad (\text{equation 2-10})$$

Thus, the crosslink density of epoxy networks can be calculated by equation 2-11:

$$\nu_e = \frac{E'_R}{3RT_R} \quad (\text{equation 2-11})$$

where the  $E'_R$  (Pa) is storage modulus of epoxy networks at the rubbery plateau,  $R$  is ideal gas constant ( $R = 8.314 \text{ J} \cdot \text{mol}^{-1} \cdot \text{K}^{-1}$ ), and  $T_R = T_\alpha + 30(\text{K})$ .

From the values of the storage modulus in the rubbery state ( $E'_R$ ) of the neat epoxy networks<sup>[28]</sup> and the theoretical features reported previously, the crosslink density ( $\nu_e$ ) of different materials was calculated and summarized in Table 2-5.



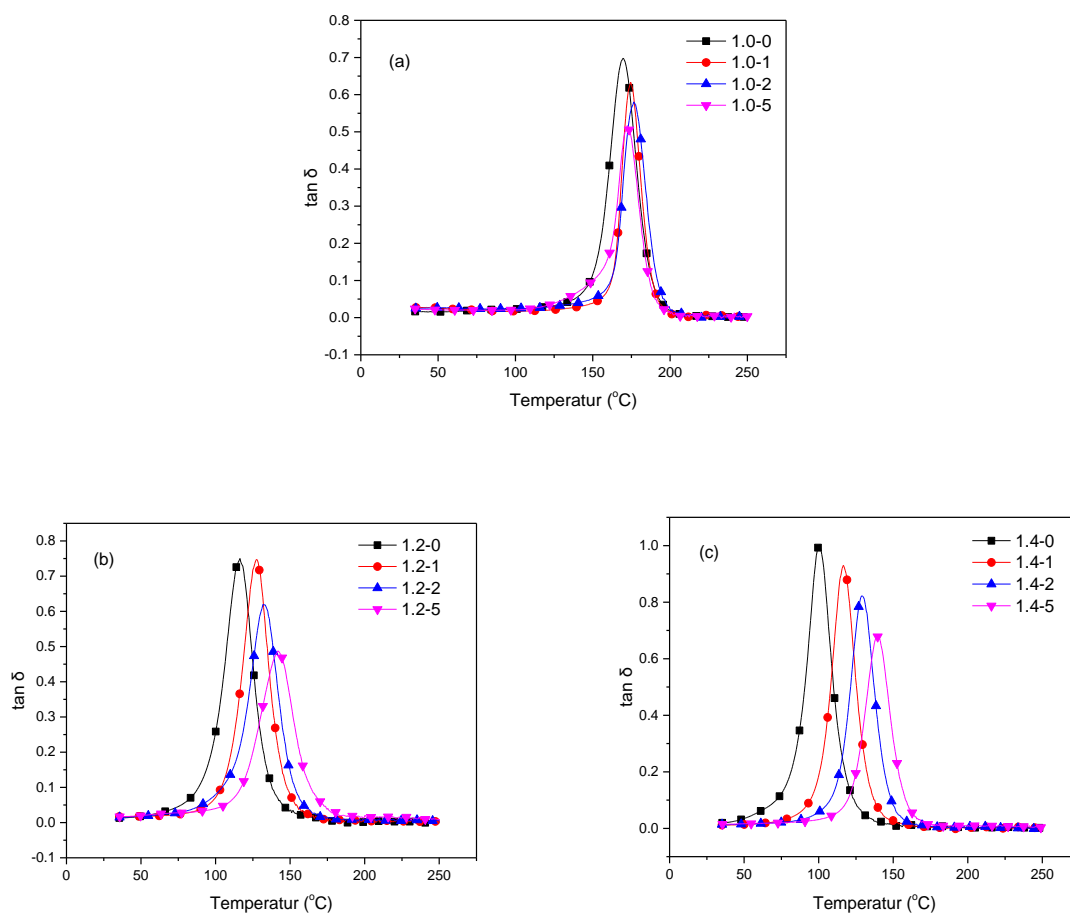


**Figure 2-10** Loss factor ( $\tan \delta$ ) as a function temperature of different epoxy-amine microcomposites (a)  $r=1.0$ ; (b)  $r=1.2$ ; (c)  $r=1.4$  (at 1Hz, heating rate  $3 \text{ K}\cdot\text{min}^{-1}$ )

**Table 2-5** Dynamic mechanical behavior of neat epoxy-amine networks and microcomposites based on different weight fractions of IL@SiO<sub>2</sub> microcapsules

Materials	$T_{\alpha}$ (°C) *	$T_R$ (°C) **	$E'_R$ (MPa) ***	max $\tan \delta$	$v_e$ (mol·m <sup>-3</sup> )
1.0-0	168	198	16.1	0.69	1371
1.0-1	175	205	32.3	0.63	/
1.0-2	176	206	38.3	0.58	/
1.0-5	173	203	36.5	0.51	/
1.2-0	116	146	10.4	0.75	997
1.2-1	128	158	16.0	0.74	/

1.2-2	132	162	17.2	0.62	/
1.2-5	142	172	32.6	0.49	/
1.4-0	100	130	8.4	1.00	838
1.4-1	116	146	11.7	0.93	/
1.4-2	129	159	13.8	0.82	/
1.4-5	140	170	29.7	0.68	/

\*  $\alpha$ -relaxation temperature obtained ( $T_\alpha$ ) from DMA at 1 Hz at the maximum  $\tan \delta$

\*\* Temperature determined at which  $E'_R$  is, *i.e.*  $T_R = T_\alpha + 30$  (K) at rubbery state

\*\*\* Storage modulus in the rubbery state

Table 2-5 reports the temperature of the  $\alpha$ -relaxation associated with the glass transition. As expected,  $T_\alpha$ , obtained from the value at the maximum  $\tan \delta$ , decreases as the epoxy-to-amino hydrogen ratio increases ( $r > 1.0$ ) for the same weight fraction of IL@SiO<sub>2</sub> microcapsules. As for  $T_g$  measured by DSC, this decrease is attributed to the reduction of the crosslink density with increasing  $r$  value. In fact, as an excessive amount of epoxy monomer is used, the average molar mass between crosslinks increases, *i.e.* decrease of the crosslink density,  $\nu_e$ . As a consequence, the storage modulus in the rubbery state,  $E'_R$ , decreases with the increasing stoichiometric ratio,  $r$ . The enhanced segmental motion of the polymer network chains could be also evidenced from the values of  $\tan \delta$  at  $T_\alpha$ .

On the other hand,  $T_\alpha$  increases as the weight fraction of IL@SiO<sub>2</sub> microcapsules increases for a given  $r$  value, in agreement with DSC results. The increase of  $T_\alpha$  with the weight fraction of microcapsules could be attributed to strong interactions created at the silica surface with the polar groups in the epoxy network. In fact, hydrogen bonds could be generated between the surface silanols and polar groups such as hydroxyls (hydroxy ethers formed from the addition reactions), epoxies, or remaining primary or secondary amines. In addition, dehydration reactions could occur between the generated hydroxyl groups and the silanols at the silica surface [56].

The existence of these interfacial physical interactions leads to the reduction of the segmental motions. Thus, as the mass fraction of IL@SiO<sub>2</sub> increases, *i.e.* as the interfacial area

increases, more and more interfacial interactions (acting as additional physical crosslinks) and potential interfacial bonds (acting as additional chemical crosslinks) are generated leading to an increase of the  $T_g$ . For microcomposites prepared from epoxy matrices having a stoichiometric ratio higher than 1.0, more epoxy groups remain unreacted and could form additional interactions with silanols.

These ones could explain the larger effect on the increase of  $T_g$  with the increasing amount of microcapsules. These interfacial interactions/reactions also contribute to increase the value of the storage modulus in the rubbery state,  $E_R'$ , which is related both on the crosslinking density and the reinforcement effect due to the presence of stiff silica particles since this improvement depends on both polymer chain ends and IL@SiO<sub>2</sub> microcapsules content. Nevertheless, as IL@SiO<sub>2</sub> microcapsules are added more than 5 wt%, a significant increase of the viscosity of the mixture is observed leading to difficulties for the processing. These of change of end groups in the molecular chains by the addition of IL@SiO<sub>2</sub> microcapsules brought a very slight influence on the surface properties, which can be seen in the supporting information.

### 2.3.3 Swelling

When the crosslinked polymer is put in a good solvent, two main factors are crucial: *i*) the solubility of monomer units in the solvent, which is mainly revealed by Flory-Huggins parameter  $\chi$ ; *ii*) the molar mass between crosslinks, *i.e.* crosslink density [57]. The relation between  $M_c$  and  $\nu_e$  can be converted by the density of polymer ( $\rho$ ) according to equation 2-12:

$$M_c = \frac{\rho}{\nu_e} \quad (\text{equation 2-12})$$

The swelling equilibrium defined by Flory-Rehner [58] is based on the hypothesis that the changes of free energy on swelling of a network can be separated and are additive [59].  $M_c$  can be calculated according to the equation 2-13, which also showed how swelling is related to the molar mass between crosslinks [60, 61].

$$M_c = -\nu_1 \times \rho_2 \frac{(V_p^{1/3} - \frac{V_p}{2})}{\ln(1-V_p) + V_p + \chi_{12} V_p^2} \quad (\text{equation 2-13})$$

where  $v_1$  is the molar volume of the solvent,  $\rho_2$  the density of polymer material,  $V_p$  the volume fraction of polymer in the swollen polymer, and  $\chi_{12}$  the Flory solvent-polymer interaction parameter between polymer and solvent. In the practical experiment, the volume fraction of polymer in the swollen polymer,  $V_p$ , could be calculated from the swelling ratio determined from swelling experiments according to the equation 2-14:

$$\frac{1}{V_p} = 1 + (\varphi_2 - 1) \frac{\rho_2}{\rho_1} \quad (\text{equation 2-14})$$

where  $\varphi_2$  is the swelling ratio (equation 2-15),  $\rho_1$  and  $\rho_2$  the density of solvent and polymer, respectively.

$$\varphi_2 = \frac{m_{swell}}{m_0} \quad (\text{equation 2-15})$$

where  $m_{swell}$  is the mass of the swollen polymer while  $m_0$  is the mass of the original dry polymer. Nevertheless, this approach to determine  $M_c$  remains limited for highly cross-linked polymers as swelling is lower than expected. As a consequence, only quantitative determination could be done from the swelling ratio <sup>[62]</sup>, *i.e.* swelling experiments are used to estimate changes in the crosslink density <sup>[63, 64]</sup>.

Tetrahydrofuran (THF) is well-known as good solvent for epoxy prepolymers. As a consequence, THF was chosen for the swelling experiments performed on epoxy-amine networks and IL@SiO<sub>2</sub> microcapsule-filed epoxy microcomposites. Different samples were immersed in the same amount of THF and left at the room temperature until the equilibrium was reached (or the sample broke). All the samples were weighted after well wiped at set intervals. The swelling ratios of different IL@SiO<sub>2</sub> microcapsule-filled epoxy-amine microcomposites as a function a time are shown in Figure 2-11. As mentioned before, the swelling by the solvent is mainly related to the Flory-Huggins parameters of the solvent and polymer chains as well as the crosslink density. It is obvious that lowly crosslinked networks will swell much more than highly crosslinked networks.

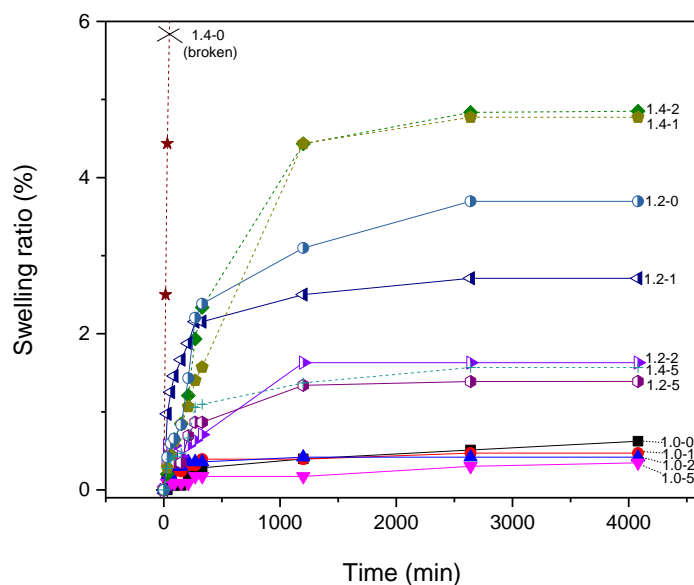


**Figure 2-11** Swelling ratio of different epoxy-amine networks and their corresponding IL@SiO<sub>2</sub> microcapsule-filled microcomposites in THF (at room temperature)

It can be seen from Figure 2-11 that epoxy-to-amino hydrogen ratio plays an important role in the solvent. Without addition of IL@SiO<sub>2</sub> microcapsules, epoxy-amine networks at stoichiometric ratio ( $r=1.0$ ) are the most stable ones in the solvent while epoxy-amine networks with  $r=1.4$  even break after being immersed in THF for 4 hours. With only 1 wt% of IL@SiO<sub>2</sub> microcapsules added in the epoxy-amine matrix ( $r=1.4$ ), the performance of microcomposites in the solvent was greatly improved. Hence, the swelling experiments have showed that the addition of IL@SiO<sub>2</sub> microcapsules in the polymer matrix can improve the dimensional stability of epoxy-amine microcomposites. For a better understanding, the graphical illustration in 3D of swelling model of IL@SiO<sub>2</sub> microcapsule-filled epoxy-amine composites is presented in Figure 2-12. As drawn, the epoxy-amine network without IL@SiO<sub>2</sub> microcapsules shows swollen macromolecules. And solvent molecules can easily penetrate the network and decrease crosslinking density. Therefore, the material may collapse from internal molecular chains as shown in the Figure 2-12 (b). While with the addition of IL@SiO<sub>2</sub> microcapsules (Figure 2-12 (d)), IL@SiO<sub>2</sub> microcapsules help the material to keep a dimensional stability in the solvent.

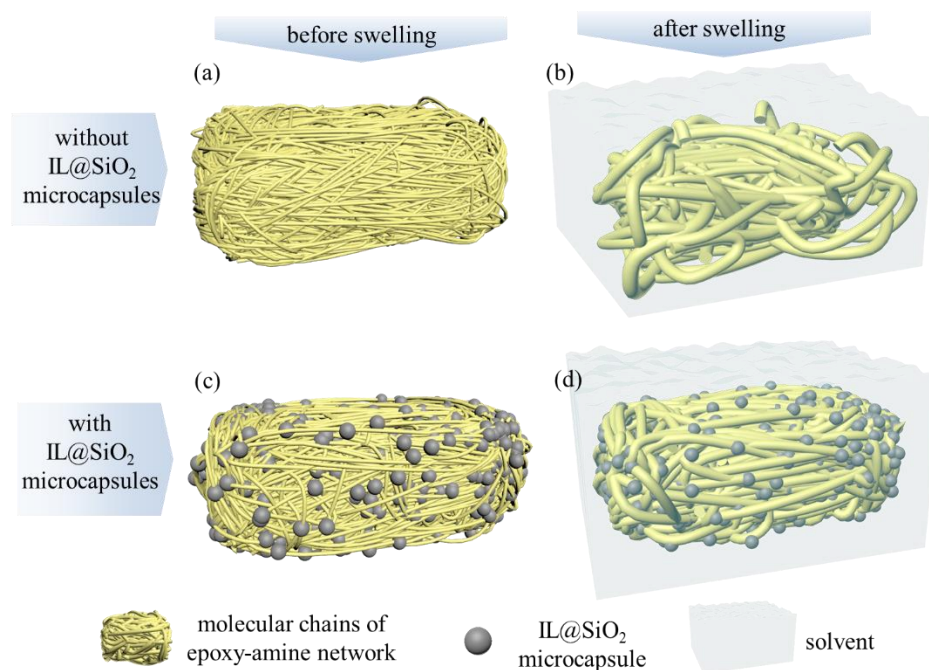


**Figure 2-12** Graphical illustration of swelling model of neat epoxy-amine network: (a) before and (b) after swelling; and IL@SiO<sub>2</sub> microcapsule-filled epoxy-amine microcomposites: (c) before and (d) after swelling

### 2.3.4 Thermal behavior of neat epoxy networks and IL@SiO<sub>2</sub> microcapsule-filled epoxy microcomposites

Thermostability and degradation behavior of IL@SiO<sub>2</sub> microcapsule-filled epoxy microcomposites were characterized by thermogravimetric analysis (TGA) under nitrogen (N<sub>2</sub>) atmosphere. The temperature at 5 wt% weight loss,  $T_{d\ 5\%}$ , was determined as the onset of weight loss temperature and the temperature at the peak of DTG curve as the maximum decomposition temperature ( $T_{d\ max}$ ). Table 2-6 reports the decomposition temperatures of all the materials (TGA and DTG curves are presented in Figure S2-5 in the Supporting Information of Chapter 2). It is obvious that all the  $T_{d\ 5\%}$  are above 350 °C except for the neat epoxy network prepared with a large excess of epoxy (material denoted 1.4-0). All the materials, *i.e.* neat epoxy networks and microcomposites, display similar  $T_{d\ max}$ . Because of the high thermal stability of IL@SiO<sub>2</sub> microcapsules<sup>[65]</sup> and additional interactions generated in between microcapsules and epoxy network in microcomposites, the microcapsules do not have negative influence on the thermal stability of epoxy microcomposites.

**Table 2-6** Degradation temperatures of epoxy-based materials obtained using TGA analysis

Materials	T <sub>d onset</sub> (°C)	T <sub>d max</sub> (°C)
1.0-0	359	378
1.0-1	361	379
1.0-2	352	378
1.0-5	353	377
1.2-0	352	380
1.2-1	359	381
1.2-2	363	380
1.2-5	359	380
1.4-0	329	380
1.4-1	363	382
1.4-2	352	383
1.4-5	356	384

### 2.3.5 Mechanical performances of IL@SiO<sub>2</sub> microcapsule-filled epoxy-amine microcomposites

According to the results of thermomechanical analyses, the IL@SiO<sub>2</sub> microcapsules generate interactions between polymer chains and silica surface. Thus, it is interesting to study the effect of such additional physical and chemical interactions due to the presence of IL@SiO<sub>2</sub> microcapsules on the large strain mechanical properties and fracture toughness of microcomposites. Therefore, compression and fracture toughness tests were performed to determine the Young's modulus,  $E$ , and the stress intensity factor,  $K_{Ic}$ , as well as critical energy release rate,  $G_{Ic}$ , of IL@SiO<sub>2</sub> microcapsules filled epoxy-amine microcomposites compared to neat epoxy-amine networks (see Figure 2-13 and Figure 2-14). The values of  $E$ ,

$K_{Ic}$  and  $G_{Ic}$  of different samples are summarized in the Figure 2-13 and Figure 2-14, respectively. The corresponding values are summarized in Table S2-2. (see the supporting information of Chapter 2).

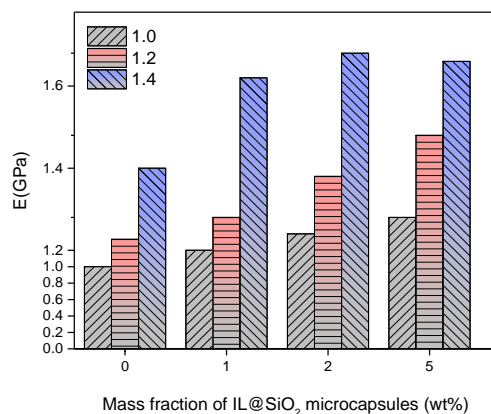


**Figure 2-13** Young's modulus epoxy-amine microcomposite filled with different weight fractions of IL@SiO<sub>2</sub> microcapsules

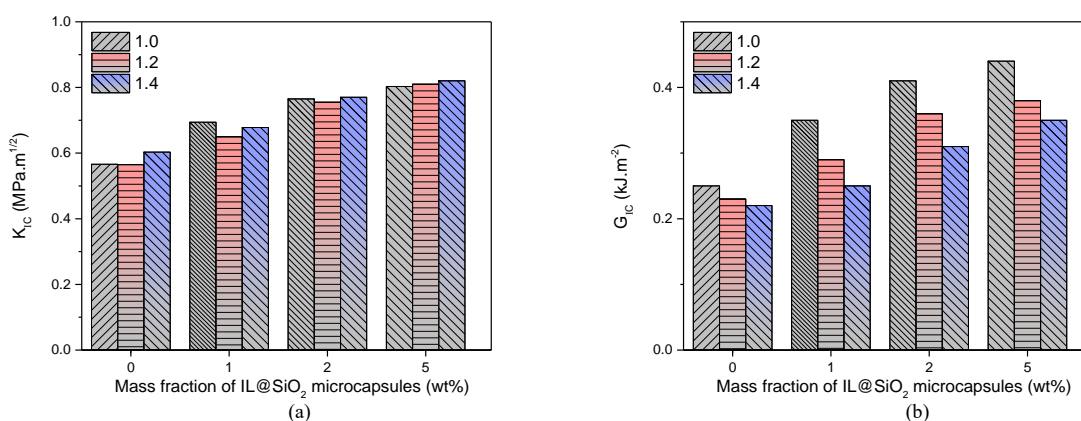


**Figure 2-14** (a)  $K_{Ic}$  and (b)  $G_{Ic}$  of epoxy-amine microcomposites filled with different weight fractions of IL@SiO<sub>2</sub> microcapsules

First of all, the dependence of the Young's modulus of the neat epoxy-amine networks with the epoxy-amino hydrogen ratio ( $r$ ) is in agreement with the ones reported in the literature [66]. In fact, the Young's modulus is not maximum for the 'closed' network, *i.e.* for  $r$  equal to 1.0, due to the antiplasticization effect related to the amplitude of the secondary relaxation  $\beta$  in the glassy state [67]. On another hand, the fracture energies of neat epoxy networks and microcomposites (for a given weight fraction of IL@SiO<sub>2</sub> microcapsules) decrease with



increased  $r$  value.

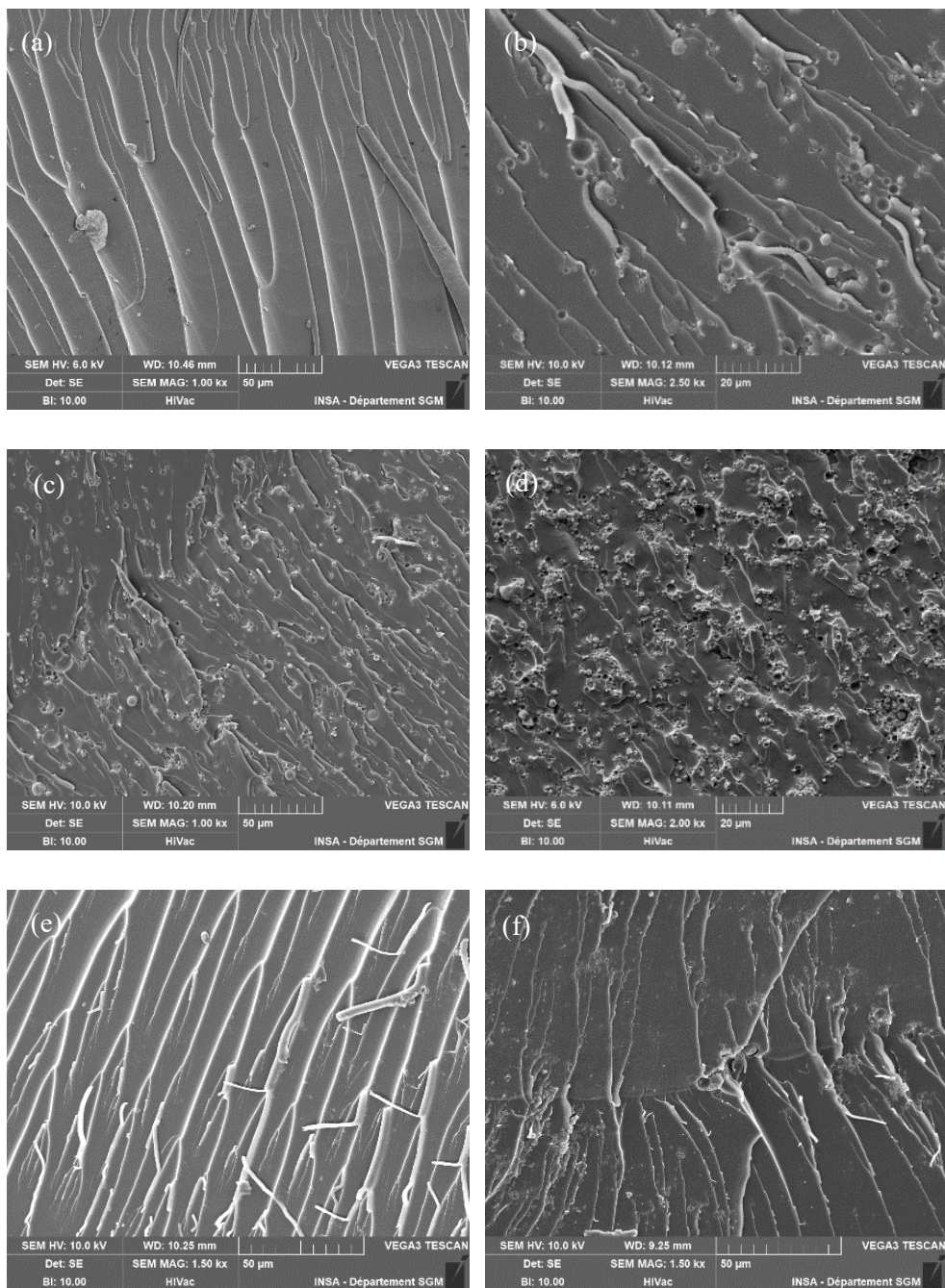
For the materials prepared with a stoichiometric ratio equal to 1.0, the modulus and fracture toughness increase with the increasing IL@SiO<sub>2</sub> microcapsules content. Contrary to some works such as those reported by Chen *et al* [68] who observed the expected increase of Young's modulus but a decrease of the glass transition temperature, the microcomposites prepared in our work display both an improvement of stiffness and toughness and no loss of thermomechanical properties. Chemical modification of silica is generally considered for improving the dispersion in the polymer matrix in order to avoid the formation of aggregates to improve the interfacial strength [69]. In our case, no surface modification of silica was applied and the dispersion is rather fine, meanwhile no negative influence on thermal properties was observed compared to previous studies on silica-based nanocomposites [50]. Nevertheless, our results are in agreement with those reported by Kausch's group [70] for epoxies filled with various types of microparticles such as silica or alumina. These authors observed that the stress intensity factor,  $K_{Ic}$ , varies linearly with the volume fraction of silica microparticles and that the surface treatment has no influence. Fracture mechanisms were proposed and will be discussed for our microcomposites in the next section (see 3.4). For microcomposites prepared with a non-stoichiometric epoxy system, *i.e.*  $r$  equal to 1.2 or 1.4, we found that microcapsules have a similar reinforcing effect for microcomposites prepared with  $r$  equal to 1.0.

From these results, one can conclude that the introduction of low amounts of IL@SiO<sub>2</sub> microcapsules can lead to an increase of the Young modulus as well as fracture energy without counterpart in terms of loss of thermal properties ( $T_g$  increases even in the presence of microcapsules). To develop a better understanding of the toughening mechanisms involved for such microcomposites and the difference with silica filled epoxy nanocomposites, further characterizations will be carried out from the observation of fracture surfaces.

### 2.3.6 Fracture mechanism of IL@SiO<sub>2</sub> microcapsule-filled epoxy-amine microcomposites

Analyzing the topography of the fracture surface of microcomposites, *i.e.* issued from the fractured CT specimens, is helpful to understand the fracture and toughening mechanisms. Thus, scanning electron microscopy (SEM) was employed to observe the fracture surfaces of the IL@SiO<sub>2</sub> microcapsule-filled epoxy-amine microcomposites. Figure 2-15 shows SEM

images of the neat epoxy-amine network and the corresponding microcomposites. A uniform dispersion of IL@SiO<sub>2</sub> microcapsules in the epoxy matrix is observed, *i.e.* no widespread agglomeration. Nevertheless, different morphologies of fractured surface were noticed for various types of microcomposites.



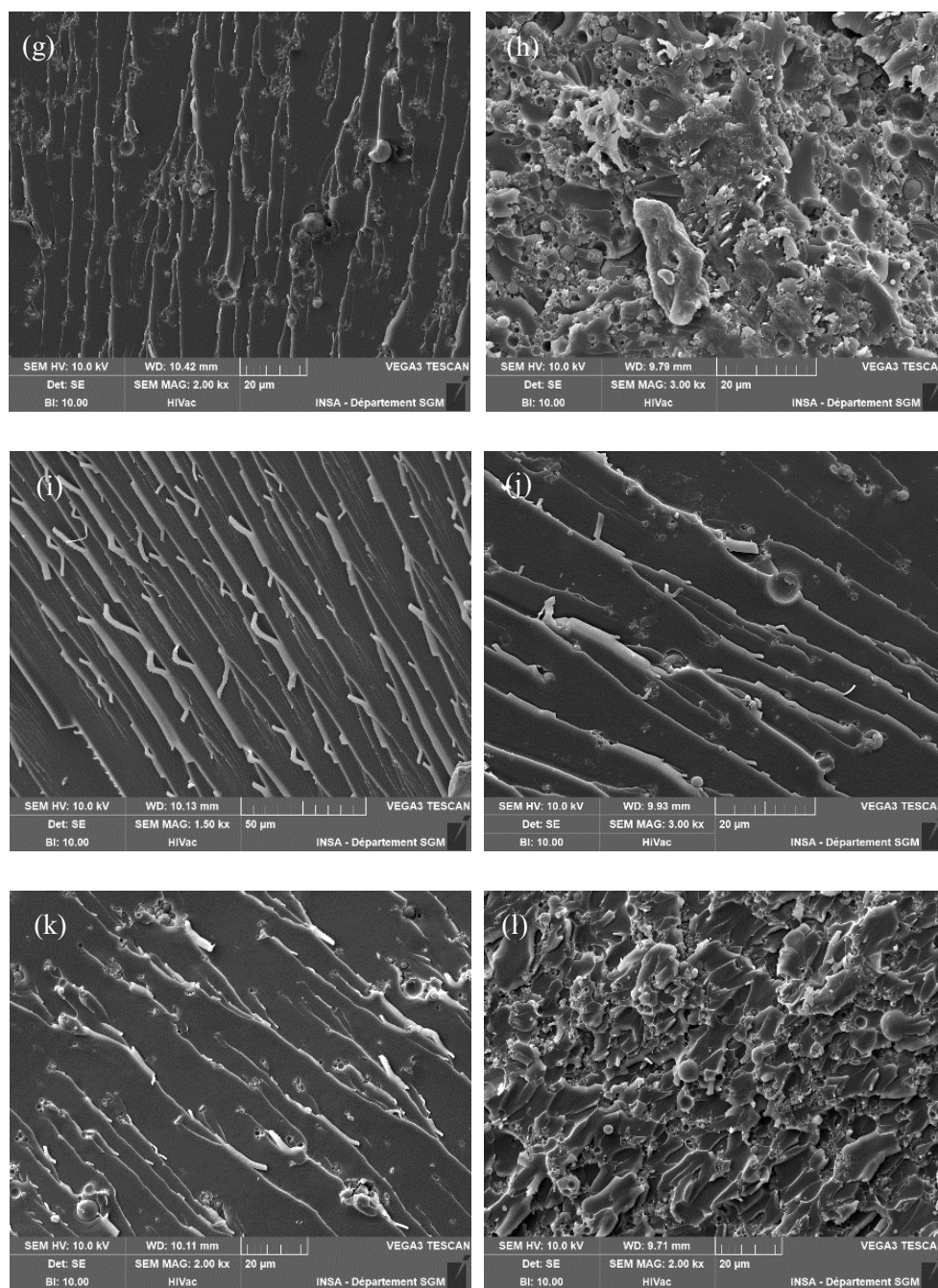


**Figure 2-15** SEM micrographs of fracture surfaces of epoxy-amine composites filled with different weight fractions of IL@SiO<sub>2</sub> microcapsules

- (a) 1.0-0; (b) 1.0-1; (c) 1.0-2; (d) 1.0-5;  
 (e) 1.2-0; (f) 1.2-1; (g) 1.2-2; (h) 1.2-5;  
 (i) 1.4-0; (j) 1.4-1; (k) 1.4-2; (l) 1.4-5

First of all, the neat epoxy-amine network displays a mirror-like fracture surface which is usual for non-modified epoxy-amine networks (see Figure 2-15 (a), (e) and (i)). The fracture

surface steps are related to the stick-slip propagation of the crack with successive arrests.

While for the IL@SiO<sub>2</sub> microcapsule-filled epoxy-amine composites, two different types of fracture surface can be distinguished from the Figure 2-15. When microcapsules are added at low content, *i.e.* 1 and 2 wt%, the distance between microcapsules is large, resulting in surface steps associated with microcapsules encountered by the moving crack front (Figure 2-15 (b), (c), (f), (g), (j), and (k)). When microcapsules are present at high content (5 wt%, Figure 2-15 (d), (h), (l)), a much more larger fracture surface is generated with multiple cracks deviations corresponding to the observed increase of  $G_{Ic}$ . These types of fracture surfaces are in agreement with the description of Lange<sup>[71]</sup> about filled epoxies.

Difference toughening mechanisms were proposed. For example, crack bifurcation or microcracking could be identified as the toughening mechanism for rubber or thermoplastic-modified epoxies<sup>[72]</sup>. Crack deflection, crack pinning, plastic deformation, and plastic void growth are universal toughening mechanisms for the nano/microparticles filled polymer composites. The mechanism may differ according to the size and shape of the fillers. Crack pinning mechanism involved for hard fillers will create the obstruction to the propagation of the crack front and led to an increasing toughness by bowing out the crack front between the particles<sup>[73]</sup>. This phenomenon was first put forward by Lange<sup>[74]</sup> and Zamanian *et al*<sup>[75]</sup> who also pointed out in their publication that crack pinning could possibly happen when the size of fillers is comparable to the crack tip opening displacement. Besides, Lange also gave the relation between the increasing fracture energy and interparticle spacing<sup>[76]</sup>, which was described in equation 2-16:

$$\Delta G_{Ic} = \frac{T}{2b} \quad (\text{equation 2-16})$$

where the  $T$  is the line energy of the crack front and the  $2b$  is the interparticle spacing. Therefore, As the weight fraction of IL@SiO<sub>2</sub> microcapsules increases, the interparticle spacing decreases. As a consequence, the fracture energy increases.

Crack deflection, crack front pinning, enhanced plastic deformation, and crack tip blunting were proposed to explain the toughening mechanisms for the particle filled glassy polymer networks<sup>[9, 71, 77]</sup>. For particle-reinforced epoxy composites, the fracture patterns identified on the SEM images reveal that crack pinning would be the possible toughening mechanism. In fact,

the propagation of cracks seems to be pinned by the microcapsules. As it is known that crack pinning could occur as the size of fillers is comparable to the crack tip opening displacement (COD,  $\delta_{tc}$ ), it is necessary to see if such a fracture criteria plays a role. Figure 8 recalls the theoretical definition of COD at the crack tip.

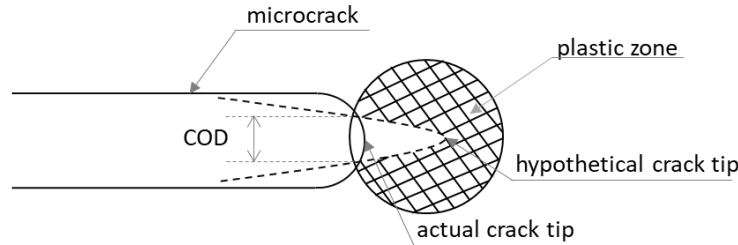


**Figure 2-16** Schematic diagram of the crack tip and crack opening displacement (COD) <sup>[77]</sup>

Under plane strain conditions, the corresponding COD value at the crack tip can be calculated from equation 2-17 <sup>[78, 79]</sup>:

$$\delta_{tc} = \frac{K_{Ic}^2}{E\sigma_y} (1 - \nu^2) = \frac{G_{Ic}}{\sigma_y} \quad (\text{equation 2-17})$$

where the  $\sigma_y$  is the yield stress of the material and  $G_{Ic}$  is the critical energy release rate in Mode I. All the values of yield stress and calculated theoretical COD values of different materials are summarized in Table 2-7, in which all the  $\delta_{tc}$  values are comparable with the size of IL@SiO<sub>2</sub> microcapsules. This fact demonstrates that crack growth can be prevented by fillers such as IL@SiO<sub>2</sub> microcapsules. In addition, it is obvious that with the increasing microcapsule content, *i.e.* the number of obstacles in the epoxy matrix, such an increase of  $\delta_{tc}$  can also be considered as an evidence of enhanced fracture toughness. In addition, crack tip blunting results from pulling out of the microcapsules as evidenced on SEM images. The resulting increase of the crack tip radius leads to a reduction of the local stress concentration. As a consequence, those toughening mechanisms lead to an increase of the volume of the process zone, *i.e.* the volume ahead of the crack tip in which plastic deformation is located. Thus, microcapsules could contribute to the fracture toughness of epoxy-microcapsules microcomposites. To sum up, epoxy amine networks without microcapsules display brittle behavior, *i.e.* have low fracture toughness, whereas the microcapsules filled epoxy microcomposites, crack pinning and crack tip blunting mechanisms contribute to a higher fracture toughness.

**Table 2-7** Yield stress and theoretical crack opening displacement values of neat epoxy-amine networks and microcomposites based on different weight fractions of IL@SiO<sub>2</sub> microcapsules

Material	$\sigma_y$ (MPa)	$\delta_{tc}$ ( $\mu\text{m}$ )*
1.0-0	95 $\pm$ 4	2.63
1.0-1	103 $\pm$ 3	3.40
1.0-2	106 $\pm$ 7	3.87
1.0-5	109 $\pm$ 5	4.04
1.2-0	96 $\pm$ 4	2.40
1.2-1	103 $\pm$ 2	2.82
1.2-2	115 $\pm$ 7	3.13
1.2-5	114 $\pm$ 2	3.33
1.4-0	84 $\pm$ 6	2.62
1.4-1	104 $\pm$ 6	2.40
1.4-2	113 $\pm$ 5	2.74
1.4-5	117 $\pm$ 4	2.99

\* calculated from the average value of  $\sigma_y$

## 2.4 Conclusion of Chapter 2

Ionic liquids (IL) core/silica shell microcapsules were successfully synthesized from the one step sol-gel hydrolysis and condensation reactions of TEOS within an IL/H<sub>2</sub>O emulsion. TEM and SEM microscopies clearly evidence the core-shell structure and spherical shape of the synthesized SiO<sub>2</sub>@IL microcapsules, *i.e.* microcontainers having a SiO<sub>2</sub>-like shell and IL trapped as the core. EDX (performed under TEM) and FTIR spectroscopies have proved that the ionic liquids IL 104 are well encapsulated in the silica shell. Thermogravimetric and elemental analyses also show that the weight fraction of ionic liquids IL and silica shell are close to 20 wt.% and 41 wt.%, respectively. Moreover, microcapsules show very good thermal stability which allow their use for being inserted in a curable system such as an epoxy-amine reactive system to design microcomposites. Consequently, it paves the way for the implementation of such ionic liquid core/silica shell microcapsules as promising additives in

epoxy networks to promote improved mechanical properties.

The obtained IL@SiO<sub>2</sub> microcapsules were incorporated in epoxy amine networks as microfillers. Even a small amount IL@SiO<sub>2</sub> microcapsules can enhance simultaneously the thermal and mechanical properties of epoxy microcomposites. For a given epoxy-to-aminohydrogen stoichiometric ratio of the epoxy matrix, by increasing weight fraction of IL@SiO<sub>2</sub> microcapsules, Young's modulus and fracture toughness of microcomposites increase as well as glass transition temperature. On another hand, for the same weight fraction of IL@SiO<sub>2</sub> microcapsules, as the stoichiometric ratio of epoxy matrix increases, these improvement effects are even more important. These enhanced thermal and thermomechanical properties could be related to the improved interactions between polymer chains and microcapsules silica surface. The increased fracture toughness could be associated to the crack front pinning and crack tip blunting mechanisms for microcapsules filled epoxy microcomposites. Thus, this work is the first to show that it is possible to introduce microcapsules into high glass transition temperature epoxy-amine matrices without impairing their thermal, thermomechanical, and fracture properties. Also, this study makes it possible to envisage the use of these microcapsules to bring new functionalities to epoxy-based materials used as matrices of composites or structural adhesives (self-repair, shape memory) and/or protective coatings (anticorrosion).

## References of Chapter 2

- [1] Jin, F.-L.; Li, X.; Park, S.-J., Synthesis and application of epoxy resins: A review. *Journal of Industrial and Engineering Chemistry*. **2015**, 29, 1-11.
- [2] Shin, H.; Kim, B.; Han, J.-G.; Lee, M. Y.; Park, J. K.; Cho, M., Fracture toughness enhancement of thermoplastic/epoxy blends by the plastic yield of toughening agents: A multiscale analysis. *Composites Science and Technology*. **2017**, 145, 173-180.
- [3] Keller, A.; Chong, H. M.; Taylor, A. C.; Dransfeld, C.; Masania, K., Core-shell rubber nanoparticle reinforcement and processing of high toughness fast-curing epoxy composites. *Composites Science and Technology*. **2017**, 147, 78-88.
- [4] Li, B.; Zhang, X.; Qi, G.; Wang, X.; Zhang, J.; Han, P.; Ru, Y.; Qiao, J., A rubber-modified epoxy composite with very high toughness and heat resistance. *Polym. Polym. Compos.* **2019**, 27, 582-586.
- [5] Mehrabi-Kooshki, M.; Jalali-Arani, A., Preparation of binary and hybrid epoxy nanocomposites containing graphene oxide and rubber nanoparticles: Fracture toughness and mechanical properties. *J. Appl. Polym. Sci.* **2019**, 136, 46988.
- [6] Di Filippo, M.; Alessi, S.; Palmese, G.; Dispenza, C., Electrospun rubber/thermoplastic hybrid nanofibers for localized toughening effects in epoxy resins. *J. Appl. Polym. Sci.* **2020**, 137, 48501.
- [7] Bajpai, A.; Alapati, A. K.; Klingler, A.; Wetzel, B., Tensile properties, fracture mechanics properties and toughening mechanisms of epoxy systems modified with soft block copolymers, rigid TiO<sub>2</sub> nanoparticles and their hybrids. *Journal of Composites Science*. **2018**, 2, 72.
- [8] Sasidharan, S.; Anand, A., Epoxy based hybrid structural composites with nanofillers: A review. *Industrial & Engineering Chemistry Research*. **2020**, 12617-12631.
- [9] Garg, A. C.; Mai, Y.-W., Failure mechanisms in toughened epoxy resins—A review. *Composites Science and Technology*. **1988**, 31, 179-223.
- [10] Pearson, R. A.; Yee, A. F., Toughening mechanisms in elastomer-modified epoxies. *Journal of Materials Science*. **1989**, 24, 2571-2580.
- [11] Bascom, W. D.; Cottington, R. L.; Jones, R. L.; Peyser, P., The fracture of epoxy- and elastomer-modified epoxy polymers in bulk and as adhesives. *J. Appl. Polym. Sci.* **1975**, 19, 2545-2562.
- [12] Domun, N.; Hadavinia, H.; Zhang, T.; Sainsbury, T.; Liaghat, G. H.; Vahid, S., Improving the fracture toughness and the strength of epoxy using nanomaterials--a review of the current status. *Nanoscale*. **2015**, 7, 10294-10329.
- [13] Vashchuk, A.; Fainleib, A. M.; Starostenko, O.; Grande, D., Application of ionic liquids



in thermosetting polymers: Epoxy and cyanate ester resins. *Express Polymer Letters*. **2018**, 12, 898-917.

[14] Nguyen, T. K. L.; Livi, S.; Soares, B. G.; Pruvost, S.; Duchet-Rumeau, J.; Gérard, J.-F., Ionic liquids: a new route for the design of epoxy networks. *ACS Sustainable Chemistry & Engineering*. **2015**, 4, 481-490.

[15] Maka, H.; Spsychaj, T.; Pilawka, R., Epoxy resin/ionic liquid systems: the influence of imidazolium cation size and anion type on reactivity and thermomechanical properties. *Industrial & Engineering Chemistry Research*. **2012**, 51, 5197-5206.

[16] Silva, A. A.; Livi, S.; Netto, D. B.; Soares, B. G.; Duchet, J.; Gérard, J.-F., New epoxy systems based on ionic liquid. *Polymer*. **2013**, 54, 2123-2129.

[17] Nguyen, T. K. L.; Soares, B. G.; Duchet-Rumeau, J.; Livi, S., Dual functions of ILs in the core-shell particle reinforced epoxy networks: curing agent vs dispersion aids. *Composites Science and Technology*. **2017**, 140, 30-38.

[18] Saurín, N.; Sanes, J.; Bermúdez, M. D., Self-Healing of Abrasion Damage in Epoxy Resin-Ionic Liquid Nanocomposites. *Tribology Letters*. **2015**, 58, 1-9.

[19] Zhou, Y.; Qu, J., Ionic Liquids as Lubricant Additives: A Review. *ACS Appl Mater Interfaces*. **2017**, 9, 3209-3222.

[20] Saurín, N.; Sanes, J.; Carrión, F. J.; Bermúdez, M. D., Self-healing of abrasion damage on epoxy resin controlled by ionic liquid. *RSC Advances*. **2016**, 6, 37258-37264.

[21] Li, H.; Wang, Q.; Wang, H.; Cui, Y.; Zhu, Y.; Wang, B., Fabrication of thermally stable polysulfone microcapsules containing [EMIm][NTf<sub>2</sub>] ionic liquid for enhancement of in situ self-lubrication effect of epoxy. *Macromolecular Materials and Engineering*. **2016**, 301, 1473-1481.

[22] Xiang, Z. Y.; Lu, Y. C.; Zou, Y.; Gong, X. C.; Luo, G. S., Preparation of microcapsules containing ionic liquids with a new solvent extraction system. *Reactive and Functional Polymers*. **2008**, 68, 1260-1265.

[23] Barbé, C.; Calleja, S.; Kong, L.; Drabarek, E.; Bush, A.; Sizgek, E.; Finnie, K., Sol-gel silica particles for controlled release applications. *MRS Online Proceedings Library Archive*. **2004**, 368-373.

[24] Rahman, I. A.; Padavettan, V., Synthesis of silica nanoparticles by sol-gel: size-dependent properties, surface modification, and applications in silica-polymer nanocomposites—a review. *Journal of Nanomaterials*. **2012**, 2012, 1-15.

[25] Tang, F.; Li, L.; Chen, D., Mesoporous silica nanoparticles: synthesis, biocompatibility and drug delivery. *Adv. Mater. (Weinheim, Ger.)*. **2012**, 24, 1504-1534.

[26] Asefa, T.; Tao, Z., Biocompatibility of mesoporous silica nanoparticles. *Chemical research in toxicology*. **2012**, 25, 2265-2284.

[27] Weiss, E.; Dutta, B.; Kirschning, A.; Abu-Reziq, R., BMIm-PF<sub>6</sub>@SiO<sub>2</sub> microcapsules: particulated ionic liquid as a new material for the heterogenization of catalysts. *Chemistry of Materials*. **2014**, 26, 4781-4787.

- [28] Yang, M.; Zhu, X.; Ren, G.; Men, X.; Guo, F.; Li, P.; Zhang, Z., Tribological behaviors of polyurethane composite coatings filled with ionic liquid core silica gel shell microcapsules. *Tribology Letters*. **2015**, *57*, 1-9.
- [29] Miller, R., Emulsifiers: Types and uses. *Encyclopedia of Food and Health*. **2016**, 498-502.
- [30] Wa, L.; Fengyun, L.; Fanlu, Z.; Mengjing, C.; Qiang, C.; Jue, H.; Weijun, Z.; Mingwei, M., Preparation of silica aerogels using CTAB/SDS as template and their efficient adsorption. *Appl. Surf. Sci.* **2015**, *353*, 1031-1036.
- [31] Li, H.; Cui, Y.; Li, Z.; Zhu, Y.; Wang, H., Fabrication of microcapsules containing dual-functional tung oil and properties suitable for self-healing and self-lubricating coatings. *Prog. Org. Coat.* **2018**, *115*, 164-171.
- [32] Ma, Y.; Li, Z.; Wang, H.; Li, H., Synthesis and optimization of polyurethane microcapsules containing [BMIm]PF<sub>6</sub> ionic liquid lubricant. *J Colloid Interface Sci.* **2019**, *534*, 469-479.
- [33] Zhang, C. Y.; Cao, Z.; Zhu, W. J.; Liu, J.; Jiang, Q.; Shuai, X. T., Highly uniform and stable cerasomal microcapsule with good biocompatibility for drug delivery. *Colloids Surf. B Biointerfaces*. **2014**, *116*, 327-333.
- [34] Tah, B.; Pal, P.; Mahato, M.; Talapatra, G. B., Aggregation behavior of SDS/CTAB catanionic surfactant mixture in aqueous solution and at the air/water interface. *J Phys Chem B*. **2011**, *115*, 8493-8499.
- [35] Zhou, D.; Liu, R.; He, Y.-B.; Li, F.; Liu, M.; Li, B.; Yang, Q.-H.; Cai, Q.; Kang, F., SiO<sub>2</sub> hollow nanosphere-based composite solid electrolyte for lithium metal batteries to suppress lithium dendrite growth and enhance cycle life. *Advanced Energy Materials*. **2016**, *6*, 1-10.
- [36] Nourafkan, E.; Alamdari, A., Study of effective parameters in silver nanoparticle synthesis through method of reverse microemulsion. *Journal of Industrial and Engineering Chemistry*. **2014**, *20*, 3639-3645.
- [37] Miraglia, D. B.; Rodríguez, J. L.; Minardi, R. M.; Schulz, P. C., Critical Micelle Concentration and HLB of the Sodium Oleate–Hexadecyltrimethylammonium Bromide Mixed System. *J. Surfactants Deterg.* **2010**, *14*, 401-408.
- [38] Gu, X.; Li, C.; Liu, X.; Ren, J.; Wang, Y.; Guo, Y.; Guo, Y.; Lu, G., Synthesis of nanosized multilayered silica vesicles with high hydrothermal stability. *The journal of Physical Chemistry C*. **2009**, *113*, 6472-6479.
- [39] Gledhill, R. A.; Kinloch, A. J., Relationship between mechanical properties of and crack propagation in epoxy resin adhesives. *Polymer*. **1978**, *19*, 574-582.
- [40] Chabane, H.; Livi, S.; Morelle, X. P.; Sonnier, R.; Loïc Dumazert; Duchet-Rumeau, J.; Gérard, J.-F., Synthesis of new ionic liquid-grafted metal-oxo nanoclusters – Design of nanostructured hybrid organic-inorganic polymer networks. *Polymer*. **2021**, *224*, 123721-123731.
- [41] Petrovic, L. B.; Sovilj, V. J.; Katona, J. M.; Milanovic, J. L., Influence of polymer–

- surfactant interactions on o/w emulsion properties and microcapsule formation. *Journal of Colloid and Interface Science*. **2010**, 342, 333-339.
- [42]Ciriminna, R.; Sciortino, M.; Alonzo, G.; Schrijver, A. d.; Pagliaro, M., From molecules to systems: sol– gel microencapsulation in silica-based materials. *Chem. Rev. (Washington, DC, U. S.)*. **2011**, 111, 765-789.
- [43]Chen, G.; Tao, D., An experimental study of stability of oil–water emulsion. *Fuel processing technology*. **2005**, 86, 499-508.
- [44]Wu, C.; Zhang, M.; Rong, M.; Friedrich, K., Silica nanoparticles filled polypropylene: effects of particle surface treatment, matrix ductility and particle species on mechanical performance of the composites. *Composites Science and Technology*. **2005**, 65, 635-645.
- [45]Constantinescu, D. M.; Apostol, D. A.; Picu, C. R.; Krawczyk, K.; Sieberer, M., Mechanical properties of epoxy nanocomposites reinforced with functionalized silica nanoparticles. *Procedia Structural Integrity*. **2017**, 5, 647-652.
- [46]Battistella, M.; Cascione, M.; Fiedler, B.; Wichmann, M. H. G.; Quaresimin, M.; Schulte, K., Fracture behaviour of fumed silica/epoxy nanocomposites. *Composites Part A: Applied Science and Manufacturing*. **2008**, 39, 1851-1858.
- [47]Donato, R. K.; Matějka, L.; Schrekker, H. S.; Pleštil, J.; Jigounov, A.; Brus, J.; Šlouf, M., The multifunctional role of ionic liquids in the formation of epoxy-silica nanocomposites. *Journal of Materials Chemistry*. **2011**, 21, 13801-13810.
- [48]Shi, T.; Livi, S.; Duchet, J.; Gérard, J.-F., Ionic liquids-containing silica microcapsules: a potential tunable platform for shaping-up epoxy-based composite materials? *Nanomaterials*. **2020**, 10, 881-892.
- [49]Pascault, J.-P.; Williams, R. J. J., Glass transition temperature versus conversion relationships for thermosetting polymers. *Journal of Polymer Science Part B: Polymer Physics*. **1990**, 18, 85-95.
- [50]Rosso, P.; Ye, L.; Friedrich, K.; Sprenger, S., A toughened epoxy resin by silica nanoparticle reinforcement. *J. Appl. Polym. Sci*. **2006**, 100, 1849-1855.
- [51]Liu, Y.-L.; Hsu, C.-Y.; Wei, W.-L.; Jeng, R.-J., Preparation and thermal properties of epoxy-silica nanocomposites from nanoscale colloidal silica. *Polymer*. **2003**, 44, 5159-5167.
- [52]D.Katz; Tobolsky, A. V., Rubber elasticity in a highly crosslinked epoxy system. *Polymer*. **1963**, 4, 417-421.
- [53]Gluck-Hirsch, J. B.; Kokini, J. L., Determination of the molecular weight between crosslinks of waxy maize starches using the theory of rubber elasticity. *J. Rheol*. **1997**, 41, 129-140.
- [54]Yang, F., Diffusion-induced stress in inhomogeneous materials: concentration-dependent elastic modulus. *Science China Physics, Mechanics and Astronomy*. **2012**, 55, 955-962.
- [55]Wall, F. T.; Mandel, F., Theory of rubberlike elasticity. *The Journal of Chemical Physics*. **1976**, 64, 1998-2001.
- [56]Ochi, M.; Takahashi, R., Phase structure and thermomechanical properties of primary and

- tertiary amine-cured epoxy silica hybrids. *J. Polym. Sci., Part B: Polym. Phys.* **2001**, 39, 1071–1084.
- [57]Singhal, R.; Tomar, R. S.; Nagpal, A. K., Effect of cross-linker and initiator concentration on the swelling behaviour and network parameters of superabsorbent hydrogels based on acrylamide and acrylic acid. *International Journal of Plastics Technology.* **2009**, 13, 22-37.
- [58]Flory, P. J., Statistical Mechanics of Swelling of Network Structures. *The Journal of Chemical Physics.* **1950**, 18, 108-111.
- [59]Neuburger, N. A.; Eichinger, B. E., Critical experimental test of the Flory-Rehner theory of swelling. *Macromolecules.* **1988**, 21, 3060-3070.
- [60]Ranjha, N. M.; Ayub, G.; Naseem, S.; Ansari, M. T., Preparation and characterization of hybrid pH-sensitive hydrogels of chitosan-co-acrylic acid for controlled release of verapamil. *J. Mater. Sci. Mater. Med.* **2010**, 21, 2805-2816.
- [61]Xue, W.; Champ, S.; Huglin, M. B., Network and swelling parameters of chemically crosslinked thermoreversible hydrogels. *Polymer.* **2001**, 42, 3665-3669.
- [62]Kenyon, A. S.; Nielsen, L. E., Characterization of Network Structure of Epoxy Resins by Dynamic Mechanical and Liquid Swelling Tests. *Journal of Macromolecular Science: Part A - Chemistry.* **1969**, 3, 275-295.
- [63]Roy, B.; Karak, N., Modification of hyperbranched epoxy by vegetable oil-based highly branched polyester resin. *Polym. Bull.* **2012**, 68, 2299-2312.
- [64]Aoki, M.; Shundo, A.; Yamamoto, S.; Tanaka, K., Effect of a heterogeneous network on glass transition dynamics and solvent crack behavior of epoxy resins. *Soft Matter.* **2020**, 16, 7470-7478.
- [65]Shi, T.; Livi, S.; Duchet, J.; Gerard, J. F., Ionic Liquids-Containing Silica Microcapsules: A Potential Tunable Platform for Shaping-Up Epoxy-Based Composite Materials? *Nanomaterials (Basel).* **2020**, 10.
- [66]Palmese, G. R.; McCullough, R. L., Effect of epoxy-amine stoichiometry on cured resin material properties. *J. Appl. Polym. Sci.* **1992**, 46, 1863-1873.
- [67]Won, Y.-g.; Galy, J.; Gérard, J.-F.; Pascault, J.-P., Internal antiplasticization in copolymer and terpolymer networks based on diepoxides, diamines and monoamines. *Polymer.* **1992**, 31, 1787-1792.
- [68]Chen, C.; Justice, R. S.; Schaefer, D. W.; Baur, J. W., Highly dispersed nanosilica-epoxy resins with enhanced mechanical properties. *Polymer.* **2008**, 49, 3805-3815.
- [69]Sprenger, S., Nanosilica-Toughened Epoxy Resins. *Polymers (Basel).* **2020**, 12, 1777-1803.
- [70]Moloney, A. C.; Kausch, H. H.; Stieger, H. R., The fracture of particulate-filled epoxide resins. *Journal of materials Science.* **1983**, 18, 208-216.
- [71]Lange, F. F.; Radford, K. C., Fracture energy of an epoxy composite system. *Journal of Materials Science.* **1971**, 6, 1197-1203.
- [72]Pearson, R. A.; FYee, A., Toughening mechanisms in thermoplastic-modified epoxies. *Polymer.* **1993**, 34, 3658-3670.

- [73]Zotti, A.; Zuppolini, S.; Zarrelli, M.; Borriello, A., Fracture Toughening Mechanisms in Epoxy Adhesives. In *Adhesives - Applications and Properties*, 2016.
- [74]Lange, F. F., The interaction of a crack front with a second-phase dispersion. *Philos. Mag.* **1970**, 22, 0983-0992.
- [75]Zamanian, M.; Mortezaei, M.; Salehnia, B.; Jam, J. E., Fracture toughness of epoxy polymer modified with nanosilica particles: Particle size effect. *Engineering Fracture Mechanics.* **2013**, 97, 193-206.
- [76]Lange, F. F., *Fracture of Brittle Matrix Particulate Composite*. Accademic Press: New York, 1974; Vol. 5: Fracture and Fatigue., p 2-44.
- [77]Donahue, R. J.; Clark, H. M.; Atanmo, P.; Kumble, R.; McEvily, A. J., Crack opening displacement and the rate of fatigue crack growth. *International Journal of Fracture Mechanics.* **1972**, 8, 209-219.
- [78]AJ, K.; YOUNG, R., Fracture Behavior of Polymers. In *Fracture behaviour of polymers*, Springer Science & Business Media: 1983.
- [79]Liebowitz, H., *Fracture: an advanced treatise. Volume VII. Fracture of nonmetals and composites*. Academic Press 1972.

## Supporting Information of Chapter 2

### 1. Synthesis of $n\text{SiO}_2$ without IL

0.20 g SDS and 0.40 g CTAB were dissolved in 54 mL deionized water and then 1.00 mL  $\text{NH}_3 \cdot \text{H}_2\text{O}$  was added to the mixture. The mixture was agitated by magnetic stirring and was kept at 68 °C for 1.5 h in order to obtain a homogeneous solution. After that, 1.50 g TEOS was dripped slowly into mixture to perform a sol-gel reaction at 68 °C for 2 h and then at 80 °C for 2 h to form the hollow silica nanoparticles. Finally, white precipitation was collected by centrifugation and they were washed three times with deionized water and then dried at 60 °C for 24 h.

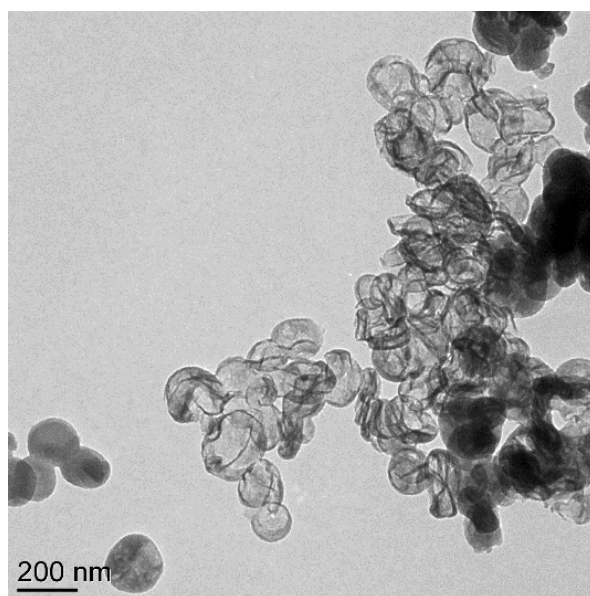


**Figure S2-1** TEM micrograph of hollow silica nanoparticles ( $n\text{SiO}_2$ )

## 2. DSC curves of IL@SiO<sub>2</sub> microcapsule-filled epoxy-amine microcomposites

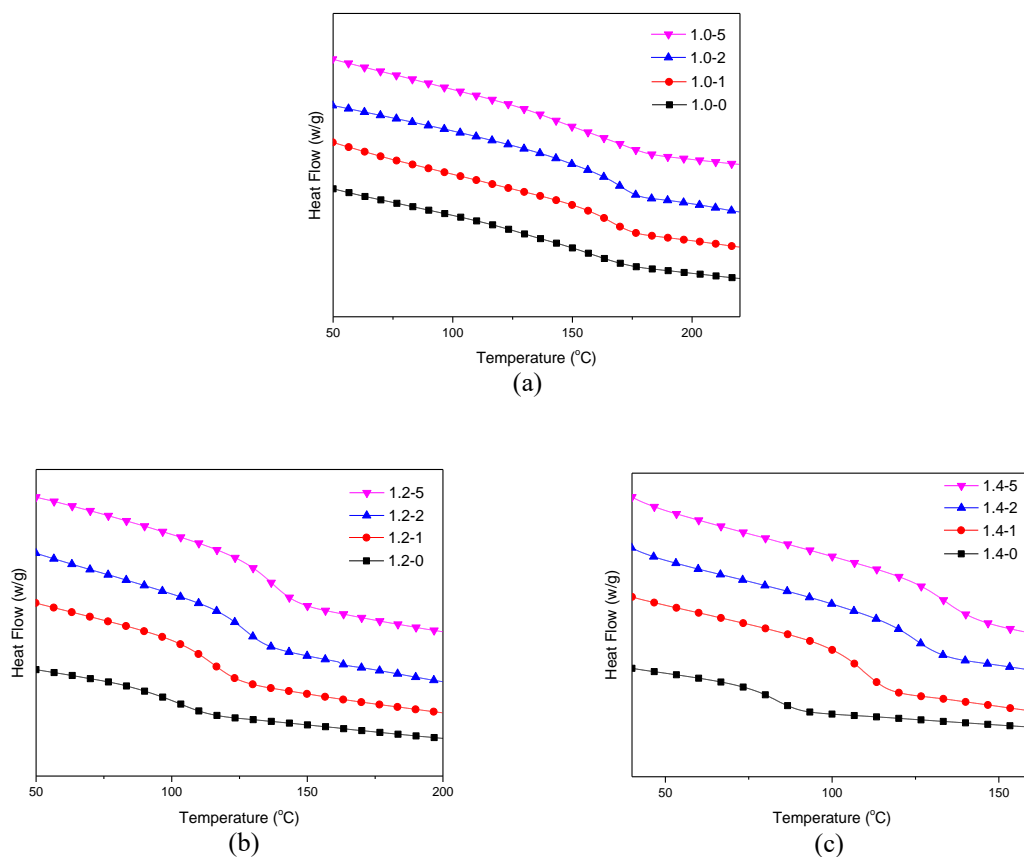


**Figure S2-2** DSC traces of epoxy-amine networks and their corresponding IL@SiO<sub>2</sub> microcapsule-filled microcomposites (N<sub>2</sub> atmosphere, heating rate: 10 K·min<sup>-1</sup>)

(a)  $r=1.0$ ; (b)  $r=1.2$ ; (c)  $r=1.4$

### 3. Storage modulus and loss modulus as a function of temperature of different IL@SiO<sub>2</sub> microcapsule-filled epoxy-amine microcomposites

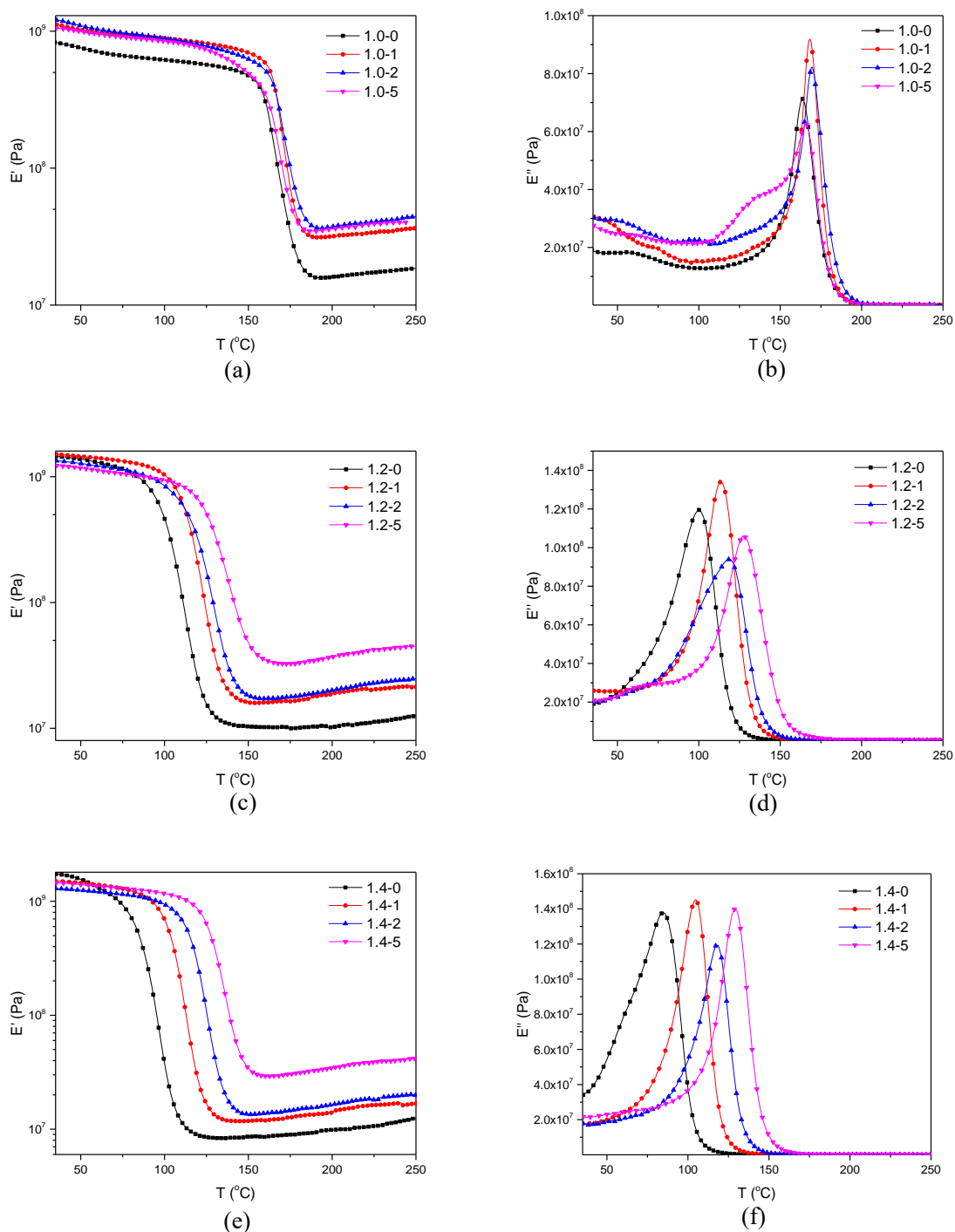


**Figure S2-3** Storage modulus and loss modulus as a function of temperature of different IL@SiO<sub>2</sub> microcapsule-filled epoxy-amine microcomposites,

Storage modulus ( $E'$ ) : (a)  $r=1.0$ ; (c)  $r=1.2$ ; (e)  $r=1.4$

Loss modulus ( $E''$ ) : (b)  $r=1.0$ ; (d)  $r=1.2$ ; (f)  $r=1.4$



#### 4. Surface property of IL@SiO<sub>2</sub> microcapsule-filled epoxy-amine composites

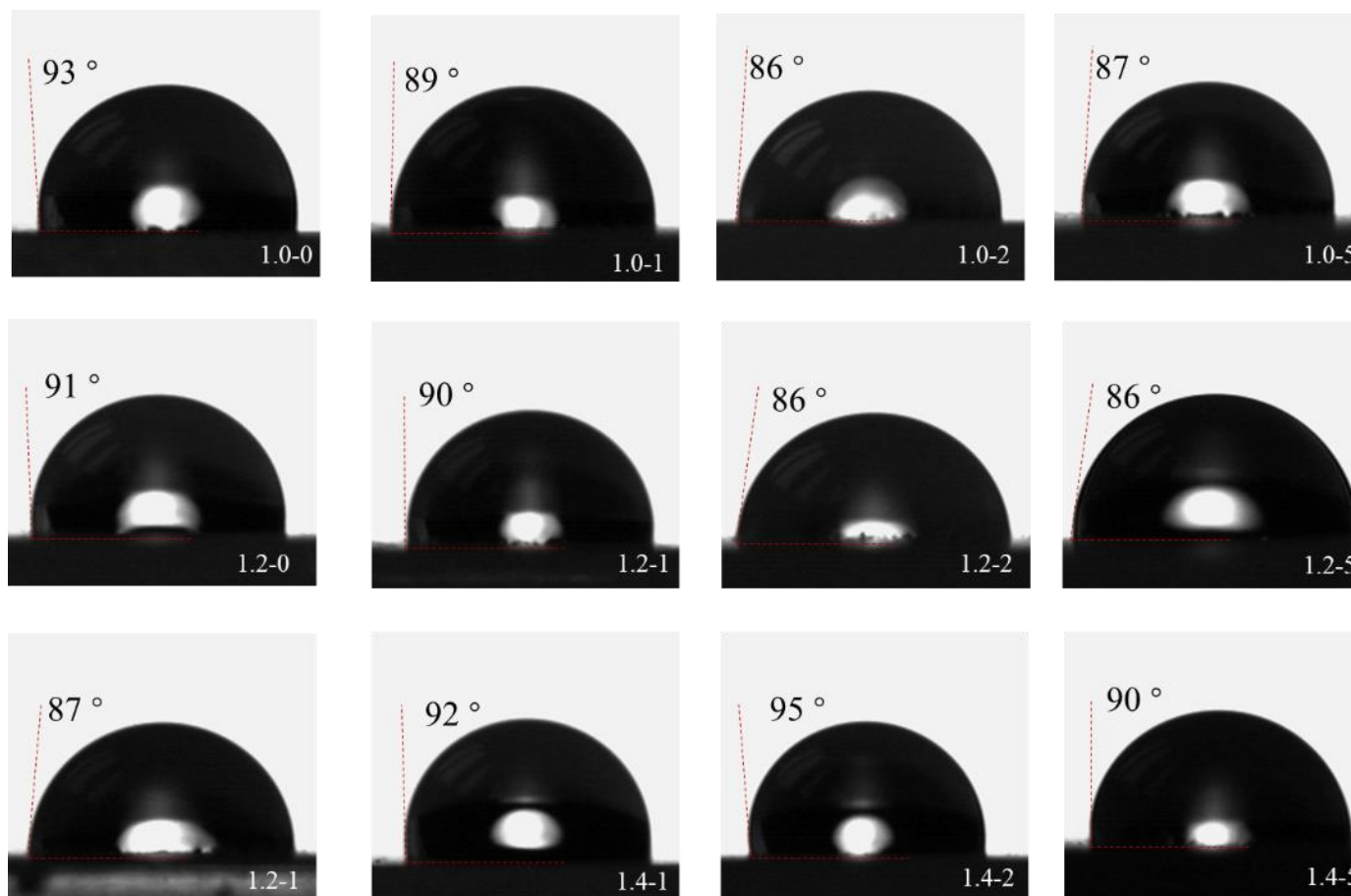


**Figure S2-4** Contact angle with H<sub>2</sub>O on the surfaces of IL@SiO<sub>2</sub> microcapsule-filled epoxy microcomposites

**Table S2-1** Contact angle and surface energy of IL@SiO<sub>2</sub> microcapsule-filled epoxy-amine microcomposites measured by sessile drop method

system	$\Theta_{water}$ (°)	$\Theta_{CH_2I_2}$ (°)	$\gamma_{non-dispersive}$ (mJ·m <sup>-2</sup> )	$\gamma_{dispersive}$ (mJ·m <sup>-2</sup> )	$\gamma_{total}$ (mJ·m <sup>-2</sup> )
1.0-0	93	37	0.4	41.3	41.7
1.0-1	89	23	0.4	47.3	47.7
1.0-2	86	35	1.6	40.6	42.2
1.0-5	87	27	0.9	44.9	45.8
1.2-0	91	34	0.6	42.3	42.9
1.2-1	90	22	0.3	47.7	48.0
1.2-2	86	20	1.0	47.1	48.1
1.2-5	86	22	0.9	46.7	47.6
1.4-0	87	17	0.6	48.4	49.0
1.4-1	92	18	0.1	49.6	49.7
1.4-2	95	26	0.4	46.7	47.1
1.4-5	90	24	0.5	46.7	47.2

### 5. TGA and DTG curves of IL@SiO<sub>2</sub> microcapsule-filled epoxy-amine microcomposites under N<sub>2</sub> atmosphere

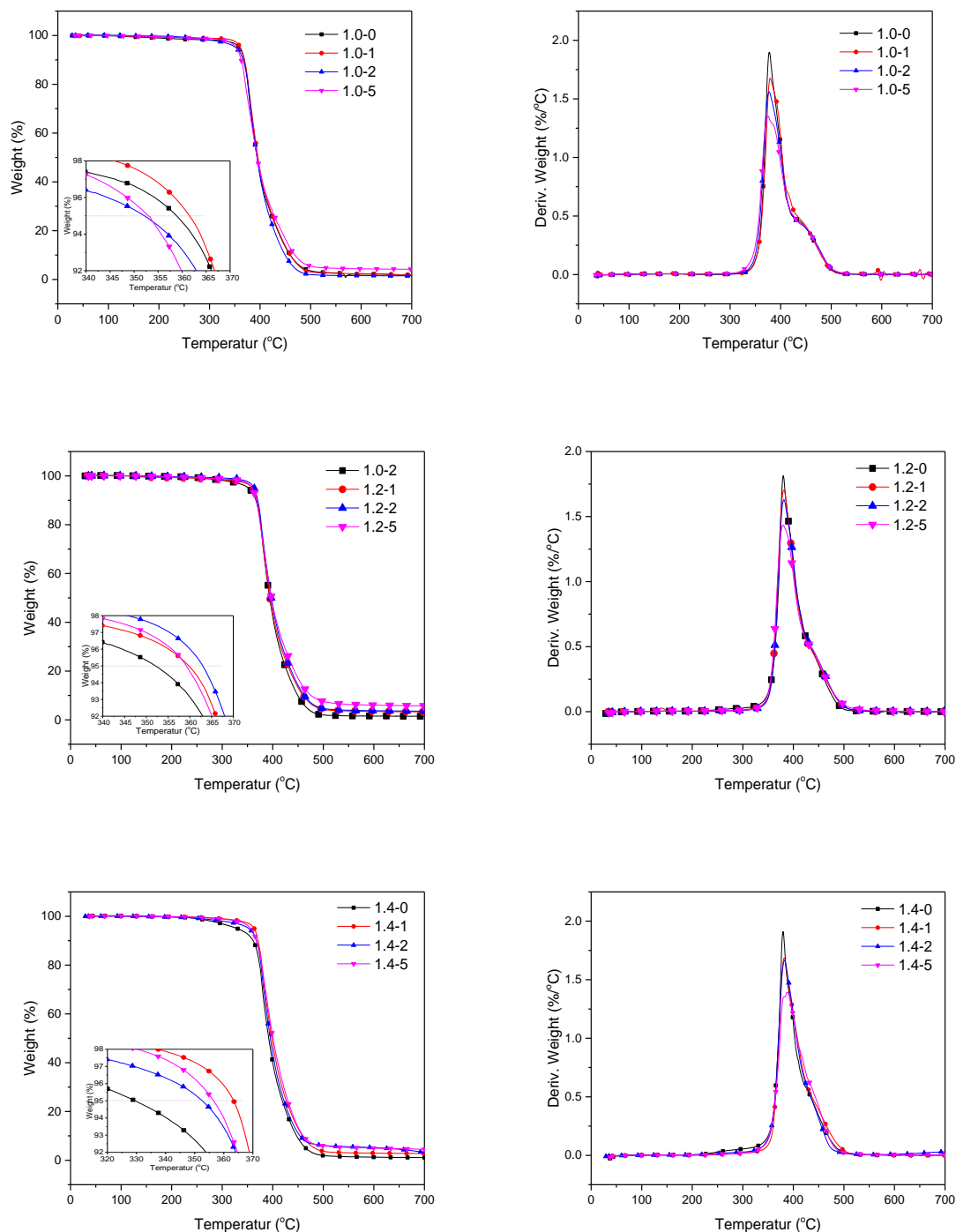


**Figure S2-5** TGA traces of different IL@SiO<sub>2</sub> microcapsule-filled epoxy-amine microcomposites (N<sub>2</sub> atmosphere, heating rate: 20 K·min<sup>-1</sup>)

6. Fracture toughness and Young's modulus IL@SiO<sub>2</sub> microcapsule-filled epoxy-amine microcomposites

**Table S2-2** Fracture toughness and Young's modulus of epoxy-amine microcomposites filled with different weight fractions of IL@SiO<sub>2</sub> microcapsules

r	1.0			1.2			1.4		
mass fraction of IL@SiO <sub>2</sub> microcapsules	<i>E</i> (GPa)	<i>K<sub>IC</sub></i> (MPa·m <sup>1/2</sup> )	<i>G<sub>IC</sub></i> <sup>*</sup> (kJ·m <sup>-2</sup> )	<i>E</i> (GPa)	<i>K<sub>IC</sub></i> (MPa·m <sup>1/2</sup> )	<i>G<sub>IC</sub></i> <sup>*</sup> (kJ·m <sup>-2</sup> )	<i>E</i> (GPa)	<i>K<sub>IC</sub></i> (MPa·m <sup>1/2</sup> )	<i>G<sub>IC</sub></i> <sup>*</sup> (kJ·m <sup>-2</sup> )
0 wt%	1.10 ± 0.04	0.55 ± 0.05	0.25	1.24 ± 0.03	0.56 ± 0.06	0.23	1.42 ± 0.05	0.60 ± 0.05	0.22
1 wt%	1.20 ± 0.05	0.69 ± 0.07	0.35	1.30 ± 0.06	0.65 ± 0.08	0.29	1.64 ± 0.06	0.68 ± 0.05	0.25
2 wt%	1.26 ± 0.06	0.76 ± 0.04	0.41	1.40 ± 0.03	0.76 ± 0.07	0.36	1.70 ± 0.04	0.77 ± 0.06	0.31
5 wt%	1.30 ± 0.04	0.80 ± 0.06	0.44	1.50 ± 0.06	0.81 ± 0.06	0.38	1.68 ± 0.05	0.82 ± 0.05	0.35

\* calculated by the mean value of *E* and *K<sub>IC</sub>*



## Chapter 3 :

# Synthesis of poly(urea-formaldehyde) microcapsules containing epoxy monomer to design self-healable epoxy-amine-IL materials

These last decades, self-healing polymer materials represent a promising generation of smart polymers having the ability to self-repair after external damage. Moreover, this self-healing ability can be used in order to extend the lifetime of the resulting materials. Based on the self-healing mechanism, two pathways have been widely reported to provide the self-healing functionality, intrinsic and extrinsic self-healing. In this chapter, extrinsic self-healing was described by using a single microcapsule-based system, *i.e.* epoxy containing poly(urea-formaldehyde) microcapsules, with an ionic liquid (IL) added in the epoxy-amine network as initiator. This chapter will introduce three parts: *i)* synthesis and characterization of EP@PUF microcapsule, including the morphology, chemical structure, and thermal properties; *ii)* the influence of IL on the curing behavior and final properties of epoxy networks and the determination of the optimal weight fraction of IL; *iii)* the preparation of epoxy-amine-IL composites including EP@PUF microcapsules and the characterization of epoxy composites, including their morphology, thermal and mechanical properties and their self-healing behavior.

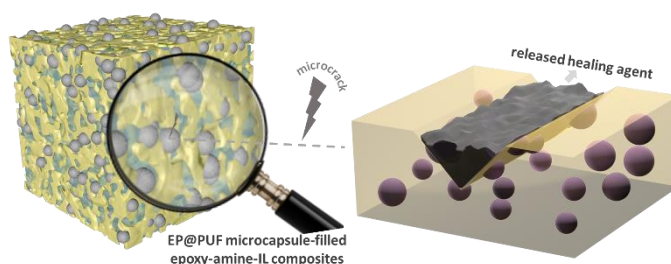


## Table of Contents

<b>3.1 Introduction .....</b>	<b>142</b>
<b>3.2 Experimental.....</b>	<b>144</b>
3.2.1 Materials.....	144
3.2.2 Characterization methods .....	146
<b>3.3 Synthesis and characterization of EP@PUF microcapsules.....</b>	<b>148</b>
3.3.1 Synthesis procedure of EP@PUF microcapsules .....	148
3.3.2 Characterization of EP@PUF microcapsules .....	149
3.3.2.1 Morphology of EP@PUF microcapsules .....	149
3.3.2.2 Determination of chemical nature of EP@PUF microcapsules.....	153
3.3.2.3 Thermal properties of EP@PUF microcapsules .....	154
<b>3.4 Preparation and characterization of epoxy-amine-IL networks.....</b>	<b>159</b>
3.4.1 Sample preparation.....	159
3.4.2 Characterization of epoxy-amine-IL networks .....	160
3.4.2.1 Curing behavior of epoxy-amine-IL networks .....	160
3.4.2.2 Morphology of epoxy-amine-IL networks .....	163
3.4.2.3 Thermal properties of epoxy-amine-IL networks .....	165
3.4.2.4 Mechanical properties of epoxy networks.....	167
<b>3.5 Preparation and characterization of self-healing epoxy-amine-ionic liquids composites filled with EP@PUF microcapsules .....</b>	<b>168</b>
3.5.1 Material processing .....	168
3.5.2 Characterization of EP@PUF microcapsule-filled epoxy-amine-IL materials .....	169
3.5.2.1 Morphology of EP@PUF microcapsule-filled epoxy-amine-IL materials .....	169
3.5.2.2 Thermal behavior of EP@PUF microcapsule-filled epoxy-amine-IL materials .....	170
3.5.2.3 Thermal stability of EP@PUF microcapsule-filled epoxy-amine-IL materials.....	172
3.5.2.4 Dynamic mechanical analysis of EP@PUF microcapsule-filled epoxy-amine-IL materials	

.....	173
3.5.2.5 Self-healing property of EP@PUF microcapsule-filled epoxy-amine-IL materials.....	176
3.5.2.6 Mechanical properties of EP@PUF microcapsule-filled epoxy-amine-IL materials .....	179
<b>3.6 Conclusion of Chapter 3 .....</b>	<b>181</b>
<b>References of Chapter 3.....</b>	<b>183</b>
<b>Supporting Information of Chapter 3 .....</b>	<b>188</b>



### 3.1 Introduction

The design of smart materials having the ability to heal the failure and to retrieve the mechanical properties of the final material is a real challenge. Developing self-healable polymer materials inspired by the living creatures in the nature could prolong the life time of the material. Two main routes to achieve self-healing in polymer materials have been reported: *i*) intrinsic self-healing based on introduction of reversible reaction and bonds and *ii*) extrinsic self-healing based on microvascular networks or microcapsules [1].

Intrinsic self-healing could be repeatable by introducing reversible interactions into the material systems, however, the design of the molecular structure of materials is necessary and complex. Extrinsic self-healing mechanism is widely used for developing self-healable polymer material due to the minimum restrictions on the intrinsic properties of the materials, in which microcapsules showed a real potential due to the shell stiffness as well as the restricted movement of core materials as external self-healing agents. Moreover, microencapsulation has been widely described in the literature for different types of applications, such as drug delivery [2], nanoreactors [3], and construction of self-healable polymer materials [4, 5], etc.

In the field of epoxy thermosets, microcapsules composed of urea and/or melamine and formaldehyde were widely used as shell forming materials due to their excellent features including high mechanical strength [6], good thermal stability [7], chemical resistance [8], long term storage stability [9] and low permeability [10]. For the first generation, microencapsulated dicyclopentadiene (DCPD) and solid Grubbs' catalyst by ring-opening metathesis polymerization were applied for epoxy composites [11-13], the released DCPD react with Grubbs' catalyst and re-bond the broken faces, while the bonding between the substrate and the poly(DCPD) was not optimal for epoxy composites [14, 15]. Later, linseed oil as self-healing agent was also reported [16, 17]. For example, linseed oil was encapsulated by poly(urea-formaldehyde) microcapsules aiming at development self-healable epoxy coating. Reported by Suryanarayana *et al* [16], an exothermic peak at 155 °C in the DSC curve of such microcapsules corresponding to the curing of linseed oil was measured, and a self-healing behavior was observed for the final epoxy coating. In addition, linseed oil acts as an oxidative healing agent avoiding the use of catalyst for the formation of a continuous film. Nevertheless, this continuous film with

crosslinked structure essentially consists of the intermolecular coupling of radicals originated by decomposition of the relatively unstable peroxide groups [18]. In fact, the presence of glycerides in linseed oil may also act as plasticizer which limits the hardening process of encapsulated linseed oil [19].

Recently, epoxy monomer was also considered as self-healing agent via microencapsulation. Yuan *et al* [7-9] and Liao *et al* [20] have studied the synthesis and the properties of microcapsules containing epoxy. These authors proved that these microcapsules have good mechanical properties and an excellent thermal stability, which leads to considering them promising additives for self-healing. However, few studies report the properties of such microcapsule-filled epoxy composites. Yin *et al* [15] encapsulated epoxy prepolymer (bisphenol-A epoxy resin, type E-51) in poly(urea-formaldehyde) microcapsules and synthesized the complex of  $\text{CuBr}_2$  and 2-methylimidazole as a latent hardener for released healing agent. The self-healing epoxy composites based on E-51 and tetraethylenepentamine system exhibited a promising recovery while the complex would be dissociated at about 130 – 170 °C [21, 22]. As a consequence, the curing of the epoxy matrix should be processed at a temperature lower than the dissociation temperature of the hardener. Except such a latent hardener, some amines, *i.e.* polyetheramine and tetraethylenepentamine were also encapsulated to design a dual microcapsules healing system with epoxy containing microcapsules [23, 24]. Dual microcapsules system may avoid the above limitations related to latent hardener, but additional synthesis procedure for encapsulating liquid amine was found to be complex as these ones are soluble in water and in most organic solvents [25]. The uniform dispersion of two types of microcapsules was found to be important for healing [26].

For these different reasons, the use of microcapsules containing epoxy monomer as a healing agent in epoxy composites has different peculiarities, including limitation of curing temperature of epoxy matrix or the raising cost for extra synthesis process for the second type of microcapsules. Therefore, a reactant for healing agent with higher thermal stability may enlarge the application of epoxy loaded microcapsules in polymer composites. According to previous research, ionic liquid (IL) can play the role of initiator for epoxy polymerization [27], leading to epoxy-IL networks having good mechanical and thermal properties [28-30]. The high thermal stability of ILs allows to consider them as an initiator for the self-healing agent of high

temperature matrices. Nevertheless, the influence of IL on the final properties of polymer composites and self-healing ability for single microcapsule systems still remain vacant.

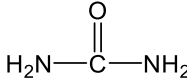
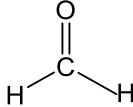
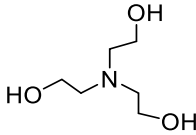
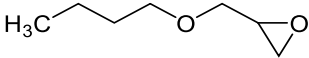
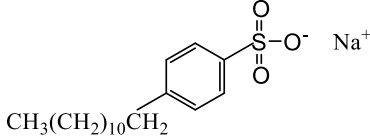
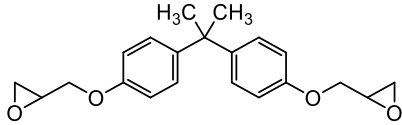
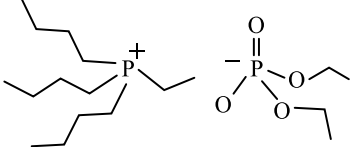
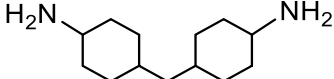
Therefore, this chapter focuses on the synthesis of poly(urea-formaldehyde) (PUF) microcapsules containing an epoxy resin and their self-healing application in high temperature cured epoxy composites. This chapter will include three parts: *i*) the synthesis and characterization of epoxy containing PUF microcapsules, denoted EP@PUF; *ii*) In the second part, the effect of the presence of the IL on the epoxy-amine network will be studied as well as the reactivity of IL in the self-healing process. The optimized composition of the epoxy matrix will be determined from the characterization of epoxy-amine networks containing different weight fractions of IL. *iii*) the preparation and characterization of EP@PUF microcapsule-filled ternary epoxy-amine-IL system. Their thermal and mechanical properties as well as self-healing ability will be investigated.

## 3.2 Experimental

### 3.2.1 Materials

Urea (U), formaldehyde solution (F, 37 wt.% in water, contains 10-15% methanol as stabilizer), triethanolamine (TEA), epoxy resin, *i.e.* bisphenol A diglycidyl ether (DEGBA D.E.R. 332), butyl 2,3-epoxypropyl ether (BGE), sulfuric acid (H<sub>2</sub>SO<sub>4</sub>, ACS reagent, 95.0-98.0%), bisphenol A diglycidyl ether (DGEBA, D.E.R. 332), sodium dodecylbenzenesulfonate (SDBS), 1-octanol, and 4,4'-methylenebis(cyclohexylamine) (PACM) were purchased from Sigma-Aldrich. The phosphonium-based ionic liquid tributyl(ethyl)phosphonium diethyl phosphate, denoted as IL 169, was provided by Cytec Solvay. Acetone was purchased from Carlo ERBA Reagent. All the chemicals were used as received without any further purification and their chemical structures were shown in Table 3-1.

**Table 3-1** Summarized chemical structures of the materials used

Chemicals and abbreviations	Chemical formula
Urea (U)	
Formaldehyde solution (F, 37 wt. % in H <sub>2</sub> O, contains 10-15% methanol as stabilizer)	
Triethanolamine (TEA)	
Butyl 2,3-epoxypropyl ether (BGE)	
Sodium dodecylbenzenesulfonate (SDBS)	
Epoxy resin Bisphenol A diglycidyl ether (DGEBA, D.E.R. 332)	
1- octanol	$\text{CH}_3(\text{CH}_2)_6\text{CH}_2\text{OH}$
tributyl(ethyl)phosphonium diethyl phosphate (IL 169)	
4,4'-methylenebis(cyclohexylamine) (PACM)	

### 3.2.2 Characterization methods

Monitoring the *in-situ* polymerization by optical microscopy was carried out using an Axio Imager A2M type optical microscope (OM) from Zeiss Co.

Scanning electron microscope (SEM) was carried out using a TESCAN VEGA3 from TESCAN ANALYTICS proceeding with an accelerating voltage of 10 kV. To prepare the specimen, dried powder of EP@PUF microcapsules and cross sections of epoxy composites were pasted on the sample holder using a carbon tape. All the specimens were coated with gold by a sputter coater to prevent charge accumulation on the surface. The sputter coating process was performed at a current of 30 mA for 90 s.

Thermogravimetric analysis coupled with infrared spectrometry (TGA-IR) was performed with test was carried out using a TGA 8000 from PerkinElmer. The evolved gas analysis was performed by interfacing a Fourier transform infrared spectrometer (FTIR, Nicolet 6700) to the exit port of the TGA furnace. 10 mg of the material was put in an alumina crucible and heated from 35 to 700 °C at a heating rate of 10 K·min<sup>-1</sup> under N<sub>2</sub> atmosphere. Infrared spectra in the optical range of 4,000–400 cm<sup>-1</sup> were recorded every 4 s.

Differential Scanning Calorimetry (DSC) measurement of EP@PUF microcapsules and epoxy composites were performed using Q 10 from TA Instrument operating at a heating rate of 10 K·min<sup>-1</sup> under nitrogen flow of 50 mL·min<sup>-1</sup>.

Thermogravimetric analyses (TGA) of epoxy composites were carried out using a Q500 Thermogravimetric Analyzer from TA Instruments. The analyses were performed from 30 to 700 °C with a heating rate of 20 K·min<sup>-1</sup> under nitrogen atmosphere.

Transmission electron microscope (TEM) was performed using a JEM-1400 Flash electron microscope operating at an accelerating voltage of 120 kV. The polymer samples were prepared by ultramicrotome on carbon film coated copper grids.

Dynamic mechanical analysis (DMA) was carried out using an ARES-G2 from TA Instruments. The analyses were carried out at 0.01% strain, at a frequency of 1 Hz and with a heating rate of 3 K min<sup>-1</sup> from 35 to 250 °C. The characterization was performed twice for the same sample in the same conditions.

Compression tests were carried out using a MTS machine operating with a 5 kN load cell.

The samples geometry was based on ISO 604:2002 standard *i.e.* 5\*5\*16 mm<sup>3</sup>. The Young's modulus ( $E$ ) was determined from  $\sigma$  (stress) vs.  $\varepsilon$  (strain) curves in the linear region.

Mode I stress intensity factor ( $K_{Ic}$ ) of epoxy-amine networks and related microcomposites were determined on compact tension specimens according to the ISO 13586:2018(E) standards (Figure 4-2). The notch was formed using a milling cutter and the initial crack also known as natural crack was made by tapping a fine razor blade into the notch. The length of initial crack to width ratio ( $\alpha/w$ ) has to keep between 0.2 and 0.8. The fracture toughness test was carried out using a MTS tensile machine equipped with a 1 kN load cell operating at tensile speed at 10 mm·min<sup>-1</sup>.  $K_{Ic}$  was calculated according to equation 3-1:

$$K_{Ic} = f(\alpha/w) \frac{F_Q}{h\sqrt{w}} \quad (\text{equation 3-1})$$

where  $\alpha$  (m) is the length of initial crack,  $w$  (m) and  $h$  (m) are the width and thickness of specimen, respectively.  $F_Q$  (N) is the final load at the first crack. The  $f(\alpha/w)$  value is a geometrical factor which can be calculated using equation 3-2:

$$f(\alpha/w) = \frac{(2+\alpha)}{(1-\alpha)^{3/2}} \times (0.886 + 4.64\alpha - 13.32\alpha^2 + 14.72\alpha^3 - 5.64\alpha^4) \quad (\text{equation 3-2})$$

The critical energy release ( $G_{Ic}$ ) can be calculated from equation 3-3 and the value of  $K_{Ic}$ , Young's modulus ( $E$ ), and Poisson's coefficient ( $\nu$ ). 0.35 for  $\nu$  were considered according to the values related in the literature for epoxy networks [31, 32].

$$G_{Ic} = \frac{(1-\nu^2) \cdot K_{Ic}^2}{E} \quad (\text{equation 3-3})$$

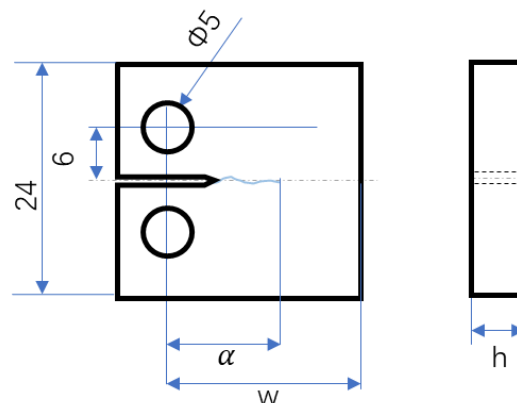


**Figure 3-1** Compact Tensile (CT) test specimen geometry

### 3.3 Synthesis and characterization of EP@PUF microcapsules

#### 3.3.1 Synthesis procedure of EP@PUF microcapsules

The synthesis of epoxy containing poly(urea-formaldehyde) microcapsules (EP@PUF) via *in-situ* polymerization mainly involved three steps: *i*) preparation of UF prepolymer, *ii*) preparation of oil in water (O/W) emulsion and *iii*) *in-situ* polymerization (encapsulation), (Figure 3-2).

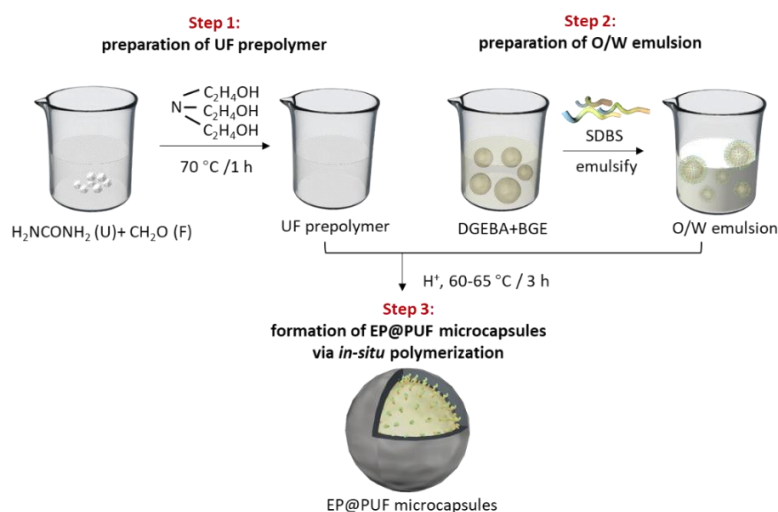


**Figure 3-2** Synthesis steps for EP@PUF microcapsules via *in-situ* polymerization

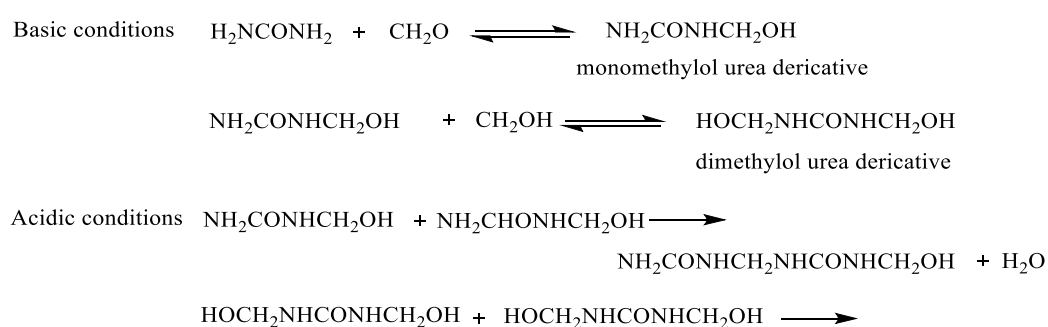
In the first step, urea (U) and formaldehyde solution (F) were added in a flask with a molar ratio of  $n_{(U)}:n_{(F)}=1:2$ . When urea is fully dissolved, a suitable amount of triethanolamine (TEA) was added to the solution until the pH value of the mixture was close to 9, and the mixture was kept at 70 °C under magnetic stirring for 1 h. After the reaction, a transparent prepolymer solution was obtained. In the meanwhile, the O/W emulsion can be prepared as follows for the second step: a mixture of DGEBA and BGE ( $m_{(DGEBA)}:m_{(BGE)}=5:1$ , to guarantee a promising viscosity for *in-situ* polymerization<sup>[9]</sup>) was added in a certain amount of 1 wt% SDBS aqueous solution (8.3 times the mass of core material) which was mechanically stirred for 1 h at 60 °C. One or two drops of 1- octanol were added to the mixture to prevent the generation of bubbles. Then, the prepolymer and O/W solution were cooled down to room temperature, and they were mixed to carry out the *in-situ* polymerization in order to obtain the EP@PUF microcapsules. Once the mixture was mixed with UF prepolymer solution, pH was slowly adjusted close to 3-

3.5 by adding 2 wt% sulfuric acid. At the same time, the temperature was slowly increased to 60-65 °C and the reaction was kept in an oil bath for 3 h. When the encapsulation process was ended, the slurry was cooled down to room temperature. The white precipitate was filtrated and washed three times by deionized water and acetone to remove the UF prepolymer and unencapsulated core material. Finally, the EP@PUF microcapsules were dried at 60 °C ready before use.

### 3.3.2 Characterization of EP@PUF microcapsules

#### 3.3.2.1 Morphology of EP@PUF microcapsules

Several researches have reported the synthesis of microcapsules with amino resins shell considering one-step method [33-35]. To avoid the competitive reaction between the addition and condensation reactions, a two-step method for synthesis EP@PUF microcapsules was considered (see section 3.3.1). Scheme 3-1 shows the chemical reaction of the PUF shell at basic or acidic conditions. Specifically, under basic conditions, urea and formaldehyde react to form monomethylol urea and dimethylol urea derivatives. Under acidic conditions, the urea derivatives continue to react including the remaining urea in the solution. Thus, the prepolymer polymerized to form a network and solidify under low pH value.



**Scheme 3-1** Reaction mechanisms of poly(urea-formaldehyde)

The formation PUF of the shell during the polymerization process was monitored by optical microscopy (OM) and the morphologies of final EP@PUF microcapsules were characterized by scanning electron microscopy (SEM). Figure 3-3 shows the OM images of the encapsulation process during the reaction at different times. Before the shell formation, Figure 3-3 (a) shows the morphology of O/W emulsion, separated epoxy droplets can be distinguished,



and a shiny surface can be seen. Figure 3-3 (b) shows the beginning of the PUF shell formation as well as EP@PUF microcapsules. At this stage, the mixture was characterized by a milky white color, indicating that the polymerization still kept going in the aqueous phase. Because of the positive charge of UF prepolymer, they are attracted toward the hydrophilic groups of anionic surfactants and keep polymerizing [36]. After the reduction of the pH by the addition of H<sub>2</sub>SO<sub>4</sub>, the continuous polymerization of the urea derivatives generated crosslinked polymer. At this step, a thin shell can be distinguished on OM images as a black circle in the image. Due to the weakness of the thin PUF shell, the newly formed PUF shell could be easily broken or collapsed when other shells impact. As the reaction takes place, the molar mass of PUF is growing which leads to an increase in PUF shell thickness. The extra PUF nanoparticles are also formed in the continuous phase and some of them are deposited on the PUF shell at the same time. The final morphology of EP@PUF microcapsules in transmission and reflection mode are shown in Figure 3-3 (c) and (d), respectively.

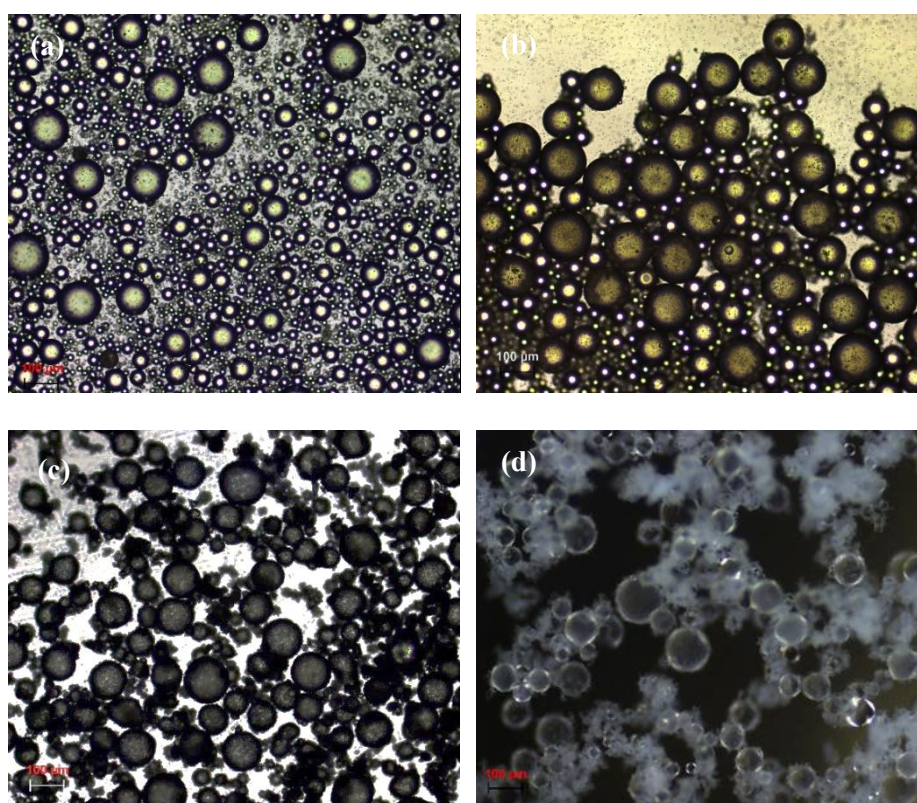


**Figure 3-3** OM images of synthetic procedure of EP@PUF microcapsules (a) O/W emulsion; (b) formation of PUF nanoparticles; (c) formation and solidification of EP@PUF microcapsules; (d) OM image of EP@PUF microcapsules in reflection mode;

As shown in Figure 3-3 (a), the core material was dispersed by mechanical stirring in the surfactant aqueous solution to form an oil in water (O/W) emulsion. Because of the continuous stirring in the aqueous solution, various flow patterns were formed in the mixture, as evidenced by the schematic representation of Figure 3-4. Therefore, the inhomogeneous flow inside an aqueous solution and heterogeneous shear force at different locations led to a broad size distribution of EP@PUF microcapsules.

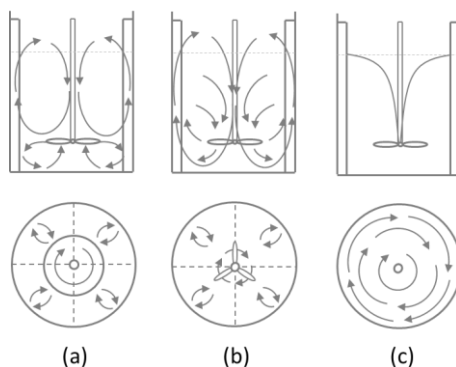


**Figure 3-4** Flow pattern (a) radial flow; (b) axial flow; (c) tangential flow

The size distribution of EP@PUF microcapsules was determined using the Image J software from counting the EP@PUF microcapsules diameters randomly. Figure 3-5 represents the size distribution of EP@PUF microcapsules. The diameter of EP@PUF microcapsules is distributed in the range of 20-150  $\mu\text{m}$  and around 80% of microcapsules have a diameter of about 50-100  $\mu\text{m}$ . Such broad size distribution corresponds to the initial size distribution of oil droplets in the O/W emulsion resulting from the inhomogeneous flow and heterogeneous shear forces. Nevertheless, this diameter range of EP@PUF microcapsules is relevant for self-healing applications.

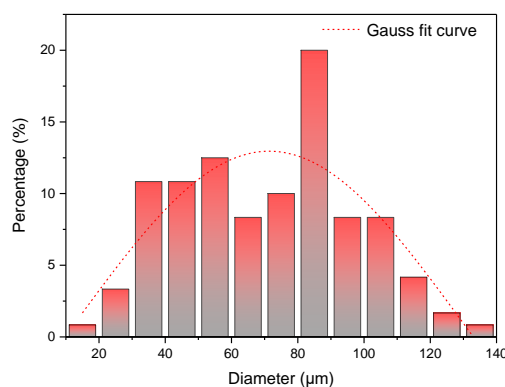


**Figure 3-5** Diameter distribution of EP@PUF microcapsules

The morphology of the EP@PUF microcapsules was characterized by SEM. Figure 3-6 (a)-(d) shows several microcapsules, individual ones, surface features, and a broken microcapsule. First of all, it can be seen that EP@PUF microcapsules have a diameter range from 50-100  $\mu\text{m}$  in agreement with previously OM measurements. A rough surface and a smooth interior surface can be distinguished on Figure 3-6 (c) and (d), confirming the formation scenario of PUF shell and deposition of PUF nanoparticles. The shell thickness of EP@PUF microcapsules can also be measured from Figure 3-6 (d), which is closed to 2-3  $\mu\text{m}$ . The value of this shell thickness is also in a relevant range and guarantees sufficient mechanical strength required for sample processing, *i.e.* mixing in the reactive polymer matrix system, and controlled release of core component [37].

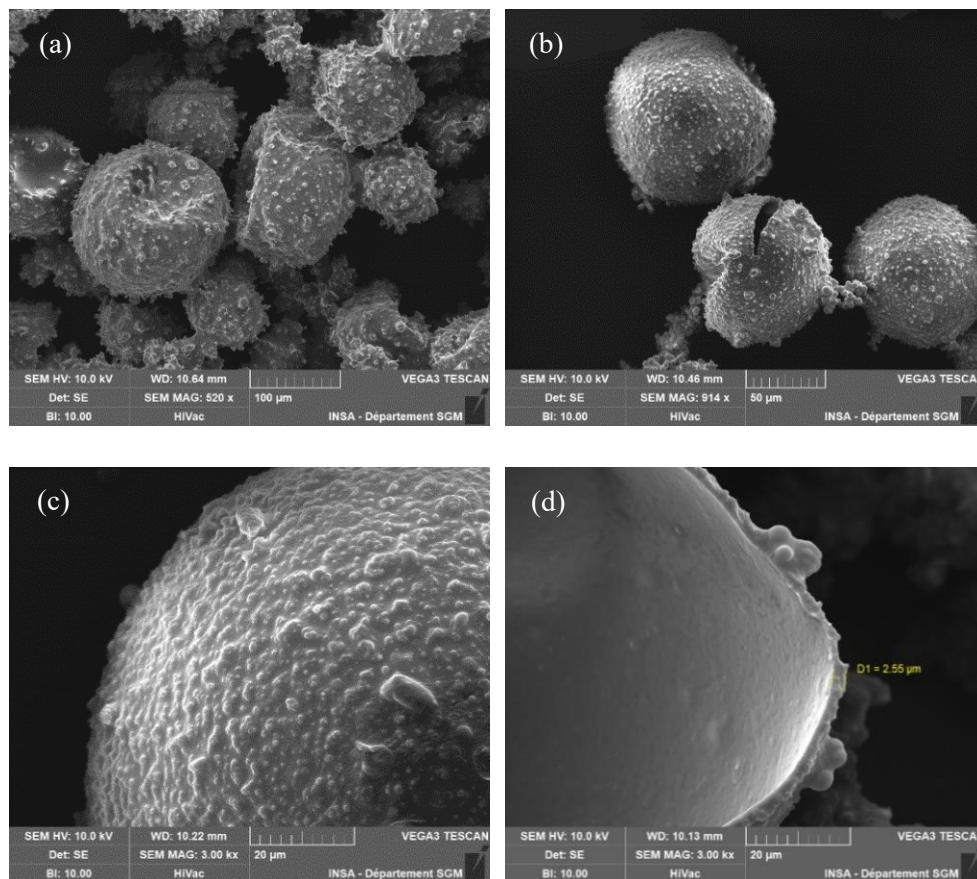


**Figure 3-6** SEM micrographs of (a), (b) EP@PUF microcapsules; (c) surface morphology of EP@PUF microcapsule; (d) broken EP@PUF microcapsule

### 3.3.2.2 Determination of chemical nature of EP@PUF microcapsules

The chemical structure of EP@PUF microcapsules and their core and shell materials were characterized by FTIR as shown in Figure 3-7. The characteristic chemical groups with their corresponding wavenumbers of absorption peaks of core (DGEBA+BGE) and shell (PUF) materials are listed in Figure 3-8. As presented in Figure 3-7 and Figure 3-8, the characteristic peaks of core materials at  $3,050\text{ cm}^{-1}$  (C-H stretching in phenyl ring),  $3,100\text{-}2,800\text{ cm}^{-1}$  (C-H stretching in methyl groups) [38],  $1,610\text{ cm}^{-1}$  (C-C stretching in phenyl ring),  $1,450\text{ cm}^{-1}$  (C-H bending in methyl groups) and  $910/830\text{ cm}^{-1}$  (epoxy groups) were observed in the spectra for both DGEBA+BGE mixture and EP@PUF microcapsules [9]. Meanwhile, the characteristic peaks at  $3,350\text{ cm}^{-1}$  (N-H stretching),  $1,640\text{ cm}^{-1}$  (C=O stretching vibration) [39],  $1,540\text{ cm}^{-1}$  (N-H bending)  $1,250\text{ cm}^{-1}$  (C-O stretching of aliphatic ether) provided from PUF [40] appeared in both spectra of PUF and EP@PUF microcapsules. Therefore, the characteristic peaks from both core and shell material were identified in the spectrum of EP@PUF microcapsules, indicating that the DGEBA and BGE as core materials were successfully encapsulated in the PUF microcapsules.

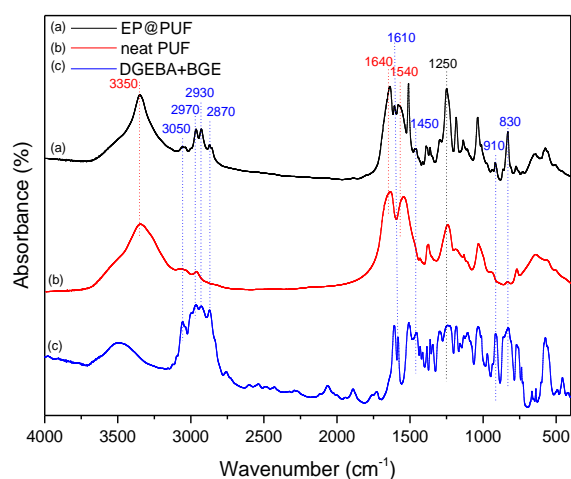


**Figure 3-7** FTIR spectra of (a) EP@PUF microcapsules and its (b) shell material: neat PUF, and (c) core materials: DGEBA+BGE

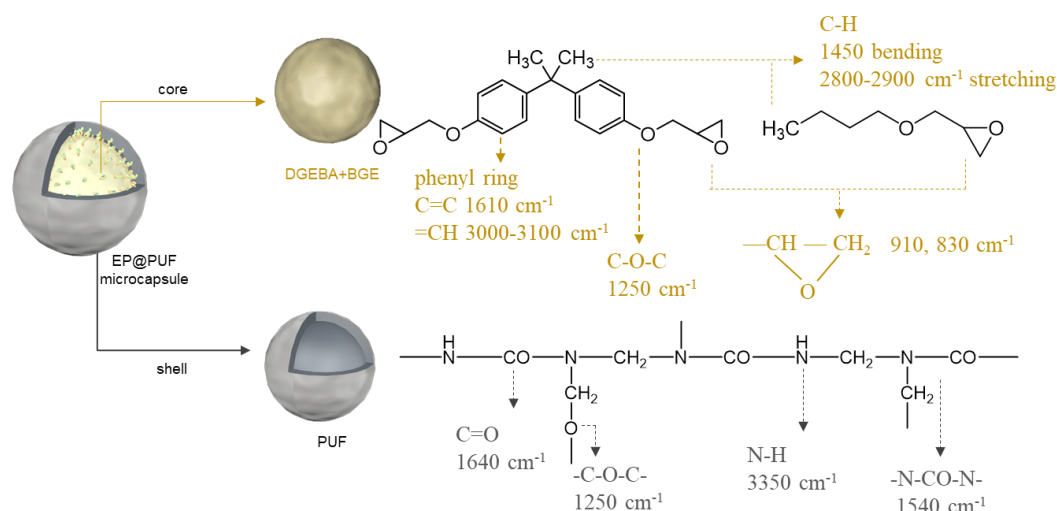


**Figure 3-8** IR-characteristic peaks of core (DGEBA+BGE) and shell (PUF) materials in EP@PUF microcapsules

### 3.3.2.3 Thermal properties of EP@PUF microcapsules

The thermal stability of EP@PUF microcapsules is a key parameter for achieving the self-healing purpose in the epoxy networks. Therefore, in order to investigate the thermal behavior and the stability of EP@PUF microcapsules during heating and self-healing, *i.e.* the further polymerization availability of healing agent inside the EP@PUF microcapsules, DSC and TGA were performed to investigate the thermal properties of the EP@PUF microcapsules.

#### Thermal behavior (DSC)

Figure 3-9 shows the DSC curves of EP@PUF microcapsules from room temperature to 350 °C under N<sub>2</sub> atmosphere. Core and shell materials were also characterized under the same conditions. For the core material, *i.e.* the mixture of DGEBA and BGE, the high thermal stability of the core material was observed. For a neat PUF shell, an endothermic peak was observed at about 230 - 250 °C, corresponding to the decomposition. For EP@PUF microcapsules, before 200 °C, these ones remained stable, *i.e.* no endothermic or exothermic phenomena were observed. With increasing temperature, an exothermic peak occurred at about 230 - 260 °C, which could be assigned to the polymerization of DGEBA encapsulated inside the PUF microcapsules. This polymerization could be initiated by the by-products decomposition product of the PUF shell [41, 42].

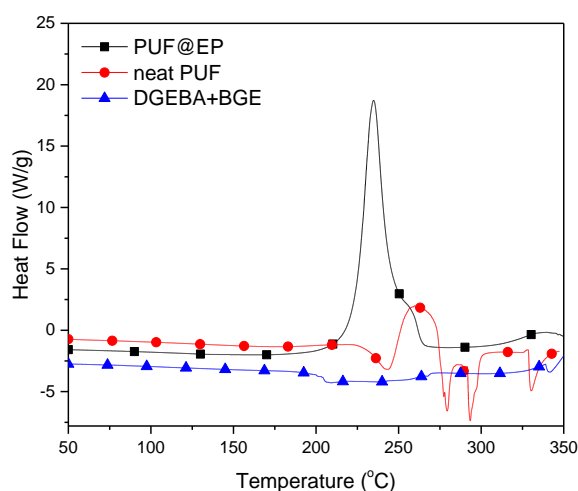


**Figure 3-9** DSC traces of core and shell materials in EP@PUF microcapsules (■) EP@PUF; (●) neat PUF; (▲) DGEBA+BGE (N<sub>2</sub> atmosphere, heating rate: 10 K·min<sup>-1</sup>)

#### **Thermal stability of EP@PUF microcapsules (TGA)**

For self-healing via microcapsules, the healing agent must maintain stable until the self-healing is required and display high thermal stability. Therefore, TGA analyses were carried out on the EP@PUF microcapsules in order to further check the chemical constitution of microcapsules as well as the availability of core compounds for self-healing in polymer matrix composites. Figure 3-10 shows the TGA and DTG traces of EP@PUF microcapsules as well as their shell and core neat materials. The temperature at 5 wt% weight loss was defined as the onset decomposition temperature ( $T_{d\ onset}$ ) and the peak temperatures on the DTG traces were defined as maximum decomposition temperature (see Table 3-2). The  $T_{d\ onset}$  for the EP@PUF microcapsules, neat PUF, and DGEBA+BGE were found to be 238, 251, and 256 °C respectively. Thus, it could be noticed that the EP@PUF microcapsules have a thermal stability due to the protection brought by the PUF shell. Thus, the onset decomposition temperature over 230 °C ensures the integrity of EP@PUF microcapsules during the curing of epoxy amine networks.

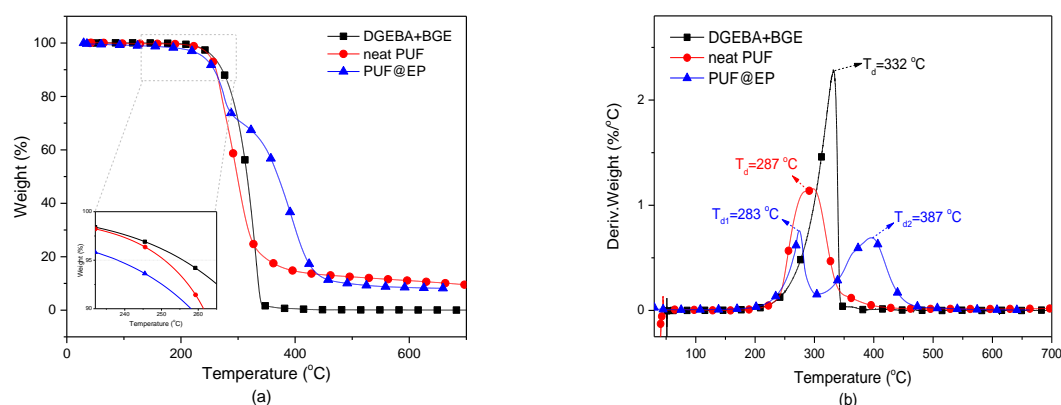


**Figure 3-10** (a) TGA (b) and DTG traces of (▲) EP@PUF microcapsules and their shell material (●, neat PUF) and core material (■, DGEBA+BGE) (N<sub>2</sub> atmosphere, heating rate 20 K·min<sup>-1</sup>)

**Table 3-2** Weight loss temperature of EP@PUF microcapsules and neat components

Material	T <sub>d onset</sub> (°C)	T <sub>d max</sub> (°C)
DGEBA+BGE	256	332
neat PUF	251	287
EP@PUF	238	T <sub>d max1</sub> = 283; T <sub>d max2</sub> = 387

In order to confirm the thermal degradation process of EP@PUF microcapsules, infrared spectroscopy analyses were also performed combined with TGA to determine the composition of the overflowing gas. Figure 3-11 presents the spectra of degradation products during the thermal degradation of EP@PUF microcapsules. The nature of the gases and their characteristic wavenumbers of absorption peaks are listed in Table 3-3. The same analyses were carried out for neat PUF and DGEBA+BGE. Their corresponding FTIR spectra of degradation products during the thermal degradation are shown in the supporting information of Chapter 3.

As shown in Figure 3-10 (b), there was one main degradation step for core or shell materials whereas there were two degradation steps for EP@PUF microcapsules. The first weight loss of EP@PUF microcapsules happened from 230 to 310 °C, *i.e.* corresponding to the degradation of PUF [7]. Ammonia (3,536-3,504 cm<sup>-1</sup>) and cyanamide (2,220 cm<sup>-1</sup>) were

identified to be related to products from PUF degradation [43]. During this step, the alkaline gas could initiate the polymerization of the core component in such higher temperature conditions, in agreement with the existence of an exothermic peak of EP@PUF microcapsules in Figure 3-9. Then, the second weight loss occurred from 310 to 500 °C, which could be associated with the degradation of the core material and further decomposition of shell material. At this step, absorption peaks at 1,260  $\text{cm}^{-1}$  and 1,178  $\text{cm}^{-1}$  belong to the stretching vibrations of aromatic ethers and the C–H hydrocarbons from the epoxy segment [44]. These features indicate that the decomposition of the core material is the main phenomenon. It is noteworthy that the second weight loss shifted to a higher temperature range compared to DGEBA+BGE. This phenomenon can be explained by: *i)* the protection of shell material and a delayed heat transfer; *ii)* the emitted alkaline gas could also initiate the polymerization of DGEBA and the resulting highly crosslinked product displays a higher degradation temperature. Therefore, the core material content in the EP@PUF microcapsules can be estimated to be closed to 60 wt%, which is in agreement with the results reported in the literature for similar studies [40, 45].

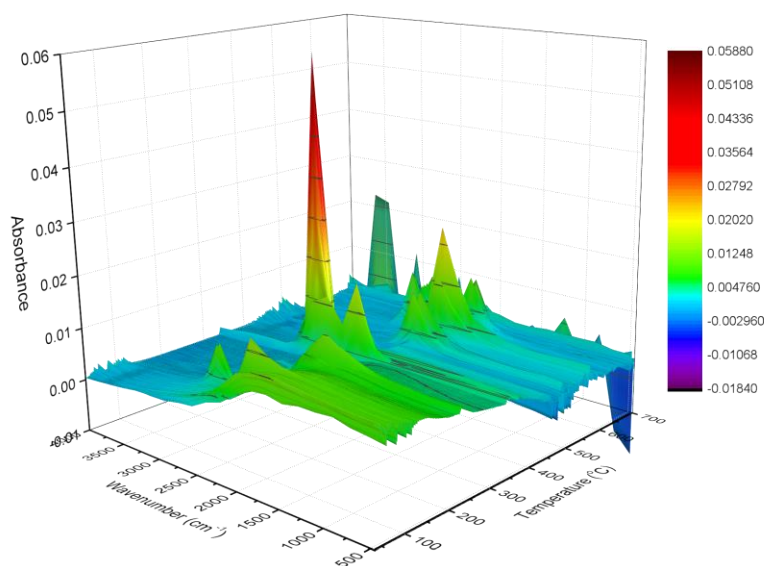


**Figure 3-11** FTIR spectra of emitted gas during degradation of EP@PUF microcapsules under N<sub>2</sub> atmosphere (heating rate: 10 K·min<sup>-1</sup>)



**Table 3-3** Emitted gas and their characterization from FTIR absorption peaks of EP@PUF microcapsules, shell (PUF), and core (DGEBA+BGE) materials during TGA analysis

PUF shell			DGEBA+BGE core			EP@PUF microcapsules		
Temperature	Gas	wavenumber (cm <sup>-1</sup> )	Temperature	Gas	Wavenumber (cm <sup>-1</sup> )	Temperature	Gas	Wavenumber (cm <sup>-1</sup> )
230 °C   360 °C	ammonia	3,536   3,504	250 °C   500 °C	C-H	2,975	240 °C   310 °C	ammonia	3,536   3,504
	cyanamide	2,260   2,220					cyanamide	2,220   2,260
	CO	2,300   2,220		methyl group	1,450	CO	2,300   2,220	
360 °C   500 °C	CO <sub>2</sub>	2,350		benzene	1,500 1,600	310 °C   500 °C	ammonia	3,536   3,504
				aromatic ethers	1,260 1,178		C-H	2,975
							benzene	1,500 1,600
			aromatic ethers				1,260 1,178	
CO <sub>2</sub>	2,350	CO <sub>2</sub>	2,350					

To conclude, the EP@PUF microcapsules have been successfully synthesized from *in-situ* polymerization in an O/W emulsion. The obtained EP@PUF microcapsules present smooth inner and rough outer surfaces which could promote the adhesion between EP@PUF microcapsules and the epoxy-amine matrix. DSC analyses have shown that the healing agent in the EP@PUF microcapsules could polymerize and the TGA analyses have proved that the obtained EP@PUF microcapsules have a good thermal stability. This later property will ensure the integrity of the healing agent during high temperature curing processes of the polymer matrix. In a next step, a phosphonium-based ionic liquid which will play the role of initiator of epoxy healing agent will be added to epoxy-amine system. Such a route will allow investigating the influence of IL on the final properties of epoxy matrix.

### 3.4 Preparation and characterization of epoxy-amine-IL networks

#### 3.4.1 Sample preparation

In order to investigate the reactivity of ionic liquid with a healing agent within the epoxy-amine matrix and determine the optimized ionic liquid content, different epoxy-amine-IL systems (see Table 3-4) were prepared and characterized by DSC.

Formulation **1** (epoxy-to-amino hydrogen ratio,  $r = 1$ , *i.e.* at the stoichiometric ratio,) and formulation **2** (epoxy combined with IL 169) were used as a reference to determine the curing behavior of epoxy prepolymer with either hardener (PACM) or catalytic curing agent (IL169). Formulation **3-5**, *i.e.* epoxy-amine networks ( $r = 1$ ) containing different amounts of IL169 addition were prepared to observe the influence of IL 169 on the curing behavior of the DGEBA-PACM network. Finally, a comparative study between formulations **4** and **6** was made to confirm the reactivity of IL 169 with the excess of epoxy prepolymer as a healing agent in the cured DGEBA-PACM system.

The materials were prepared according to the following procedure: DGEBA and PACM mixture with or without IL 169 were mixed at 60 °C and stirred by mechanical stirring until a homogeneous mixture was formed. Then, the mixture was degassed in a vacuum bell jar to remove the bubbles inside. Finally, the mixture was poured into a silicon mold and cured in an oven during 2 h at 80 °C and 2 h at 160 °C.

**Table 3-4** Formulations considered to design epoxy-amine-ionic liquids networks

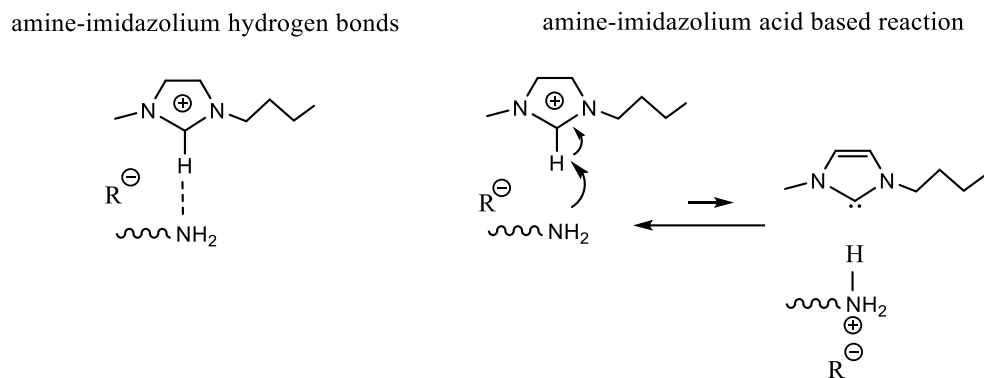
Composition	Epoxy (D.E.R 332) (phr)	Diamine (PACM) (phr)	Ionic liquid (IL 169) (phr)
<b>1</b> ( $r = 1$ )	100	30	0
<b>2</b>	100	0	10
<b>3</b>	100	30	5
<b>4</b>	100	30	10
<b>5</b>	100	30	20
<b>6</b>	100	20	10

### 3.4.2 Characterization of epoxy-amine-IL networks

#### 3.4.2.1 Curing behavior of epoxy-amine-IL networks

Different ionic liquids (IL) can be used as initiators for epoxy polymerization <sup>[27, 29]</sup> either via cation or via anion. For a same cation, the reactivity of IL is strongly dependent on anions nature as they reacted with epoxy compounds <sup>[46]</sup>. B. Soares *et al* <sup>[47]</sup> reported the large influence of IL on the curing behavior of epoxy-amine or epoxy-anhydride networks. Soares and Livi *et al* <sup>[47]</sup> have demonstrated that the use of imidazolium-based IL N,N'-dioctadecylimidazolium iodide ([DiOImid][I]) catalyzed the curing process of epoxy and 4,4'-methylenebis(3-chloro-2,6-diethylaniline) (MCDEA). The onset curing temperature of epoxy-MCDEA-[DiOImid][I] mixture decreases of 50 K as only 5 phr of [DiOImid][I] is applied. In addition, a significant shift of the exothermic peak temperature towards lower temperature indicated the reaction between the imidazolium-based IL and DGEBA. In the epoxy-amine networks, imidazolium-based IL could form hydrogen bonds with amine, combined with a N-heterocyclic carbene mechanism leading to a reduction of the curing onset temperature and a decrease of temperature at maximum curing rate <sup>[46, 48]</sup> (see Scheme 3-2).

However, for phosphonium-based IL, the counter anion initiates the opening of epoxy functionality depending on the chemical nature of the counter anions, and an influence on the curing behavior between phosphonium-based IL and epoxy prepolymer exerted a marginal effect on the curing process of epoxy and MCEDA for temperature higher than 200 °C <sup>[49]</sup>. Some phosphonium-based ILs have been studied as initiators of epoxy networks. Lower reactivity was found for the phosphate anion in comparison with the phosphinate anion which has a longer alkyl chain with inductive donor effect <sup>[50]</sup>. According to this phenomenon, tributyl(ethyl)phosphonium diethyl phosphate, denoted as IL 169, which can initiate the polymerization of epoxies at higher temperatures <sup>[29]</sup> was studied to act as an initiator for the encapsulated healing agent.



**Scheme 3-2** Hydrogen bond between amine and imidazolium IL

To study the curing behavior of epoxy-amine with IL 169 and to verify the reactivity of IL 169 for the healing agent (an excess of epoxy), DSC was used to study the reaction between epoxy resin and diamine (PACM) with different weight fractions of IL 169 (Table 3-4).

First of all, epoxy-amine mixtures at stoichiometric ratio ( $r = 1$ ) with different weight fractions of IL 169 were investigated to study the influence of IL 169 on the curing behavior of epoxy-amine. The DSC traces are reported in Figure 3-12. It can be seen that there is no large influence of IL 169 on the curing behavior of the epoxy-PACM network as the IL 169 content is lower than 10 wt%. Nevertheless, as the addition of IL 169 is 20 wt%, a slight shift of the curing temperature towards lower temperatures was observed. Taking into account the reaction mechanism between epoxy and amine (Scheme 3-3), the pair of electrons on the very electronegative nitrogen atom of the primary amine makes them nucleophilic and allows them to attack the electrophilic carbon next to the epoxide oxygen. This phenomenon is the rate determining step of the reaction between epoxy and amine. The PACM amine used in this work has high reactivity, *i.e.* its copolymerization could occur at low temperatures. For IL 169, a higher temperature is required to open epoxy ring because of its low basicity<sup>[50]</sup>. Nevertheless, the mobility of IL 169 may be limited as the viscosity of the reactive system increases after gelation.

For the epoxy-amine with phosphonium-based IL systems, Leclère *et al*<sup>[51]</sup> have mentioned that there is a competition between the epoxy-amine addition reaction and the anionic polymerization initiated by the phosphonium-based IL via the etherification reaction. Therefore, in the epoxy-PACM-IL 169 formulation, epoxy-PACM reaction was prior to one of epoxy with IL 169. As a consequence, a large part of the IL 169 remains unreacted in the epoxy-

amine networks as shown in Figure 3-12 [51].

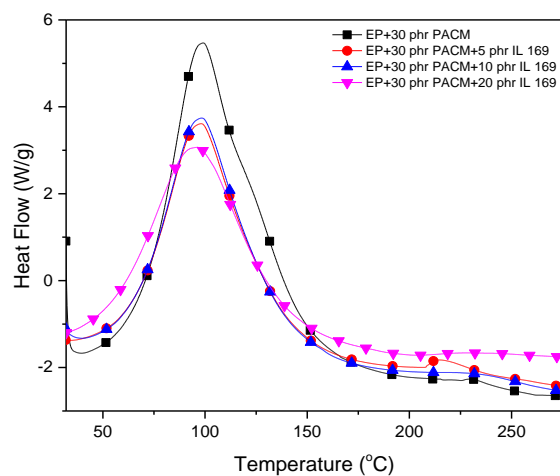


**Figure 3-12** DSC traces of curing process of epoxy-amine at stoichiometric ratio with different amount of ionic liquid (■) EP + 30 phr PACM; (●) EP + 30 phr PACM+ 5 phr IL169; (▲) EP + 30 phr PACM + 10 phr IL169; (▼) EP + 30 phr PACM + 20 phr IL169 (N<sub>2</sub> atmosphere, heating rate: 10 K·min<sup>-1</sup>)



**Scheme 3-3** General mechanism for epoxy-amine curing [52]

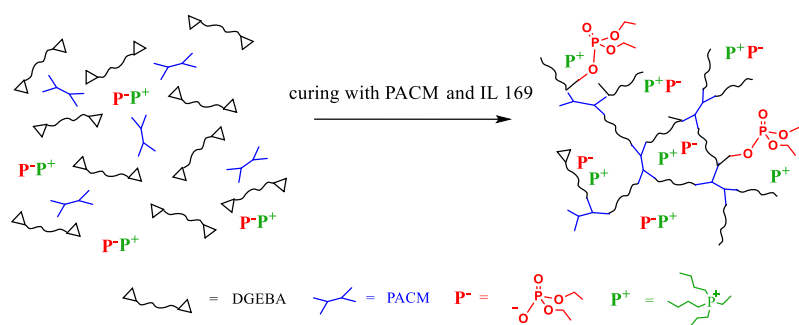


**Figure 3-13** The possible polymerization and structure of epoxy-amine-IL network [51]

In order to verify the reactivity of free IL 169 with additional epoxy monomer, *i.e.* encapsulated epoxy monomer as a healing agent, epoxy-amine network with  $r > 1$  was used. Thus, 10 phr of IL 169 was added in the mixture with epoxies in excess (EP + 20 phr PACM + 10 phr IL 169). The corresponding DSC traces, as well as the references, are shown in Figure 3-14.

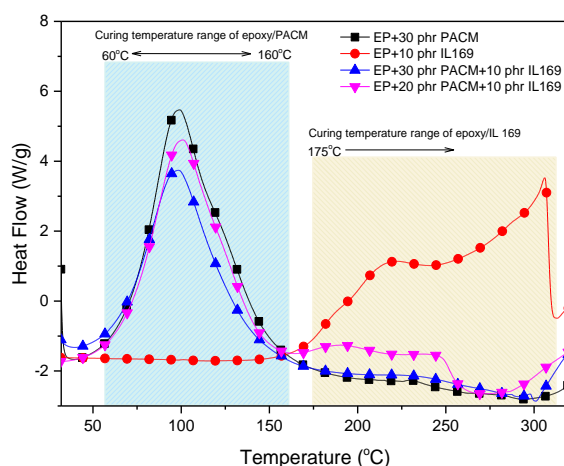


**Figure 3-14** DSC traces of curing of different epoxy-amine-ionic liquid systems (■) EP + 30 phr PACM; (●) EP + 10 phr IL169; (▲) EP + 30 phr PACM + 10 phr IL169; (▼) EP + 20 phr PACM + 10 phr IL169 (N<sub>2</sub> atmosphere, heating rate: 10 K·min<sup>-1</sup>)

For EP + 30 phr PACM and EP + 30 phr PACM + 10 phr IL 169 system, epoxy was cured with PACM at stoichiometric ratio ( $r = 1.0$ ) and a single exothermic peak could be evidenced from 60 to 160 °C. This feature indicates the rapid reaction between epoxy and PACM. 10 phr of IL 169 does not influence the curing behavior of epoxy-PACM. For EP + 10 phr IL 169 system, an exothermic process above 175 °C highlighted the chain growth polymerization of epoxy initiated by IL 169 with low basicity. For the EP+20 PACM+10 IL169 system, a second exothermic behavior after 175 °C coinciding with the temperature range of EP + 10 phr IL169 system was highlighted after the main reaction of epoxy-PACM. Therefore, the reactivity of IL 169 with the excess of epoxies was confirmed by the comparison of the above four systems.

In summary, one can confirm that IL 169 could keep its reactivity, *i.e.* be able to initiate the polymerization of epoxy excess in the cured epoxy-amine network. Epoxy and amine (PACM) cured at stoichiometric ratio ( $r = 1$ ) is necessary but the IL 169 content in the epoxy networks needs to be optimized.

### 3.4.2.2 Morphology of epoxy-amine-IL networks

The distribution of IL 169 and the optimal weight fraction in the epoxy-amine matrix need to be investigated. Therefore, epoxy-amine network cured at stoichiometric ratio ( $r = 1$ ) with a different mass fraction (from 5 to 20 phr) of IL 169 were prepared and characterized. First of

all, their morphology was characterized by TEM. Figure 3-15 (a)-(c) shows the TEM images of ultrathin sections of different epoxy-amine-IL networks at lower magnification and a homogeneous morphology can be observed, indicating a good distribution of IL 169 in the epoxy-amine network. Figure 3-15 (d)-(f) show the corresponding TEM micrographs at high magnification, a difference in electronic densities between phases due to IL 169 <sup>[53]</sup> is observed and it is more obvious with an increasing percentage of IL 169. This can be explained by the limited miscibility between phosphonium salt and the growing species during curing <sup>[29]</sup>. As a summary, the phosphonium-based ionic liquid (IL 169) is dispersed homogeneously in the epoxy-amine network and a very fine nanosized phase was observed with the increasing amount of IL 169. This homogeneous distribution of IL 169 within epoxy-amine network is beneficial for further initiating the polymerization of the released healing agents.

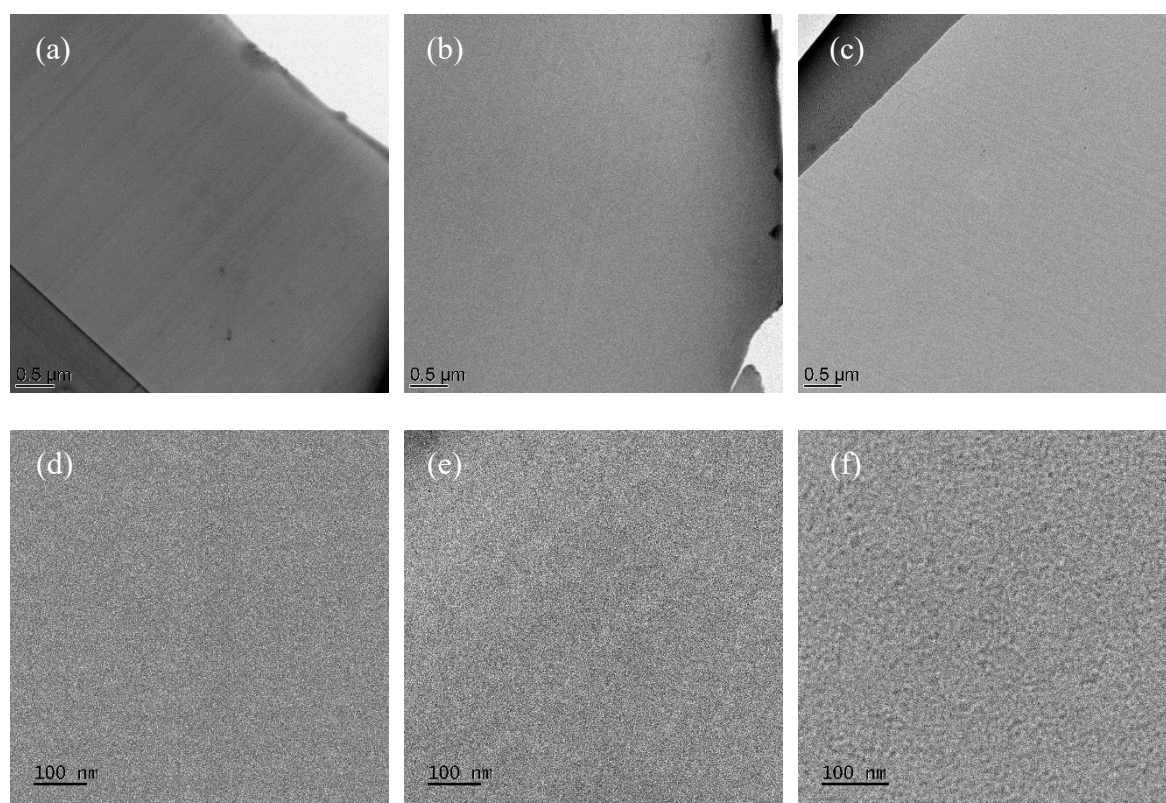


**Figure 3-15** TEM micrographs of cured epoxy-amine-IL networks, *i.e.* DGEBA combined with 30 phr PACM with addition of (a,d) 5 phr IL 169; (b, e) 10 phr IL 169; (c, f) 20 phr IL 169

### 3.4.2.3 Thermal properties of epoxy-amine-IL networks

It is well known that the addition of low molar mass component in thermoset polymers always influences the thermal properties of the resulting material. Thus, it is necessary to take into consideration similarly the effect on the thermal properties brought by IL 169. Therefore, the thermal properties of epoxy-amine networks with different IL contents were characterized. This will help to determine the optimal IL 169 content. Figure 3-16 presents the DSC traces of epoxy-amine networks ( $r = 1$ ) with different IL 169 contents and the corresponding  $T_g$  values. It can be seen that with the addition of IL 169, the  $T_g$  decreases compared to the neat epoxy-amine network ( $T_g = 156\text{ }^\circ\text{C}$ , see Table 2-4 in Chapter 2). According to the literature, after the polyaddition reaction of epoxies and amines, IL may open residual epoxy rings from anion to form phosphonium alcoholates [27, 51]. DSC traces for curing epoxy-amine-IL 169 (Figure 3-14) indicate that epoxy reacts with amine in the early stage of curing, and IL 169 remains ions pairs within the epoxy-amine network. As a consequence, IL 169 plays a role of plasticizer and decreases the  $T_g$  [54, 55].

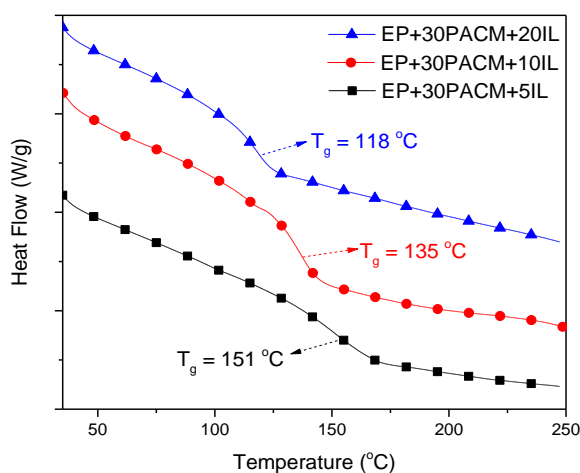


**Figure 3-16** DSC traces of epoxy-amine-IL systems: (■) EP + 30 phr PACM + 5 phr IL169; (●) EP + 30 phr PACM + 10 phr IL169; (▲) EP + 30 phr PACM + 20 phr IL169 (N<sub>2</sub> atmosphere, heating rate: 10 K·min<sup>-1</sup>)

The influence of IL 169 on the thermal degradation of epoxy-amine networks as well as the one of neat IL 169 were characterized by TGA as shown in Figure 3-17. The onset decomposition temperature ( $T_{d\text{ onset}}$ , temperature at 5 wt% weight loss) and the maximum



decomposition temperature ( $T_{d\ max}$ ) were summarized in Table 3-5. It can be seen that neat IL 169 has the lowest  $T_{d\ onset}$  (266 °C) and two steps of thermal degradation were evidenced. Compared with EP + 10 phr IL 169 system ( $T_{d\ onset}$  = 341 °C) [50], free IL 169 in the epoxy-amine network may decrease the  $T_{d\ onset}$  values of final materials with increasing mass fraction of free IL 169 (see Table 3-5). Moreover,  $T_{d\ max}$  values of epoxy-amine-IL networks are shifted to lower temperature as well and the shoulder (Figure 3-17 (b), pointed by arrows) on the DTG curves corresponds obviously with the increasing amount of IL 169, to the second degradation of IL 169. Therefore, free IL 169 in the epoxy-amine networks may decrease the  $T_{d\ onset}$  of the resulting epoxy-amine-IL system with increasing weight fraction.

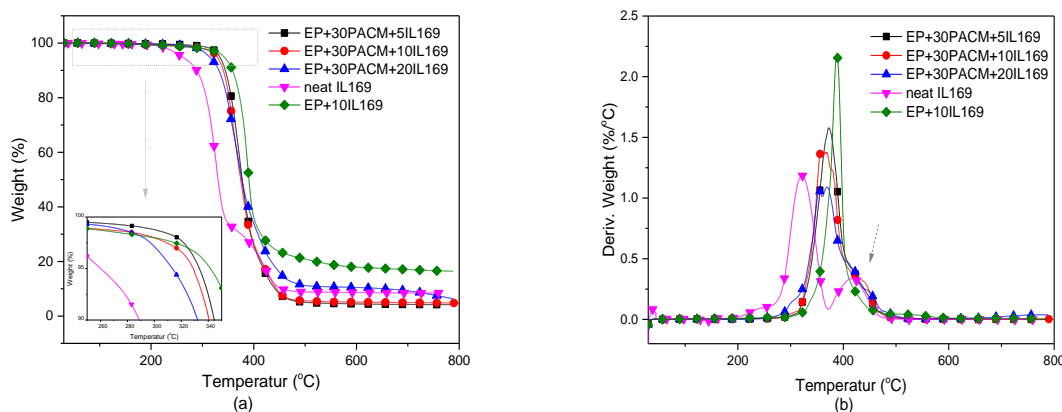


**Figure 3-17** (a) TGA and (b) DTG traces of epoxy-amine-IL networks

(■) EP + 30 phr PACM + 5 phr IL169; (●) EP + 30 phr PACM + 10 phr IL169; (▲) EP + 30 phr PACM + 20 phr IL169; (▼) neat IL169 ; (◆) EP + 10 phr IL169 (N<sub>2</sub> atmosphere, heating rate: 20 K·min<sup>-1</sup>)

**Table 3-5** Weight loss temperatures of epoxy-amine-IL networks and neat IL 169

Material	$T_{d\ onset}$ (°C)	$T_{d\ max}$ (°C)
EP + 30 PACM+5 IL 169	333	370
EP+30 PACM+10 IL 169	328	365
EP+30 PACM+20 IL 169	313	364
neat IL 169	260	$T_{d\ max1} = 320; T_{d\ max2} = 420$
EP + 10 phr IL169	341	388
EP + 30 PACM	359	378

#### 3.4.2.4 Mechanical properties of epoxy networks

The mechanical properties of epoxy-amine-IL networks were investigated to determine the optimal weight fraction of IL 169. The Young's modulus and fracture toughness were characterized and the results are summarized in Table 3-6. The Young's modulus and fracture toughness increased simultaneously. This could be explained by the nanoscale dispersion of IL 169 within the epoxy-amine network. The uniform dispersion as nanophases of IL 169 in the polymer matrix (see Figure 3-15) could also explain the increase of fracture toughness. In fact, ionic liquid as nanophases could increase plastic deformation at the crack tip during crack propagation leading to an increase of the fracture toughness [56].

**Table 3-6** Mechanical properties of different epoxy-amine-IL networks

Materials	$E$ (GPa)	$K_{IC}$ (MPa·m <sup>1/2</sup> )
EP+30 PACM	1.1 ± 0.04	0.55 ± 0.05
EP+30 PACM +5 IL	1.3 ± 0.02	0.60 ± 0.05
EP+30 PACM +10 IL	1.6 ± 0.03	0.63 ± 0.04
EP+30 PACM +20 IL	1.6 ± 0.02	0.68 ± 0.04

To conclude, IL 169 could be considered as potential initiator for a released healing agent from EP@PUF microcapsules for self-healing purposes. It is necessary to make sure that IL 169 is well dispersed and remains reactive. Therefore, the curing behavior, thermal and mechanical properties of different epoxy-amine-IL 169 networks were studied. The results have shown that IL 169 played a role of plasticizer and lower the decomposition temperature of epoxy-amine networks. However, the homogeneous distribution of IL 169 as nanophases helped to prevent the crack propagation by plastic deformation and improved the mechanical properties. Therefore, after considering the disadvantages of thermal properties and advantages of mechanical properties provided by IL 169 in the epoxy-amine network, the optimal addition of IL 169 was determined to be 10 phr.

### 3.5 Preparation and characterization of self-healing epoxy-amine-ionic liquids composites filled with EP@PUF microcapsules

#### 3.5.1 Material processing

After determining the optimal weight fraction of IL 169 in the epoxy-amine networks, to provide the self-healing behavior, the EP@PUF microcapsules were added in the epoxy-amine-IL formulation to prepare the epoxy composites. Different weight fractions of EP@PUF microcapsules (5 to 20 wt%) were considered (Table 3-7).

**Table 3-7** Weight fractions of each component of EP@PUF microcapsule-filled epoxy-amine-IL composites

Material	D.E.R. 332 (phr)	PACM (phr)	IL 169 (phr)	EP@PUF (wt%)
1	100	30	10	0
2	100	30	10	5
3	100	30	10	10
4	100	30	10	15
5	100	30	10	20

Figure 3-18 describes the preparation protocol of EP@PUF microcapsule-filled epoxy-amine-IL composites. In a first step, EP@PUF microcapsules were dispersed into epoxy monomer under ultrasounds. Before adding diamine (PACM), 10 wt% of IL 169 of epoxy resin were added to the initial mixture. This one was then stirred in an oil bath at 60 °C for 15 min. Then, PACM diamine hardener was added considering a stoichiometric ratio equal to 1 (epoxy-to-amino hydrogen ratio). The mixture was stirred for another 15 min at 60 °C. Finally, the mixture was degassed, casted, and cured in an oven. The curing process was carried out as follows: 2 h at 80 °C followed by 2 h at 160 °C. Finally, the materials were cooled down to room temperature.

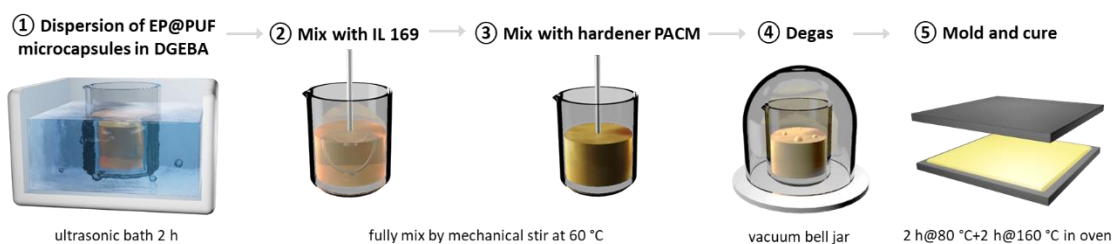
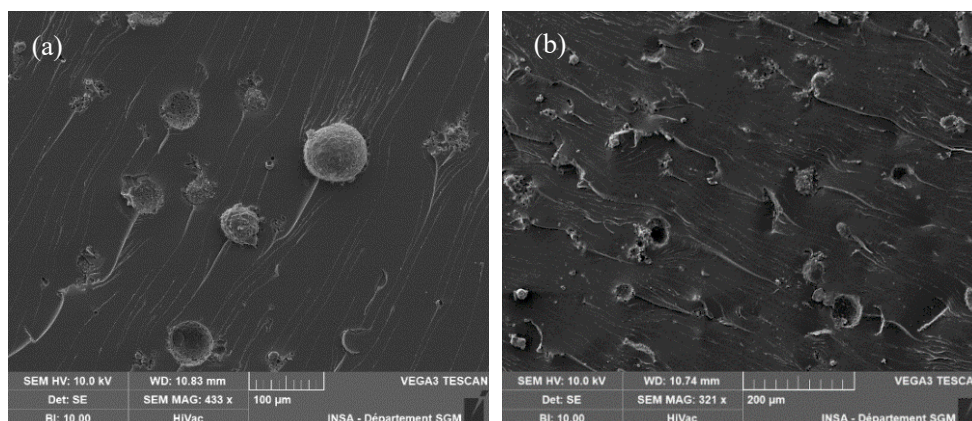


**Figure 3-18** Design of EP@PUF microcapsule-filled epoxy-amine-IL composites

### 3.5.2 Characterization of EP@PUF microcapsule-filled epoxy-amine-IL materials

#### 3.5.2.1 Morphology of EP@PUF microcapsule-filled epoxy-amine-IL materials

The dispersion of state of EP@PUF microcapsule-filled epoxy-amine-IL composites was characterized by SEM (Figure 3-19). Figure 3-19 (a)-(d) shows the SEM images of fractured surfaces of EP@PUF microcapsule-filled epoxy-amine-IL composites with 5, 10, 15, and 20 wt% EP@PUF microcapsules contents. Figure 3-19 (e)-(h) show the intact or broken EP@PUF microcapsule and the interfaces in the epoxy composites. As shown in Figure 3-19 (a) - (d), a good dispersion of EP@PUF microcapsules and broken ones can be seen on the fracture surfaces. Moreover, tails, *i.e.* the hackle markings were observed on the fractured surface and these tails were formed by the rapid advancement of the crack front the path that required the minimum energy [57, 58]. The interfacial strength is also very important for self-healing ability for composites filled with microcapsules. A good interface can guarantee the rupture of microcapsules during the crack propagation for further release of healing agent. Figure 3-19 (e) - (f) shows the individual EP@PUF microcapsules and the good interface with the epoxy-amine-IL network. In Figure 3-19 (g) and (h), the interface can be seen clearly. As a consequence, on the fractured surfaces, tails were observed evidencing crack pinning leading to advancement of fracture toughness. Therefore, the rapid crack propagation and the good interfaces between the EP@PUF microcapsules and the epoxy-amine network could ensure the breakage and the release of healing agent, and the good distribution of EP@PUF microcapsules could be in favor of achieving self-healing.



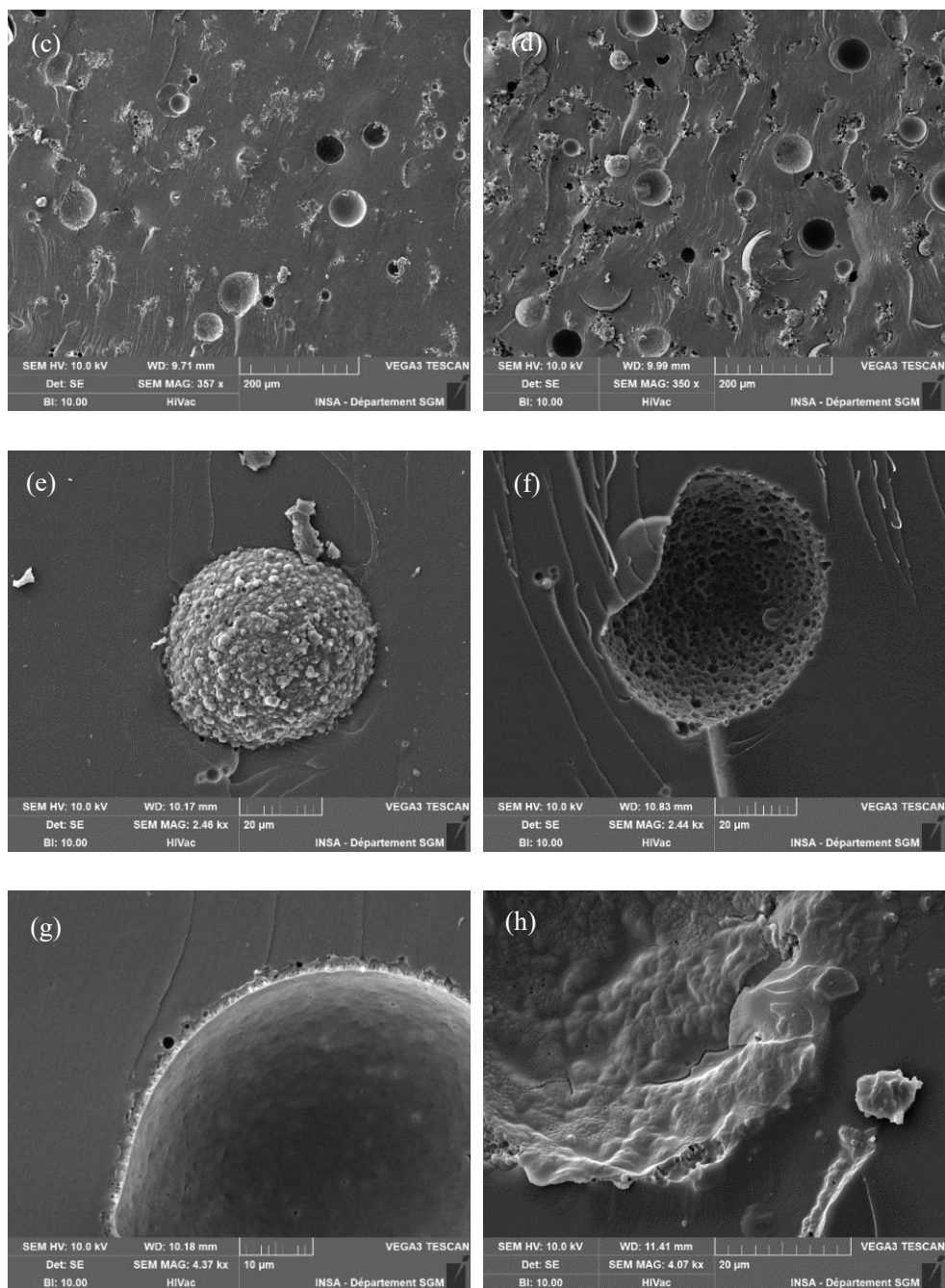


**Figure 3-19** SEM micrographs of fractured surface of epoxy-amine-IL composites filled with (a) 5 wt%; (b) 10 wt%; (c) 15 wt%; (d) 20 wt% of EP@PUF microcapsules; and (e)-(f) intact/broken EP@PUF microcapsules and the interfaces

### 3.5.2.2 Thermal behavior of EP@PUF microcapsule-filled epoxy-amine-IL materials

The thermal behavior of EP@PUF microcapsule-filled epoxy composites was characterized from DSC measurement (Figure 3-20). Glass transition temperature ( $T_g$ ) was

summarized in Table 3-8. First, a decrease of  $T_g$  values EP@PUF microcapsule-filled epoxy composites was observed compared with the neat epoxy-amine-IL network, which is mainly due to the addition of EP@PUF microcapsules. In addition, it should be noticed that for all the EP@PUF microcapsule-filled epoxy-amine-IL networks, an exothermic peak from 200 to 250 °C is evidenced on the DSC trace, indicating the polymerization of released epoxy healing agent from the EP@PUF microcapsules occurs. On the opposite, the epoxy-amine-IL network did not show such an exothermic peak as no polymerization reaction occurs. Therefore, the reactivity of the EP@PUF microcapsules as potential self-healing agent is verified.

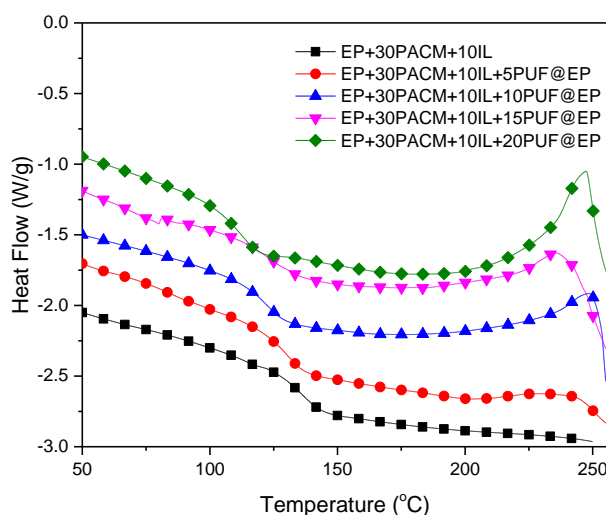


**Figure 3-20** DSC traces of EP@PUF microcapsule-filled epoxy-amine-IL composites ( $N_2$  atmosphere, heating rate:  $10\text{ K}\cdot\text{min}^{-1}$ )

**Table 3-8**  $T_g$  of different EP@PUF microcapsule-filled epoxy-amine-IL materials

Symbol in Figure 3-20	Material	$T_g$ (°C)
■	EP+30PACM+10IL	135
●	EP+30PACM+10IL+5EP@PUF	130
▲	EP+30PACM+10IL+10EP@PUF	124
▼	EP+30PACM+10IL+15EP@PUF	123
◆	EP+30PACM+10IL+20EP@PUF	113

### 3.5.2.3 Thermal stability of EP@PUF microcapsule-filled epoxy-amine-IL materials

Thermal stability of EP@PUF microcapsule-filled epoxy-amine-IL composites was characterized by TGA, and the TGA and the corresponding DTG traces were shown in Figure 3-21. The onset decomposition temperature ( $T_{d\ onset}$ , temperature at 5 wt% weight loss) and maximum decomposition temperature ( $T_{d\ max}$ , temperature at the peak of DTG curve) are summarized in Table 3-9.

It can be seen that when the weight fraction of EP@PUF microcapsules increases,  $T_{d\ onset}$  decreases while  $T_{d\ max}$  does not change. The decrease of  $T_{d\ onset}$  can be attributed to the facts that EP@PUF microcapsules have a  $T_{d\ onset}$  around 238 °C (see Table 3-2), which is lower than the one of epoxy-amine-IL network (328 °C). Therefore, increasing the EP@PUF microcapsules content will lower the  $T_{d\ onset}$  of EP@PUF microcapsules filled epoxy-amine-IL composite.

For  $T_{d\ max}$ , similar values and degradation behavior can be evidenced in Figure 3-21 for all materials. Epoxy-amine-IL networks filled with 10, 15, and 20 wt% EP@PUF microcapsules showed three steps of decomposition, *i.e.* two maxima on the DTG traces. However, epoxy materials with only 5 wt% of EP@PUF microcapsules did not have the first peak. The first decomposition close to 260 °C ( $T_{d\ max1}$ ) evidenced with a low intensity peak on the DTG traces corresponds to the decomposition of the PUF shell. Therefore, the more EP@PUF microcapsules added in the epoxy matrix, the highest first degradation peak is on the DTG traces. On the other hand,  $T_{d\ max2}$  close to 370 °C for all the samples did not vary and is associated with the degradation of the polymer matrix. The shoulder close to 420-470 °C on DTG traces can be attributed to the further degradation of polymerized healing agent and IL 169. According to the TGA results, the EP@PUF microcapsule-filled epoxy-amine-IL materials display a very good thermal stability. The addition of EP@PUF microcapsules slightly decreases the  $T_{d\ onset}$  but the microcapsules do not have any influence on the degradation behavior of the resulting materials.

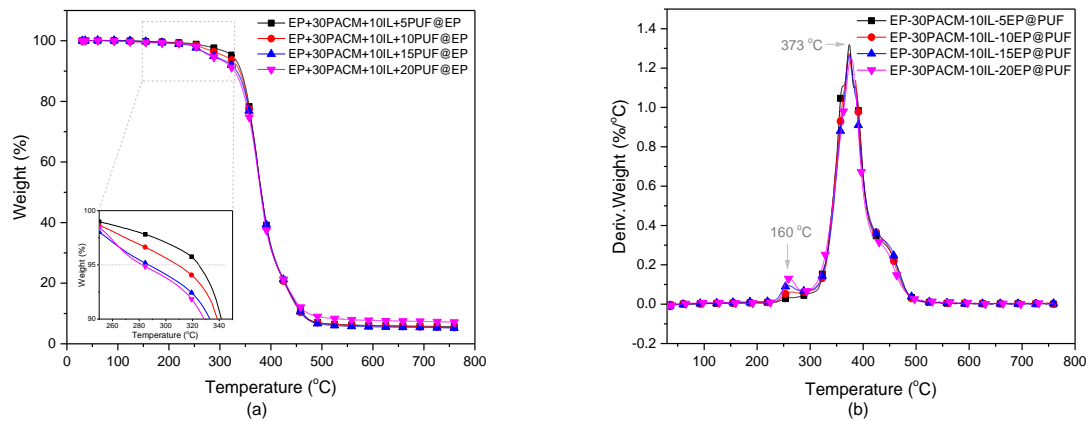


**Figure 3-21** (a) TGA and (b) DTG traces of EP@PUF microcapsule-filled epoxy composites under N<sub>2</sub> atmosphere (■) EP + 30PACM + 10IL + 5EP@PUF; (●) EP + 30PACM + 10IL + 10EP@PUF; (▲) EP + 30PACM + 10IL + 15EP@PUF; (▼) EP + 30PACM + 10IL + 5EP@PUF (N<sub>2</sub> atmosphere, heating rate: 20 K·min<sup>-1</sup>)

**Table 3-9** Weight loss temperature of EP@PUF microcapsule-filled epoxy-amine-IL materials

Material	T <sub>d</sub> onset (°C)	T <sub>d</sub> max	
		T <sub>d</sub> max1 (°C)	T <sub>d</sub> max2 (°C)
EP + 30 PACM+10 IL	328	365	
EP + 30PACM + 10 IL + 5 EP@PUF	324	--	374
EP + 30 PACM + 10 IL + 10 EP@PUF	308	264	373
EP + 30 PACM + 10 IL + 15 EP@PUF	287	257	375
EP + 30 PACM + 10 IL + 20 EP@PUF	282	258	377

### 3.5.2.4 Dynamic mechanical analysis of EP@PUF microcapsule-filled epoxy-amine-IL materials

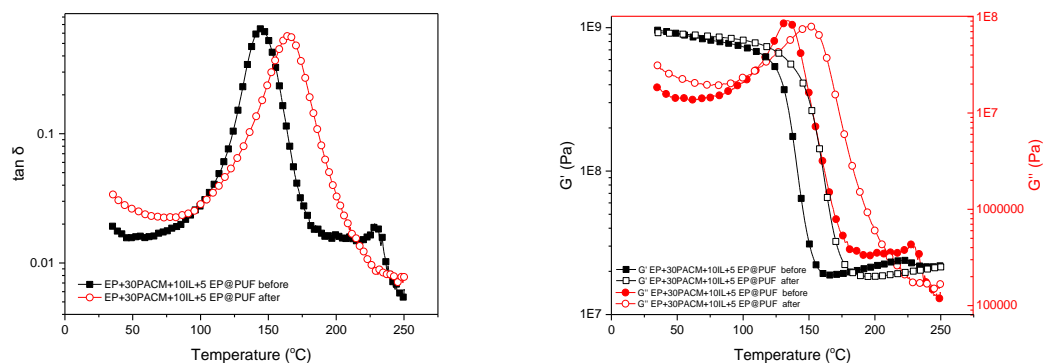
Dynamic mechanical analysis (DMA) was performed to characterize EP@PUF filled epoxy-amine-IL materials. Two characterizations for the same sample in the same conditions were performed to simulate the self-healing process. The loss factor (tan δ), storage modulus



( $G'$ ), and loss modulus ( $G''$ ) as a function of temperature of different materials are presented in Figure 3-22.

As shown in Figure 3-22, the glass transition of epoxy matrix is evidenced on the  $\tan \delta$  vs. temperature (T) curves, corresponding to the main peak and relaxation ( $\alpha$ ). A second peak after the main relaxation from 200 to 250 °C could be also evidenced on  $\tan \delta$  - T and  $G''$  -T curves in the first heating run. In the same temperature range, an increase of  $G''$  can be seen as well. This can be explained by the beginning of decomposition of the PUF shell and the polymerization of the healing agent in the EP@PUF microcapsules. In fact, polymerization started with the breakage of the PUF shell. Meanwhile, the released healing agent, *i.e.* epoxy, polymerized from the initiation of IL 169 in the epoxy matrix explains the increase of  $G''$ .

The  $T_\alpha$  values of EP@PUF microcapsule-filled epoxy materials increase after the first heating run, as shown in Table 3-10. To explain this, the graphical representation of possible structures of healed materials with the healing agent is shown in Figure 3-23. In the EP@PUF microcapsule-filled epoxy composites, the released healing agent polymerized from the initiation of IL 169 heals the cracks of the polymer matrix by forming a cured network. As a consequence, an increase of  $T_\alpha$  was observed. Furthermore, because of the polymerized healing agent in the matrix, a strengthened material has been formed compared with the original material. Thus, the self-healing ability of EP@PUF microcapsules filled epoxy-amine-IL composites was verified and the mechanical performances of healed composites are improved.



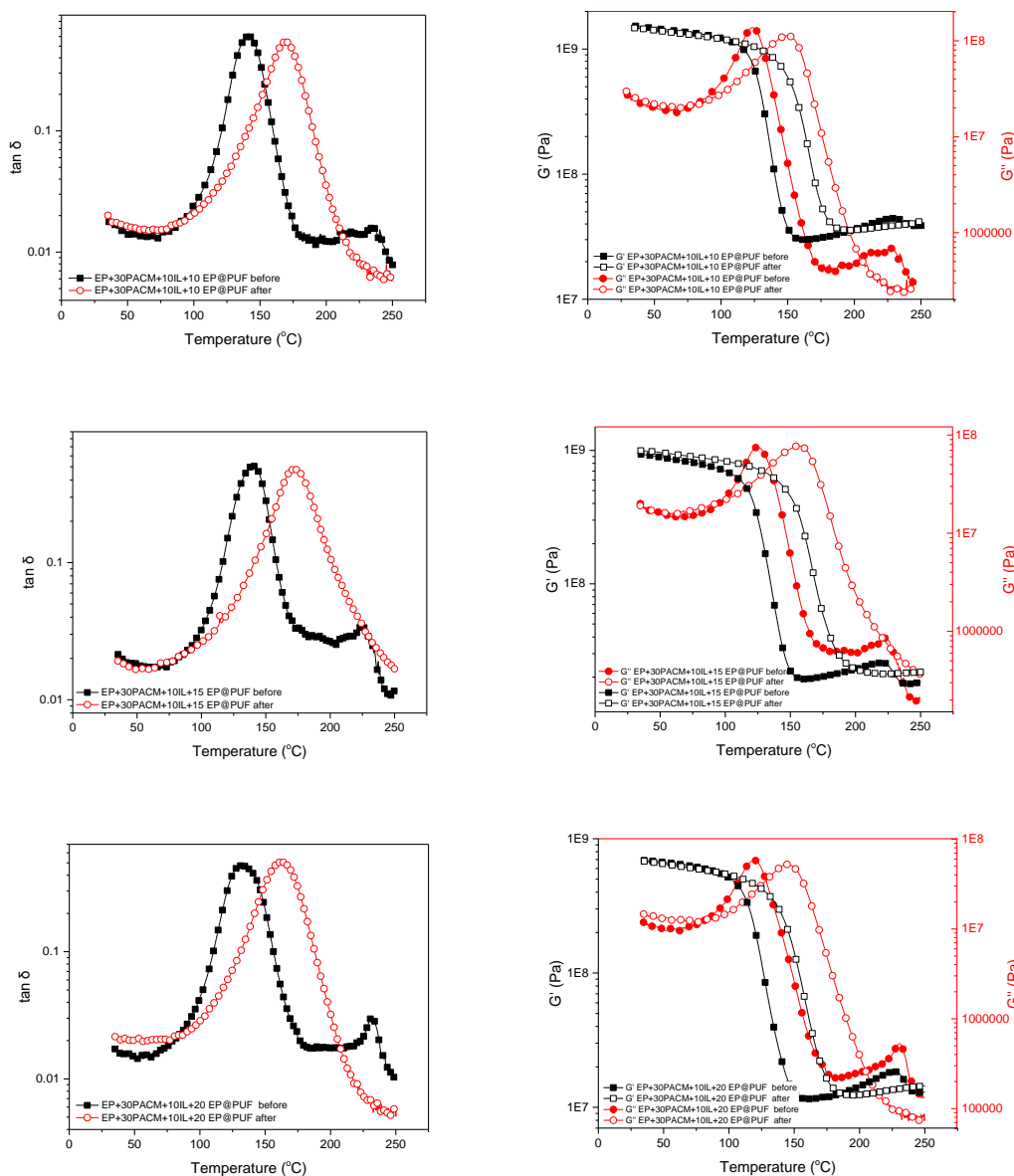


**Figure 3-22**  $\tan \delta$ ,  $G'$ , and  $G''$  vs. temperature curves of EP@PUF microcapsule-filled epoxies (at 1Hz, heating rate  $3 \text{ K} \cdot \text{min}^{-1}$ )

**Table 3-10**  $\alpha$  transition temperatures of different EP@PUF microcapsule-filled epoxy-amine-IL materials

Material	$T_{\alpha}$ ( $^{\circ}\text{C}$ ) before	$T_{\alpha}$ ( $^{\circ}\text{C}$ ) after
EP + 30 PACM + 10 IL + 5 EP@PUF	144	164
EP + 30 PACM + 10 IL + 10 EP@PUF	140	163
EP + 30 PACM + 10 IL + 15 EP@PUF	138	166
EP + 30 PACM + 10 IL + 20 EP@PUF	132	162

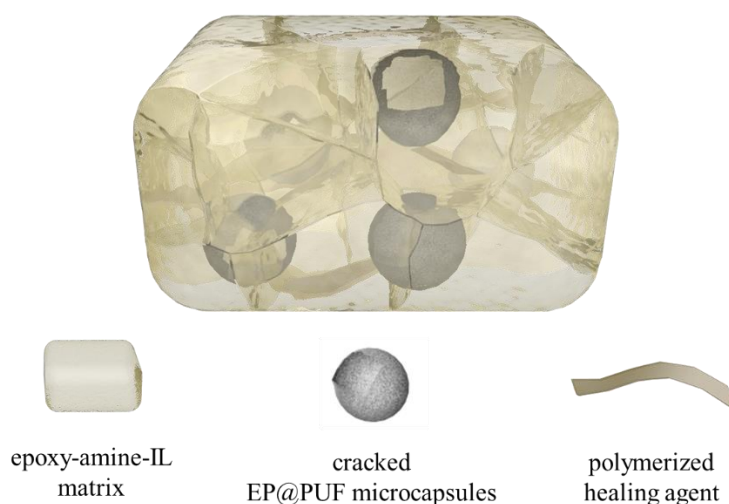


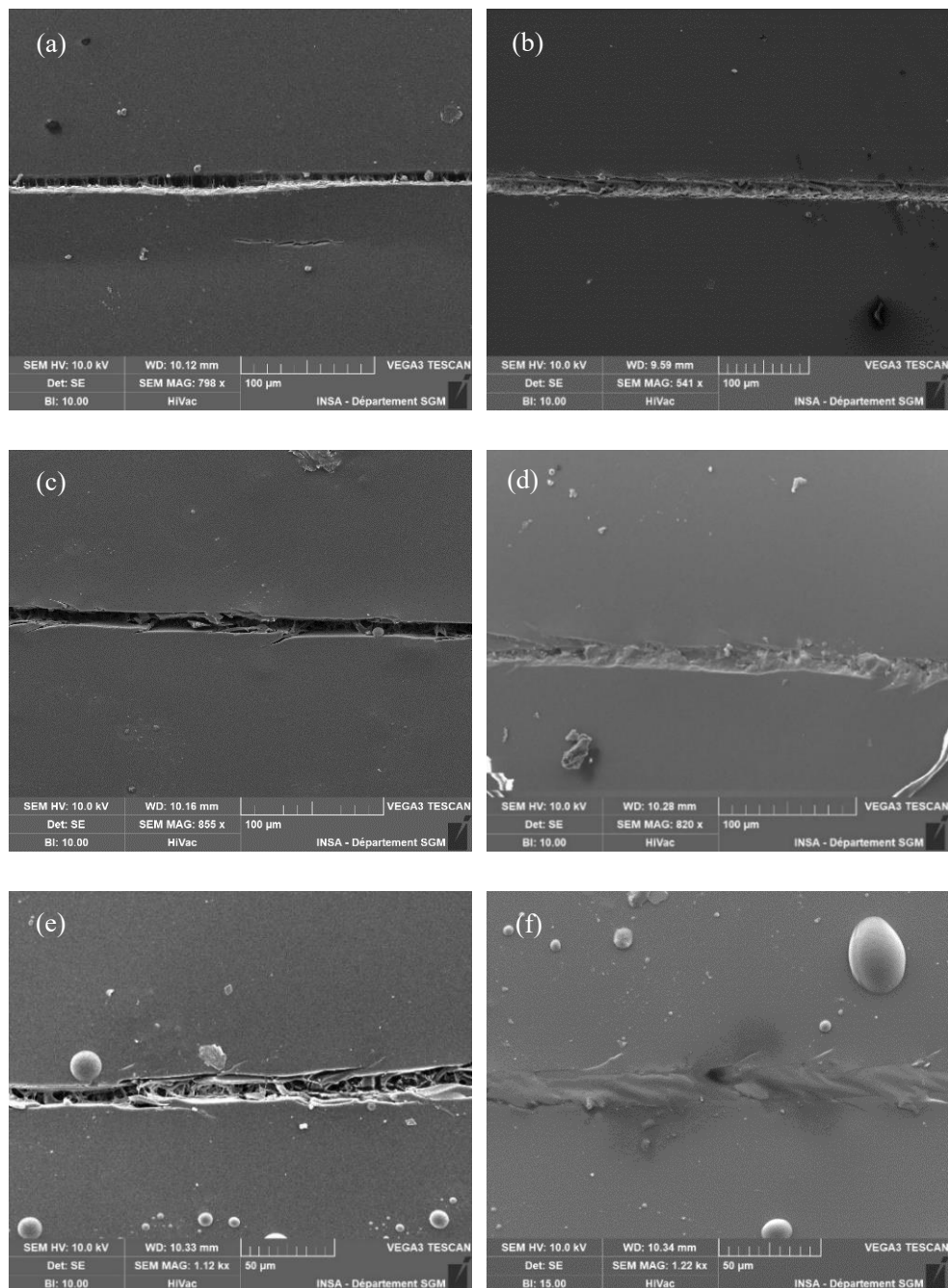
**Figure 3-23** Graphical representation of possible structure after the healing process

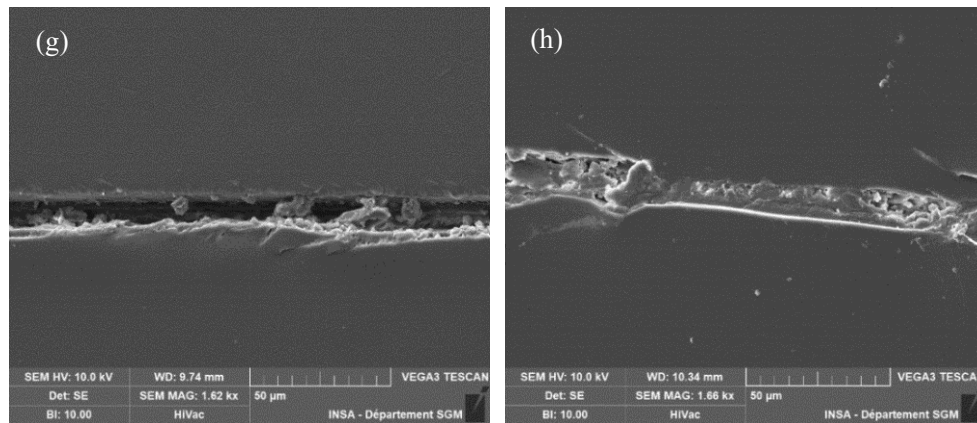
### 3.5.2.5 Self-healing property of EP@PUF microcapsule-filled epoxy-amine-IL materials

Finally, the self-healing ability of the prepared material was characterized by comparing a scratch created on the material before and after self-healing using SEM microscopy. A scratch was made by a razor blade on the materials and the scratched materials were placed in an oven to carry out the self-healing process at 80 °C for 2h, 160 °C for 3h, and 200 °C for 3h. The SEM images of scratches on the epoxy-amine-IL networks filled with different weight fractions of EP@PUF microcapsules before (left) and after (right) the self-healing process were represented in Figure 3-24. The width of the scratches made by the razor blade was controlled around 10 to 15  $\mu\text{m}$ , which should be smaller than the diameter but bigger than the shell thickness of the EP@PUF microcapsules, to ensure the breakage of the PUF shell and the release of the self-healing agent.

As shown in Figure 3-24, the self-healing ability depends on the weight fraction of the EP@PUF microcapsules in the epoxy composites. As shown in Figure 3-24 (b), the epoxy-amine-IL composites filled with only 5 wt% of EP@PUF microcapsules did not show a release for filling the crack and polymerization of the healing agent. Thus, no self-healing effect was observed due to the too low number of EP@PUF microcapsules in the polymer matrix. As the interspace among EP@PUF microcapsules is large, the scratch could pass through the polymer matrix without damaging the EP@PUF microcapsules. Nevertheless, if the mass fraction of EP@PUF microcapsules was increased up to 10 wt%, the healing effect of the scratch can be

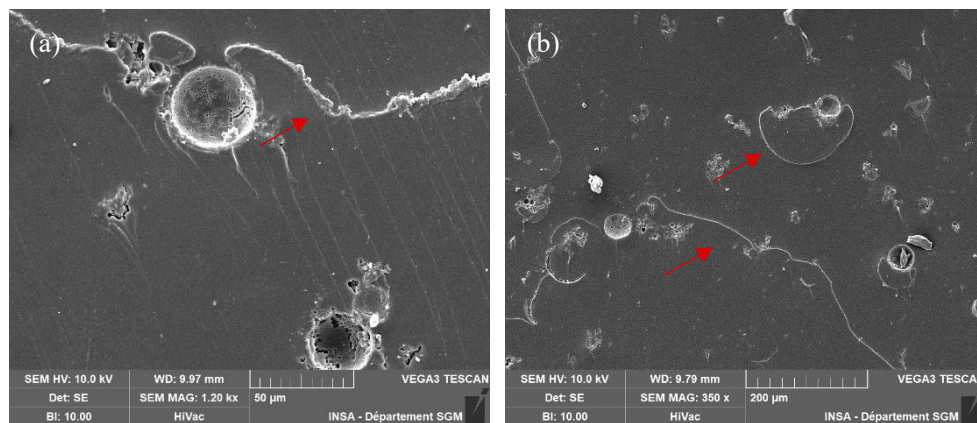
effective as shown in Figure 3-24 (d). The release of healing agent and its polymerization in the scratch as well as the self-healing effect can also be evidenced when the weight fraction of EP@PUF microcapsules is higher, *i.e.* 15 wt% (Figure 3-24 (f)) to 20 wt% (Figure 3-24 (h)).





**Figure 3-24** SEM micrographs of scratches on the EP@PUF microcapsule-filled epoxy-amine-IL materials before (left) and after (after) healing: (a)(b) 5 wt%; (c)(d) 10 wt%; and (e)(f) 15 wt% and (g)(h) 20 wt% of EP@PUF microcapsules addition

In addition, after the fracture toughness test, the samples were submitted to the same healing process in the oven, and the fractured surfaces after the healing process were also observed by SEM. As shown in Figure 3-25, the released polymerized healing agent could be observed (pointed out by the arrows in Figure 3-25). It can be seen that the healing agent was released by the broken EP@PUF microcapsules and polymerized at the fractured surface. However, the healed material did not recover mechanical properties similar to the original ones. In fact, a large quantity of the healing agent is needed to rebond the two large fractured surfaces for a well cured material. Nevertheless, the polymerized film formed by the released healing agent in Figure 3-25 evidences the self-healing ability of EP@PUF microcapsules introduced epoxy-amine-IL networks.



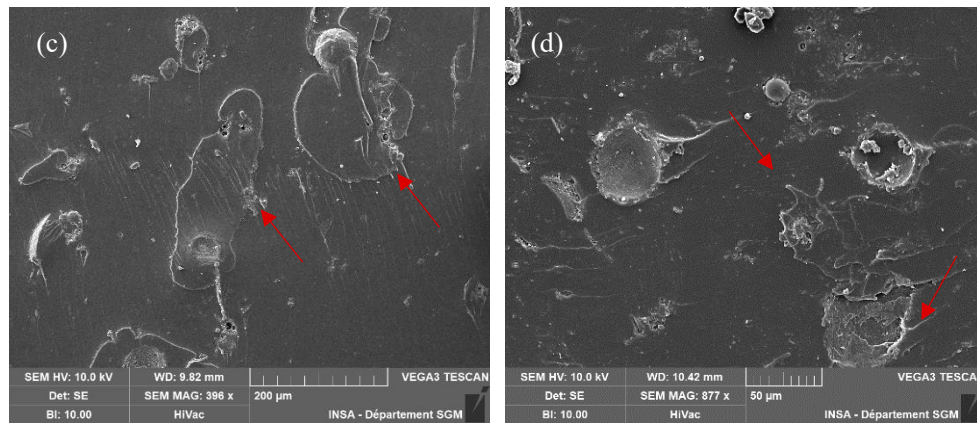


**Figure 3-25** SEM micrographs of healing surface after fractured toughness test of EP@PUF microcapsule-filled epoxy-amine-IL materials (arrow indicated the release and polymerized healing agent at the fracture surface)

### 3.5.2.6 Mechanical properties of EP@PUF microcapsule-filled epoxy-amine-IL materials

According to the previous studies, more than 10 wt% of EP@PUF are enough to achieve an efficient self-healing effect of the scratch into the epoxy-amine-IL materials, because increasing the number of EP@PUF microcapsules will lead to a negative effect on the thermal properties of the final epoxy materials. Let us consider the influence of EP@PUF microcapsules on the mechanical properties of epoxy-amine-IL composites by characterizing their Young's modulus and fracture toughness.

Table 3-11 summarizes Young's modulus and the fractures of epoxy-amine-IL networks with and without EP@PUF microcapsules. It can be seen that more than 5 wt% of EP@PUF microcapsules addition leads to a decrease of Young's modulus of epoxy materials and this decrease is even higher with increasing weight fraction of EP@PUF microcapsules. The decrease of Young's modulus is in agreement with the one observed for other amino-microcapsule-filled polymers both for single or dual microcapsules systems. For example, Yan *et al* [59] and Li *et al* [23] have also reported that the reduced modulus is due to the addition of single and dual microcapsules in polymers. There are two reasons that can explain the negative influence of EP@PUF microcapsules on Young's modulus : *i*) the EP@PUF microcapsules filled with healing agent act as defects at the cross section of composites; the lack of chemical bonds at the interface or stronger molecular interactions between EP@PUF microcapsule and

the polymer matrix led to a weak or brittle interface; *ii*) soft segment of the molecular chains slipping of EP@PUF microcapsule surface from its original position within the epoxy matrix during the characterization led to a reduction in Young's modulus of epoxy composite [60].

An increase in the fracture toughness of EP@PUF microcapsule-filled epoxy materials resulting from additional EP@PUF microcapsules can be evidenced. This one could be attributed to the addition of microcapsules that can absorb the fracture energy and prevent the propagation of cracks, corresponding to the tails in Figure 3-19. As described in Chapter 2, the tails around the fillers explained the crack pinning toughen mechanism. Nevertheless, additional mechanisms are present. Lee *et al* [61] studied the micromechanical behavior of epoxy loaded microcapsules by nanoindentation. These authors demonstrated that the epoxy loaded microcapsules with a PUF shell behaved like a viscoelastic material. Therefore, the “Crack path deflection” mechanism could also contribute to the increased fracture toughness [62, 63]. The viscoelastic character of polymer shell makes the crack deviate from its main plane and increase the energy for crack propagation [64, 65]. In addition, the fracture of microcapsules from the microcracks propagation can undergo debonding from the matrix and increase the crack tip radius (of the diameter of the fractured microcapsules) [66]. Therefore, increasing number of EP@PUF microcapsules in the epoxy-amine matrix brings more defects in the matrix. The low mechanical strength of EP@PUF microcapsules compared to highly crosslinked matrix contributed to the decreased Young's modulus. Nevertheless, increasing number of EP@PUF microcapsules also improve the toughness from the increasing tortuosity of the cracks during propagation.

**Table 3-11** Mechanical properties of different EP@PUF microcapsule-filled epoxy-amine-IL materials

Material	$E$ (GPa)	$K_{IC}$ (MPa·m <sup>1/2</sup> )
EP+30PACM+10IL	1.6±0.03	0.63±0.04
EP+30PACM+10IL+5EP@PUF	1.6±0.01	0.66±0.02
EP+30PACM+10IL+10EP@PUF	1.5±0.05	0.71±0.03
EP+30PACM+10IL+15EP@PUF	1.5±0.02	0.77±0.02
EP+30PACM+10IL+20EP@PUF	1.4±0.02	0.81±0.05

To conclude, EP@PUF microcapsules in the epoxy-amine-IL network can play a role of additive self-healing according to the extrinsic self-healing mechanism, in which 10 phr of IL 169 was added in the matrix as initiator for the polymerization of released healing agent. Results have shown that more than 10 wt% of EP@PUF microcapsules could bring a promising self-healing effect of scratches and improve the fracture toughness at the same time for the final material. However, an increasing number of EP@PUF microcapsules in the matrix will also bring a negative effect on the thermal properties and on resulting stiffness.

### 3.6 Conclusion of Chapter 3

In this chapter, an epoxy monomer was encapsulated in a poly(urea-formaldehyde) (PUF) shell material as EP@PUF microcapsules. The obtained EP@PUF microcapsules have a rough surface and a size distribution of around 20 - 150  $\mu\text{m}$ . Good thermal stability and polymerization ability of core material make the EP@PUF microcapsules behave as self-healing additives in the polymer composites.

An ionic liquid tributyl(ethyl)phosphonium diethyl phosphate (IL 169) was considered as the initiator of the polymerization of a healing agent, *i.e.* encapsulated epoxies, due to the different cure temperature ranges required for the copolymerization with 4,4'-methylenebis(cyclohexylamine) (PACM). Thus, IL 169 can react with the released epoxy healing agent as EP@PUF microcapsules are broken. Different characterization methods including DCS, TGA, and TEM have been employed to optimize the weight fraction of IL 169 in the epoxy-amine network. We showed that IL 169 added to the epoxy-networks acts as a plasticizer and is able to initiate the polymerization of excess epoxies. Nevertheless, the homogeneous distribution of IL 169 as nanophases promotes the initiation of the polymerization after releasing healing agent and helps to improve the mechanical behavior. After balancing the both advantages and disadvantages of IL 169 in the epoxy-amine network, the optimal addition of IL 169 in epoxy-amine networks was 10 phr.

Finally, different weigh fractions of EP@PUF microcapsules were added in the epoxy-amine-IL network as self-healing additives. Their thermal properties, self-healing ability, and mechanical properties were investigated. DSC and TGA analyses showed that the addition of EP@PUF microcapsules slightly affected  $T_g$  and degradation temperature of resulting material



due to lack of chemical interactions and the lower decomposition temperature of EP@PUF microcapsules compared to epoxy matrix. SEM observation of the scratch before and after the self-healing process was used to characterize the self-healing ability of the resulting materials. A threshold of the numbers of EP@PUF microcapsules ( $> 10$  wt%) in the epoxy matrix was found. Over this threshold, the healing agent is released sufficiently and the self-healing effect is effective. However, the addition of EP@PUF microcapsules in the epoxy matrix lowers Young's modulus and thermal properties but improves the fracture toughness of the resulting materials, which is mainly due to the viscoelastic characteristic of such EP@PUF microcapsules.

## References of Chapter 3

- [1] Song, M. M.; Wang, Y. M.; Liang, X. Y.; Zhang, X. Q.; Zhang, S.; Li, B. J., Functional materials with self-healing properties: a review. *Soft Matter*. **2019**, 15, 6615-6625.
- [2] R, P. N.; A, P. D.; D, B. P.; Vikram, P.; Darshan, M., Microsphere as a novel drug delivery. *International Journal of Pharmacy & Life Sciences*. **2011**, 2, 992-997.
- [3] Lensen, D.; Vriezema, D. M.; van Hest, J. C., Polymeric microcapsules for synthetic applications. *Macromol. Biosci*. **2008**, 8, 991-1005.
- [4] Blaiszik, B. J.; Caruso, M. M.; McIlroy, D. A.; Moore, J. S.; White, S. R.; Sottos, N. R., Microcapsules filled with reactive solutions for self-healing materials. *Polymer*. **2009**, 50, 990-997.
- [5] Szabó, T.; Molnár-Nagy, L.; Bognár, J.; Nyikos, L.; Telegdi, J., Self-healing microcapsules and slow release microspheres in paints. *Prog. Org. Coat*. **2011**, 72, 52-57.
- [6] Sun, G.; Zhang, Z., Mechanical properties of melamine-formaldehyde microcapsules. *J Microencapsul*. **2001**, 18, 593-602.
- [7] Yuan, L.; Liang, G.-Z.; Xie, J.-Q.; Guo, J.; Li, L., Thermal stability of microencapsulated epoxy resins with poly(urea-formaldehyde). *Polymer Degradation and Stability*. **2006**, 91, 2300-2306.
- [8] Yuan, L.; Liang, G.-Z.; Xie, J.-Q.; Li, L.; Guo, J., The permeability and stability of microencapsulated epoxy resins. *Journal of Materials Science*. **2007**, 42, 4390-4397.
- [9] Yuan, L.; Liang, G.; Xie, J.; Li, L.; Guo, J., Preparation and characterization of poly(urea-formaldehyde) microcapsules filled with epoxy resins. *Polymer*. **2006**, 47, 5338-5349.
- [10] Liu, X.; Sheng, X.; Lee, J. K.; Kessler, M. R., Synthesis and Characterization of Melamine-Urea-Formaldehyde Microcapsules Containing ENB-Based Self-Healing Agents. *Macromolecular Materials and Engineering*. **2009**, 294, 389-395.
- [11] Gilford III, J.; Hassan, M. M.; Rupnow, T.; Barbato, M.; Okeil, A.; Asadi, S., Dicyclopentadiene and sodium silicate microencapsulation for self-healing of concrete. *J. Mater. Civ. Eng*. **2014**, 26, 886-896.
- [12] Naveen, V.; Raja, S.; Deshpande, A. P., A two-step approach for synthesis, characterization and analysis of dicyclopentadiene-urea formaldehyde-siloxane-based double-walled microcapsules used in self-healing composites. *International Journal of Plastics Technology*. **2019**, 23, 157-169.
- [13] Wang, R.; Hu, H.; He, X.; Liu, W.; Li, H.; Guo, Q.; Yuan, L., Synthesis and characterization of chitosan/urea - formaldehyde shell microcapsules containing dicyclopentadiene. *J. Appl. Polym. Sci*. **2011**, 121, 2202-2212.

- [14] Kessler, M.; Sottos, N.; White, S., Self-healing structural composite materials. *Composites Part A: applied science and manufacturing*. **2003**, *34*, 743-753.
- [15] Yin, T.; Rong, M.; Zhang, M.; Yang, G., Self-healing epoxy composites – Preparation and effect of the healant consisting of microencapsulated epoxy and latent curing agent. *Composites Science and Technology*. **2007**, *67*, 201-212.
- [16] Suryanarayana, C.; Rao, K. C.; Kumar, D., Preparation and characterization of microcapsules containing linseed oil and its use in self-healing coatings. *Prog. Org. Coat.* **2008**, *63*, 72-78.
- [17] Jadhav, R. S.; Hundiwale, D. G.; Mahulikar, P. P., Synthesis and characterization of phenol – formaldehyde microcapsules containing linseed oil and its use in epoxy for self-healing and anticorrosive coating. *J. Appl. Polym. Sci.* **2011**, *119*, 2911-2916.
- [18] Juita; Dlugogorski, B. Z.; Kennedy, E. M.; Mackie, J. C., Low temperature oxidation of linseed oil: a review. *Fire Science Reviews*. **2012**, *1*, 1-36.
- [19] Lazzari, M.; Chiantore, O., Drying and oxidative degradation of linseed oil. *Polymer Degradation and Stability*. **1999**, *65*, 303-313.
- [20] Liao, L.; Zhang, W.; Xin, Y.; Wang, H.; Zhao, Y.; Li, W., Preparation and characterization of microcapsule containing epoxy resin and its self-healing performance of anticorrosion covering material. *Chin. Sci. Bull.* **2011**, *56*, 439-443.
- [21] Dowbenko, R.; Anderson, C.; Chang, W.-H., Imidazole complexes as hardeners for epoxy adhesives. *Industrial & Engineering Chemistry Product Research and Development*. **1971**, *10*, 344-351.
- [22] Kaplan, M. L.; Wayda, A. L.; Lyons, A. M., Lanthanide–imidazole complexes as latent curing agents for epoxy resins. *Polymer Chemistry*. **1990**, *28*, 731-740.
- [23] Li, Q.; Kim, N. H.; Hui, D.; Lee, J. H., Effects of dual component microcapsules of resin and curing agent on the self-healing efficiency of epoxy. *Composites Part B: Engineering*. **2013**, *55*, 79-85.
- [24] Yi, H.; Deng, Y.; Wang, C., Pickering emulsion-based fabrication of epoxy and amine microcapsules for dual core self-healing coating. *Composites Science and Technology*. **2016**, *133*, 51-59.
- [25] Hu, H.; Zhang, L.; Yu, R.; Yuan, L.; Yang, Y.; He, X.; Wang, J.; Li, Z., Microencapsulation of ethylenediamine and its application in binary self-healing system using dual-microcapsule. *Materials & Design*. **2020**, *189*, 108535-108545.
- [26] Jin, H.; Mangun, C. L.; Stradley, D. S.; Moore, J. S.; Sottos, N. R.; White, S. R., Self-healing thermoset using encapsulated epoxy-amine healing chemistry. *Polymer*. **2012**, *53*, 581-587.
- [27] Silva, A. A.; Livi, S.; Netto, D. B.; Soares, B. G.; Duchet, J.; Gérard, J.-F., New epoxy systems based on ionic liquid. *Polymer*. **2013**, *54*, 2123-2129.
- [28] Sonnier, R.; Dumazert, L.; Livi, S.; Nguyen, T. K. L.; Duchet-Rumeau, J.; Vahabi, H.; Laheurte, P., Flame retardancy of phosphorus-containing ionic liquid based epoxy networks.

*Polymer Degradation and Stability*. **2016**, 134, 186-193.

[29] Nguyen, T. K. L.; Livi, S.; Soares, B. G.; Pruvost, S.; Duchet-Rumeau, J.; Gérard, J.-F., Ionic liquids: a new route for the design of epoxy networks. *ACS Sustainable Chemistry & Engineering*. **2015**, 4, 481-490.

[30] Saurín, N.; Sanes, J.; Bermúdez, M., Self-healing of abrasion damage in epoxy resin-ionic liquid nanocomposites. *Tribology Letters*. **2015**, 58, 1-9.

[31] Gledhill, R. A.; Kinloch, A. J., Relationship between mechanical properties of and crack propagation in epoxy resin adhesives. *Polymer*. **1978**, 19, 574-582.

[32] Chabane, H.; Livi, S.; Morelle, X. P.; Sonnier, R.; Loïc Dumazert; Duchet-Rumeau, J.; Gérard, J.-F., Synthesis of new ionic liquid-grafted metal-oxo nanoclusters – Design of nanostructured hybrid organic-inorganic polymer networks. *Polymer*. **2021**, 224, 123721-123731.

[33] Brown, E. N.; Kessler, M. R.; Sottos, N. R.; White, S. R., In situ poly (urea-formaldehyde) microencapsulation of dicyclopentadiene. *Journal of microencapsulation*. **2003**, 20, 719-730.

[34] Fan, C.; Tang, J.; Zhou, X., Role of ammonium chloride in preparing poly (urea - formaldehyde) microcapsules using one - step method. *J. Appl. Polym. Sci.* **2013**, 129, 2848-2856.

[35] Chuanjie, F.; Juntao, T.; Xiaodong, Z., Effects of process parameters on the physical properties of poly (urea-formaldehyde) microcapsules prepared by a one-step method. *Iranian polymer journal*. **2013**, 22, 665-675.

[36] Hussain, S. I.; Kalaiselvam, S., Nanoencapsulation of oleic acid phase change material with Ag<sub>2</sub>O nanoparticles-based urea formaldehyde shell for building thermal energy storage. *Journal of Thermal Analysis and Calorimetry*. **2019**, 140, 133-147.

[37] Li, Q.; Mishra, A. K.; Kim, N. H.; Kuila, T.; Lau, K.-t.; Lee, J. H., Effects of processing conditions of poly(methylmethacrylate) encapsulated liquid curing agent on the properties of self-healing composites. *Composites Part B: Engineering*. **2013**, 49, 6-15.

[38] Mao, J.; Yang, H.; Zhou, X., In situ polymerization of uniform poly(urea-formaldehyde) microcapsules containing paraffins under the high-speed agitation without emulsifier. *Polym. Bull.* **2012**, 69, 649-660.

[39] Li, G.; Feng, Y.; Gao, P.; Li, X., Preparation of mono-dispersed polyurea-urea formaldehyde double layered microcapsules. *Polym. Bull.* **2008**, 60, 725-731.

[40] Parsaee, S.; Mirabedini, S. M.; Farnood, R.; Alizadegan, F., Development of self - healing coatings based on urea - formaldehyde/polyurethane microcapsules containing epoxy resin. *J. Appl. Polym. Sci.* **2020**, 137, 49663-49677.

[41] Yuan, L.; Gu, A.; Liang, G., Preparation and properties of poly (urea-formaldehyde) microcapsules filled with epoxy resins. *Materials Chemistry and Physics*. **2008**, 110, 417-425.

[42] Chowdhury, R. A.; Hosur, M. V.; Nuruddin, M.; Tcherbi-Narteh, A.; Kumar, A.; Boddu, V.; Jeelani, S., Self-healing epoxy composites: preparation, characterization and healing

- performance. *Journal of Materials Research and Technology*. **2015**, 4, 33-43.
- [43]Camino, G.; Operti, L.; Trossarelli, L., Mechanism of thermal degradation of urea-formaldehyde polycondensates. *Polymer Degradation and Stability*. **1983**, 5, 161-172.
- [44]Chen, K.; Tian, C.; Liang, S.; Zhao, X.; Wang, X., Effect of stoichiometry on the thermal stability and flame retardation of polyisocyanurate foams modified with epoxy resin. *Polymer Degradation and Stability*. **2018**, 150, 105-113.
- [45]Tzavidi, S.; Zotiadis, C.; Porfyrus, A.; Korres, D. M.; Vouyiouka, S., Epoxy loaded poly(urea - formaldehyde) microcapsules via in situ polymerization designated for self - healing coatings. *J. Appl. Polym. Sci*. **2020**, 137, 49323-49333.
- [46]Maka, H.; Spsychaj, T.; Pilawka, R., Epoxy resin/ionic liquid systems: the influence of imidazolium cation size and anion type on reactivity and thermomechanical properties. *Industrial & Engineering Chemistry Research*. **2012**, 51, 5197-5206.
- [47]Soares, B. G.; Livi, S.; Duchet-Rumeau, J.; Gerard, J.-F., Synthesis and characterization of epoxy/MCDEA networks modified with imidazolium-based ionic liquids. *Macromolecular Materials and Engineering*. **2011**, 296, 826-834.
- [48]Canal, J. P.; Ramnial, T.; Dickie, D. A.; Clyburne, J. A., From the reactivity of N-heterocyclic carbenes to new chemistry in ionic liquids. *Chem Commun (Camb)*. **2006**, 1809-1818.
- [49]Guenther Soares, B.; Livi, S.; Duchet-Rumeau, J.; Gerard, J. F., Preparation of epoxy/MCDEA networks modified with ionic liquids. *Polymer*. **2012**, 53, 60-66.
- [50]Nguyen, T. K. L. New generation of epoxy networks based on ionic liquids: From structuration to final properties. PhD Thesis, Université de Lyon, 2016.
- [51]Leclère, M.; Livi, S.; Maréchal, M.; Picard, L.; Duchet-Rumeau, J., The properties of new epoxy networks swollen with ionic liquids. *RSC Advances*. **2016**, 6, 56193-56204.
- [52]Ehlers, J.-E.; Rondan, N. G.; Huynh, L. K.; Pham, H.; Marks, M.; Truong, T. N., Theoretical Study on Mechanisms of the Epoxy–Amine Curing Reaction. *Macromolecules*. **2007**, 40, 4370-4377.
- [53]Maka, H.; Spsychaj, T.; Pilawka, R., Epoxy resin/phosphonium ionic liquid/carbon nanofiller systems: Chemorheology and properties. *Express Polymer Letters*. **2014**, 8, 723-732.
- [54]Shi, Y.-Q.; Fu, T.; Xu, Y.-J.; Li, D.-F.; Wang, X.-L.; Wang, Y.-Z., Novel phosphorus-containing halogen-free ionic liquid toward fire safety epoxy resin with well-balanced comprehensive performance. *Chem. Eng. J*. **2018**, 354, 208-219.
- [55]Soares, B. G.; Silva, A. A.; Pereira, J.; Livi, S., Preparation of epoxy/jeffamine networks modified with phosphonium based ionic liquids. *Macromolecular Materials and Engineering*. **2015**, 300, 312-319.
- [56]Fonseca, E.; Demétrio da Silva, V.; Klitzke, J. S.; Schrekker, H. S.; Amico, S. C., Imidazolium ionic liquids as fracture toughening agents in DGEBA-TETA epoxy resin. *Polym. Test*. **2020**, 87, 106556-106565.
- [57]Katouezadeh, E.; Zebarjad, S. M.; Janghorban, K., Mechanical properties of epoxy

- composites embedded with functionalized urea-formaldehyde microcapsules containing an oxidizable oil. *Materials Chemistry and Physics*. **2021**, 260, 124106-124117.
- [58]Blaiszik, B. J.; Sottos, N. R.; White, S. R., Nanocapsules for self-healing materials. *Composites Science and Technology*. **2008**, 68, 978-986.
- [59]Yuan, Y. C.; Rong, M. Z.; Zhang, M. Q.; Chen, J.; Yang, G. C.; Li, X. M., Self-healing polymeric materials using epoxy mercaptan as the healant. *Macromolecules*. **2008**, 41, 5197-5202.
- [60]Ahangaran, F.; Hayaty, M.; Navarchian, A. H.; Pei, Y.; Picchioni, F., Development of self-healing epoxy composites via incorporation of microencapsulated epoxy and mercaptan in poly(methyl methacrylate) shell. *Polym. Test*. **2019**, 73, 395-403.
- [61]Lee, J.; Zhang, M.; Bhattacharyya, D.; Yuan, Y. C.; Jayaraman, K.; Mai, Y. W., Micromechanical behavior of self-healing epoxy and hardener-loaded microcapsules by nanoindentation. *Materials Letters*. **2012**, 76, 62-65.
- [62]Keller, M. W.; Sottos, N. R., Mechanical Properties of Microcapsules Used in a Self-Healing Polymer. *Experimental Mechanics*. **2006**, 46, 725-733.
- [63]Tripathi, M.; Rahamtullah; Kumar, D.; Rajagopal, C.; Kumar Roy, P., Influence of microcapsule shell material on the mechanical behavior of epoxy composites for self-healing applications. *J. Appl. Polym. Sci*. **2014**, 131, 40572-40580.
- [64]Pearson, R. A.; FYee, A., Toughening mechanisms in thermoplastic-modified epoxies. *Polymer*. **1993**, 34, 3658-3670.
- [65]Rubinstein, A. A., Mechanics of the crack path formation. *International Journal of Fracture* **1991**, 47, 291-305.
- [66]Brown, E. N.; White, S. E.; Sottos, N. R., Microcapsule induced toughening in a self-healing polymer composite. *Journal of Materials Science*. **2004**, 39, 1703-1710.

## Supporting Information of Chapter 3

### 1. FTIR spectra of emitted gas from PUF@EP microcapsules during thermal degradation under N<sub>2</sub> atmosphere (10 K·min<sup>-1</sup>)

#### (1) EP@PUF microcapsules

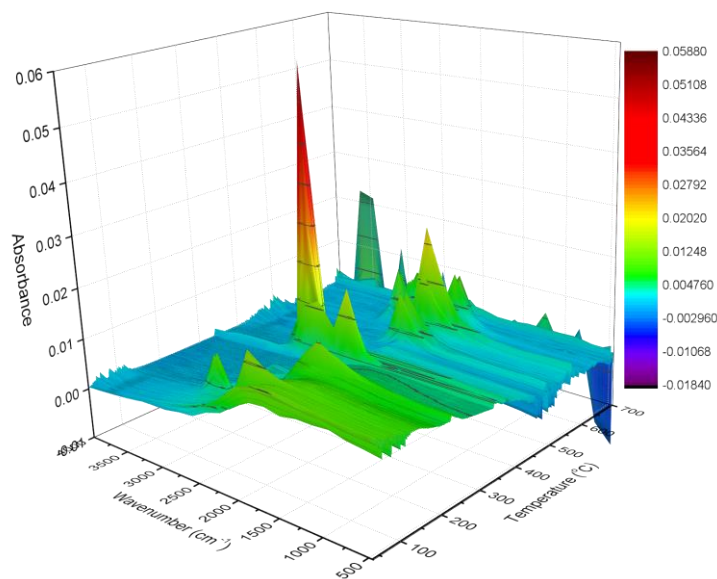


**Figure S3-1** FTIR spectra of emitted gas during degradation of EP@PUF microcapsules under N<sub>2</sub> atmosphere

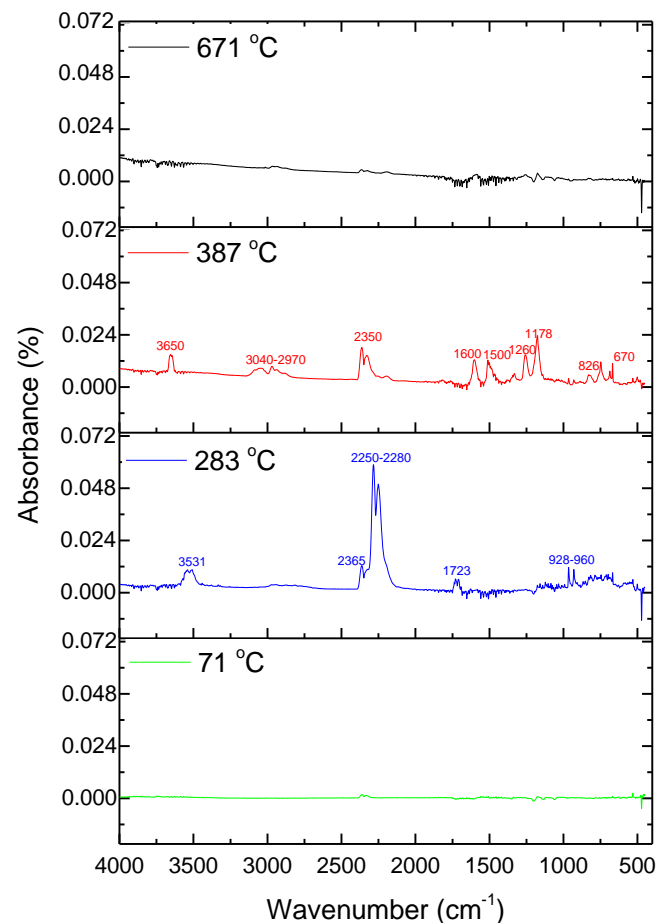


**Figure S3-2** FTIR spectra of emitted gas at different temperatures EP@PUF microcapsules under N<sub>2</sub> atmosphere

(2) core material: DGEBA+BGE

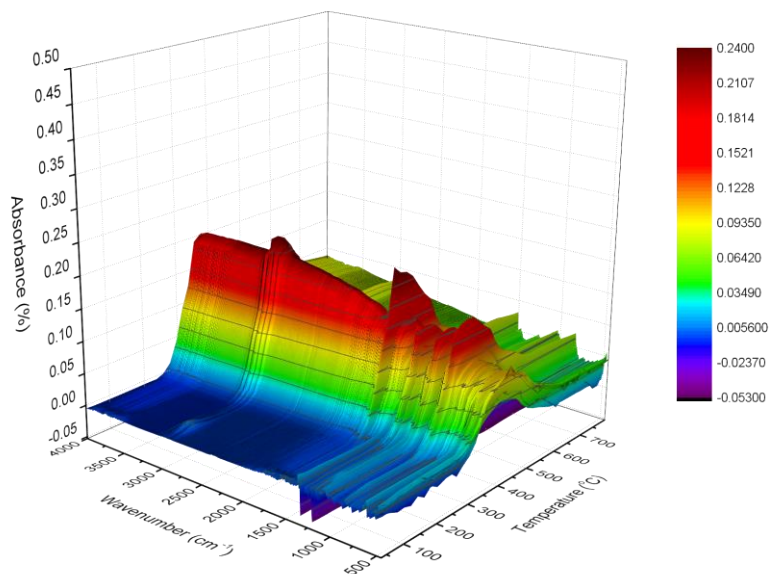


**Figure S3-3** FTIR spectra of emitted gas during degradation of DGEBA+BGE under N<sub>2</sub> atmosphere

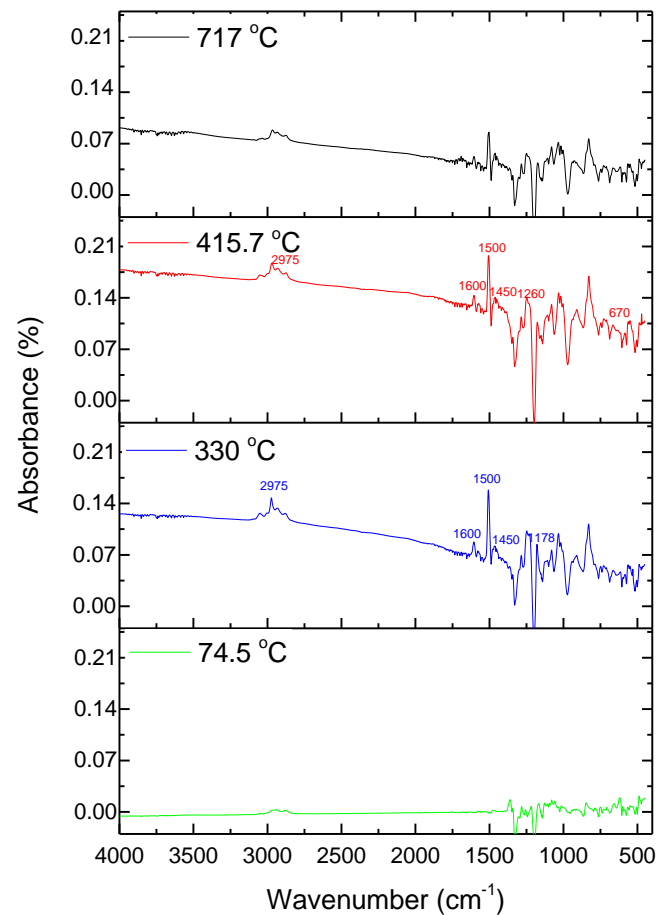


**Figure S3-4** FTIR spectra of emitted gas at different temperatures DGEBA+BGE under N<sub>2</sub> atmosphere



(2) shell material: neat PUF

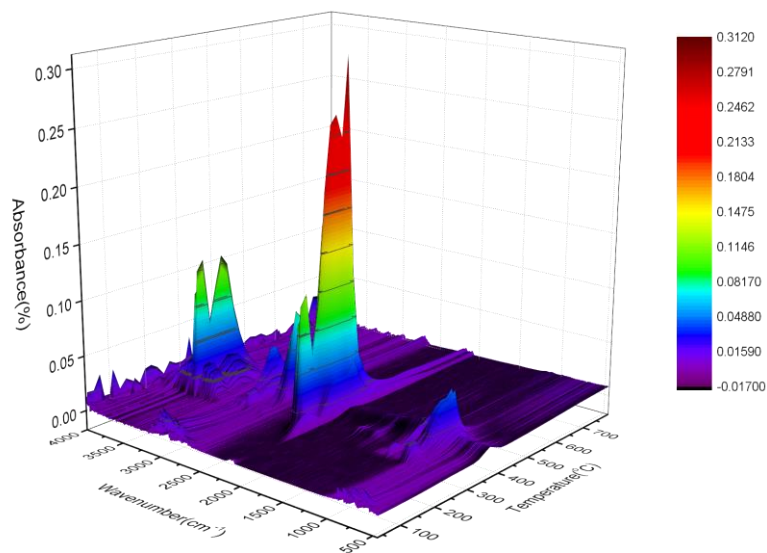


Figure S3-5 FTIR spectra of emitted gas during degradation of neat PUF under N<sub>2</sub> atmosphere

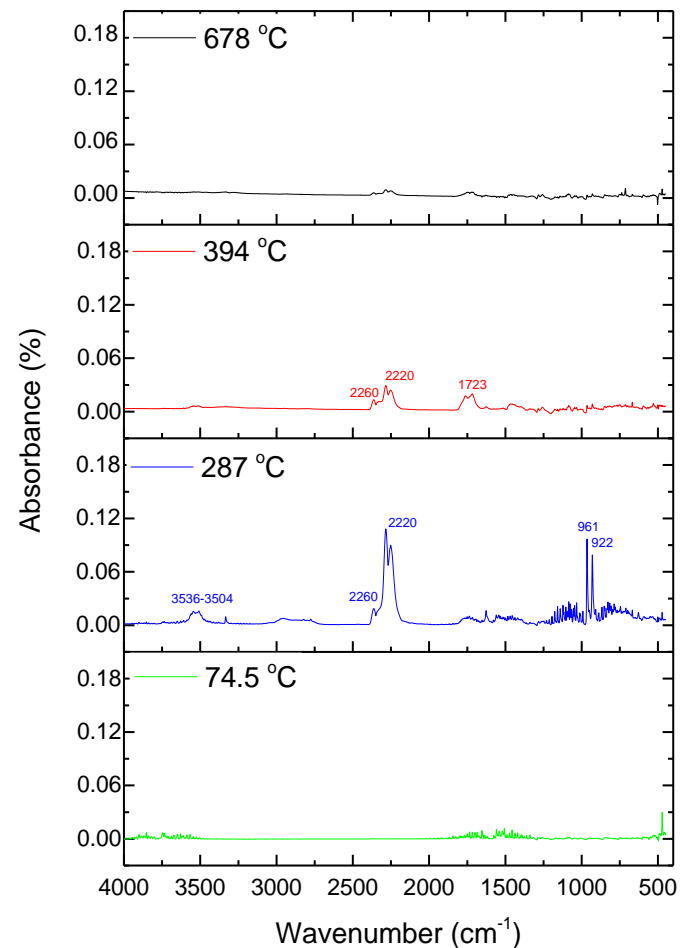
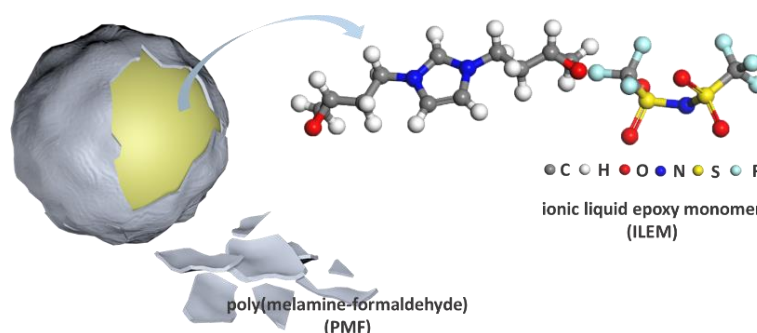


Figure S3-6 FTIR spectra of emitted gas at different temperatures neat PUF under N<sub>2</sub> atmosphere

## Chapter 4:

# Encapsulation of ionic liquid epoxy monomer and their self-healing application in epoxy-amine networks

Introduction of microcapsules for achieving self-healing is a convenient and promising strategy for polymer materials as reported in Chapter 3. Nevertheless, the previously described route requires the presence of an initiator for healing agent. Therefore, an ionic liquid epoxy monomer (ILEM) with self-curing ability was encapsulated in poly(melamine-formaldehyde) microcapsules as a healing agent. However, few studies have been done about the encapsulation using this route and its application as a self-healing additive in polymer composites. Therefore, this chapter focuses on the synthesis and characterization of ILEM containing poly(melamine-formaldehyde) (PMF) microcapsules (ILEM@PMF) and the properties of final epoxy composites cured with different amines. Three sections are included in this chapter: *i*) Synthesis and characterization of ILEM and ILEM@PMF microcapsules; *ii*) Influence of synthesis parameters on the morphology and size distribution of ILEM@PMF microcapsules; *iii*) Investigation of final properties of ILEM@PMF microcapsules filled epoxy-amine composites cured with different amines as the hardener.



## Table of contents

<b>4.1 Introduction .....</b>	<b>194</b>
<b>4.2 Experimental.....</b>	<b>195</b>
4.2.1 Materials.....	195
4.2.2 Characterization.....	197
<b>4.3 Synthesis and characterization of ILEM@PMF microcapsules .....</b>	<b>200</b>
4.3.1 Synthesis of ILEM.....	200
4.3.2 Synthesis of ILEM@PMF microcapsules .....	201
4.3.3 Characterization of ILEM@PMF microcapsules .....	202
4.3.3.1 Selection of the best surfactant to obtain ILEM/H <sub>2</sub> O emulsion .....	202
4.3.3.2 Monitoring ILEM@PMF microcapsules synthesis .....	203
4.3.3.3 Influence of synthesis parameters on the morphology and size distribution of ILEM@PMF microcapsules .....	205
4.3.3.4 Chemical structure of ILEM@PMF microcapsules .....	210
4.3.3.5 Thermal behavior and stability of ILEM@PMF microcapsules.....	211
<b>4.4 Preparation and characterization of ILEM@PMF microcapsule-filled epoxy-amine materials.....</b>	<b>214</b>
4.4.1 Material Processing .....	215
4.4.2 Results and discussion.....	215
4.4.2.1 Local temperature of different epoxy-amine networks.....	215
4.4.2.2 Morphology of ILEM@PMF microcapsule-filled epoxy-amine materials .....	216
4.4.2.3 Thermal properties of ILEM@PMF microcapsule-filled epoxy-amine materials.....	218
4.4.2.4 Dynamic mechanical properties of ILEM@PMF microcapsule-filled epoxy-amine materials .....	219
4.4.2.5 Self-healing property of ILEM@PMF microcapsule-filled epoxy-amine materials .....	220
4.4.2.6 Mechanical properties of ILEM@PMF microcapsule-filled epoxy-amine materials.....	222

<b>4.5 Conclusion.....</b>	<b>223</b>
<b>References of Chapter 4.....</b>	<b>224</b>
<b>Supporting Information of Chapter 4 .....</b>	<b>229</b>

## 4.1 Introduction

Microcapsules can facilitate the delivery of encapsulated components which is the main strategy of the extrinsic self-healing mechanism [1]. Self-healing happens as the healing agent is released by breaking microcapsules and further polymerization under given stimuli including initiator, reaction with a hardener and temperature [2]. These stimuli for polymerization of the healing agent depend of course on the nature of the encapsulated healing agent.

Several reactive components were encapsulated as microcapsules for self-healing applications, such as dicyclopentadiene (DCPD) [3], methylmethacrylate acrylate (MMA), and epoxy monomer [4, 5], etc. According to the nature of the healing agents, various strategies were considered for the polymerization : Grubbs' catalyst for DCPD [6], triethylborane (TEB) for MMA [7], heat oxidation for linseed oil [8], etc. However, several problems remain when extra hardeners or initiators were used. For example, the reactivity of Grubbs' catalyst may be influenced by the presence of reactants, such as amines [9] and a poor dispersion of the catalyst may lead to a poorer healing efficiency [10]. A color change was observed in epoxy-amine network embedded with Grubbs' catalyst indicating a partial or complete dissolution of Grubbs' catalyst during curing processing, which may also affect self-healing efficiency [11]. Ionic liquid is considered as initiator for the healing agent, *i.e.* epoxy monomer, but can behave as plasticizer of the epoxy matrix as shown in Chapter 3. Besides, highly reactive compounds such as amines [12] are considered to react with the healing agent, but the protection of reactive components requires an additional synthesis step. Therefore, a more efficient healing agent and single type microcapsule self-healing system may help to expand the field of self-healing materials and avoid these limitations.

Recently, ionic liquid monomers (ILM) have attracted the huge attention of researchers to design new multifunctional polymer materials with promising properties [13-15]. Such ILM can be polymerized for designing new multifunctional polymers for various applications, such as gas sorption [16, 17], polymer electrolytes [18, 19], antibacterial membranes [20, 21] and self-healable materials [22]. Ionic liquid epoxy monomers (ILEM) can be polymerized to prepare high performance materials. For example, Livi *et al* [23] have designed a facile and robust way to design polyfunctional imidazolium monomers bearing an aromatic ring and two epoxy functions. These compounds can be cured with an amine to build epoxy networks with enhanced thermal property, mechanical property and ionic conductivity. Similarly, Radchenko *et al* [24] have synthesized a bisimidazolium-based ILEM for development shape memory materials. The

authors also reported that imidazolium-based ILEM was able to undergo self-curing from the thermally latent cationic initiation of imidazolium fragments [25] or the extractable proton [26]. By changing the structure of cations and counteranions in the imidazolium-based ILEM, thermal stability as well as their polymerization temperature can be tailored [15]. Therefore, ILEM could be applied for self-healing considering a single microcapsule system, *i.e.* without any extra catalyst/initiator in the polymer matrix. To our knowledge, no work has been carried out in this area.

For shell material of the microcapsules, different compounds can be considered : silica [27], polymethyl methacrylate (PMMA) [28], polysaccharides [29], polysulfone [30, 31], and amino polymers including poly (urea-formaldehyde) (PUF) or poly (melamine-formaldehyde) (PMF). However, PUF and PMF polymers are the most widely used as shell material for self-healing applications because of the good mechanical strength required for processing and breakability required at the self-healing step. Compared with urea in PUF, melamine in PMF displays a higher functionality and shows a higher reactivity, leading to a shorter time for PMF shell microcapsules synthesis [32]. The higher stiffness and brittleness of PMF shell compared to PUF [33] can guarantee a higher healing efficiency.

Therefore, this chapter focuses on the synthesis of an epoxy-functionalized imidazolium ionic liquid monomer, its encapsulation in a PMF shell to obtain ILEM containing microcapsules (ILEM@PMF), and their application in epoxy-amine materials. The first attempt was to encapsulate ILEM in polymer shell microcapsules via *in-situ* polymerization. Thus, suitable surfactants for stabilizing ILEM droplets in aqueous emulsions were researched. The influence of synthesis parameters on the morphology and size distribution of ILEM@PMF microcapsules were investigated. The chemical structure and thermal properties of ILEM@PMF microcapsules were also characterized. ILEM@PMF microcapsules were then added in different epoxy-amine networks to study their self-healing performance in different thermoset polymer composites. This work tried for the first time to design ILEM containing microcapsules as a single microcapsule system, to achieve self-healing purposes epoxy networks. Therefore, our study proposes a strategy for reaching self-healing and avoiding the use of a hardener or an initiator in the matrix.

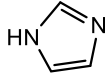
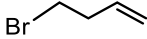
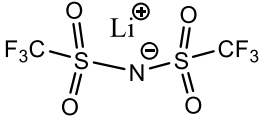
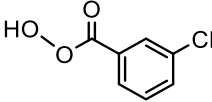
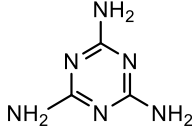
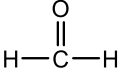
## 4.2 Experimental

### 4.2.1 Materials

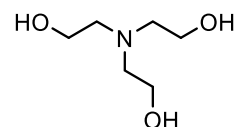
Imidazole, sodium hydride (NaH, 60 % dispersion in mineral oil), 4-bromo-1-butene, lithium bis(trifluoromethanesulfonyl)imide ( $\text{Li}^+\text{NTf}_2^-$ ), meta-chloroperoxybenzoic acid

(mCPBA), melamine (M), formaldehyde solution (F, 37 wt. % in H<sub>2</sub>O, contains 10-15% methanol as stabilizer), triethanolamine (TEA), sodium dodecylbenzenesulfonate (SDBS), poly(vinyl alcohol) (PVA, M<sub>w</sub> 13,000-23,000, 87-89% hydrolyzed), epoxy resin, *i.e.* bisphenol A diglycidyl ether (DEGBA, D.E.R. 332), 4,4'-methylenebis(cyclohexylamine) (PACM), and triethylenetetramine (TETA) were purchased from Sigma-Aldrich and used as received. Epikure 3223 curing agent, containing mainly diethylenetriamine (DETA) was purchased from Silmid Co. Anhydrous solvents including acetonitrile (CH<sub>3</sub>CN), tetrahydrofuran (THF), and acetone (CH<sub>3</sub>COCH<sub>3</sub>) were obtained using a PURESOLV SPS400 apparatus developed by InnovativeTechnology Inc. The chemical structures of all the materials are shown in Table 4-1.

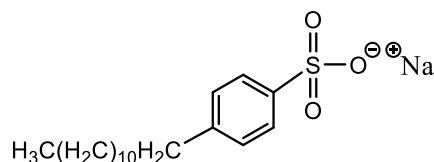
**Table 4-1** Chemical structures of the products used

Materials and abbreviations	Chemical structures
Imidazole	
4-bromo-1-butene	
lithium bis(trifluoromethanesulfonyl)imide (Li <sup>+</sup> NTf <sub>2</sub> <sup>-</sup> )	
meta-chloroperoxybenzoic acid (mCPBA)	
Melamine (M)	
formaldehyde solution (F, 7 wt. % in H <sub>2</sub> O)	

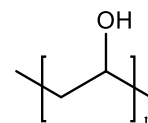
triethanolamine  
(TEA)



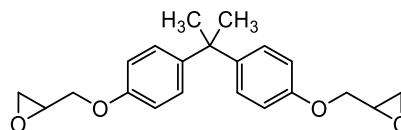
sodium dodecylbenzenesulfonate (SDBS)



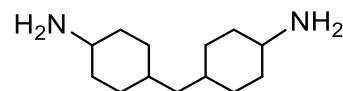
poly(vinyl alcohol)  
(PVA,  $M_w$  13,000-23,000, 87-89% hydrolyzed)



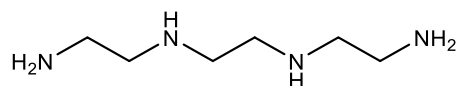
bisphenol A diglycidyl ether  
(DEGBA, D.E.R. 332)



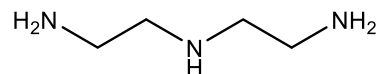
4,4'-methylenebis(cyclohexylamine) (PACM)



Triethylenetetramine (TETA)



Epikure 3223 (diethylenetriamine, DETA)



---

## 4.2.2 Characterization

$^1\text{H}$  and  $^{19}\text{F}$  NMR spectra were recorded using a Bruker Avance III 400 MHz at 298K. Samples were dissolved in deuterated chloroform ( $\text{CDCl}_3$ ), methanol (MeOD) or acetonitrile ( $\text{CD}_3\text{CN}$ ). The chemical shifts ( $\delta$ ) are expressed in ppm relative to the internal reference tetramethylsilane for  $^1\text{H}$  and  $^{19}\text{F}$  nuclei, and coupling constants are indicated in Hz. Abbreviations for signal coupling are as follows: s=singlet; d=doublet; dd=doublet of doublets; t=triplet; m=multiplet.



Thermogravimetric analysis coupled with infrared spectrometry (TGA-IR) was performed using TGA 8000 machine from PerkinElmer and the evolved gas analysis was performed by interfacing a Fourier transform infrared spectrometer (FTIR, Nicolet 6700 spectrophotometer) to the exit part of the TGA furnace. Analyses were carried out under N<sub>2</sub> atmosphere at a heating rate of 10 K·min<sup>-1</sup> to 800 °C. Over 10.0 mg of the sample was put in an alumina crucible and heated from 35 to 700 °C at a heating rate of 10 K·min<sup>-1</sup> K under N<sub>2</sub> atmosphere. Infrared spectra in the optical range of 400 - 4000 cm<sup>-1</sup> were recorded every 4 s.

Monitoring the *in-situ* polymerization by optical microscopy was carried out on an Axio Imager A2M type optical microscope from Zeiss Co.

Differential Scanning Calorimetry (DSC) measurements were carried out by using Q10 TA instrument at a heating rate of 10 K·min<sup>-1</sup> under N<sub>2</sub> flow of 50 mL·min<sup>-1</sup>.

Q500 Thermogravimetric analyzer from TA Instruments was used for thermogravimetric analysis. The characterization was performed at a heating rate of 20 K·min<sup>-1</sup> under a N<sub>2</sub> atmosphere.

Morphology characterization was carried out by TESCAN VEGA3 type SEM from Tescan Analytcs. All the specimens were coated with gold by a sputter coater to prevent charge accumulation on the surface. The sputter coating process was performed at a current of 30 mA for 90 s.

Self-healing was characterized from the observation of the healing of a scratch notch on the polymer surface. Cured epoxy film with a thickness about 100 - 150 µm was notched by a razor blade. Then the notched film was placed in an oven to conduct self-healing protocol ( 4 h at 100 °C followed by 4 h at 200 °C). The samples before and after the self-healing protocol were observed by SEM.

The local temperature of samples during the curing process was measured by YC 747 UD type data logger thermometer from TCSA company. Epoxy and hardener were mixed and poured into an aluminum vessel and the thermocouple was placed and fixed inside the mixture. The temperature was recorded during the curing process (Figure 4-1).

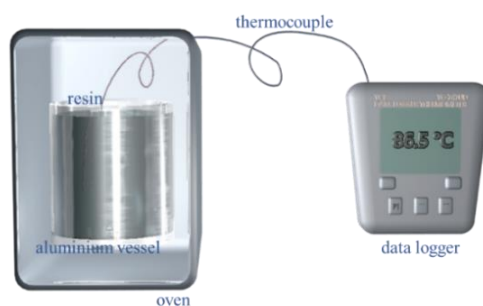


**Figure 4-1** Local temperature recording of the sample during curing

Dynamic mechanical analysis (DMA) was carried out using an ARES-G2 from TA Instruments. The analyses were carried out for 0.01% dynamic strain at a frequency of 1 Hz and a heating rate of 3 K min<sup>-1</sup> from 35 to 250 °C. The characterizations were performed twice for the same material under the same conditions.

Compression tests were carried out using a MTS machine operating with a 5 kN load cell. The samples geometry was based on ISO 604:2002 standard *i.e.* 5\*5\*16 mm<sup>3</sup>. The Young's modulus ( $E$ ) was determined from  $\sigma$  (stress) vs.  $\varepsilon$  (strain) curves in the linear region.

Mode I stress intensity factor ( $K_{IC}$ ) of epoxy-amine networks and related microcomposites were determined on compact tension specimens according to the ISO 13586:2018(E) standards (Figure 4-2). The notch was formed using a milling cutter and the initial crack also known as natural crack was made by tapping a fine razor blade into the notch. The length of initial crack to width ratio ( $\alpha/w$ ) has to keep between 0.2 and 0.8. The fracture toughness test was carried out using a MTS tensile machine equipped with a 1 kN load cell operating at tensile speed at 10 mm·min<sup>-1</sup>.  $K_{IC}$  was calculated according to equation 4-1:

$$K_{IC} = f(\alpha/w) \frac{F_Q}{h\sqrt{w}} \text{ (equation 4-1)}$$

where  $\alpha$  (m) is the length of initial crack,  $w$  (m) and  $h$  (m) are the width and thickness of specimen, respectively.  $F_Q$  (N) is the final load at the first crack. The  $f(\alpha/w)$  value is a geometrical factor which can be calculated using equation 4-2:

$$f(\alpha/w) = \frac{(2+\alpha)}{(1-\alpha)^{3/2}} \times (0.886 + 4.64\alpha - 13.32\alpha^2 + 14.72\alpha^3 - 5.64\alpha^4) \text{ (equation 4-2)}$$

The critical energy release ( $G_{IC}$ ) can be calculated from equation 4-3 and the value of  $K_{IC}$ , Young's modulus ( $E$ ), and Poisson's coefficient ( $\nu$ ). 0.35 for  $\nu$  were considered according to the values related in the literature for epoxy networks [34, 35].

$$G_{IC} = \frac{(1-\nu^2) \cdot K_{IC}^2}{E} \text{ (equation 4-3)}$$

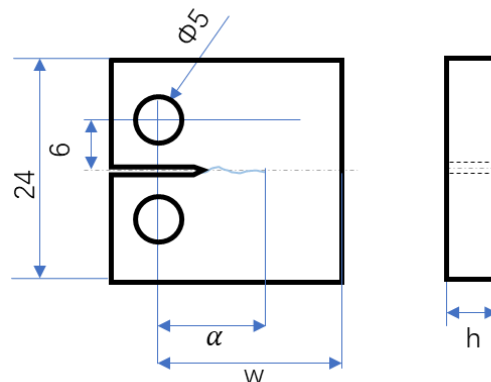


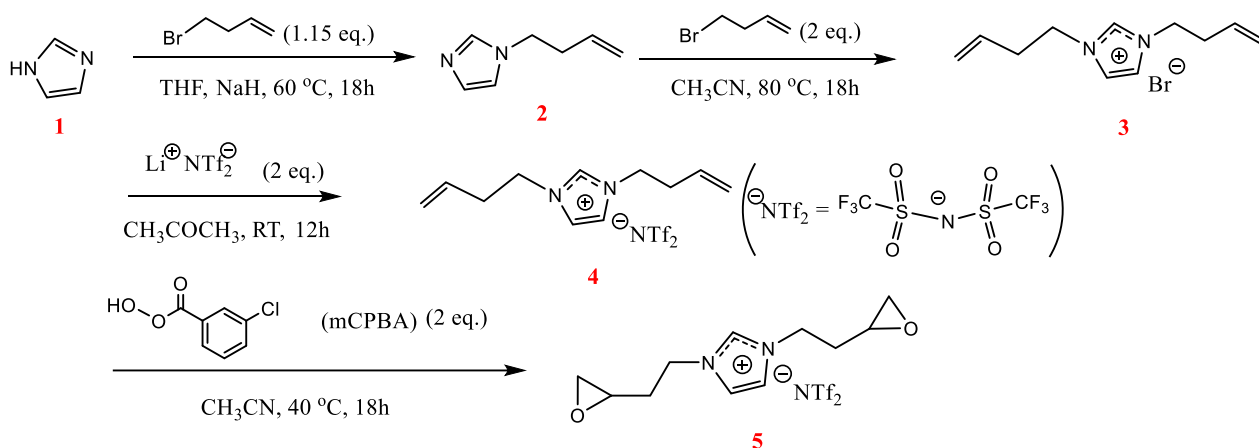
**Figure 4-2** Compact Tension (CT) test specimen geometry

### 4.3 Synthesis and characterization of ILEM@PMF microcapsules

#### 4.3.1 Synthesis of ILEM

The synthesis of imidazolium ionic liquid monomer (ILEM) with two epoxy groups was described by Scheme 4-1. The imidazolium ionic liquid epoxy monomer **5** (ILEM) was synthesized by four steps from imidazole. First, 1,4-dibromobutane (1.15 equiv) was added to imidazole **1** to form compound **2**. Then, 2.0 equivalent of 1,4-dibromobutane was reacted with **2** to obtain **3**. After an anionic exchange of bromide with NTf<sub>2</sub><sup>-</sup> by using Li<sup>+</sup>NTf<sub>2</sub><sup>-</sup> salt in order to obtain the corresponding imidazolium salt **4** with 98% of yield. Finally, the diepoxide **5** was obtained quantitatively by the Prilezhaev reaction with mCPBA (2 equiv) in CH<sub>3</sub>CN at 40 °C for 18h.

ILEM was characterized by NMR (see Figure S4-1 – Figure S4-5 in the supporting information of Chapter 4): <sup>1</sup>H NMR (400 MHz, Chloroform-d) δ 8.93 (s, 1H), 7.36 (d, J = 0.8 Hz, 2H), 4.40 (t, J = 6.7 Hz, 4H), 3.01 (m, 2H), 2.79 (dd, 2H), 2.52 (dd, 2H), 2.47 – 2.34 (dd, 2H), 1.85 (dd, 2H). <sup>19</sup>F NMR (376 MHz, Acetonitrile-d<sub>3</sub>) δ -80.11.



**Scheme 4-1** Synthesis of the imidazolium ionic liquid epoxy monomer (ILEM)

The thermal behavior of ILEM was characterized by DSC and TGA. The characteristic temperatures were obtained and are summarized in Table 4-2. A homo-polymerization can be evidenced from an onset temperature ( $T_{p \text{ onset}}$ ) close to 227 °C (see Figure S4-6). Since the imidazolium fragment can act as a thermally latent cationic initiator<sup>[25]</sup>, ILEM may be a good candidate as a self-healing agent as its curing temperature is higher than that of the reactive systems used for matrices. As shown in Table 4-2, the  $T_{d \text{ onset}}$  (temperature at 5 wt% weight loss) of ILEM was close to 290 °C. Moreover, two steps degradation of ILEM was observed with maxima on DTG curves (see Figure S4-7), corresponding to the two maximum degradation

temperatures in Table 4-2 ( $T_{d\ max1} = 320\ ^\circ\text{C}$  and  $T_{d\ max2} = 456\ ^\circ\text{C}$ ). Thus, ILEM shows a good thermal stability which is favorable for *in-situ* microencapsulation process and self-healing application.

**Table 4-2** Thermal properties of ILEM

Characterizations	Characteristic Temperatures ( $^\circ\text{C}$ )
DSC	$T_{p\ onset} = 227$
TGA	$T_{d\ onset} = 290$ $T_{d\ max1} = 320; T_{d\ max2} = 456$

### 4.3.2 Synthesis of ILEM@PMF microcapsules

As described in Chapter 3, the synthesis of poly(melamine-formaldehyde) (PMF) shell microcapsules (ILEM@PMF) containing ILEM via *in-situ* polymerization was similar to the EP@PUF microcapsules. Thus, the procedure is summarized in Figure 4-3. The synthesis is composed of three steps: *i*) preparation of melamine (M) and formaldehyde solution (F) prepolymer, *ii*) preparation of ILEM in water solution (ILEM/H<sub>2</sub>O) solution, and *iii*) *in-situ* polymerization and encapsulation.

First, 0.7 g of M and 2.1 g of F solution were added in a flask and with a mass ratio of  $m_{(M)}:m_{(F)}=1:3$ , and 2.1 g of water was also added in order to lower the concentration of MF prepolymer in the aqueous solution. Then, 10 wt% of triethanolamine (TEA) aqueous solution was added dropwise in the previous solution until the pH value was around 9. The mixture was kept at 70  $^\circ\text{C}$  under magnetic stirring for 1 h. After reaction, a transparent MF prepolymer solution was obtained. The ILEM/H<sub>2</sub>O emulsion was prepared by adding different amounts of ILEM in the aqueous solution with surfactants and mechanically stirred at a given speed according to Table 4-3. Finally, transparent MF prepolymer was added in the ILEM/H<sub>2</sub>O emulsion, 2 wt% of sulfuric acid aqueous solution was used to tune pH around 4 for starting the *in-situ* polymerization. Once the reaction was completed, the mixture was cooled down to room temperature and the white precipitate was filtrated and washed three times with deionized water and acetone to remove the unencapsulated ILEM. In a last step, the microcapsules were dried in an oven. The neat ILEM and ILEM@PMF microcapsules were shown in Figure 4-4.

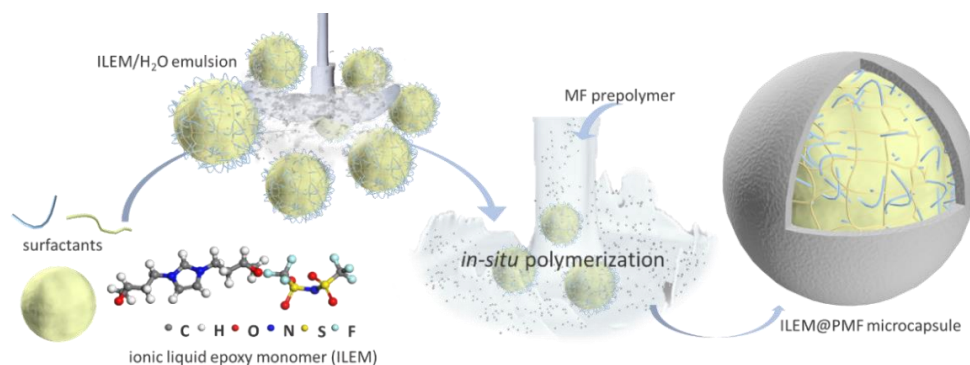


**Figure 4-3** Synthesis route of ILEM@PMF microcapsules via *in-situ* polymerization



**Figure 4-4** ILEM (left) and ILEM@PMF microcapsules (right)

### 4.3.3 Characterization of ILEM@PMF microcapsules

#### 4.3.3.1 Selection of the best surfactant to obtain ILEM/H<sub>2</sub>O emulsion

For *in-situ* polymerization, stable droplets and good dispersion of the core material are key parameters [36,37]. Thus, surfactants including ionic, polymeric, and a combination of both types were tried to obtain stable ILEM droplets in water emulsion (ILEM/H<sub>2</sub>O). Thus, different surfactants were first dissolved in deionized water (1 wt%) to form a transparent aqueous solution. ILEM was added to each aqueous solution and stirred mechanically at 300 rpm. After 1h, a sample was taken from each emulsion and observed by optical microscope (OM). Figure 4-5 shows the OM images of ILEM/H<sub>2</sub>O emulsions stabilized by different types of surfactants.

As can be seen in Figure 4-5, a mixture of surfactants SDBS and PVA with weight ratio 9:1 is a good compromise to stabilize ILEM droplets in an aqueous solution. In fact, a stable emulsion with spherical droplets having a diameter from 8 to 15  $\mu\text{m}$  was observed. However, demulsification and coacervation of ILEM can be observed over time (Figure 4-5 (a) (c) and (d)). These observations can be explained by the numerous adsorption sites of the PVA - molecule chains at the oil-water interface. On the opposite, SDBS can increase the electrostatic repulsions between ILEM oil droplets in water [38]. In addition, if only PVA is considered to stabilize the ILEM droplets, at low concentrations, it is difficult to obtain a stable emulsion. In

addition, at high concentration, the viscosity increases due to the high molar mass of the PVA. Such a high viscosity is not favorable for the deposition of shell material on the surface of ILEM droplets to obtain a spherical shape of microcapsules [39]. Consequently, a combination of SDBS and PVA was considered to obtain a stable ILEM/H<sub>2</sub>O emulsion.

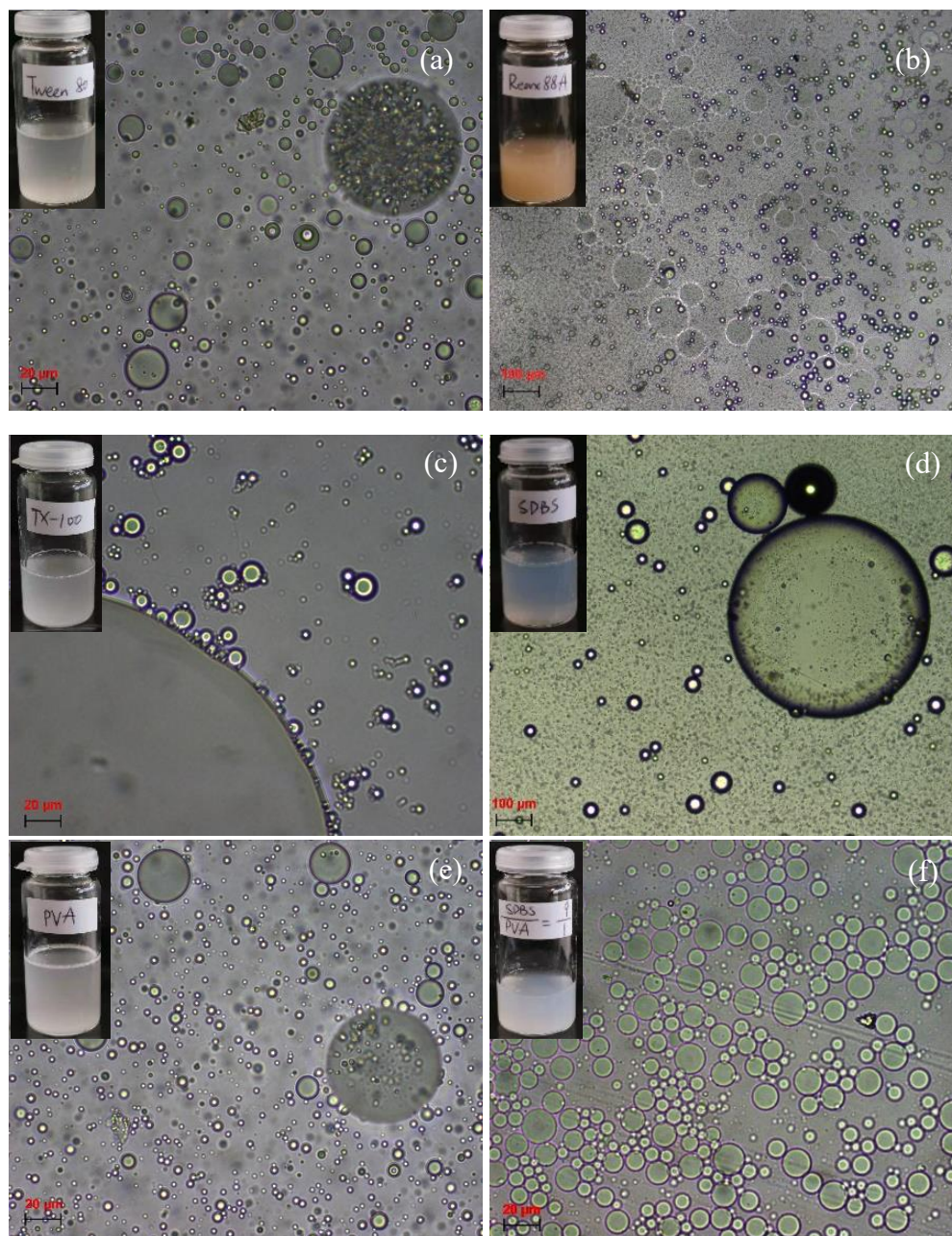


**Figure 4-5** Optical microscope images of ILEM/H<sub>2</sub>O emulsion stabilized by (a) Tween 80; (b) Reax 88A; (c) TX-100; (d) SDBS; (e) PVA; (f) SDBS:PVA=9:1 (surfactant concentration: 1wt%)

#### 4.3.3.2 Monitoring ILEM@PMF microcapsules synthesis

The *in-situ* polymerization and the formation of ILEM@PMF microcapsules were also

monitored by OM. A drop of liquid was taken from the reaction system at different times and observed by OM (Figure 4-6). The reaction mechanism of PMF is described in Scheme 4-2.

First of all, Figure 4-6 (a) shows that the ILEM droplets are stabilized in the aqueous phase by the combination of SDBS and PVA and form a stable and homogeneous emulsion. After adding the MF prepolymer, acid was added to change the basic medium to acidic one to initiate the condensation reaction of MF prepolymer, as described in Scheme 4-2 (b). The morphology before adding MF prepolymer is the one reported in Figure 4-6 (a) ( $t = 0$  min). As the pH was tuned to 4-5, the MF nanoparticles started to form in the emulsion and to migrate to the surface of the ILEM droplets. Therefore, the mixture (Figure 4-6 (b)) appeared cloudy at 120 min due to the increase of MF polymer molar mass and the generation of PUF nanoparticles in the suspension. Then, the reaction system was kept in acidic conditions for a given temperature. Along reaction time, the PMF nanoparticles are deposited continuously on the surface of ILEM droplets to form the PMF shell. ILEM@PMF microcapsules were observed at 180 min (Figure 4-6 (c), (d)).

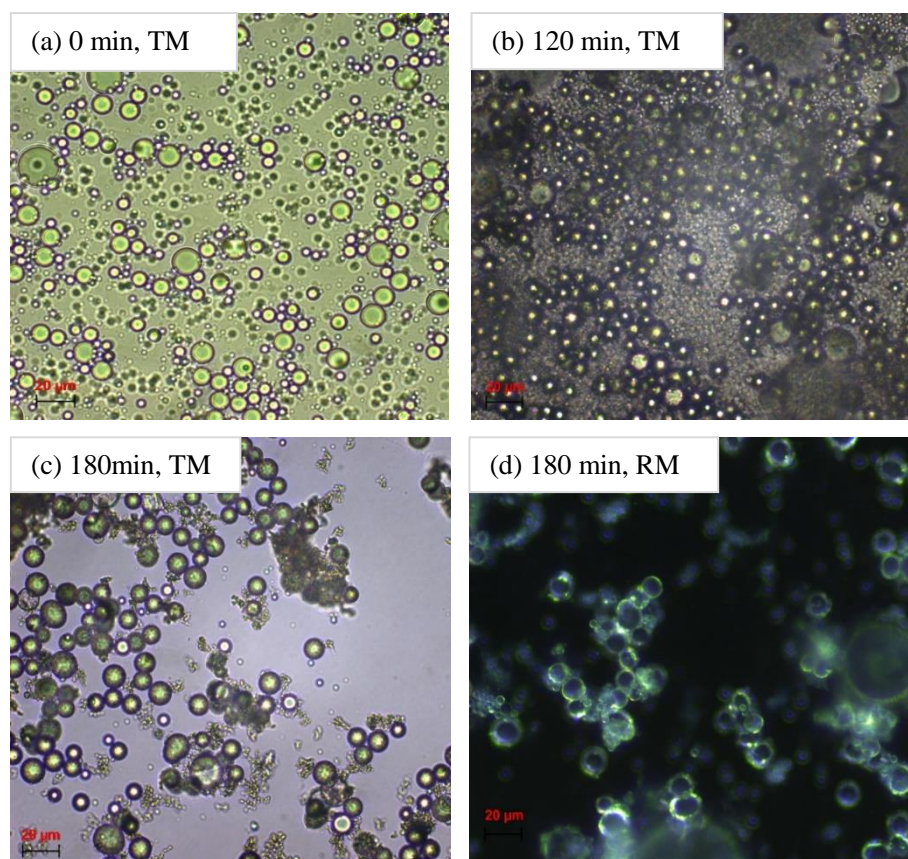
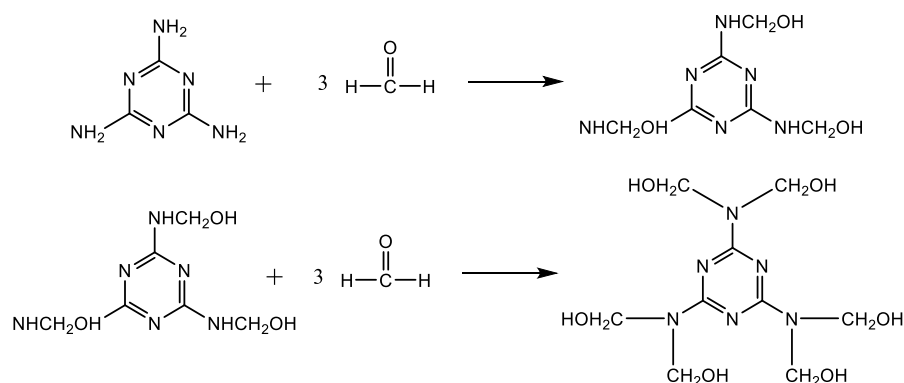


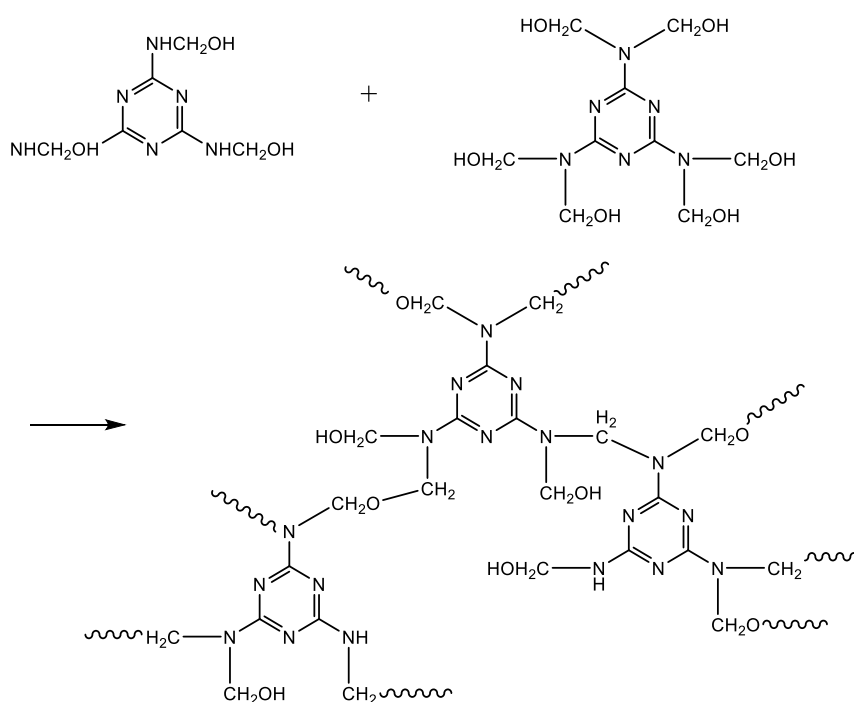
**Figure 4-6** Optical microscope images of the formation of ILEM@PMF microcapsules at different times after mixing with prepolymer (TM= transmission mode, RM=reflection mode)

(a) 0 min, TM; (b) 120 min TM; (c) 180 min, TM; (d) 180 min, RM

(a) basic condition



(b) acid condition



**Scheme 4-2** Reaction mechanisms of poly(melamine-formaldehyde) (PMF)

#### 4.3.3.3 Influence of synthesis parameters on the morphology and size distribution of ILEM@PMF microcapsules

Several parameters influence the morphology of microcapsules prepared by *in-situ* polymerization [40-42]. First, pH and temperature during the *in-situ* polymerization have a huge influence on the condensation rate of PMF. Compared to the reaction rate for the synthesis of microcapsules in Chapter 3, the addition reaction of formaldehyde with melamine is easier compared to formaldehyde and urea. Melamine has a higher amine functionality (presence of three amino groups). Thus, hexa-hydroxymethyl melamine can be formed to facilitate the further condensation reactions [43]. Kim *et al* [44] also reported that PMF resin required lower



activation energy than the PUF one, *i.e.* the condensation reactions proceed faster at a given temperature.

To study the influence of two other important parameters, *i.e.* core/shell ratio and stirring speed, on the morphology of ILEM@PMF microcapsules, an orthogonal experiment was designed as shown in Table 4-3. All the microcapsules were prepared with the same concentration of co-surfactants, heating rate, final pH, temperature, and weight content of ILEM in the aqueous solution. The morphology of different resulting microcapsules and their size distribution are presented in Figure 4-7.

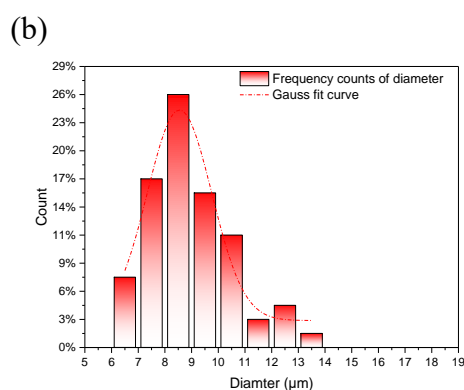
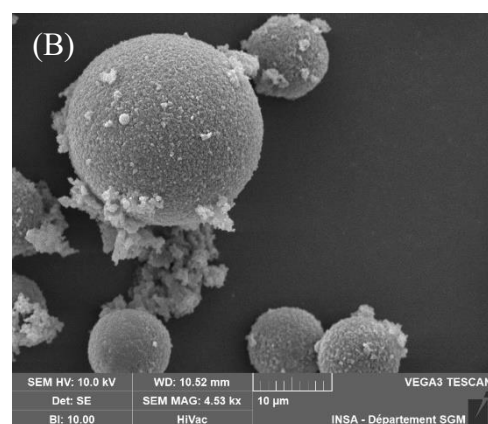
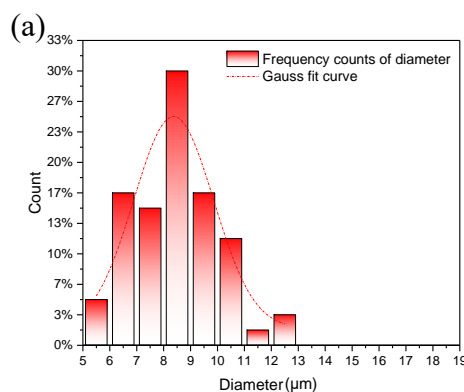
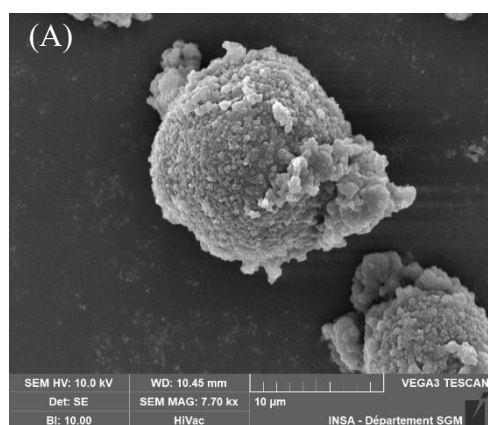
**Table 4-3** Different synthesis parameters considered for the preparation of ILEM@PMF microcapsules and its serial number of corresponding SEM micrographs

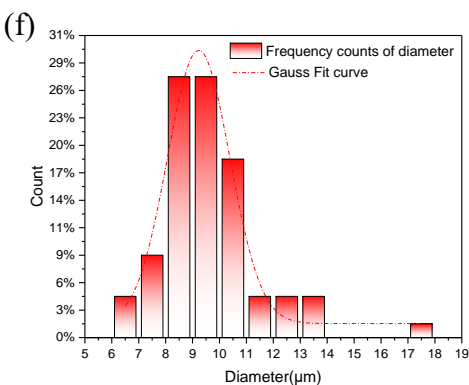
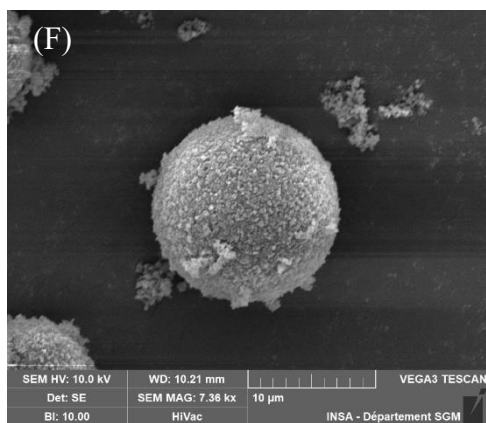
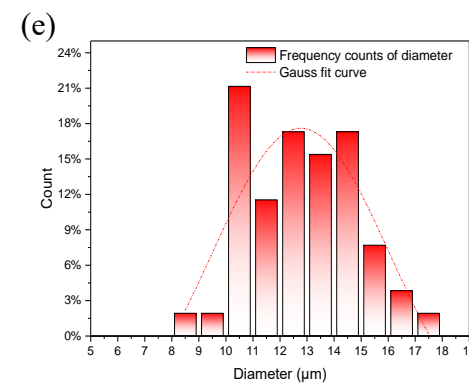
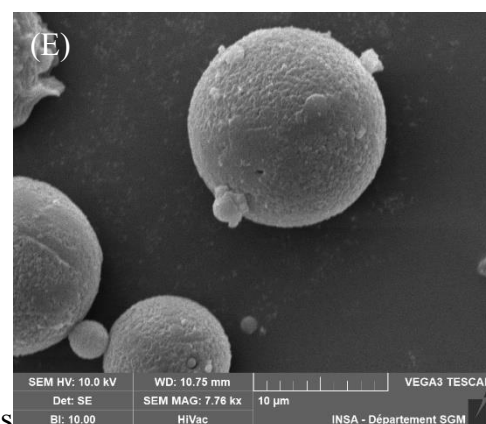
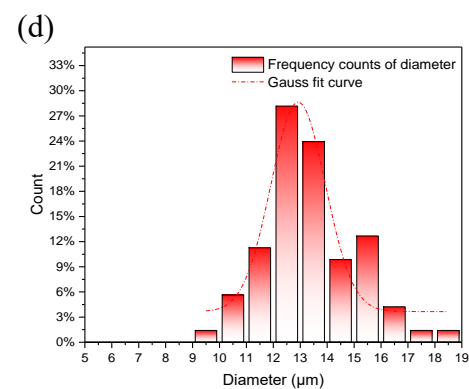
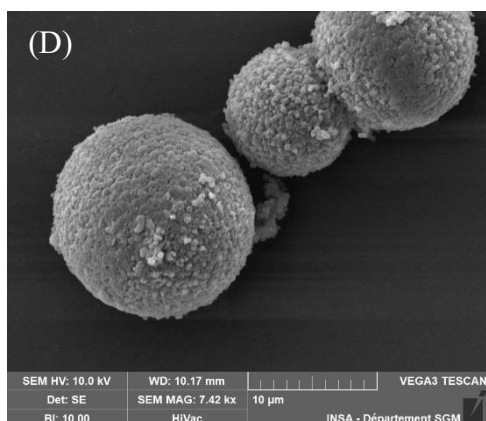
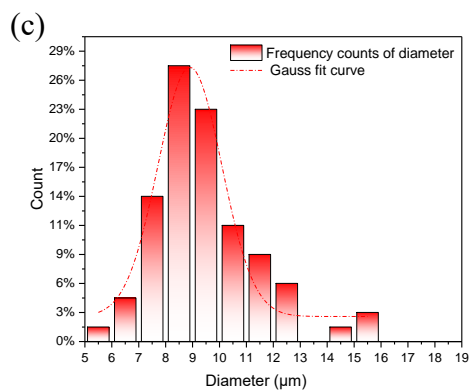
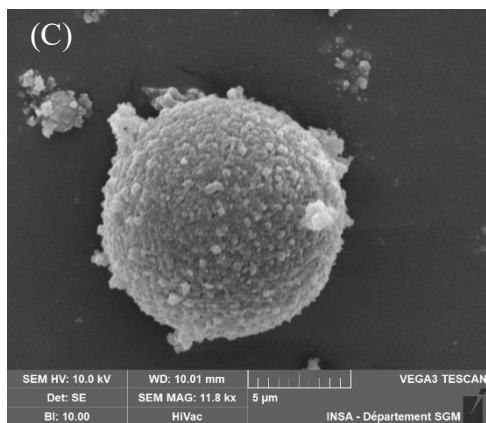
Microcapsules	Synthesis parameters		Serial number of SEM images (A-G) and size distribution (a-g)
	(Surfactants : SDBS:PVA=9:1, 1 wt%) core/shell ratio	stirring speed (rpm)	
<b>1</b>	0.95	300	(A)/(a)
<b>2</b>	1.08	300	(B)/(b)
<b>3</b>	1.22	300	(C)/(c)
<b>4</b>	1.31	300	(D)/(d)
<b>5</b>	1.42	300	(E)/(e)
<b>6</b>	1.22	250	(F)/(f)
<b>7</b>	1.22	350	(G)/(g)

First of all, microcapsules **1-5** were synthesized considering the same stirring speed and different core/shell ratios. As shown in Figure 4-7 (a) to (e), the diameter of ILEM@PMF microcapsules increases with a higher core/shell ratio while their size distribution is not extended. As the microcapsules have the same weight fraction of ILEM in the aqueous solution, an increase of diameter can be explained by the decreased number of MF prepolymer in the aqueous solution. MF prepolymer behaves as UF prepolymer to decrease the interfacial tension [45, 46]. Thus, a low MF concentration may help to form bigger ILEM droplets because a high core/shell weight ratio results in a lower weight fraction of MF prepolymer in the aqueous solution, *i.e.* weight fraction in aqueous solution remains always the same. Despite the influence of the core/shell ratio on the diameter of ILEM@PMF microcapsules, the number of PMF nanoparticles has also an impact. From microcapsules **1-5** (Figure 4-7 (A) to (E)), one can conclude that the number of individual PMF nanoparticles or stuck on the ILEM@PMF microcapsules surface decreased. The excessive MF polymer polymerized as nanoparticles and

precipitated in the aqueous solution, and a proper core/shell ratio reduced the excessive PMF nanoparticles. Therefore, ILEM@PMF microcapsules with a higher core/shell ratio display a more regular shape.

Then, microcapsules **6**, **3** and **7** have the same core/shell ratio but were prepared under different stirring speeds. From Figure 4-7 (f), (c) and (g), one can conclude that the stirring speed does not influence the maximum value of diameter of ILEM@PMF microcapsules. However, it plays a key role in the size distribution of ILEM@PMF microcapsules and the number of PMF nanoparticles. As mentioned before, the mechanical stirring contributed to the stabilization of the ILEM/H<sub>2</sub>O emulsion while the anisotropic shear forces led to a size distribution of the ILEM/H<sub>2</sub>O emulsion. Figure 4-7 (F), (C), and (G) reported the morphologies of microcapsules for different stirring speed. The microcapsules prepared under the highest stirring speed (350 rpm) (microcapsules **7**, Figure 4-7 (G)) have the narrow size distribution but more PMF nanoparticles. This can be explained by the strong shear force at high stirring speed, which helps to disperse ILEM but breaks the soft PMF shell at the early stages of the synthesis process. For the ILEM@PMF microcapsules prepared at 350 rpm with a core/shell ratio higher than 1.22:1, the strong shear force destroyed the newly formed ILEM/H<sub>2</sub>O microcapsules and leading to a reduced yield.





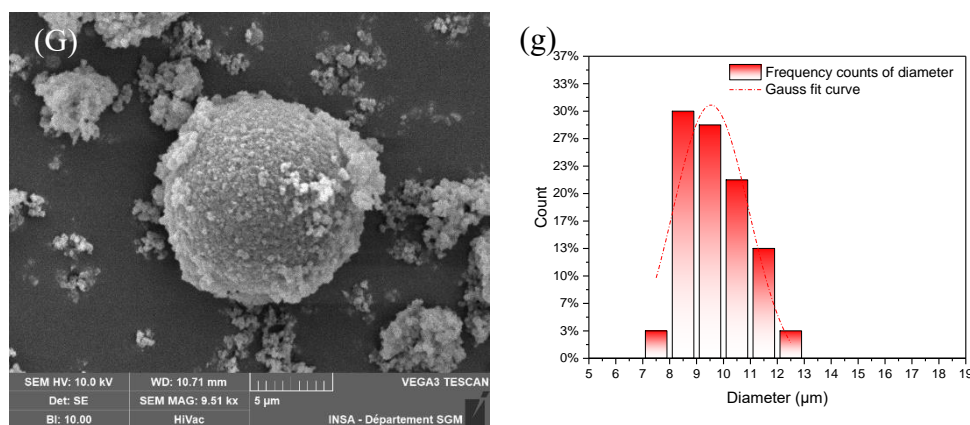


**Figure 4-7** SEM micrographs ((A)-(G)) and size distributions ((a)-(g)) of ILEM@PMF microcapsules prepared with different parameters

According to the SEM images (Figure 4-7), two type of microcapsules, *i.e.* 4 and 5 (Figure 4-7 (d) and (e)), display the suitable morphologies. Additional morphology characterizations were performed. Apparently, a reduced amount of PMF nanoparticles could be observed for microcapsules 5 (Figure 4-8 (d)) but their shell thickness (0.51 μm, Figure 4-8 (e)) is smaller compared to microcapsules 4 (0.82 μm, Figure 4-8 (b)). It is worth noting that the shell thickness will have a large influence on the integrity of ILEM@PMF microcapsules in the subsequent processing steps required for epoxy composites.

Therefore, ILEM@PMF microcapsules 4 and 5 were added in the same epoxy-amine network as ones considered in Chapter 3 (polymer matrix: D.E.R 332 cured with TETA, see section 4.4.1). As shown in Figure 4-8 (f), ILEM@PMF microcapsules 5 could be easily broken due to their thin and brittle PMF shell, during processing and curing processes<sup>[47]</sup>. By contrast, ILEM@PMF microcapsules 4 remained intact after processing in the epoxy-amine matrix. Therefore, a relatively low core/shell ratio allows to increase the shell thickness of ILEM@PMF microcapsules providing good mechanical strength against the mechanical forces exerted during the processing of epoxy materials.

To sum up, considering the morphology of ILEM@PMF microcapsules and their mechanical strength, the optimized synthesis parameters of ILEM@PMF microcapsules for self-healing application in epoxy-amine composites are the followings: core/shell ratio = 1.31, stirring speed = 300 rpm.

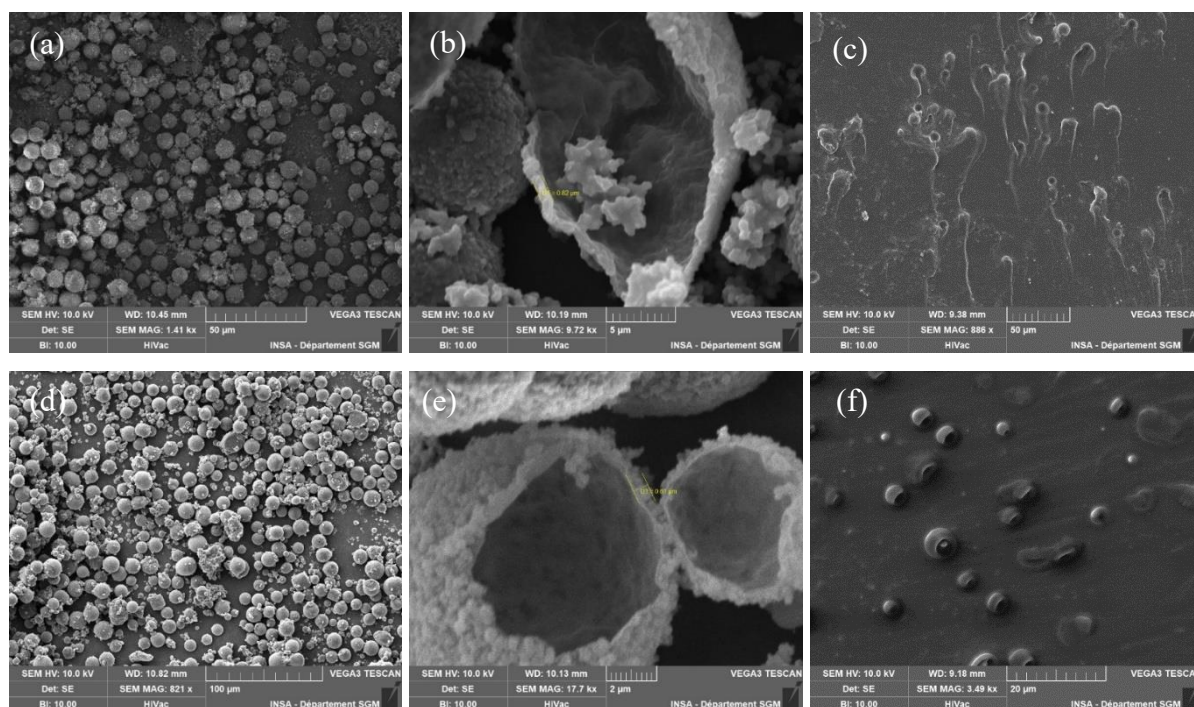


**Figure 4-8** ILEM@PMF microcapsules **4** (a) (b) and **5** (d) (e) and morphologies of epoxy-amine networks containing microcapsules **4** (c) and **5** (f)

#### 4.3.3.4 Chemical structure of ILEM@PMF microcapsules

The chemical structure of ILEM@PMF microcapsules, *i.e.* core and shell were characterized by FTIR as shown in Figure 4-9. These ones are schematically represented in Figure 4-10. For the core, the characteristic peaks of counter anions ( $\text{NTf}_2^-$ ) could be evidenced as the symbol for ILEM monomer in the FTIR spectrum. To be more specific, the characteristic peak at  $1,350\text{ cm}^{-1}$  and  $1,056\text{ cm}^{-1}$  are assigned to the stretching vibration of S=O bonds from sulfoxide<sup>[48]</sup> while the peak at  $1,195\text{ cm}^{-1}$  was assigned to the stretching vibration of C-F bonds in  $\text{CF}_3$  groups<sup>[49, 50]</sup>. In addition, the characteristic peaks for epoxy groups at  $830\text{ cm}^{-1}$  and  $910\text{ cm}^{-1}$ <sup>[51]</sup> can be also seen in the spectra of ILEM and ILEM@PMF microcapsules. For the PMF shell, 1,3,5-triazine rings having C=N bonds display absorption peaks at  $1,558\text{ cm}^{-1}$  and  $1,497\text{ cm}^{-1}$ . Besides, the absorption peaks around  $3,300\text{ -}2,800\text{ cm}^{-1}$  are the stretching vibration of C-H in alkane chains. Therefore, FT-IR analysis indicated that ILEM@PMF microcapsules have been successfully synthesized.

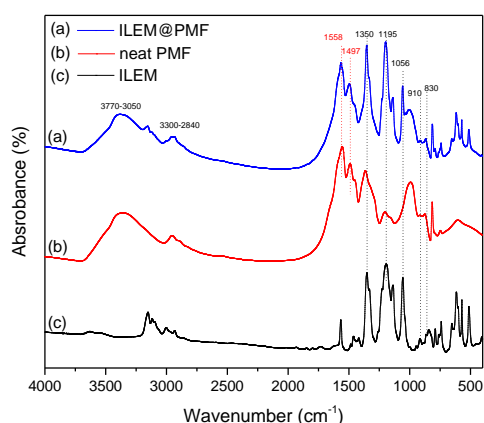


**Figure 4-9** FTIR spectra of ILEM@PMF microcapsules, core, and shell materials  
(a) ILEM@PMF microcapsules; (b) shell: neat PMF; (c) core: ILEM

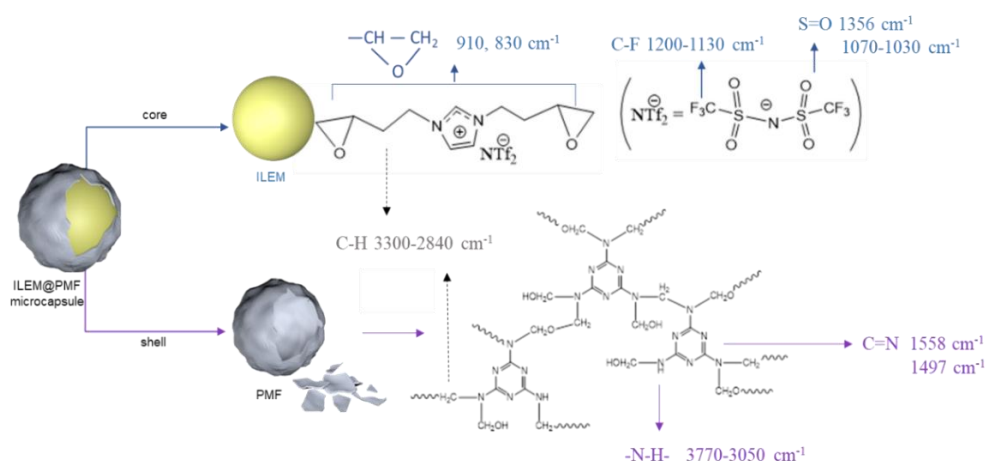


**Figure 4-10** Characteristic peaks in FTIR spectra of core and shell materials of ILEM@PMF microcapsules

#### 4.3.3.5 Thermal behavior and stability of ILEM@PMF microcapsules

The thermal behavior of ILEM@PMF microcapsules as well as their core (ILEM) and shell (PMF) were characterized by DSC as shown in Figure 4-11. Exothermic peaks observed on DSC traces for ILEM and ILEM@PMF during heating indicate the polymerization of ILEM. Compared to neat ILEM, a shift to lower temperature was observed for ILEM@PMF microcapsules. We speculate that this phenomenon is associated to the presence of remaining amines in the PMF shell. This lower temperature reminded us the curing temperature of the polymer matrix should be kept lower than the polymerization temperature of encapsulated ILEM. At about 150°C, for PMF and ILEM@PMF microcapsules, the release of absorbed moisture and free formaldehyde could also be observed [52, 53]. Therefore, the ability of ILEM to polymerize has proved the potential for ILEM in the ILEM@PMF microcapsules for self-

healing applications. Nevertheless, the decrease of the temperature of polymerization for ILEM in the microcapsules will impose a limit curing temperature of the epoxy polymer matrix.

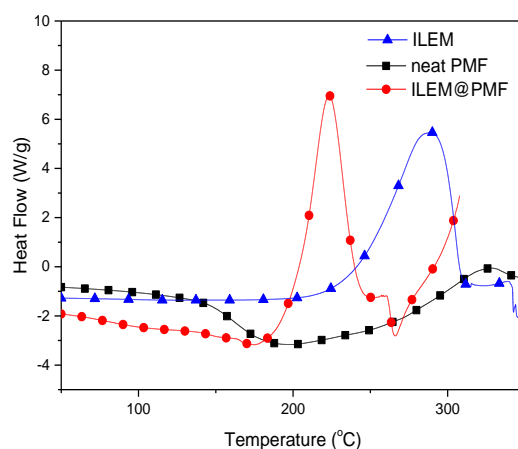


**Figure 4-11** DSC traces of (▲) ILEM (■) neat PMF, and (●) ILEM@PMF microcapsules (N<sub>2</sub> atmosphere, heating rate 10 K·min<sup>-1</sup>)

The thermal degradation of ILEM@PMF microcapsules was characterized by TGA under N<sub>2</sub> atmosphere. The TGA traces and DTG traces of ILEM@PMF microcapsules as well as the ones of core and shell materials are presented in Figure 4-12. Four stages of weight loss for the ILEM@PMF microcapsules can be evidenced in Figure 4-12. The first and second weight losses occurring at low temperature (below 300 °C) could be associated to the evaporation of absorbed water and free formaldehyde, as for neat PMF [54]. Due to the high thermal stability of ILEM and PMF [55], the third and fourth steps of weight losses occurring at high temperature (> 300 °C) correspond to the decomposition of polymerized ILEM and PMF shell.

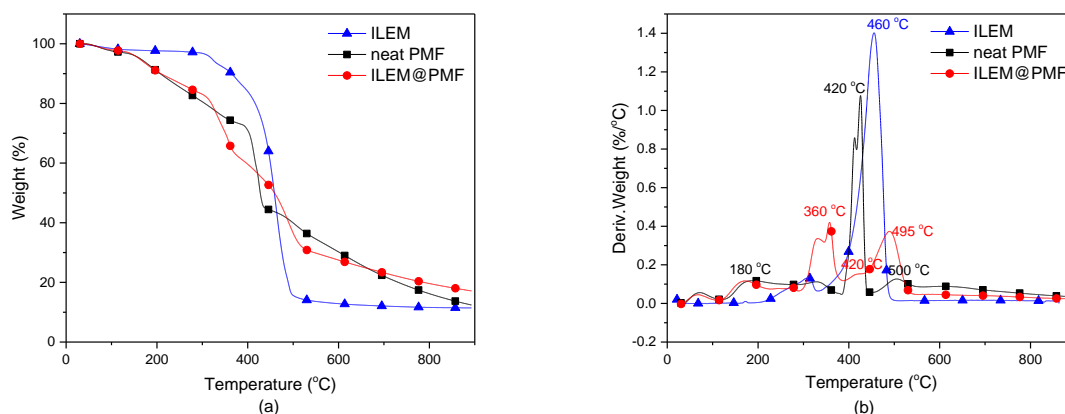


**Figure 4-12** (a) TGA and (b) DTG traces of (▲) core material ILEM and (■) shell material neat PMF and (●) ILEM@PMF microcapsules (N<sub>2</sub> atmosphere, heating rate 20 K·min<sup>-1</sup>)

In order to investigate the degradation behavior of ILEM@PMF microcapsules, the emitted gases during TGA were characterized by FTIR. The FTIR spectra as a function of the temperature are given in Figure 4-13. The detected chemical components and their characteristic wavenumbers are summarized in Table 4-4. The FTIR spectra and corresponding absorption peaks of emitted gases for core and shell materials of ILEM@PMF microcapsules are shown in the supporting information of Chapter 4.

According to the FTIR spectra of emitted gases, the first weight loss corresponds to the evaporation of absorbed water and free formaldehyde from the deformaldehyde reaction of PMF prepolymer at elevated temperatures. The second weight loss of ILEM@PMF microcapsules occurred from 300 to 380 °C. The presence of alkanes and amides evidenced that the decomposition of the PMF shell occurs at this stage. The third weight loss took place from 380 to 450 °C. At this stage, presence of trifluoromethane ( $\text{CHF}_3$ ) and sulfone in the released gases is a proof of the decomposition of anions ( $\text{NTf}_2^-$ ) in ILEM. The final weight loss occurred from 450 to 600 °C, related to the further decomposition of ILEM core and PMF shell. The degradation of ILEM almost finished at 500 °C, but there was a temperature shift of about 40 K for ILEM compared to ILEM@PMF microcapsules. Therefore, the ILEM core is well protected by the PMF shell and is not decomposed before PMF shell when heating.

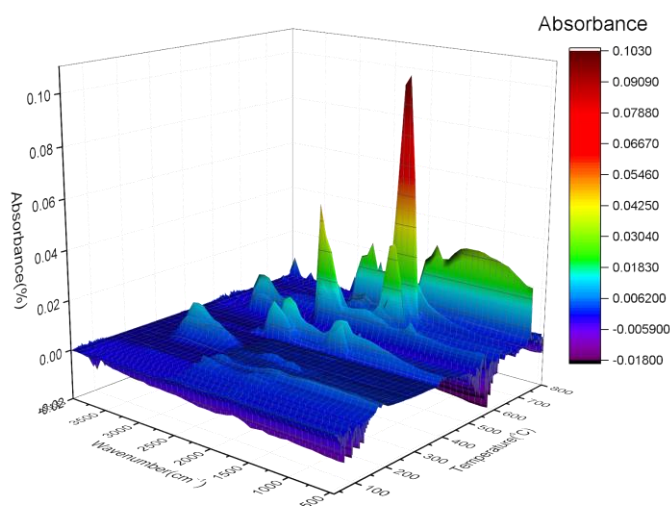


**Figure 4-13** FTIR spectra of emitted gas during thermal degradation of ILEM@PMF microcapsules under  $\text{N}_2$  atmosphere



**Table 4-4** Emitted gas characterization from FTIR for ILEM@PMF microcapsules and their corresponding shell (PMF) and core (ILEM) materials by TGA-IR analyses

PMF shell			ILEM core			ILEM@PMF microcapsules		
Temperature range	Gas	wavenumber (cm <sup>-1</sup> )	Temperature range	Gas	Wavenumber (cm <sup>-1</sup> )	Temperature range	Gas	Wavenumber (cm <sup>-1</sup> )
130 °C   260 °C	formal- ehyde	1,730 2,830-2,695	310 °C   380 °C	imine	1,711	160 °C   200 °C	formal- ehyde	1,730 2,830-2,695
260 °C   500 °C	oxhydril	3,500-3,420		aliphatic ether	1,150	300 °C   380 °C	alkane	1,450
	amide	1,600	amide				1,600	
	alkane	1,450	trifluoro- methane	1,150	380 °C   450 °C	trifluoro- methane	1,150	
	methylen e	710				amide	1,600	
500 °C   600 °C	cyanuric	1,600	380 °C   500 °C	sulfone	1,380 1,425	450 °C   600 °C	cyanuric	1,600
							trifluoro- methane	1,150
	CO <sub>2</sub>	2,350	CO <sub>2</sub>	2,350	sulfone	1,380 1,425	CO <sub>2</sub>	2,350

#### 4.4 Preparation and characterization of ILEM@PMF microcapsule-filled epoxy-amine materials

The previous study has demonstrated that the ionic liquid epoxy monomer (ILEM) could be successfully encapsulated in the PMF shell as microcapsules. In addition, ILEM is able to polymerize by thermal activation without any additional initiators or comonomers. These ILEM can be a good candidate for self-healing additives of epoxy-amine networks. Nevertheless, the potential reactivity of the ILEM trapped into ILEM@PMF microcapsules with the remaining amino groups on the shell limit the curing temperature. Therefore, ILEM@PMF microcapsules were added into epoxy-amine systems cured under different temperature conditions to investigate their self-healing performances.

#### 4.4.1 Material Processing

ILEM@PMF microcapsules were added in different epoxy-amine networks. The preparation method is described in Figure 4-14. First, ILEM@PMF microcapsules were added in epoxy monomer and the mixture was placed in an ultrasound bath to disperse the ILEM@PMF microcapsules. Then, different types of amine comonomers were added according to epoxy-to-amino hydrogen ratio equal to 1.0. The reactive mixtures were put under mechanical stirring for about 10 min. The mixtures were placed in a vacuum bell jar for 10 min to remove the trapped bubbles. Then, different curing protocols were applied depending on the chemical nature of the hardeners.

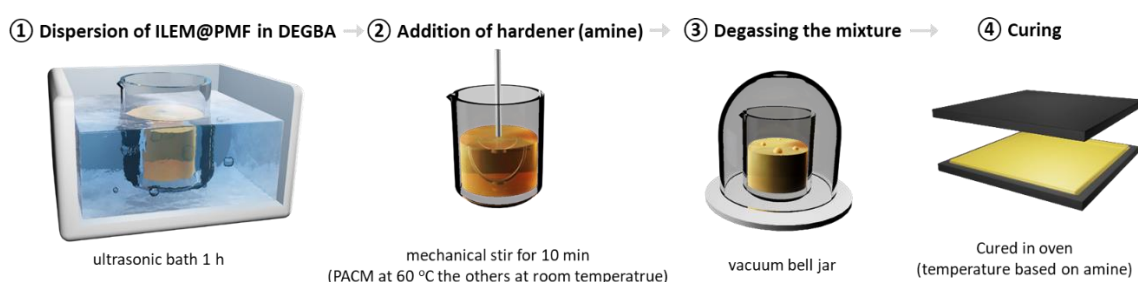


**Figure 4-14** Preparation of ILEM@PMF microcapsule-filled epoxy-amine materials

#### 4.4.2 Results and discussion

As demonstrated before, the ILEM in the ILEM@PMF microcapsules is able to polymerize. The curing temperature of polymer matrix may affect the self-healing performances of ILEM@PMF microcapsules. Therefore, the ILEM@PMF microcapsules were added by 10 wt% in the different epoxy-amine systems: *i*) epoxy-PACM; *ii*) epoxy-TETA; *iii*) epoxy-Epikure 3223. These reactive matrices were cured at stoichiometric ratio and within different temperature to see the performance of ILEM@PMF microcapsules as self-healing additive in the epoxy-amine composites.

##### 4.4.2.1 Local temperature of different epoxy-amine networks

PACM was considered firstly as hardener. The curing protocol of DGEBA-PACM reactive system was the same as one considered before: 80 °C for 2 h and 160 °C for 2 h. The linear aliphatic amine TETA which is much more reactive was copolymerized with DGEBA at : 60 °C at 2h, 80 °C at 3h, 110 °C at 3h, and 120 °C at 1h. Finally, a commercial room temperature curing agent Epikure 3223, mainly based on diethylenetriamine (DETA) which has an even higher reactivity compared to TETA was considered. DETA-epoxy resin is able to undergo

gelation and set hard at room temperature within a very short period. The curing was performed at temperature for 48 h followed by 6 h at 120 °C.

As mentioned in 4.3.3.5 section, the curing temperature of epoxy-amine matrix should be below the polymerization temperature of ILEM contained in the ILEM@PMF microcapsules. Therefore, the temperature of epoxy-amine mixture was measured in the bulk (Figure 4-15). In fact, as the condensation reaction between epoxy and amine is exothermic (100 kJ/mol) [56, 57], the calculated maximum temperature caused by the exothermic reaction for an ideal adiabatic process leading to a full conversion could reach 338 to 390 °C [58]. In real condition, heating occurs due to poor heat dissipation of the cavity or mold in which the system reacts. For the epoxy-PACM (Figure 4-15 (a)) and epoxy-TETA systems (Figure 4-15 (b)), the temperature reached high values for a relatively short time of reaction (up to 20 min for the first system). The temperature maximum at 187 °C reached by the epoxy-PACM system may cause the polymerization of ILEM in the ILEM@PMF microcapsules.

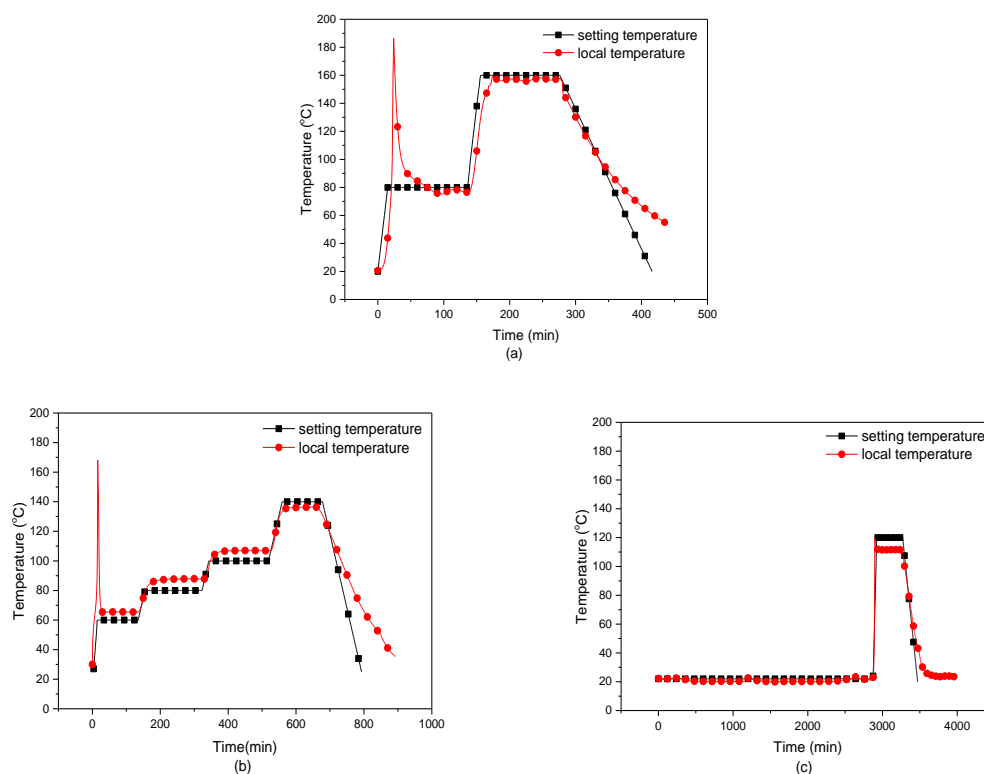


**Figure 4-15** Settled and recorded temperature (in the bulk) vs. time during curing of (a) epoxy-PACM; (b) epoxy-TETA; (c) epoxy-Epikure 3223 systems

#### 4.4.2.2 Morphology of ILEM@PMF microcapsule-filled epoxy-amine materials

SEM was used to characterize the cross sections of ILEM@PMF microcapsules filled epoxy-amine materials (Figure 4-16). As shown in Figure 4-16 (a) (d) and (g), ILEM@PMF

microcapsules display a good distribution in different epoxy-amine matrices. Different morphologies of individual ILEM@PMF microcapsules could be distinguished.

In the epoxy-PACM matrix, almost no intact ILEM@PMF microcapsules can be observed. The broken microcapsules have solid-like core instead of cavities (Figure 4-16 (a), (b) and (c)). These broken microcapsules with solid core indicate that the temperature is too high leading to the polymerization of ILEM in agreement with the temperature recording (Figure 4-15 (a)). However, in the epoxy-TETA and epoxy-Epikure 3223 matrices, intact/broken and pulled out ILEM@PMF microcapsules can be evidenced (Figure 4-16 (d) and (g)). A good interface can also be observed (Figure 4-16 (e) and (h)). At higher magnifications, a hollow structure can be seen for broken ILEM@PMF microcapsules (Figure 4-16 (f) and (i)), indicating that ILEM did not undergo polymerization.

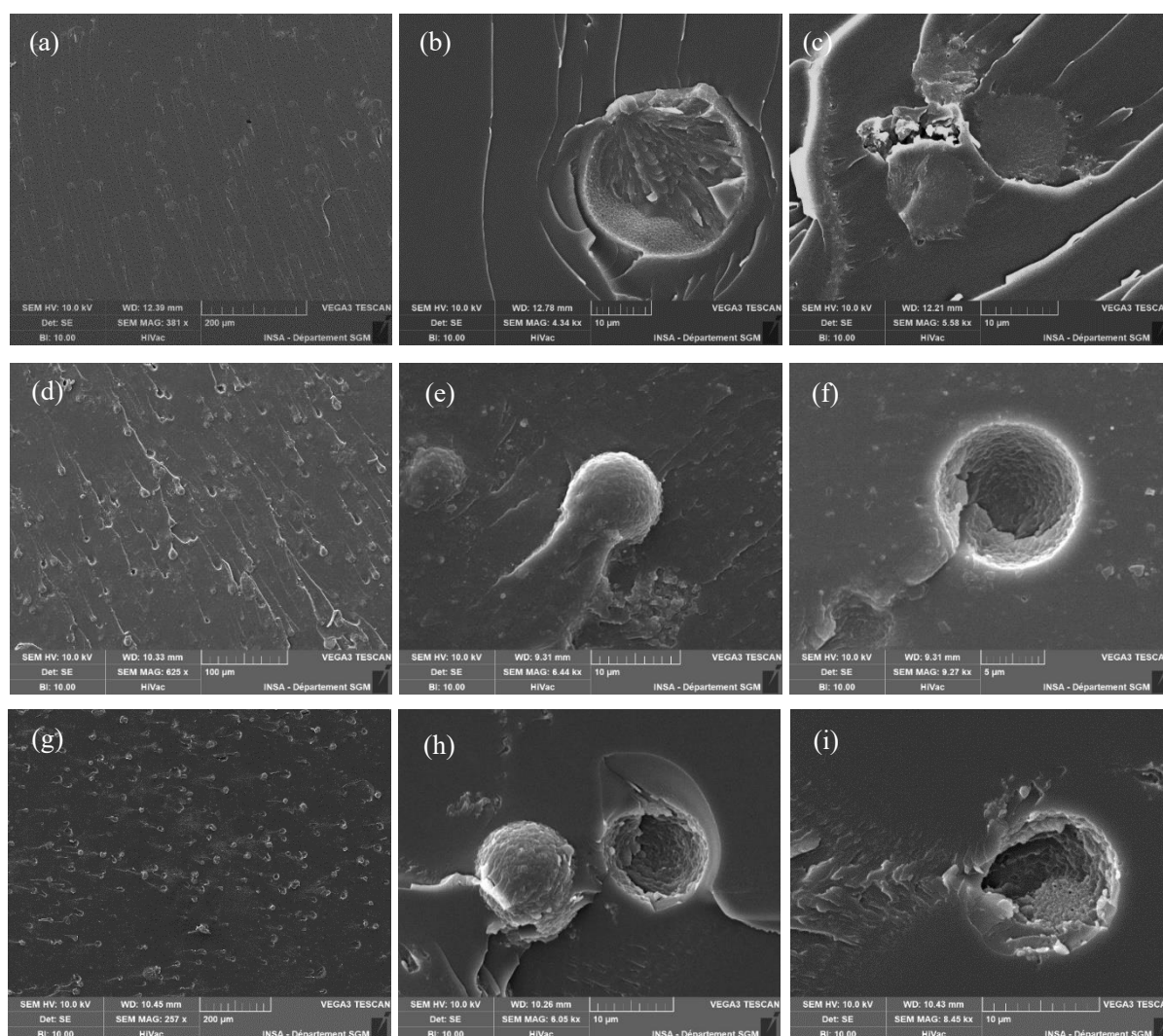


**Figure 4-16** SEM micrographs of ILEM@PMF microcapsules filled (a)-(c) epoxy-PACM; (d)-(f) epoxy-TETA; (g)-(i) epoxy-Epikure 3223 materials

#### 4.4.2.3 Thermal properties of ILEM@PMF microcapsule-filled epoxy-amine materials

The thermal properties of ILEM@PMF microcapsules filled epoxy-amine composites were characterized by DSC (Figure 4-17). First, a decrease of  $T_g$  of the ILEM@PMF microcapsules filled networks compared to the corresponding neat epoxy-amine networks can be observed, which is more obvious for epoxy-TETA/epoxy-Epikure 3223-based materials resulting from a lack of interfacial bonding between PMF shell and epoxy matrix. An exothermic peak close to 200 °C could be evidenced for ILEM@PMF microcapsules filled epoxy-TETA and epoxy-Epikure 3223 materials. This exotherm could be attributed to the polymerization of ILEM. However, no exothermic peak was noticed for epoxy-PACM system, indicating that ILEM had already polymerized during curing of the matrix due to the high local temperature.

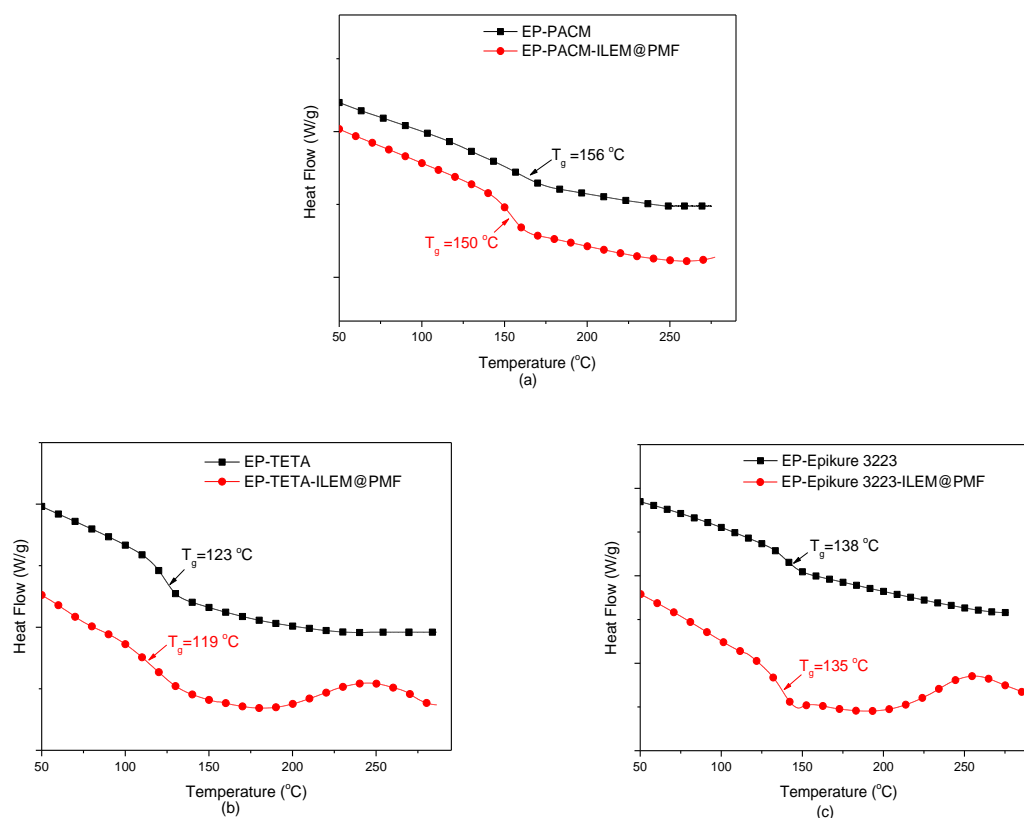


**Figure 4-17** DSC traces of (a) epoxy-PACM; (b) epoxy-TETA; (c) epoxy-Epikure 3223 based materials ( $N_2$  atmosphere, heating rate  $10\text{ K}\cdot\text{min}^{-1}$ )

Thermal stability of ILEM@PMF microcapsules filled epoxy-amine materials was characterized by TGA (see Figure S4-14 to Figure S4-16 in the supporting information). The corresponding onset decomposition ( $T_{d\text{ onset}}$ ) and maximum decomposition ( $T_{d\text{ max}}$ )

temperatures of each material are summarized in Table 4-5. A decrease of  $T_{d\ onset}$  and  $T_{d\ max}$  of ILEM@PMF filled epoxy composites compared to the corresponding neat epoxy-amine networks was observed. Referring back to Figure 4-12 and Table 4-4, the decomposition of ILEM@PMF microcapsules could start from the PMF shell which is lower than that of epoxy-amine networks, *i.e.* the first decomposition step of ILEM@PMF microcapsules occurs close to 300 °C.

**Table 4-5** Degradation temperatures of ILEM@PMF microcapsule-filled epoxy-amine composites (N<sub>2</sub> atmosphere, heating rate 20 K·min<sup>-1</sup>)

Materials	$T_{d\ onset}$ (°C)	$T_{d\ max}$ (°C)
epoxy + PACM	359	378
epoxy + PACM + ILEM@PMF	330	368
epoxy + TETA	341	367
epoxy + TETA + ILEM@PMF	329	362
epoxy + Epikure 3223	350	371
epoxy + Epikure 3223 + ILEM@PMF	330	364

#### 4.4.2.4 *Dynamic mechanical properties of ILEM@PMF microcapsule-filled epoxy-amine materials*

Dynamic mechanical analyses were also performed for the ILEM@PMF microcapsules filled epoxy-amine materials.  $\tan \delta$  and  $G'/G''$  vs. temperature spectra are given in Figure 4-18. First, a low relaxation peak above the main relaxation could be observed for epoxy-TETA and epoxy-Epikure 3223 based materials corresponding to the polymerization of ILEM. Besides, an increase of  $G'$  for the epoxy-TETA and epoxy-Epikure 3223 based materials is evidenced during a second heating which also is a proof of the ILEM polymerization. Whereas, those features related to the polymerization of ILEM were not observed for the epoxy-PACM based material, confirming for the consumption of ILEM, *i.e.* during curing.

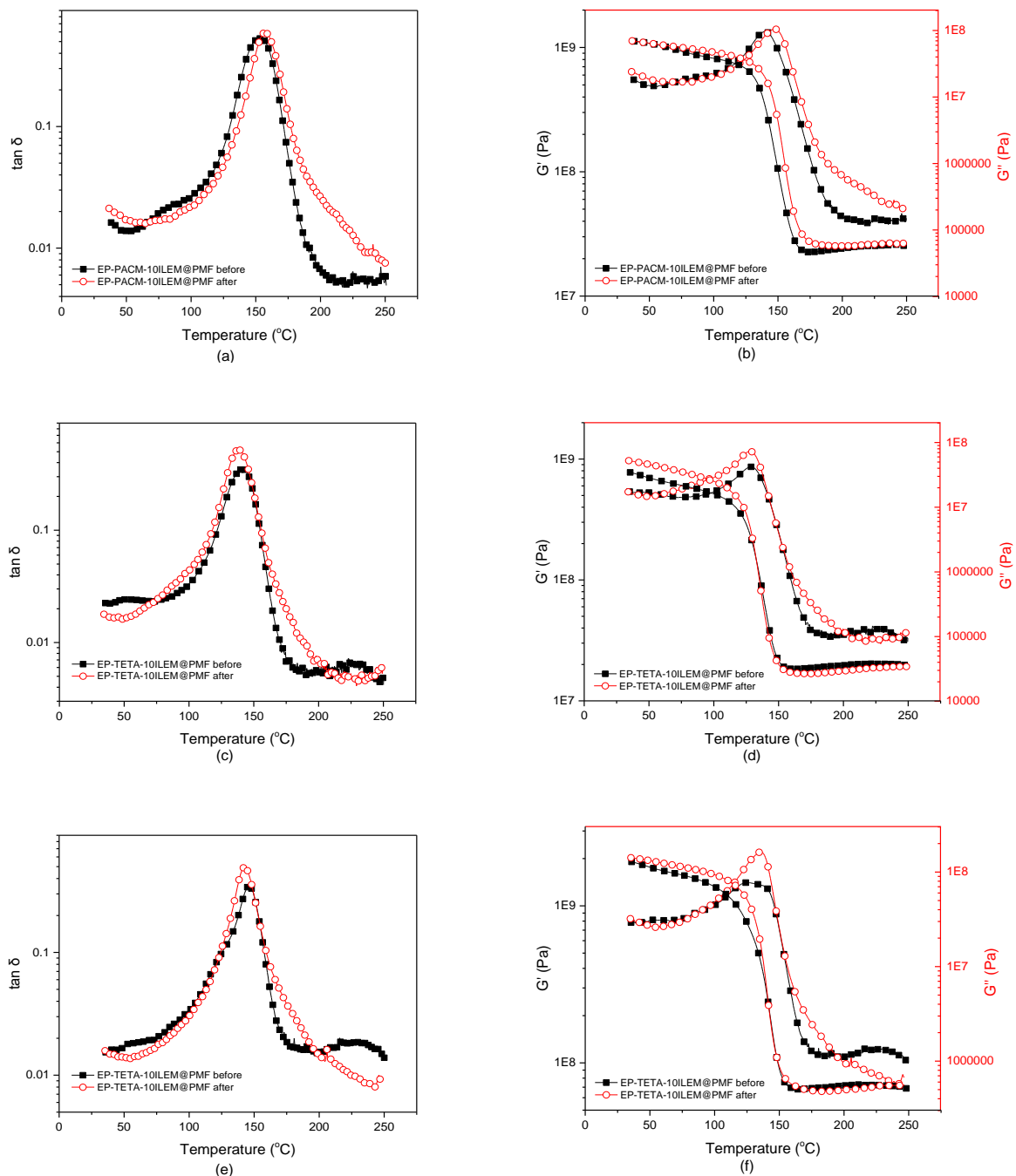


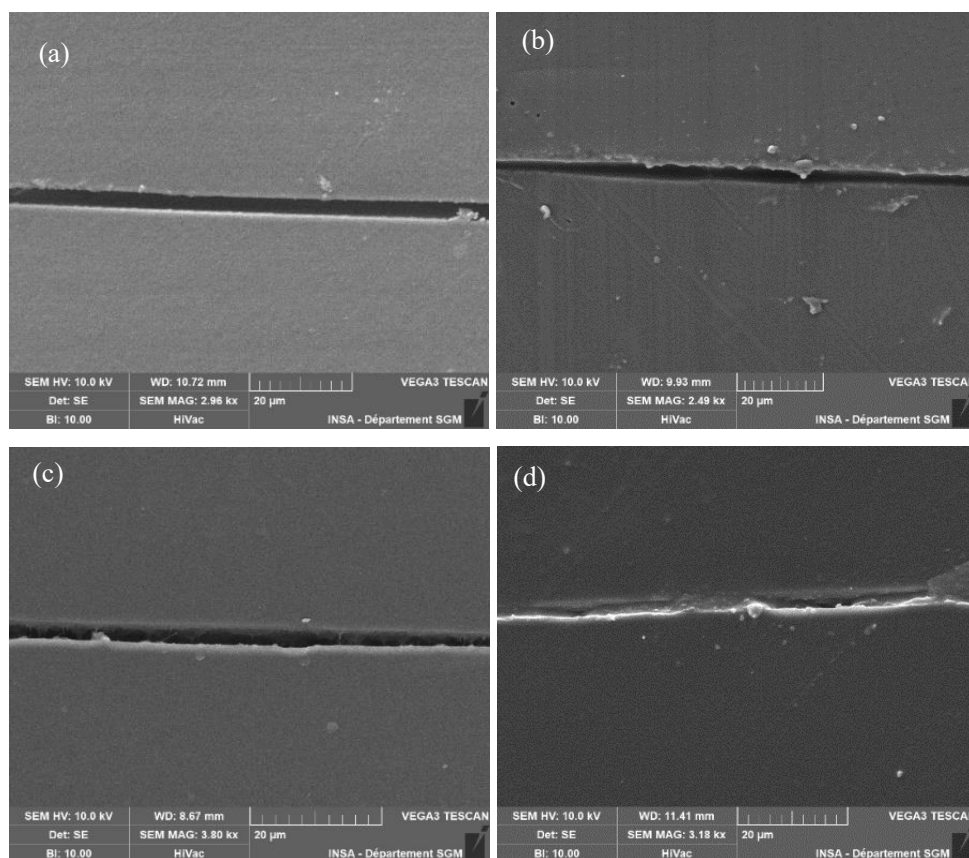
**Figure 4-18**  $\tan \delta$ ,  $G'/G''$  vs. temperature spectra of ILEM@PMF microcapsules filled (a), (b) epoxy-PACM; (c), (d) epoxy-TETA; (e), (f) epoxy-Epikure 3223 materials (at 1Hz, heating rate  $3 \text{ K} \cdot \text{min}^{-1}$ )

#### 4.4.2.5 Self-healing property of ILEM@PMF microcapsule-filled epoxy-amine materials

The self-healing property of ILEM@PMF microcapsules filled epoxy-amine material was characterized by the same method used in Chapter 3. The corresponding SEM images of scratches before and after self-healing are shown in Figure 4-19. Nevertheless, a decrease of

width for the scratch was considered according to the smaller diameter of ILEM@PMF microcapsules, *i.e.* in order to guarantee the breakage of ILEM@PMF microcapsules and the release of healing agent into the scratch.

Owing to the consumption of healing agent before the self-healing process, no healing of scratch can be get for ILEM@PMF microcapsules filled epoxy-PACM material (Figure 4-19 (b)). Whereas ILEM@PMF microcapsules have good self-healing performances for low temperature epoxy-amine networks. For epoxy-TETA (Figure 4-19 (d)) and epoxy-Epikure 3223 (Figure 4-19 (f))-based materials, a healing effect of the scratches due to the better preservation of ILEM in the corresponding composites was observed. Unreacted ILEM could diffuse and polymerize after mild curing temperatures of the epoxy-amine matrix. Therefore, a curing temperature lower than the polymerization temperature of encapsulated ILEM is necessary to achieve self-healing purpose for ILEM@PMF filled epoxy-amine materials. Even though the temperature could be a limitation of ILEM@PMF as self-healing additive, this could be the first attempt of encapsulated ILEM and their application in thermoset material. Various choices of shell material and core material for self-healing can be proposed and development of more materials can be expected.





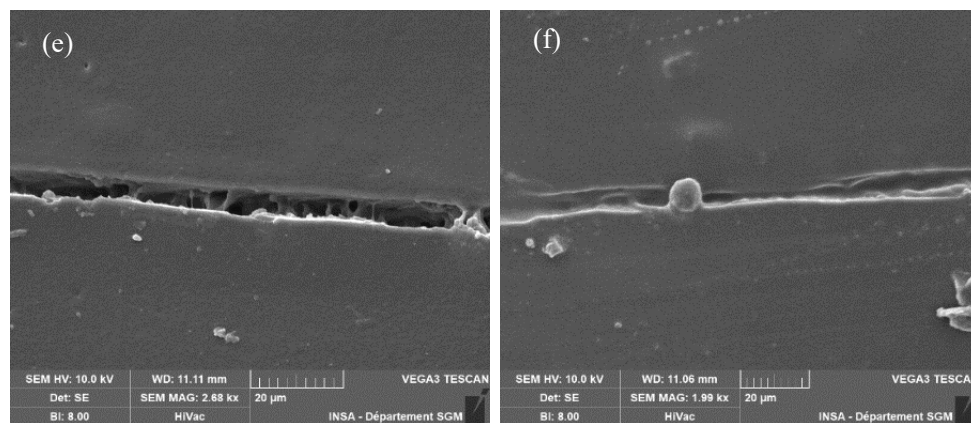


**Figure 4-19** SEM micrographs of scratches before (up) and after (down) self-healing for ILEM@PMF microcapsule-filled (a), (b) epoxy-PACM; (c), (d) epoxy-TETA; (e), (f) epoxy-Epikure 3223-based materials

#### 4.4.2.6 Mechanical properties of ILEM@PMF microcapsule-filled epoxy-amine materials

The mechanical properties including Young's modulus ( $E$ ) and fracture toughness ( $K_{IC}$ ) of ILEM@PMF microcapsules filled epoxy-amine materials were characterized (Table 4-6). The addition of microcapsules with stiff polymer shell can be regarded as viscoelastic material [59]. The weak interfaces due to lack of chemical interaction and the soft segments slipping on of ILEM@PMF microcapsules during the characterization lead to a decrease the Young's modulus of epoxy materials [60-62]. Besides, PMF as shell material for microcapsules displayed a high strength and hardness [33, 63]. As a consequence, ILEM@PMF microcapsule-filled epoxy materials still display good mechanical properties compared to the corresponding neat epoxy-amine networks. The tails generated by crack propagation and breakage of microcapsules indicate the absorption of energy during fractures propagation, as shown in Figure 4-16. Thus, the addition of ILEM@PMF microcapsules may improve the fracture toughness of the epoxy materials.

**Table 4-6** Mechanical properties of ILEM@PMF microcapsule-filled epoxy-amine material at room temperature

Materials	$E$ (GPa)	$K_{IC}$ (MPa·m <sup>1/2</sup> )
EP+TETA	1.6 ± 0.02	0.64 ± 0.04
EP + TETA + ILEM@PMF	1.5 ± 0.04	0.72 ± 0.06
EP + Epikure 3223	1.5 ± 0.05	0.65 ± 0.02
EP + Epikure 3223 + ILEM@PMF	1.4 ± 0.02	0.73 ± 0.06

## 4.5 Conclusion

A difunctional ionic liquid-type epoxy monomer, denoted as ILEM, was successfully synthesized. ILEM have good thermal stability and shows a self-curing behavior induced by heat under a given temperature. Thus, ILEM could be considered as a potential self-healing agent released from a single microcapsule.

The ILEM was encapsulated in the poly(melamine-formaldehyde) (PMF) shell by *in-situ* polymerization method, to design ILEM@PMF microcapsules. The selection of surfactants and the influence core/shell ratio and stirring speed on the morphology of the ILEM@PMF microcapsules were investigated. It was found that SDBS and PVA co-surfactants can stabilize the ILEM droplets in the aqueous solution due to the synergistic effect between the adsorption sites provided by PVA and electrostatic repulsion interactions of SDBS. The optimized core/to shell ratio and stirring speed were 1.31:1 and 300 rpm, respectively. The obtained ILEM@PMF microcapsules showed a good thermal stability and ILEM as core was able to polymerize, making ILEM@PMF microcapsules a good additive for achieving self-healing purpose in epoxy-amine materials.

As encapsulated ILEM is able to polymerize above a given temperature, this one imposes a limited range of the curing temperature of epoxy-amine systems. Therefore, the self-healing performances of ILEM@PMF microcapsules were investigated in different epoxy-amine systems cured under different temperature conditions. According to the curing temperature for amines, PACM (80 °C- 160 °C), TETA (60 °C- 125 °C), and Epikure 3223 (DETA, 20 °C - 120 °C) were chosen as curing agents. Among the three epoxy-amine systems, ILEM@PMF microcapsules exhibited good self-healing properties for epoxy-TETA and epoxy-Epikure 3223-based materials rather than in epoxy-PACM-based one. Due to the high temperature of epoxy-PACM system, ILEM is consumed, *i.e.* ILEM polymerized, before the self-healing process. Besides, the addition of such ILEM@PMF microcapsules slightly affected the thermal and mechanical properties. However, based on this first attempt of encapsulation of ILEM, new applications and new materials could be expected in the future.

## References of Chapter 4

- [1] Blaiszik, B. J.; Kramer, S. L. B.; Olugebefola, S. C.; Moore, J. S.; Sottos, N. R.; White, S. R., Self-healing polymers and composites. *Annu. Rev. Mater. Res.* **2010**, 40, 179-211.
- [2] Gan, S. N.; Shahabudin, N., Applications of microcapsules in self-healing polymeric materials. *Microencapsulation-Processes, Technologies and Industrial Applications.* **2019**, 79-124.
- [3] White, S. R.; Sottos, N. R.; Geubelle, P. H.; Moore, J. S.; Kessler, M. R.; Sriram, S.; Brown, E. N.; Viswanathan, S., Autonomic healing of polymer composites. *Nature.* **2001**, 409, 794-797.
- [4] Liu, X.; Zhang, H.; Wang, J.; Wang, Z.; Wang, S., Preparation of epoxy microcapsule based self-healing coatings and their behavior. *Surface and Coatings Technology.* **2012**, 206, 4976-4980.
- [5] Yuan, L.; Liang, G.; Xie, J.; Li, L.; Guo, J., Preparation and characterization of poly (urea-formaldehyde) microcapsules filled with epoxy resins. *Polymer.* **2006**, 47, 5338-5349.
- [6] Brown, E. N.; Sottos, N. R.; White, S. R., Fracture testing of a self-healing polymer composite. *Experimental mechanics.* **2002**, 42, 372-379.
- [7] Yang, Z.; Hollar, J.; He, X.; Shi, X., A self-healing cementitious composite using oil core/silica gel shell microcapsules. *Cem. Concr. Compos.* **2011**, 33, 506-512.
- [8] Suryanarayana, C.; Rao, K. C.; Kumar, D., Preparation and characterization of microcapsules containing linseed oil and its use in self-healing coatings. *Prog. Org. Coat.* **2008**, 63, 72-78.
- [9] Jones, A. S.; Rule, J. D.; Moore, J. S.; White, S. R.; Sottos, N. R., Catalyst morphology and dissolution kinetics of self-healing polymers. *Chemistry of Materials.* **2006**, 18, 1312-1317.
- [10] Gan, S. N.; Shahabudin, N., Applications of microcapsules in self-healing polymeric materials. *Microencapsulation-Processes, Technologies and Industrial Applications.* **2019**.
- [11] Liu, X.; Sheng, X.; Lee, J. K.; Kessler, M. R.; Kim, J. S., Rheokinetic evaluation of self-healing agents polymerized by Grubbs catalyst embedded in various thermosetting systems. *Composites Science and Technology.* **2009**, 69, 2102-2107.
- [12] Jin, H.; Mangun, C. L.; Stradley, D. S.; Moore, J. S.; Sottos, N. R.; White, S. R., Self-healing thermoset using encapsulated epoxy-amine healing chemistry. *Polymer.* **2012**, 53, 581-587.
- [13] Green, M. D.; Long, T. E., Designing imidazole-based ionic liquids and ionic liquid monomers for emerging technologies. *Polym. Rev. (Philadelphia, PA, U. S.).* **2009**, 49, 291-314.
- [14] Muldoon, M. J.; Gordon, C. M., Synthesis of gel - type polymer beads from ionic liquid monomers. *J. Polym. Sci., Part A: Polym. Chem.* **2004**, 42, 3865-3869.
- [15] Chardin, C.; Durand, A.; Jarsalé, K.; Rouden, J.; Livi, S.; Baudoux, J., Sulfonimides versus ketosulfonamides as epoxidized imidazolium counterions: towards a new generation of

ionic liquid monomers. *New J. Chem.* **2021**, 45, 2953-2957.

[16] McDanel, W. M.; Cowan, M. G.; Barton, J. A.; Gin, D. L.; Noble, R. D., Effect of monomer structure on curing behavior, CO<sub>2</sub> solubility, and gas permeability of ionic liquid-based epoxy-amine resins and ion-gels. *Industrial & Engineering Chemistry Research.* **2014**, 54, 4396-4406.

[17] Tang, J.; Tang, H.; Sun, W.; Radosz, M.; Shen, Y., Poly(ionic liquid)s as new materials for CO<sub>2</sub> absorption. *J. Polym. Sci., Part A: Polym. Chem.* **2005**, 43, 5477-5489.

[18] Susan, M. A. B. H.; Kaneko, T.; Noda, A.; Watanabe, M., Ion gels prepared by in situ radical polymerization of vinyl monomers in an ionic liquid and their characterization as polymer electrolytes. *Journal of the American Chemical Society.* **2005**, 127, 4976-4983.

[19] Nakajima, H.; Ohno, H., Preparation of thermally stable polymer electrolytes from imidazolium-type ionic liquid derivatives. *Polymer.* **2005**, 46, 11499-11504.

[20] Livi, S.; Lins, L. C.; Capeletti, L. B.; Chardin, C.; Halawani, N.; Baudoux, J.; Cardoso, M. B., Antibacterial surface based on new epoxy-amine networks from ionic liquid monomers. *European Polymer Journal.* **2019**, 116, 56-64.

[21] Guo, J.; Xu, Q.; Zheng, Z.; Zhou, S.; Mao, H.; Wang, B.; Yan, F., Intrinsically antibacterial poly(ionic liquid) membranes: the synergistic effect of anions. *ACS Macro Letters.* **2015**, 4, 1094-1098.

[22] Cui, J.; Nie, F.-M.; Yang, J.-X.; Pan, L.; Ma, Z.; Li, Y.-S., Novel imidazolium-based poly(ionic liquid)s with different counterions for self-healing. *Journal of Materials Chemistry A.* **2017**, 5, 25220-25229.

[23] Livi, S.; Chardin, C.; Lins, L. C.; Halawani, N.; Pruvost, S.; Duchet-Rumeau, J.; Gérard, J.-F.; Baudoux, J., From ionic liquid epoxy monomer to tunable epoxy-amine network: reaction mechanism and final properties. *ACS Sustainable Chemistry & Engineering.* **2019**, 7, 3602-3613.

[24] Radchenko, A. V.; Chabane, H.; Demir, B.; Searles, D. J.; Duchet-Rumeau, J.; Gérard, J.-F.; Baudoux, J.; Livi, S., New epoxy thermosets derived from a bisimidazolium ionic liquid monomer: an experimental and modeling investigation. *ACS Sustainable Chemistry & Engineering.* **2020**, 8, 12208-12221.

[25] Radchenko, A. V.; Duchet-Rumeau, J.; Gérard, J.-F.; Baudoux, J.; Livi, S., Cycloaliphatic epoxidized ionic liquids as new versatile monomers for the development of shape memory PIL networks by 3D printing. *Polymer Chemistry.* **2020**, 11, 5475-5483.

[26] Lee, S.-B.; Park, Y.-S.; Lee, K.-W.; Endo, T., Hydrazinium Salts as Novel Thermally Latent Brønsted Acid-Inducing Initiators. *Chem. Lett.* **1995**, 24, 287-288.

[27] Shi, T.; Livi, S.; Duchet, J.; Gérard, J.-F., Ionic liquids-containing silica microcapsules: a potential tunable platform for shaping-up epoxy-based composite materials? *Nanomaterials.* **2020**, 10, 881-892.

[28] Sari, A.; Alkan, C.; Karaipekli, A., Preparation, characterization and thermal properties of PMMA/n-heptadecane microcapsules as novel solid-liquid microPCM for thermal energy storage. *Appl. Energy.* **2010**, 87, 1529-1534.

[29] Ye, S.; Wang, C.; Liu, X.; Tong, Z.; Ren, B.; Zeng, F., New loading process and release properties of insulin from polysaccharide microcapsules fabricated through layer-by-layer assembly. *Journal of controlled release.* **2006**, 112, 79-87.

[30] Li, H.; Wang, Q.; Wang, H.; Cui, Y.; Zhu, Y.; Wang, B., Fabrication of thermally stable

- polysulfone microcapsules containing [EMIm][NTf<sub>2</sub>] ionic liquid for enhancement of in situ self-lubrication effect of epoxy. *Macromolecular Materials and Engineering*. **2016**, 301, 1473-1481.
- [31] Gao, H.; Xing, J.; Xiong, X.; Li, Y.; Li, W.; Liu, Q.; Wu, Y.; Liu, H., Immobilization of ionic liquid [BMIM][PF<sub>6</sub>] by spraying suspension dispersion method. *Industrial & Engineering Chemistry Research*. **2008**, 47, 4414-4417.
- [32] Wang, H.-p.; Hu, S.-q.; Cai, S.-j.; Yu, F., Preparation and properties of bisphenol A epoxy resin microcapsules coated with melamine-formaldehyde resin. *Polym. Bull.* **2014**, 71, 2407-2419.
- [33] Yuan, Y. C.; Rong, M. Z.; Zhang, M. Q., Preparation and characterization of microencapsulated polythiol. *Polymer*. **2008**, 49, 2531-2541.
- [34] Gledhill, R. A.; Kinloch, A. J., Relationship between mechanical properties of and crack propagation in epoxy resin adhesives. *Polymer*. **1978**, 19, 574-582.
- [35] Chabane, H.; Livi, S.; Morelle, X. P.; Sonnier, R.; LoïcDumazert; Duchet-Rumeau, J.; Gérard, J.-F., Synthesis of new ionic liquid-grafted metal-oxo nanoclusters – Design of nanostructured hybrid organic-inorganic polymer networks. *Polymer*. **2021**, 224, 123721-123731.
- [36] Nguon, O.; Lagugné-Labarthe, F.; Brandys, F. A.; Li, J.; Gillies, E. R., Microencapsulation by in situ polymerization of amino resins. *Polym. Rev. (Philadelphia, PA, U. S.)*. **2017**, 58, 326-375.
- [37] Khakzad, F.; Alinejad, Z.; Shirin-Abadi, A. R.; Ghasemi, M.; Mahdavian, A. R., Optimization of parameters in preparation of PCM microcapsules based on melamine formaldehyde through dispersion polymerization. *Colloid and Polymer Science*. **2013**, 292, 355-368.
- [38] Weiss, E.; Gertopski, D.; Gupta, M. K.; Abu-Reziq, R., Encapsulation of ionic liquid BMIm[PF<sub>6</sub>] within polyurea microspheres. *Reactive and Functional Polymers*. **2015**, 96, 32-38.
- [39] Zhang, H.; Wang, X., Fabrication and performances of microencapsulated phase change materials based on n-octadecane core and resorcinol-modified melamine-formaldehyde shell. *Colloids and Surfaces A: Physicochemical and Engineering Aspects*. **2009**, 332, 129-138.
- [40] Lee, H.; Lee, S.; Cheong, I.; Kim, J., Microencapsulation of fragrant oil via in situ polymerization: effects of pH and melamine-formaldehyde molar ratio. *Journal of microencapsulation*. **2002**, 19, 559-569.
- [41] Yuan, L.; Liang, G.; Xie, J.; Li, L.; Guo, J., Preparation and characterization of poly(urea-formaldehyde) microcapsules filled with epoxy resins. *Polymer*. **2006**, 47, 5338-5349.
- [42] Salaün, F.; Devaux, E.; Bourbigot, S.; Rumeau, P., Influence of process parameters on microcapsules loaded with n-hexadecane prepared by in situ polymerization. *Chem. Eng. J.* **2009**, 155, 457-465.
- [43] Jeong, B.; Park, B.-D.; Causin, V., Influence of synthesis method and melamine content of urea-melamine-formaldehyde resins to their features in cohesion, interphase, and adhesion performance. *Journal of Industrial and Engineering Chemistry*. **2019**, 79, 87-96.
- [44] Kim, S.; Kim, H.-J.; Kim, H.-S.; Lee, Y.-K.; Yang, H.-S., Thermal analysis study of viscoelastic properties and activation energy of melamine-modified urea-formaldehyde resins.

*Journal of Adhesion Science and Technology*. **2006**, 20, 803-816.

[45] Guo, H. L.; Zhao, X. P.; Wang, J. P., The relation between narrow-dispersed microcapsules and surfactants. *J Microencapsul.* **2005**, 22, 853-862.

[46] Mao, J.; Yang, H.; Zhou, X., In situ polymerization of uniform poly(urea–formaldehyde) microcapsules containing paraffins under the high-speed agitation without emulsifier. *Polym. Bull.* **2012**, 69, 649-660.

[47] Zhao, H.; Fei, X.; Cao, L.; Zhao, S.; Zhou, J., Changes in microcapsules under heating: the effect of particle size on thermal stability and breakability. *Journal of Materials Science*. **2019**, 55, 3902-3911.

[48] Ao, Y.; Peng, J.; Yuan, L.; Cui, Z.; Li, C.; Li, J.; Zhai, M., Identification of radiolytic products of [C<sub>4</sub>mim][NTf<sub>2</sub>] and their effects on the Sr<sup>2+</sup> extraction. *Dalton Trans.* **2013**, 42, 4299-4305.

[49] Hanke, K.; Kaufmann, M.; Schwaab, G.; Havenith, M.; Wolke, C. T.; Gorlova, O.; Mark, A. Johnson; Kar, B. P.; Sander, W.; Sanchez-Garcia, E., Understanding the ionic liquid [NC<sub>4111</sub>][NTf<sub>2</sub>] from individual building blocks: an IR-spectroscopic study. *Phys Chem Chem Phys.* **2015**, 17, 8518-8529.

[50] Osipov, V. Y.; Romanov, N. M.; Kogane, K.; Touhara, H.; Hattori, Y.; Takai, K., Intrinsic infrared absorption for carbon–fluorine bonding in fluorinated nanodiamond. *Mendeleev Commun.* **2020**, 30, 84-87.

[51] Mustățã, F.; Bicu, I., Multifunctional epoxy resins: synthesis and characterization. *J. Appl. Polym. Sci.* **2000**, 77, 2430-2436.

[52] Yuan, Y. C.; Ye, X. J.; Rong, M. Z.; Zhang, M. Q.; Yang, G. C.; Zhao, J. Q., Self-healing epoxy composite with heat-resistant healant. *ACS Appl Mater Interfaces.* **2011**, 3, 4487-4495.

[53] Zhu, D. Y.; Cao, G. S.; Qiu, W. L.; Rong, M. Z.; Zhang, M. Q., Self-healing polyvinyl chloride (PVC) based on microencapsulated nucleophilic thiol-click chemistry. *Polymer.* **2015**, 69, 1-9.

[54] Yuan, L.; Liang, G.-z.; Xie, J.-q.; He, S.-B., Synthesis and characterization of microencapsulated dicyclopentadiene with melamine–formaldehyde resins. *Colloid and Polymer Science.* **2007**, 285, 781-791.

[55] Konuklu, Y.; Paksoy, H. O.; Unal, M.; Konuklu, S., Microencapsulation of a fatty acid with Poly(melamine–urea–formaldehyde). *Energy Convers. Manage.* **2014**, 80, 382-390.

[56] López, J.; Rico, M.; Montero, B.; Díez, J.; Ramírez, C., Polymer blends based on an epoxy-amine thermoset and a thermoplastic. *Journal of Thermal Analysis and Calorimetry* **2009**, 95, 369-376.

[57] Ferdosian, F.; Yuan, Z.; Anderson, M.; Xu, C., Sustainable lignin-based epoxy resins cured with aromatic and aliphatic amine curing agents: curing kinetics and thermal properties. *Thermochim. Acta.* **2015**, 618, 48-55.

[58] Kroutilová, I.; Matějka, L.; Sikora, A.; Souček, K.; Staš, L., Curing of epoxy systems at sub-glass transition temperature. *J. Appl. Polym. Sci.* **2006**, 99, 3669-3676.

[59] Lee, J.; Zhang, M.; Bhattacharyya, D.; Yuan, Y. C.; Jayaraman, K.; Mai, Y. W., Micromechanical behavior of self-healing epoxy and hardener-loaded microcapsules by nanoindentation. *Materials Letters.* **2012**, 76, 62-65.

[60] Tripathi, M.; Rahamtullah; Kumar, D.; Rajagopal, C.; Kumar Roy, P., Influence of

microcapsule shell material on the mechanical behavior of epoxy composites for self-healing applications. *J. Appl. Polym. Sci.* **2014**, 131, 40572-40580.

[61] Pearson, R. A.; FYee, A., Toughening mechanisms in thermoplastic-modified epoxies. *Polymer*. **1993**, 34, 3658-3670.

[62] Rubinstein, A. A., Mechanics of the crack path formation. *International Journal of Fracture* **1991**, 47, 291-305.

[63] Chong, Y. B.; Sun, D.; Zhang, X.; Yue, C. Y.; Yang, J., Robust multifunctional microcapsules with antibacterial and anticorrosion features. *Chem. Eng. J.* **2019**, 372, 496-508.

## Supporting Information of Chapter 4

### 1. NMR spectra of ILEM and intermediate products

$^1\text{H}$  NMR (400 MHz, Chloroform- $d$ )  $\delta$  8.93 (s, 1H), 7.36 (d,  $J = 0.8$  Hz, 2H), 4.40 (t,  $J = 6.7$  Hz, 4H), 3.01 (m, 2H), 2.79 (dd, 2H), 2.52 (dd, 2H), 2.47 – 2.34 (dd, 2H), 1.85 (dd, 2H).

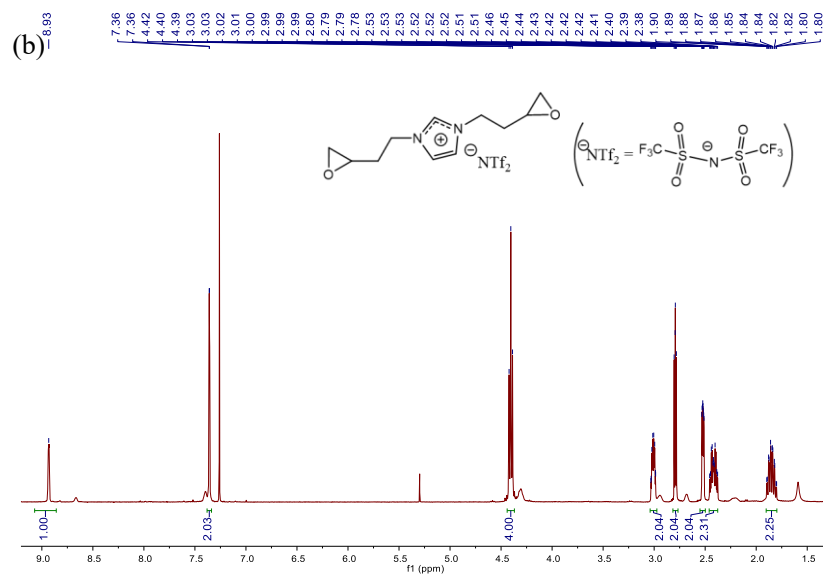


Figure S4-1  $^1\text{H}$  spectrum of ILEM (Chloroform- $d$ )

$^{19}\text{F}$  NMR (376 MHz, Acetonitrile- $d_3$ )  $\delta$  -80.11.

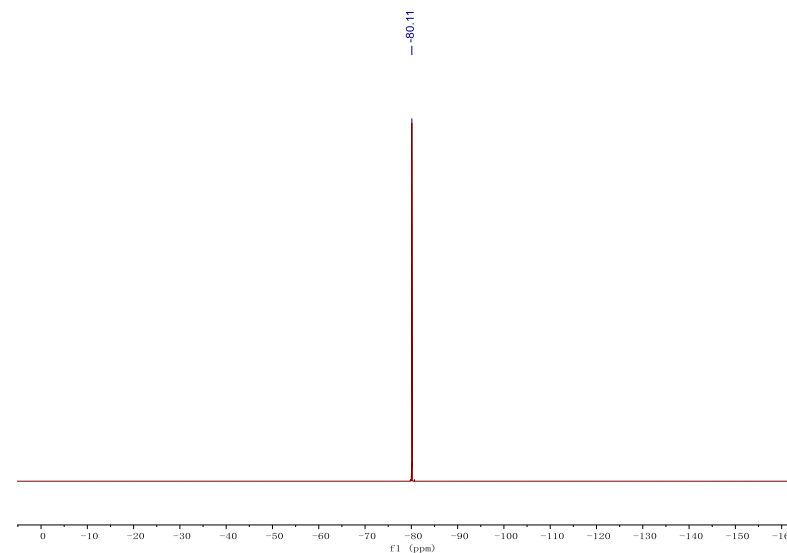


Figure S4-2  $^{19}\text{F}$  NMR spectrum of ILEM (Acetonitrile- $d_3$ )



$^1\text{H}$  NMR (400 MHz, Chloroform- $d$ )  $\delta$  7.45 (s, 1H), 7.04 (s, 1H), 6.90 (s, 1H), 5.77 (m, 1H), 5.39 – 4.67 (m, 2H), 4.00 (t, 3H), 2.48 – 2.53 (m, 2H).

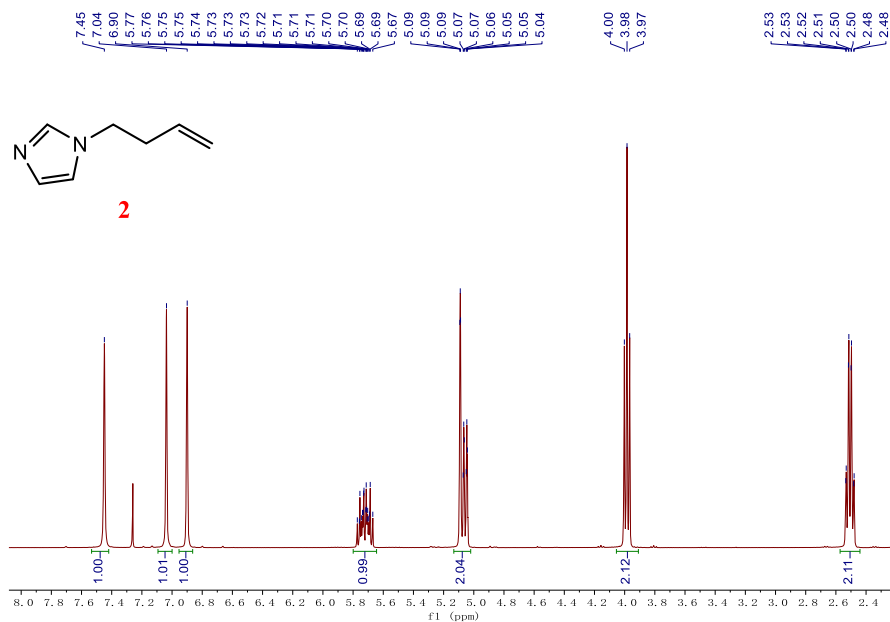


Figure S4-3  $^1\text{H}$  spectrum of compound **2** (Chloroform- $d$ )

$^1\text{H}$  NMR (400 MHz, Chloroform- $d$ )  $\delta$  8.86 (s, 1H), 7.24 (d,  $J = 1.6$  Hz, 2H), 5.74 (ddt, 2H), 5.22 – 4.98 (m, 4H), 4.29 (t, 4H), 2.69 – 2.50 (m, 4H).

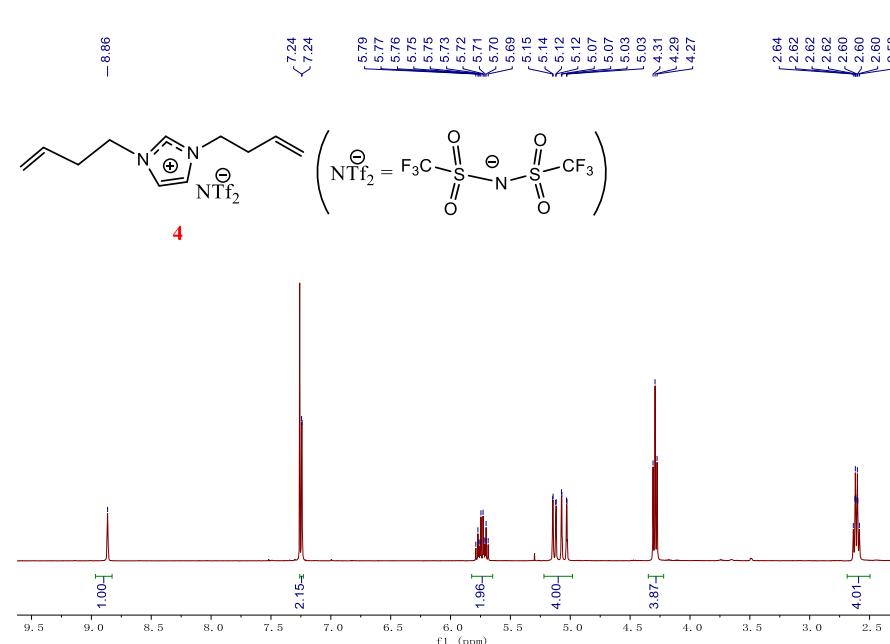
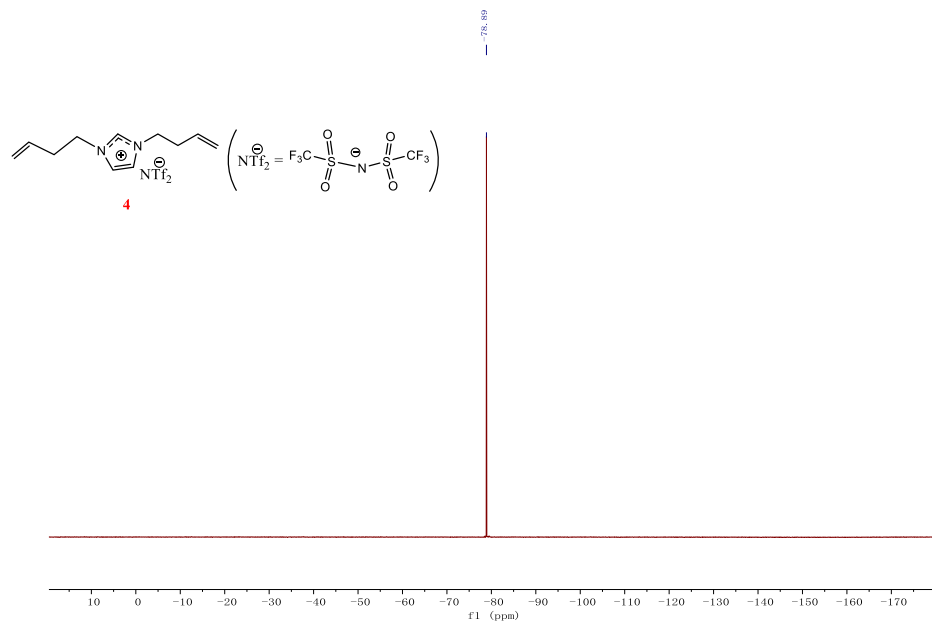


Figure S4-4  $^1\text{H}$  spectrum of compound **4** (Chloroform- $d$ )

$^{19}\text{F}$  NMR (376 MHz, Chloroform-d)  $\delta$  -78.89 .



**Figure S4-5**  $^{19}\text{F}$  spectrum of compound **4** (Chloroform-d)

## 2. DSC curve of ILEM

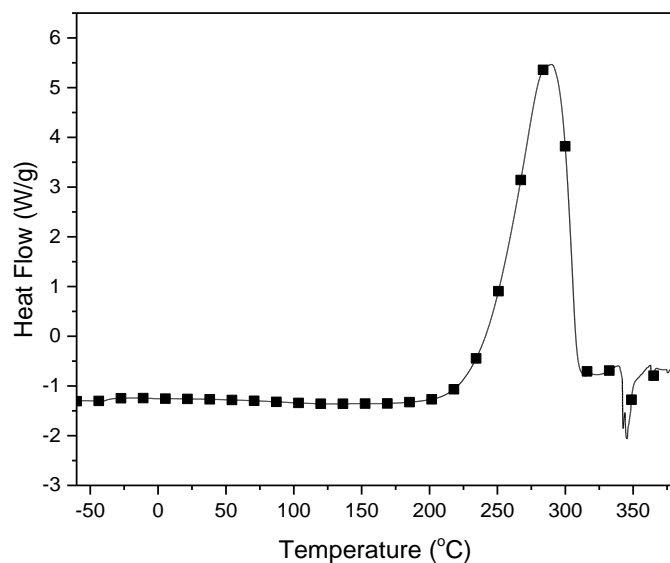


**Figure S4-6** DSC trace of ILEM (N<sub>2</sub> atmosphere, heating rate 10 K·min<sup>-1</sup>)

## 3. TGA and DTG curves of ILEM

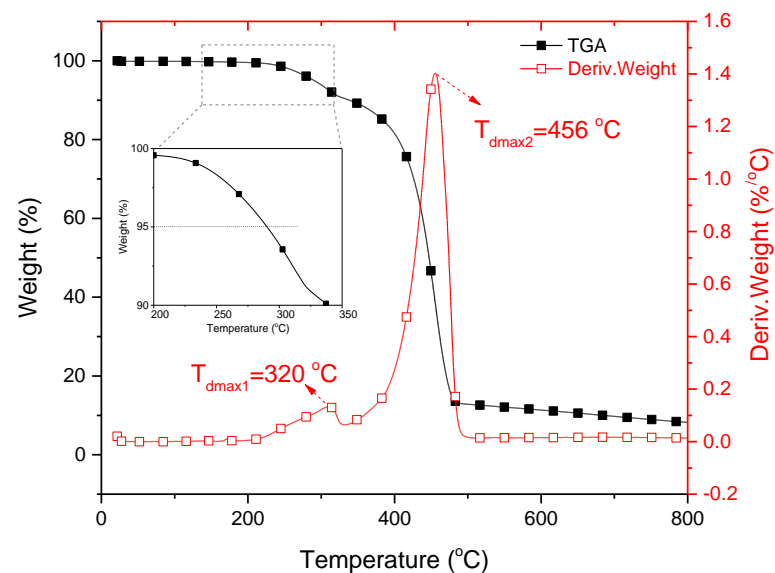


**Figure S4-7** TGA (■) and DTG (□) traces of ILEM (N<sub>2</sub> atmosphere, heating rate 20 K·min<sup>-1</sup>)

### 3. FTIR spectra of emerged gas of PMF@EP microcapsules and neat ILEM (core) and PMF (shell) at different temperature during thermal degradation at N<sub>2</sub> atmosphere

(1) ILEM@PMF microcapsule

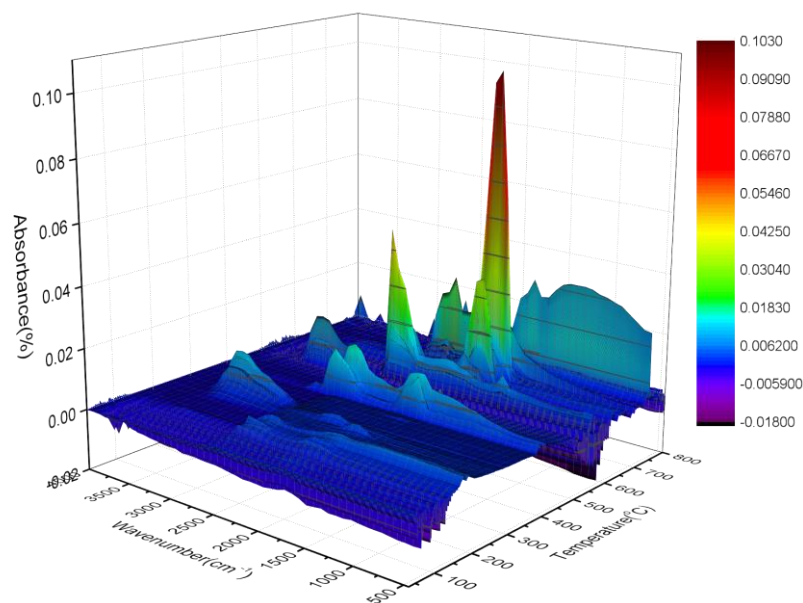


**Figure S4-8** FTIR spectra of emitted gas during degradation of ILEM@PMF microcapsules under N<sub>2</sub> atmosphere

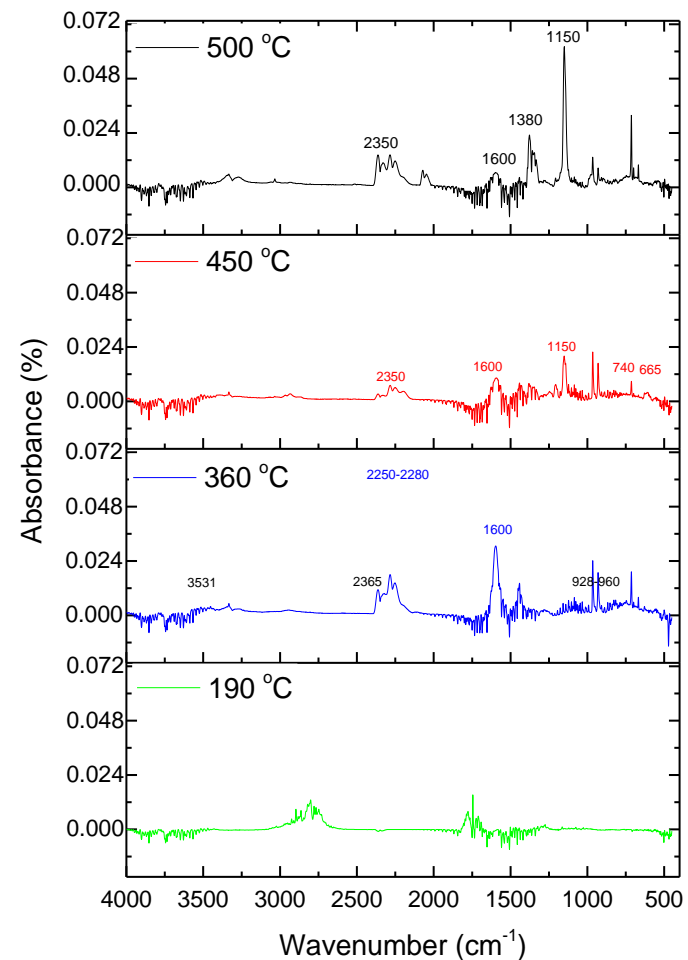


**Figure S4-9** FTIR spectra of emitted gas at different temperatures of ILEM@PMF microcapsules under N<sub>2</sub> atmosphere

(2) Neat ILEM

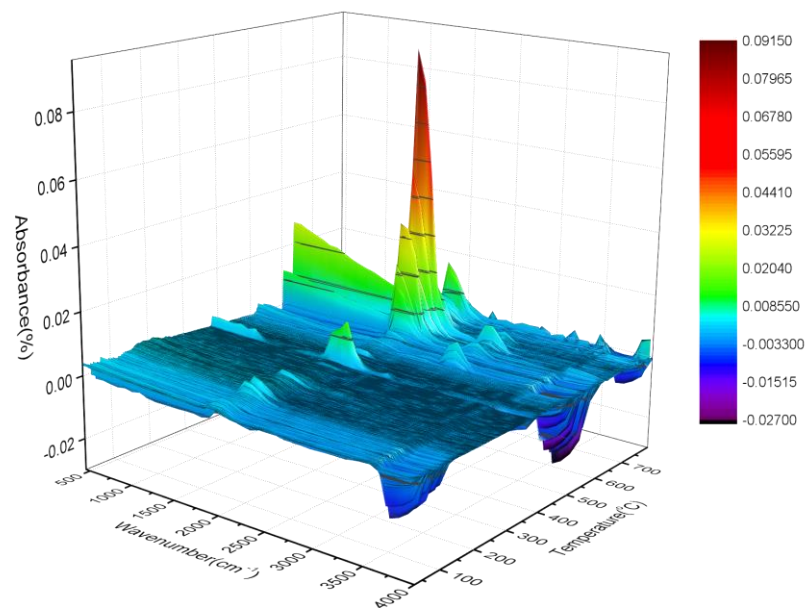


**Figure S4-10** FTIR spectra of emitted gas during degradation of ILEM under N<sub>2</sub> atmosphere

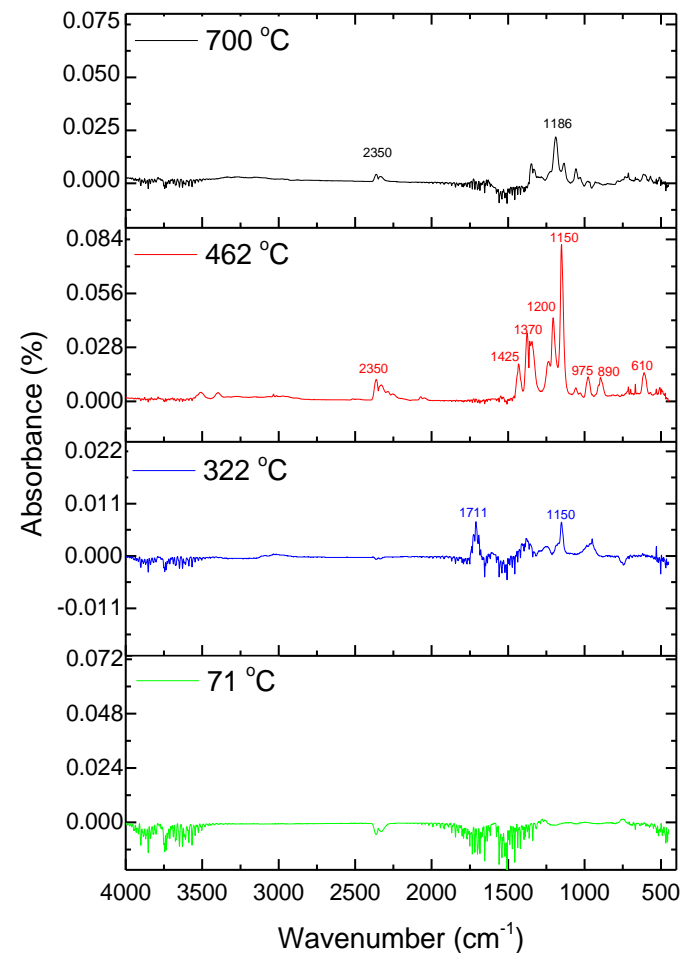


**Figure S4-11** FTIR spectra of emitted gas at different temperatures of ILEM microcapsules under N<sub>2</sub> atmosphere

(3) Neat PMF

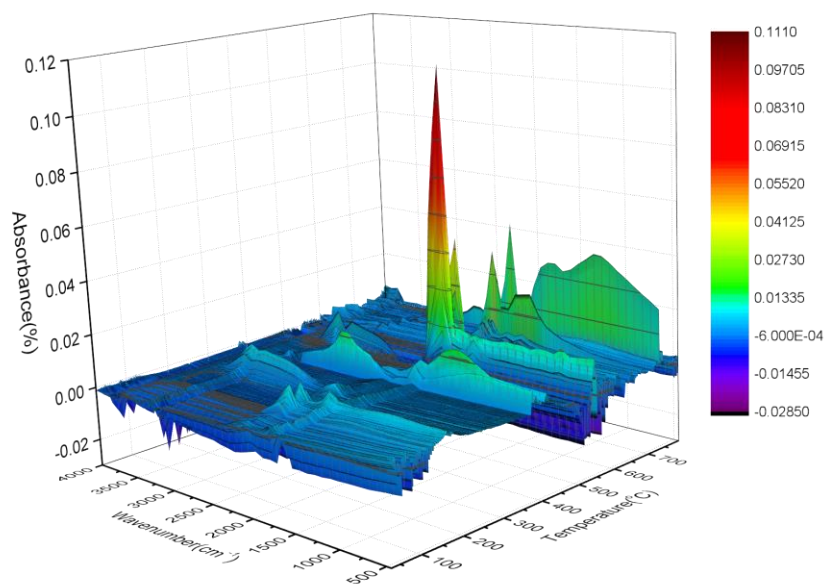


**Figure S4-12** FTIR emitted of emitted gas during degradation of neat PMF under N<sub>2</sub> atmosphere

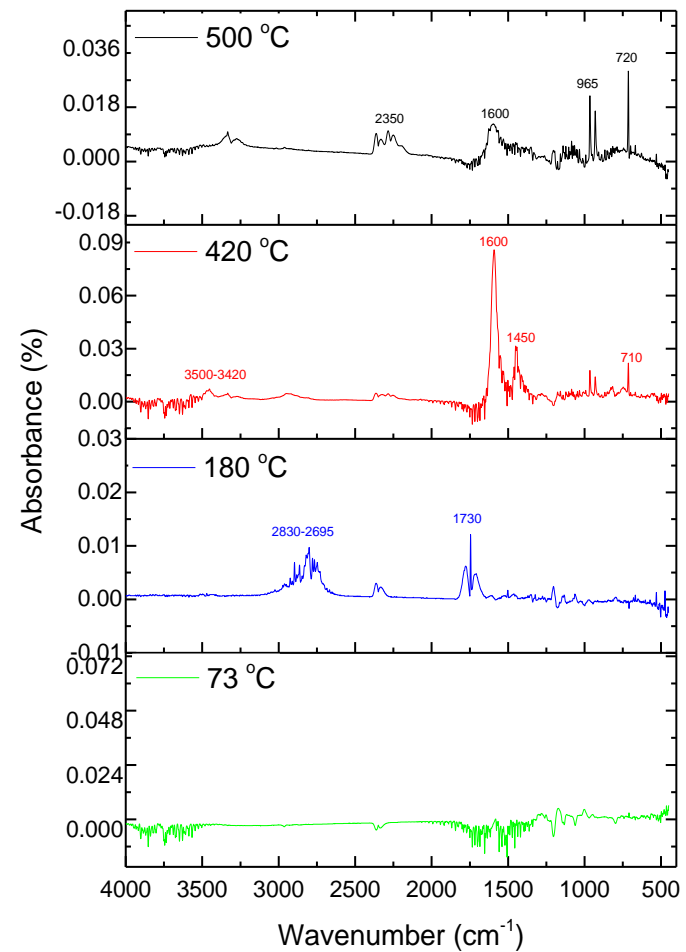


**Figure S4-13** FTIR spectra of emitted gas at different temperatures of neat PMF under N<sub>2</sub> atmosphere

#### 4. Thermal stability of ILEM@PMF microcapsules filled epoxy-amine composites

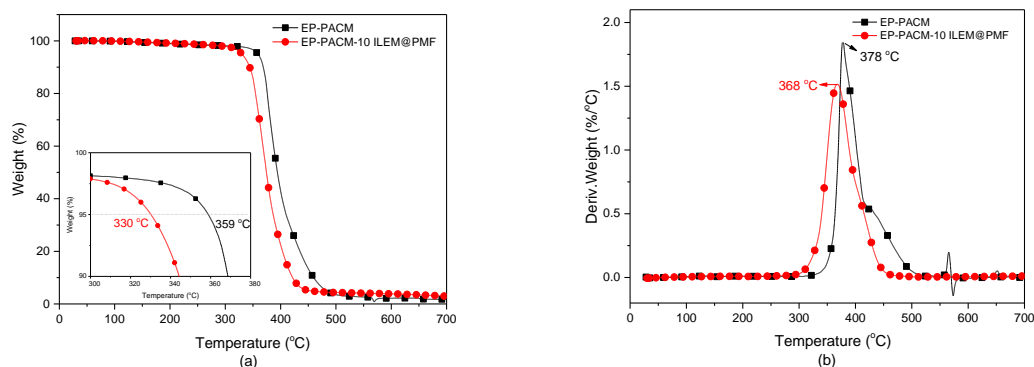


**Figure S4-14** (a) TGA and (b) DTG traces of (■) neat epoxy-PACM networks and (●) ILEM@PMF microcapsule-filled epoxy-PACM materials (N<sub>2</sub> atmosphere, heating rate 20 K·min<sup>-1</sup>)

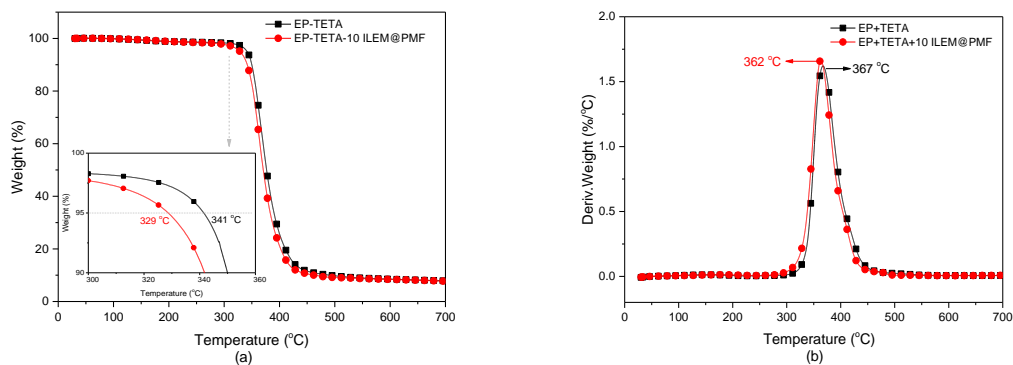


**Figure S4-15** (a) TGA and (b) DTG traces of (■) neat epoxy-TETA networks and (●) ILEM@PMF microcapsule-filled epoxy-TETA materials (N<sub>2</sub> atmosphere, heating rate 20 K·min<sup>-1</sup>)

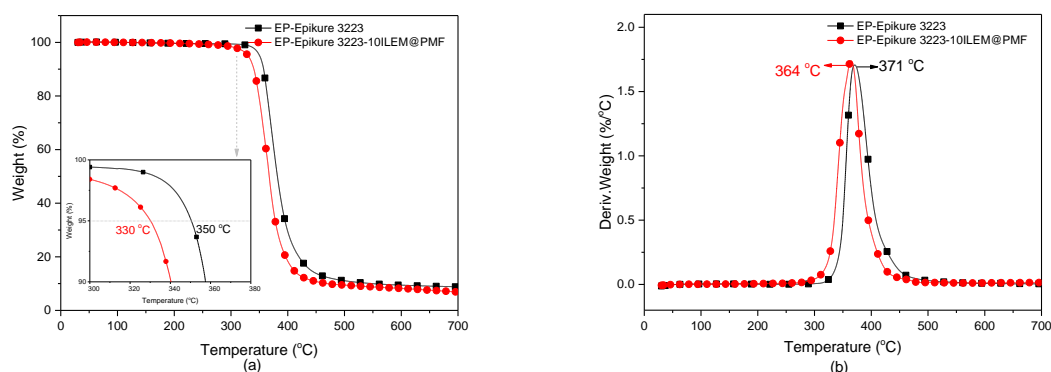


**Figure S4-16** (a) TGA and (b) DTG traces of (■) neat epoxy-Epikure 3223 networks and (●) ILEM@PMF microcapsule-filled epoxy-Epikure 3223 materials (N<sub>2</sub> atmosphere, heating rate 20 K·min<sup>-1</sup>)

## Chapter 5

# Conclusions and perspectives

This work aims at the improvement of fracture toughness and achieving self-healing of epoxy composites combined with ionic liquids (ILs) through the microencapsulation strategy. Based on this purpose, different microcapsules were synthesized as fillers in epoxy-amine composites. Meanwhile, ILs played different roles in the epoxy-amine composites.

In the first chapter, a phosphonium-based IL named tetradecyl(trihexyl)phosphonium bis-(2,4,4-trimethylpentyl) phosphinate was used as core material encapsulated in silica microcapsules via ionic liquid-in-water emulsion combined with a sol-gel process. The IL containing silica microcapsules (IL@SiO<sub>2</sub>) present a spherical morphology (2-3 μm) and an expected core-shell structure in which shell was estimated at 100 nm. They have good thermal stability and high mechanical strength. These features make them act as toughening particles in epoxy-amine networks. This study highlighted that these IL@SiO<sub>2</sub> microcapsules improved the fracture toughness and the mechanical performances of the epoxy-amine networks while keeping their thermal stability. Compared to the literature concerning the use of silica nanoparticles into epoxy nanocomposites, IL@SiO<sub>2</sub> microcapsules are well-dispersed in epoxy-amine networks preventing crack propagation. Compared to crack deflection toughening mechanism reported for nanofillers, the crack pinning mechanism seems to be the main contribution for preventing crack propagation. Non-stoichiometric epoxy systems were also investigated to get even higher reinforcing effect of IL@SiO<sub>2</sub> microcapsules.

In the second part of this work, conventional epoxy prepolymer, *i.e.* DGEBA, was encapsulated in a poly(urea-formaldehyde) shell in order to obtain epoxy containing microcapsules (EP@PUF). Such microcapsules were designed for achieving self-healing properties for epoxy-based materials. To obtain the self-healing capacity, another phosphonium-based ionic liquid denoted tributyl(ethyl)phosphonium diethyl phosphate (IL169)



was used as a co-initiator/curing agent in the bulk of epoxy-amine network. Due to the higher thermal stability of IL 169, it can be used as initiator of the epoxy prepolymer contained into PUF microcapsules. The strategy for self-healing proceeds from the reaction of the epoxy released by breaking EP@PUF microcapsules with IL 169. Therefore, EP@PUF microcapsules were synthesized and characterized in the first step. Then, a reactivity study was carried out to investigate the influence of IL 169 on the formation of epoxy-amine network in order to determine the optimized content of IL169. With 10 phr of IL 169, a negligible effect on the curing behavior of epoxy-amine system was observed. Nevertheless, a plasticizing effect was highlighted when an amount higher than 10 phr was introduced. Finally, different weight fractions of EP@PUF microcapsules were added to the epoxy-amine-IL network to prepare a self-healable epoxy material. The thermal and mechanical properties as well as the self-healing properties were investigated. It was showed that more than 10 wt% of EP@PUF microcapsules are required to get self-healing. Nevertheless, a balance was found to keep good mechanical properties due to the weak interfacial interactions and the microcapsules surface. As a consequence, this work has highlighted that the use of IL 169 as co-initiator and the epoxy prepolymer containing microcapsules induced a self-healing ability for epoxy-based materials, preventing the use of solid catalyst for high temperature cured epoxy composites.

In the third part of this work, to avoid the use of an additional initiator or encapsulated hardener as healing agent, ionic liquid monomer based on epoxidized imidazolium ILs denoted ILEM was synthesized and was encapsulated to prepare poly(melamine-formaldehyde) (PMF) microcapsules (ILEM@PMF). First, the synthesis conditions of ILEM@PMF microcapsules were carefully investigated. It was highlighted the good thermal properties and self-curing behavior of ILEM leading to ILEM@PMF microcapsules as a promising self-healing additive for epoxy-amine-based materials. Therefore, ILEM@PMF microcapsules were added in different epoxy-amine networks to study their self-healing performances. Three different epoxy-amine systems cured at different temperatures were selected. It was found that the ILEM@PMF microcapsules have a better self-healing performance for intermediate and room temperature-cured epoxy composites due to ILEM core polymerization during curing of the epoxy material requiring high cure temperature.

This work has proposed different strategies to synthesize different microcapsules as additives in epoxy-based materials. Commercial ionic liquid and synthesized ionic liquids were involved to achieve different purposes for epoxy materials combined with the microencapsulation techniques. Different solved issues were identified:

- Phosphonium-based ionic liquid was firstly encapsulated into silica microcapsules (IL@SiO<sub>2</sub>), and their performance as reinforcement was investigated. The toughening mechanism was also studied;
- A single microcapsule-based system was achieved from epoxy monomer containing microcapsules (EP@PUF) in the epoxy-amine-ILs ternary network. The use of IL 169 avoids the influence of high curing temperature on the conventional latent hardener and extra synthesis for a dual microcapsules system;
- Ionic liquid epoxy monomer (ILEM) was firstly confined into poly(melamine-formaldehyde) PMF microcapsules to play a role of self-healing additive in epoxy materials. This strategy avoided using any extra initiator or hardener to achieve self-healing purpose for epoxy-amine composites.

This work could be new tools for introducing different types of microcapsules into various types of epoxy matrices to design new multifunctional thermosets. For the future researches several studies could be considered:

- Electrospinning or coaxial electrospinning processing involving ILs for designing microvascular networks for epoxy composites or functional membranes;
- ILEM having different types of anions or structures of cations could be also designed for encapsulation in microcapsules or hollow fibers.

Actually, we have already done a few attempts for further studies. For example, we have tried to dissolve Polyethersulfone (PES) and IL 169 in the same solvent for electrospinning, aiming at obtaining fibers from phase separation. As shown in SEM micrographs (Figure 5-1) of electrospun PES fibers with 20 wt% of IL 169, the ionic liquid migrated to the surface of PES fibers. Further studies are required to design electrospun fibers having an IL core and PES shell in order to use such microfibrils as a microvascular self-healing system. Coaxial electrospinning technique could be of interest.

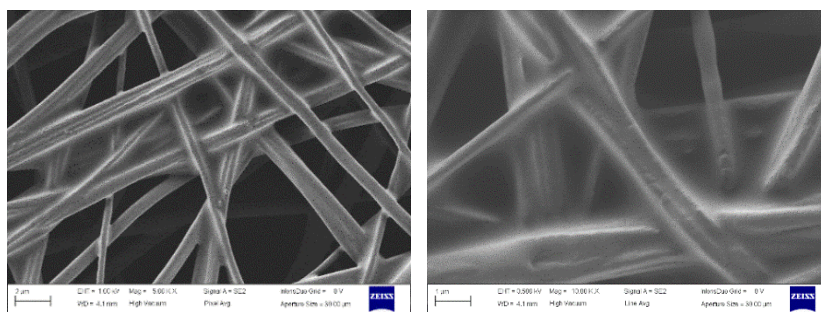


**Figure 5-1** SEM images of PES-IL fibers by electrospinning





## FOLIO ADMINISTRATIF

### THESE DE L'UNIVERSITE DE LYON OPEREE AU SEIN DE L'INSA LYON

NOM : SHI

DATE de SOUTENANCE : 29/03/2022

Prénom : Ting

TITRE : INTRODUCTION OF IONIC LIQUID VIA MICROENCAPSULATION TO DESIGN ENHANCED AND SELF-HEALABLE EPOXY-AMINE COMPOSITES

NATURE : Doctorat

Numéro d'ordre : 2022LYSEI026

Ecole doctorale : Matériaux de Lyon

Spécialité : Matériaux Polymères et Composites

RESUME : La résine époxy, en tant que l'un des matériaux thermodurcissables les plus largement utilisés, est confrontée au problème de la fragilité élevée et de la faible ténacité, ce qui a limité leur application dans certaines occasions spécifiques. Par conséquent, améliorer la ténacité pour empêcher la propagation des fissures et guérir les microfissures initiales dans la matrice époxy pourrait prolonger la durée de vie des composites époxy. Le liquide ionique (LI) a été appliqué pour concevoir une composition époxy à plus haute performance en raison des excellentes propriétés intrinsèques avec une combinaison abondante de cations et d'anions. Par conséquent, ces travaux se concentrent sur l'amélioration de la ténacité et de la capacité d'auto-guérison des composites époxy-amine traditionnels via une méthodologie populaire — la microencapsulation. Dans la première section, le liquide ionique de type phosphonium a d'abord été encapsulé dans une coque de silice sous forme de microcapsules pour améliorer la ténacité du réseau époxy-amine et le mécanisme de ténacité a également été discuté. Dans la deuxième section, le monomère époxy a été encapsulé dans une coque en poly(urée-formaldéhyde) en tant qu'agent cicatrisant extrinsèque et un liquide ionique a été incorporé dans un réseau époxy-amine-LI, qui visait à obtenir une auto-cicatrisation dans des composites époxy durcis à haute température. Dans la dernière section, un monomère époxy liquide ionique a été synthétisé et il a d'abord été encapsulé dans des microcapsules de poly(mélamine-formaldéhyde) et ils ont été ajoutés dans différentes matrices époxy-amine pour concevoir un système d'auto-guérison de microcapsules uniques. Par conséquent, ce travail s'est concentré sur différentes propriétés à travers différentes combinaisons de liquides ioniques et de microcapsules dans les composites époxy, ce qui a élargi le champ d'application du liquide ionique et inspirera l'étude de suivi.

MOTS-CLÉS : réseau époxy-amine ; liquides ioniques ; microencapsulation ; dureté ; auto-guérison.

Laboratoire de recherche : Ingénierie des Matériaux Polymères - UMR 5223 INSA de Lyon

Directeur de thèse : GERARD Jean-François

Co-directeurs de thèse : DUCHET-RUMEAU Jannick, LIVI Sébastien

Président de jury : BONGIOVANNI Roberta

Composition du jury :

BONGIOVANNI Roberta

KENNY José Maria

DEFOORT Brigitte

GERARD Jean-François

DUCHET-RUMEAU Jannick

LIVI Sébastien

Professeur (Politecnico di Torino)

Professeur (Università degli Studi di Perugia)

Docteur, HDR (ArianeGroup)

Professeur (INSA Lyon)

Professeur (INSA Lyon)

Maître de Conférences, HDR (INSA Lyon)

Examinatrice

Rapporteur

Rapporteur

Directeur de thèse

Co-directrice de thèse

Co-directeur de thèse